Mécanismes de photo-commutation réversible des protéines fluorescentes

Aline Regis Faro Regis Faro

UNIVERSITÉ DE GRENOBLE

THÈSE

Pour obtenir le grade de

DOCTEUR DE L'UNIVERSITÉ DE GRENOBLE

Spécialité: **Physique pour les Sciences du Vivant**

Arrêté ministériel : 7 août 2006

Présentée par **Aline REGIS FARO**

Thèse dirigée par **Dominique BOURGEOIS**

préparée au sein du **L'institut de Biologie Structurale JP. EBEL**
dans **l'École Doctorale de Physique**

Mécanismes de photo-commutation réversible des protéines fluorescentes

Thèse soutenue publiquement le **27 Septembre 2012**,
devant le jury composé de :

Mme Fabienne MEROLA
Dr au Laboratoire de Chimie Physique (Université Paris-Sud), Paris, Rapporteur
Mr Jean Denis PEDELACQ
Dr à l'Institut de Pharmacologie et de Biologie Structurale, Toulouse, Rapporteur
Mme Isabelle DEMACHY
Dr au Laboratoire de Chimie Physique (Université Paris-Sud), Paris, Examinateur
Mr Ranieri BIZZARRI
Dr à Scuola Normale Superiore and Istituto Nanoscienze, Pise - Italie, Examinateur
Mr Martin WEIK
Dr à l'Institut de Biologie Structurale, Grenoble, Examinateur
Mr Dominique BOURGEOIS
Dr à l'Institut de Biologie Structurale, Grenoble, Directeur de thèse

à minha mãe, Isabel Regis Peixoto Faro

REMERCIEMENTS / AGRADECIMENTOS

Ces quatre années en France ont été pour moi une très riche expérience, tant au niveau scientifique que personnel. Des nombreuses personnes ont participé directement et indirectement à réalisation de ce travail et je souhaiterai les remercier pour leurs conseils, leur aide et leur soutien.

Tout d'abord je voudrais remercier ma famille.
«Obrigada Manda por esta tão perto mesmo estando tão longe, pai pelo seu apoio e incentivo e eu serei eternamente grata à minha mãe por tudo que ela fez por mim, sua dedicaçao e amor. Ao todo resto da minha familia obrigada pela compreenção pela minha ausência. Uma lembraça muito especial à minha querida tia Cida».

Ensuite, je souhaiterai exprimer mes plus sincères remerciements à mon Directeur de thèse Dominique BOURGEOIS. Dominique m'a donné l'opportunité de réaliser cette thèse, il m'apporté son enthousiasme, sa vision de la science et ensemble nous avons relevé le « chalenge » d'écrire cette thèse en anglais. Je remercie également l'ensemble des personnes avec lesquelles j'ai travaillé pendant ces années: Eve DE ROSNY, Philippe CARPENTIER, Virgile ADAM, Sébastien VIOLOT, Claudine DARNAULT, Guillaume POMPIDOR, Delphine ARCIZET, Chenxi DUAN, Martin BYRDIN et Laurent GUYON. Je remercie Eva PEBAY–PEYROULA Directrice de l'Institut de Biologie Structurale de Grenoble, pour m'avoir permis d'effectuer ma thèse dans cet établissement. Je remercie aussi l'ensemble des membres du jury pour avoir accepté d'endosser leurs fonctions respectives.

Je souhaiterai adresser un grand merci tout spécial à Antoine MASURE pour sa patience et les bons moments passés ensemble. Merci aussi à la famille MASURE et BATHILY, vous êtes merveilleux. Merci à tous les amis que m'ont beaucoup aidé avec ses conseilles et ses corrections pendant la rédaction de cette thèse: Cécile TRON, Eleni POLYMENOPOULOU, Yiannis GEORGIOU « Σας ευχαριστούμε για όλα, την επόμενη φορά που θα γράψω στα ελληνικά », Alex VIENNE, Alexia ESSERY, Paul LEDBETTER, Fleur CHAPPELLE et Marcel NOGUEIRA.

En dernier lieu, je voudrais exprimer ma reconnaissance aussi envers mes anciens collègues de Labo (IFSC) et spécialement à Lucas BLEICHER pour m'avoir aidé à choisir mon sujet de thèse. Merci aussi à Glaucius OLIVA, Otávio THIEMANN pour vos recommandations et à mes amis Funda KOZANOGLU et à Oumaima BOUSLAMA pour m'avoir aidé à préparer mon entretien à Paris.

.

RÉSUMÉ

Mécanismes de photo-commutation réversible des protéines fluorescents (RSFPs) FARO, A. R. 2012. 232 pages. Thèse – Institut de Biologie Structurale Jean-Pierre Ebel, CEA, Université e Joseph Fourier, Grenoble, FRANCE 2012.

La propriété d'être réversiblement commutable de certaines protéines fluorescentes homologues à la GFP ouvre un vaste champ d'applications possibles: notamment le bio-stockage de données à haute densité et la microscopie à super résolution. Parmi ces protéines, on trouve plusieurs variantes de la GFP, notamment la protéine jaune YFP, et des protéines fluorescentes issues d'espèces marines Anthozoaires, comme Dronpa ou Padron. Plusieurs études structurales indiquent que ces protéines fluorescentes photochromiques commutent par isomérisation et protonation couplées du chromophore. Cependant, la synchronisation entre ces deux événements, le détail des mécanismes de photo-commutation, et le rôle de la dynamique conformationelle restent incomplètement compris. Par l'utilisation combinée de la cristallographie cinétique et de la spectroscopie optique in cristallo à basse température, nous avons comparé le comportement des protéines YFP, Dronpa et IrisFP, et nous avons étudié en détail le mécanisme photo-physique de commutation chez la protéine Padron. Contrairement à Dronpa et IrisFP, la photo-commutation d'YFP est plus efficace à basse température qu'à température ambiante. Nos résultats suggèrent que le mécanisme de commutation d'YFP n'implique pas de changement conformationel majeur, mais plutôt une protonation photo-induite du chromophore ne nécessitant pas d'isomérisation. Au contraire, les études réalisées sur la protéine Padron nous ont permis de montrer que, dans ce cas, l'isomérisation du chromophore peut se produire indépendamment de sa protonation, et, étonnamment, à température cryogénique. De plus, deux états intermédiaires ont pu être caractérisés au cours du processus de photo-commutation. La protéine Padron a permis de mettre à jour le premier marqueur codable génétiquement qui soit efficacement photo-commutable à température cryogénique.

Mot-clés: protéines fluorescentes, photo-commutation, RSFPs, états intermédiaires, protonation photo-induite, cryo-nanoscopie.

RESUMO

Mecanismo de foto comutação reversível de proteínas fluorescentes (RSFPs) FARO, A. R. 2012. 232 páginas. Tese – Institut de Biologie Structurale Jean-Pierre Ebel, CEA, Université e Joseph Fourier, Grenoble, FRANCE 2012.

A propriedade de ser reversivelmente comutável de algumas proteínas fluorescentes homólogas à GFP abre um vasto campo para possíveis aplicações: principalmente a bioestocagem de dados de alta densidade e a microscopia de super-resolução. Entre estas proteínas se encontra diversas variantes da GFP, em especial variante amarela YFP, e proteínas fluorescentes provenientes de espécies marinhas Antozoárias, como Dronpa e Padron. Diversos estudos estruturais indicam que estas proteínas fluorescentes fotocrômicas comutam por meio da união da isomerização mais a protonação do cromóforo. No entanto a sincronização entre estes dois eventos, detalhes do mecanismo, e o funcionamento da dinâmica conformacional permanecem desconhecidos. Através da combinação da cristalografia cinética e da espectroscopia óptica in cristallo à baixas temperaturas, nos comparamos o comportamento das proteínas YFP, Dronpa e IrisFP e estudamos em detalhe o mecanismo foto-físico de comutação da proteína Padron. De forma contrária à Dronpa e IrisFP, a foto-comutação da YFP é mais eficaz à baixa temperatura que a temperatura ambiente. Nossos resultados sugerem que o mecanismo de foto-comutação da YFP não envolve grandes mudanças conformacionais, mas uma protonação induzida do cromóforo que não necessita da isomerização. Inversamente, os estudos realisados com Padron nos permitiu mostrar que, neste caso, a isomerização do cromóforo pode ser produzida independentemente da protonação e surpreendentemente à temperatura criogênica. No mais, dois estados intermediários puderam ser caracterizados durante o processo de foto-comutação. A proteína Padron permitiu desenvolver o primeiro marcador geneticamente codável que foto-comuta eficazmente à temperatura criogênica.

Palavras-chave: proteínas fluorescentes, fotocomutação, RSFPs, estados intermediários, protonação foto induzida, crio-nanoscopia

ABSTRACT

Reversible photoswitching mechanism of the Fluorescent Proteins (RSFPs).
FARO, A. R.2012. 232 pages. Thesis – Institut de Biologie Structurale Jean-Pierre Ebel, CEA, Université e Joseph Fourier, Grenoble, FRANCE 2012

The property to be reversible switchable of some homologues fluorescents protein of GFP open a large field for possible applications: such as, high-density data bio-storage and super-resolution microscopy. Between these proteins, we find several variants of GFP, such as yellow fluorescent protein, YFP, and fluorescents protein from marine Anthozoary species, as Dronpa or Padron. Several structural studies suggest that these fluorescent proteins switch via isomerization coupled with the protonation of the chromophore. However, the synchronization between these processes, the detail about the photo-switching mechanism, and the role of conformational dynamics remains unclear. In combination of the kinetic crystallography and the optic spectroscopy in cristallo at low temperature, we have compared the YFP behavior, Dronpa and IrisFP, and we have studied in detail the photo-physic mechanism of Padron switching. In contrast to Dronpa and IrisFP, the YFP photoswitching is more efficient at low temperature than at room temperature. Our results suggest that theYFP switching is not associated to large structural rearrangements, but mostly a photo-induced protonation of the chromophore without isomerization. On the contrary, the studies done with Padron allowed us to show, in this case, the chromophore isomerization can be produced independently of the protonation, at cryo-temperatures. Moreover, two intermediate states were revealed in the photo-pathway. Padron fluorescent protein allows to advance the first genetically inserted dye, being photo-switchable at cryogenic temperature.

Keywords: fluorescent proteins, photoswitching, RSFPs, intermediate state, photo induced protonation, cryo-nanoscopy.

TABLE OF CONTENTS

CHAPTER 1

INTRODUCTION

CHAPTER 2

RESULTS AND DISCUSSIONS

REFERENCES

ANNEX 1

LOW-TEMPERATURE PHOTOINDUCED PROTONATION IN PHOTOCHROMIC FLUORESCENT PROTEINS. FARO, ALINE REGIS; ADAM, VIRGILE; CARPENTIER, PHILIPPE; DARNAULT, CLAUDINE; BOURGEOIS, DOMINIQUE; DE ROSNY, EVE. **PHOTOCHEMICAL & PHOTOBIOLOGICAL SCIENCES, 2008.**

ANNEX 2

LOW-TEMPERATURE CHROMOPHORE ISOMERIZATION REVEALS THE PHOTOSWITCHING MECHANISM OF THE FLUORESCENT PROTEIN PADRON. FARO, ALINE REGIS; CARPENTIER, PHILIPPE; JONASSON, GABRIELLA; POMPIDOR, GUILLAUME; ARCIZET, DELPHINE; DEMACHY, ISABELLE; BOURGEOIS, DOMINIQUE.**JOURNAL OF THE AMERICAN CHEMICAL SOCIETY, 2011.**

LIST OF ACRONYMS

FPs: Fluorescent Proteins;

YFP: Yellow Fluorescent Protein;

PTFPs: Photo-Transformable Fluorescent Proteins;

RSFPs: Reversible Switchable Fluorescent Proteins;

QC/MM: Quantum Chemical /Molecular Mechanics.

PALM: PhotoActivated Localization Microscopy;

STED: STimulated Emission Depletion;

RESOLFT: Reversible Saturable Optical Linear Fluorescence Transitions;

OLID: Optical Lock-In Detection;

pcFRET: photochromic Förster Resonance Energy Transfer;

SSIM: Saturated Structured Illumination Microscopy;

EM: Eletron Miscrocopy;

ESPT: Excited State Proton Transfer;

p-HBI: 4-(p-hydroxybenzylidene)-5-imidazolinone;

LIST OF FIGURES

Chapter 1

INTRODUCTION

1.1 FLUORESCENT PROTEINS: WHO ARE THEY?

Fluorescent proteins (FPs) are the homologous proteins of Green Fluorescent Protein (GFP), the first noticed fluorescent protein. The GFP was discovered in the mid 1970s, when O. Shimomura (Shimomura et al., 1962; Shimomura, 1995) took an interest in understanding the nature of the brightness of the jellyfish Aequorea Victoria, and isolated what he considered to be the source of the light. After four decades, this protein family continues to be extensively studied due to its qualities in the dyes world. Two factors are advantageous with FPs:

- compared to synthetic dyes, the FPs have the advantage that they can be genetically inserted in the organism of interest, providing non-invasive and specific labeling.
- compared to other proteins that can also fluoresce, they do not require any cofactor except molecular oxygen.

The structure responsible for light emission is the chromophore, p-hydroxybenzylideneimidazolinone (HBDI), positioned in the center of the protein scaffold (**Figure 1.1**).

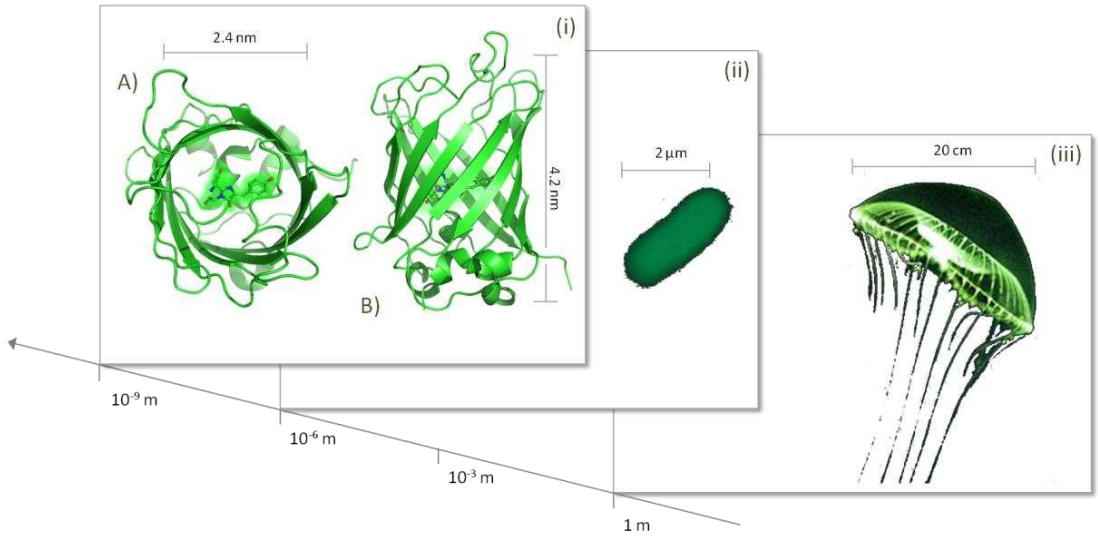

Figure 1.1) Size comparison between **(i)** Cartoon representation of the Green Fluorescent Protein (GFP) **(A)** top view and **(B)** in overall (the chromophore is represented in stick), **(ii)** E. coli cell and (**iii**) Fluorescent jellyfish.

1.1.1 FLUORESCENT PROTEINS IN NATURE

Homologues of GFP were identified in several marine organisms in the phylum Cnidaria, including Hydrozoa and reef-corals of the class Anthozoa (Matz et al., 1999; Labas et al., 2002). These proteins were also identified in evolutionarily distant species from Arthropoda (Shagin et al., 2004), Chordata (Deheyn et al., 2007; Li et al., 2009), and Ctenophora (Haddock et al., 2010) (**Figure 1.2**).

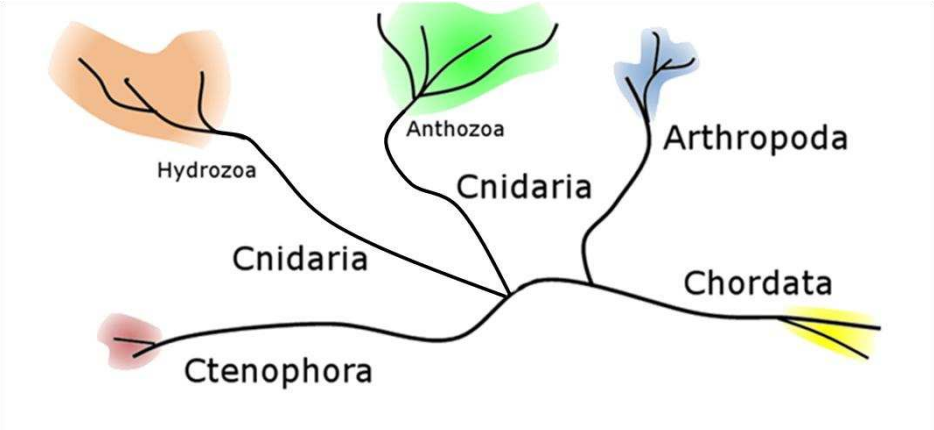

Figure 1.2) Unrooted tree for the four phyla, Cnidaria, Arthropoda, Chordata, Ctenophora, in which homologues of GFP were found. Cnidaria phylum groups the two biggest classes, Anthozoa and Hydrozoa.

The biological function of fluorescent proteins remains unclear. It is possible that the GFP function is not necessarily associated with light emission, since non-fluorescent GFP homologues have been described in Hydrozoa and Anthozoa (Alieva et al., 2008; Gurskaya et al., 2003). Several authors proposed different hypotheses to explain the biological function of FPs, based on experimental evidences that are not completely accepted. Alieva et al have reported an evolutionary study using 40 different fluorescent proteins from reef corals (class Anthozoa) (Alieva et al., 2008). Based on a probabilistic sampling approach, they proposed that FPs play a biological role in the context of a symbiosis with other marine organisms, for example a **photoprotection** role (Field et al., 2006). An alternative explanation was given by Agmon and co-authors (Shinobu et al., 2010). They have published the high-resolution GFP

structure at 0.9 Å, where they have identified several proton wires including a proton-collecting apparatus. In their view, GFP works as a **proton pump** capable of direct light conversion into proton gradients. Lukyanov and co-authors (Bogdanov et al., 2009) have also suggested a biological function of GFPs. Upon 488 nm illumination in the presence of electron acceptors, GFP undergoes green-to-red photo conversion through a two-electron oxidation process. Based on oxidative redding of GFPs from diverse species, they suggested that the function of GFP is to induce a **light-driven electron transfer**. The three hypotheses described above are only some of the possibilities for the biological function of FPs. In addition, the possibility that FPs may act in more than only one biological role in nature is not excluded.

1.1.2 FLUORESCENT PROTEINS IN SCIENCE

It is thanks to its scientific applications that FPs won their important reputation. The Nobel prize of Chemistry was awarded to Osamu Shimomura, Martin Chalfie and Roger Tsien in 2008 (Nobelprize.org, 2008) for the discovery and development of GFP and its variants (**Figure 1.3**). These proteins then quickly became widely used markers that allow the spatio-temporal tracking of the dynamic behavior of living systems at the molecular level (Ehrenberg, 2008).

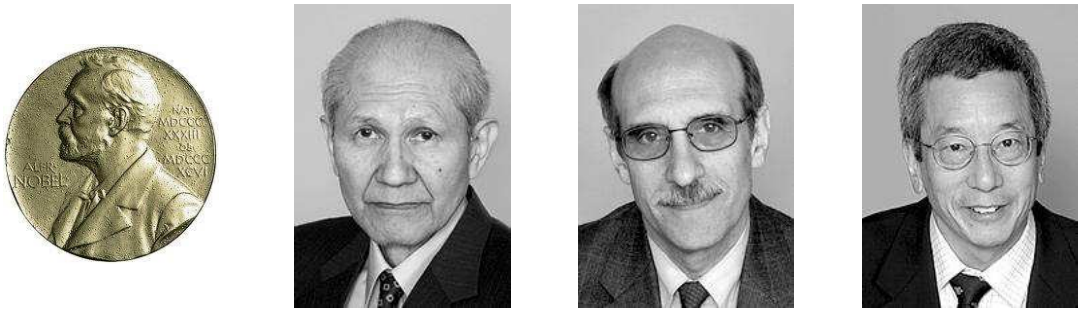

Figure 1.3) The Nobel Prize in Chemistry 2008: Osamu Shimomura, Martin Chalfie, Roger Y. Tsien

The wide rainbow of FP biosensors offers the possibility to perform **multicolor imaging experiments** (Livet et al., 2007) and to develop pairs of dyes suitable for studies based on Föster resonance energy transfer (**FRET**) (Chudakov et al., 2010). The development of red fluorescent proteins (RFP), triggered by the discovery of homologues GFP from Anthozoa, was an important improvement for applications in **imaging living cells and tissues** that require low spectral activity in UV-to-green spectral region (Subach et al., 2011a). The fluorescent proteins from Anthozoa also provide more sophisticated imaging techniques through the development of Photo-Transformable Fluorescent Proteins (PTFPs), which possess the advantage to display spectral properties that can be modulated by actinic illumination. Within the PTFPs group, photo-activatable fluorescent proteins (PAFPs) and photo-convertible fluorescent proteins (PCFPs) are particularly useful to achieve single molecule localization-based super resolution microscopy and to probe dynamic cellular events in living cells via pulse-chase imaging. For example, performing powerful variants of the fluorescence recovery after photobleaching techniques (**FRAP**). In this thesis, we have studied the photo-switchable fluorescent proteins (RSFPs). These proteins can switch between a fluorescent and a non-fluorescent form repeatedly. RSFPs are promising nano-devices for the development of **rewritable data storage** (Grotjohann et al., 2011). Moreover, they allow photochromic FRET and facilitate **super-resolution microscopy techniques**, such powerful variants of stimulated emission depletion (**STED**) microscopy (Hell and Wichmann, 1994; Klar et al., 2000; Willig et al., 2011) and structured illumination microscopy (**SIM**) (Rego et al., 2012). Further details about these RSFP's applications are described later in the text (see subchapter 1.4).

1.2 HOW DO FLUORESCENT PROTEINS WORK?

1.2.1 CHROMOPHORE FORMATION

The molecular structure of GFP is constituted of 230 amino acids, which adopt a secondary structure essentially made of β-strands that fold into a nearly cylindrical β-barrel, with 4.2 nm and 2.4 nm dimensions (Tsien, 1998) (Figure 1.1). Concomitantly with protein folding, a series of chemical reactions called maturation generate the chromophore that will be buried in the middle of the central helix and formed from the combination of three amino acids residues, **Ser65-Tyr66-Gly67** (**Figure 1.4**).

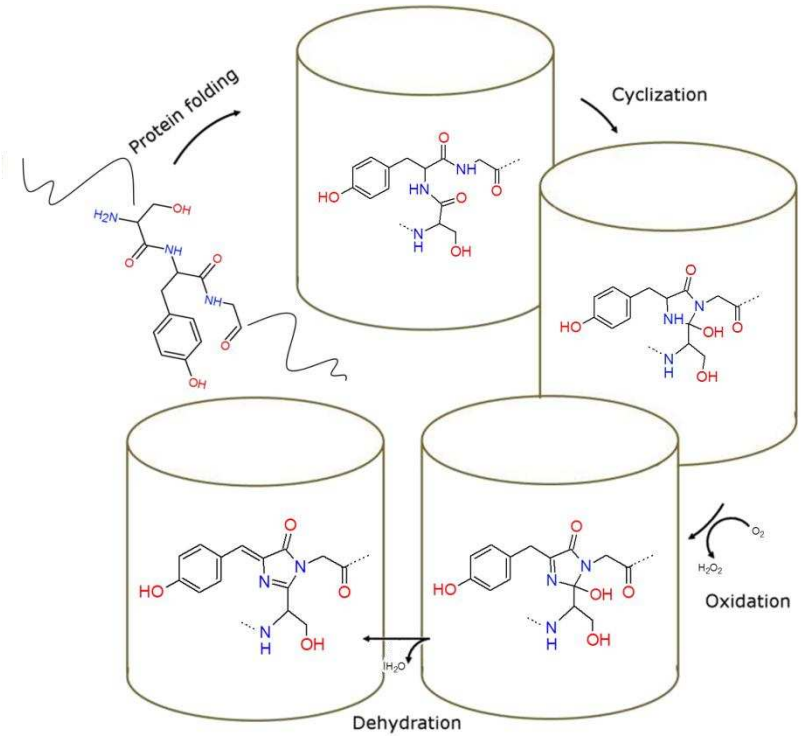

Figure 1.4) Schematic diagram of the autocatalytic process of formation of the chromophore from the amino acids Ser65-Tyr66-Gly67 in the GFP (Zhang et al., 2006).

The maturation of the chromophore is an autocatalytic process, where in the first step the **cyclization** of Gly and Ser is favored by the confinement inside of the β-barrel. Kinetic studies of hydrogen peroxide release, combined with mass spectroscopy analysis, have revealed that the second and limiting step during in vitro GFP maturation is an **oxidation** step

(Zhang et al., 2006). The hydrogen peroxide is the product of the oxidation reaction that requires molecular oxygen to occur. During oxidation, a hydroxylated cyclic imine is formed (Pouwels et al., 2008). Finally, **dehydration** converts the imine to the double-bonded imidazolinone ring yielding the fully conjugated mature chromophore. This step of reaction is probably assisted by the nature of Tyr66, since the mutation of this residue does not interfere with the cyclization or oxidation steps, but only with the dehydration (Zhang et al., 2006).

The maturation of the chromophore is a common process between all fluorescent proteins that may vary from hours to a few days depending on FP. Indeed, depending on the group of proteins other steps occur, as Verkhusha and other authors have demonstrated recently (Bravaya et al., 2012). In particular, they have shown that red-variants of fluorescent proteins, such as DsRed, TagRFP, fluorescent timers and PAmCherry, pass by a blue anionic intermediate structure, through a single oxidation step, before the mature chromophore is formed.

Once synthesized, the mature chromophore is relatively well shielded from the environment by the β-barrel. It is stabilized by a complex network of electrostatic, H-bonding, van der Waals or stacking interactions with its surrounding residues. This stabilization of the chromophore is strongly responsible for the high fluorescence emission. Due to this, the chromophoric moiety in the absence of the β-barrel does not fluoresce under normal conditions (Niwa et al., 1996). Similarly, the denaturation product of fluorescent proteins is not fluorescent although FPs recover their fluorescence when they refold (Ward and Bokman, 1982).

Several residues have a central importance in both the maturation process and the ability to fluoresce. In the chromophore triad, only the amino-acid Gly67 is essential to ensure maturation. Tyr66 can be mutated to a tryptophan or to a histidine, giving origin to two other

fluorescent proteins, the cyan variant (CFP) and the blue variant (BFP) (Tsien, 1998). The GFP brightness is improved ≈ 10 times upon excitation at 488 nm, when Ser65 is mutated into a threonine (Heim et al., 1995). The F64L is known to improve the folding efficiency, which is advantageous for living cell experiments (Cormack et al., 1996). The S65T and/or F64L mutations in the fluorescent proteins from Aequorea victoria (**AFP**s) yields the **enhanced fluorescent proteins** (eGFP, eBFP, eCFP and eYFP). Other residues are fundamental in changing the behavior of GFP, such as E222 and S205 and their roles will be described later in the text.

1.2.2 SPECTROSCOPIC BEHAVIOR OF GFPS

The GFP absorption spectrum is constituted of two broad bands: one band with a maximum at ~ 398 nm and another with a maximum at ~ 478 nm (Heim et al., 1994, 1995; Tsien, 1998). At physiological pH, the ratio between these bands is six to one. The 398 nm band is associated to the protonated form of the chromophore (**A form**). The 478 nm band is associated with the anionic form of chromophore (**B form**). The chromophore in its anionic conformation is highly fluorescent. It exhibits a strong emission peak at 503 nm. The protonated chromophore is intrinsically weakly fluorescent. However, when it is excited near its absorption maximum, it exhibits an emission peak close to the B fluorescence peak (Heim et al., 1994).

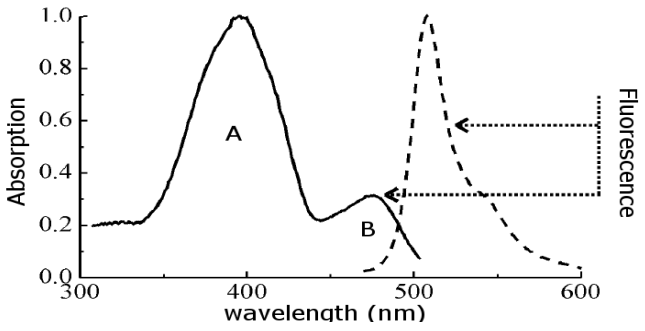

Figure 1.5) Spectroscopic behavior of GFP (Tsien, 1998).

1.2.3 EXCITED STATE PROTON TRANSFER (ESPT)

Boxer and co-worker in 1996 were the first to explain why excitation of the protonated band produces a fluorescence emission similar to that of the anionic band (Chattoraj et al., 1996). Their hypotheses are based on the analysis of steady-state absorbance and fluorescence emission spectra and also on ultrafast time-resolved fluorescence excitation with and without deuterium isotopic labeling at low temperatures. The phenomenon is being caused by a proton transfer occurring in the excited state (**ESPT**) between the hydroxybenzylidene moiety of the chromophore and the nearby H-bond network, leaving the chromophore in an anionic intermediate I state which is structurally close to A and spectroscopically close to B (Fang et al., 2009) (**Figure 1.6**).

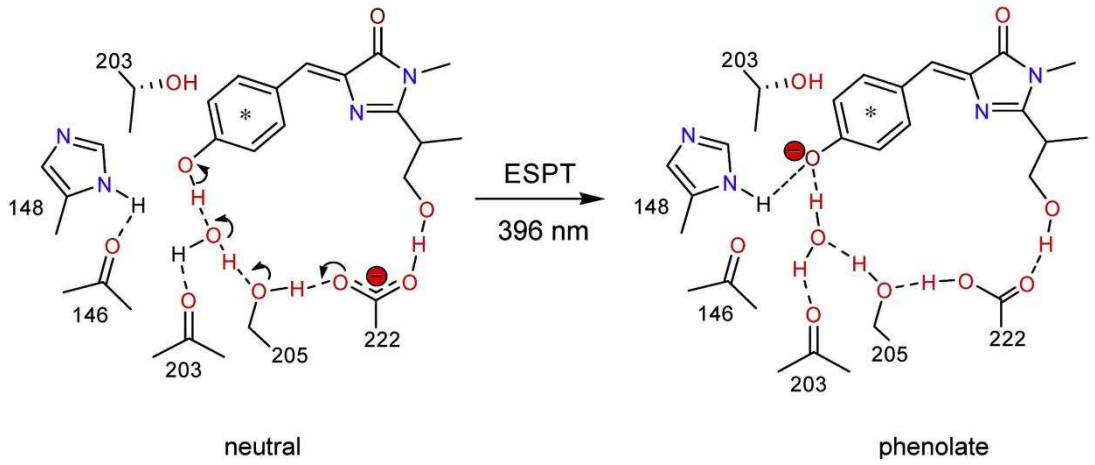

Figure 1.6) Excited state proton transfer between hydroxybenzylidene moiety of the chromophore and the nearby H-bond network in the GFP.

This first mention of ESPT was done without knowing the precise molecular structure of GFP. Some months later, two different teams published the first molecular structure of GFP (Ormo, 1996; Yang et al., 1996). Together with the GFP structure, the Tsien group also introduced a yellow variant of eGFP, called **eYFP** (Ormo, 1996) .

1.3 REVERSIBLE PHOTOSWITCHING OVER THE YEARS

1.3.1 PHOTOSWITCHING AT THE SINGLE MOLECULES LEVEL

The first time that the reversible photoswitching of a fluorescent protein was described in the literature was through single molecules experiments on YFP, done by Dickson et al in 1997 (Dickson et al., 1997). At physiological pH, the YFP absorption spectrum displays only a deprotonated band at 514 nm corresponding to the anionic chromophore (B form). The YFP[a] differs from GFP by three amino acid residues S65G/T203Y/S72A (**Figure 1.7**). The highly polarizable phenol of Tyr203 assumes an almost coplanar π–π stacking with the chromophore allowing a red shift of ≈ 20 nm of the fluorescence emission (λ_{em} = 527 nm) (Wachter et al., 1998).

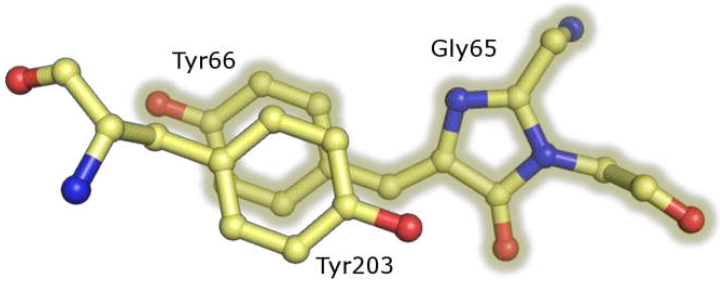

Figure 1.7) Chromophore of YFP (PDB: 1YFP) (Wachter et al., 1998).

Dickson et al. showed that single immobilized YFP proteins are light-driven to a long-lived non-fluorescent state (off-state) after long exposure (~10^6 photons) at 488 nm. The protein can recover its emission (on-state) after some minutes in the dark, or upon illumination at 405 nm. This means that, at the single molecule level, the on-off switching cycles can be repeated in a controlled way by alternation of illumination with 488 nm and

[a] YFP used in Dickson (Dickson et al., 1997) et al is a variant of the YFP 10C described in Wachter et al (Wachter et al., 1998) with an extra mutation V68L.

405 nm light. The photoswitching was also demonstrated for the variant S65G/S72A/T203F (denoted T203F) of GFP, but it exhibits a less efficient activation/inactivation of the fluorescence than YFP (Dickson et al., 1997).

In this work the authors discuss the blinking: another process that also involves the reversible transformation from a fluorescent state to the non-fluorescent state. In contrast to the photoswitching, photoblinking is the stochastic fluctuation of the fluorescence, is essentially uncontrolled, and takes place on a much faster timescale than the switching. Blinking can be observed upon continuous illumination with a single wavelength, reminiscent of spectral and amplitude fluctuation, noticed also in other fluorophores, at the single molecule level (Lu and Xie, 1997).

1.3.2 PHOTOSWITCHING AT ENSEMBLES OF MOLECULES LEVEL

i. Photoswitching at low and ultra-low temperature

On and off photoswitching in fluorescent proteins at the ensemble level was observed at ultra-low temperature on GFP and some red-shifted derivatives, using hole-burning spectroscopy (Creemers et al., 1999, 2000; Creemers, TM H Lock et al., 2002). Many of the thermally induced conversions are blocked at low temperature and, therefore, discrimination amongst individual species is facilitated (Creemers et al., 2000). The structured spectra obtained at low temperature allow to identify the protonated (A), the anionic (B) and the intermediate (I) states and to propose the pathway of photo-conversion between them.

The intermediate state I between B and A states, proposed to explain the ESPT, was first observed for GFP. It was also found in the photo-mechanism of red-shifted derivatives: RS-GFP (F64M, S65G and Q69L) and YFP (S65G, V68L, S72A and T203Y). Summarizing,

the authors suggest that illumination at the anionic excitation peak (≈ 488 nm) can excite the B and I forms. When excited, B can fluoresce or eventually be converted to the I state. In turn, if the I state is excited it can fluoresce or be converted to the B or A forms. At wavelengths less than the protonated excitation peak maximum (≈ 446 nm), the A state can be exited to fluoresce or be re-converted to the I form. The reaction can be described by:

$$A \underset{k_{-1}}{\overset{k_1}{\rightleftharpoons}} I \underset{k_{-2}}{\overset{k_2}{\rightleftharpoons}} B$$

As shown in **Figure 1.7,** RS-GFP[b] exhibits an excitation peak at 495 nm (blue line) and an emission peak at 503 nm (red line). These bands are ascribed to the intermediate state I due to its spectroscopic similarities with that of GFP. Upon illumination at 495 nm, we observe the intermediate state reduction with concomitantly an increase of the B and A states and a reduction of the fluorescence (**Figure 1.8a**). Upon illumination at 434 nm, the A-peak decreases whereas the I-peak increases (not shown). Subsequent illumination into I increases the population of A again (**Figure 1.8b**).

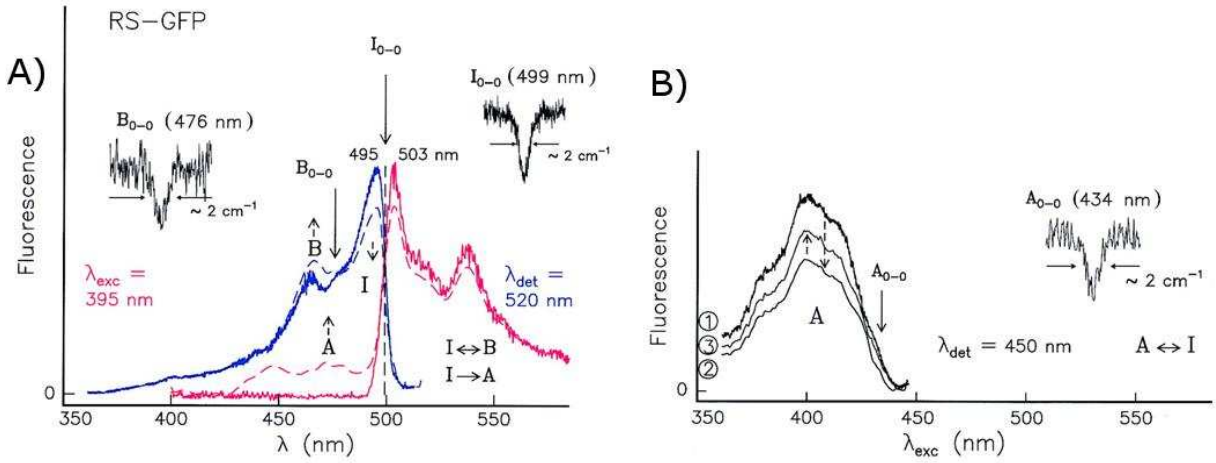

Figure 1.8) Scheme of RS-GFP model at 1.6 K. Reprinted from (Creemers, TM H Lock et al., 2002). (**A**) Interconversion from I to A and B upon illumination 495 nm with concomitantly reduction of fluorescence. (**B**) Decrease of the A band upon illumination 434 nm and subsequent increase upon illumination at 495 nm.

[b] In the paper Creemers and co-authors have described RS-GFP as Red Shifted-GFP (Delagrave et al., 1995), not to be confounded with rs-GFP published recently (Grotjohann et al., 2011).

The approach based on low temperature spectroscopy, used to decipher the reaction pathway in these works (Creemers et al., 1999, 2000; Creemers, TM H Lock et al., 2002), is close with the approach that will be used in the Results chapter of this Thesis (see Chapters 2.1 and 2.2).

ii. Partial photoswitching at room temperature

Miyawaki and Tsien have observed that in cells expressing eYFP and in pure protein solutions after bleaching at 540 nm, it is possible to recover partially the fluorescence. About 20% of the initial fluorescence is retrieved by illuminating at 340 nm at room temperature (Miyawaki and Tsien, 2000). Furthermore, the recovery can be induced by thermal relaxation, as well as by actinic illumination. However, in these bulk experiments, photoswitching is not induced with the same illumination scheme as in single-molecule experiments. Surprisingly, illumination at 405 nm does not recover the fluorescence, in contrast, it induces further decay (McAnaney et al., 2005; Sinnecker et al., 2005).

Based on stopped-flow, pressure-jump and time-resolved experiments, McAnaney et al. have detailed the kinetics of protonation, photobleaching and photoactivation in YFP 10C (McAnaney et al., 2005). At room temperature, they observed only a weak recovery of the fluorescence, similar to the observation by Miyawaki and Tsien (Miyawaki and Tsien, 2000). They described two absorption peaks at 340/460 nm that would be responsible for fluorescence recovery after illumination, and differ from the protonated peak at 390 nm. In the same year, another observation of photo-switching upon illumination at various wavelengths of samples of eYFP, citrine, CFP and GFP, was described in Sinnecker et al. They showed that a dynamical equilibrium between a reversibly and a non-reversibly photo-bleached population is established after prolonged exposure followed by thermal relaxation (Sinnecker et al., 2005).

The common feature of all these processes is the fact that photoswitching in these GFP derivatives is only weakly reversible, 10 – 40% depending on the experimental conditions. A possible interpretation for these results would be the presence of non-interchangeable populations in the photo-pathway of these proteins: one reversibly photoswitchable and the other not. For example, a first anionic fluorescent state, B_1, could undergo reversible switching to a weak or non-fluorescent state A, and concomitantly another B_2 anionic state would only be able to undergo irreversible bleaching to a dark state, D.

$$A \underset{k_{-1}}{\overset{k_1}{\rightleftharpoons}} B_1 \qquad B_2 \xrightarrow{k_2} D$$

The structural mechanisms that could be responsible for these effects are not clear. In all cases, protonation of the chromophore can be observed by inspecting the absorption spectrum. However, the sole protonation cannot explain the long-lived dark state, and this process needs to couple to at least a minimal structural rearrangement (McAnaney et al., 2005). Isomerization of the chromophore has been hypothesized as being the responsible structural rearrangement causing this effect (Weber et al., 1999; Nifosı et al., 2003). Although Raman results have showed spectroscopic signatures suggesting such cis-trans isomerization in other variants of YFP (EYQ1) (Luin et al., 2009), further evidence is missing to understand the partial photo-switching. To date, for AFPs, there are no structural results showing isomerization of the chromophore (trans conformation). It is, however, a common consensus that the matrix of the chromophore should play a fundamental role in switching mechanisms (Follenius-Wund et al., 2003; Maddalo and Zimmer, 2006; Fang et al., 2009).

1.3.3 DISCOVERY OF THE FLUORESCENT PROTEINS FROM CORALS

In 1999 Lukyanov and co-authors announced the discovery of GFP homologues isolated from reef corals (Matz et al., 1999). Although these proteins display a β-barrel tertiary structure similar to GFP, the new chromophore and amino acid interactions not only extend the existing FP color palette, but also reveal unprecedented photo-physical properties (Lukyanov et al., 2000). These new fluorescent proteins are "photo-transformable" (PTFPs): proper actinic illumination can modulate their fluorescence behavior. This property introduces unique possibilities for precision labeling and tracking of objects of interest in living systems, enhancement of signal-to-noise ratio, and, most importantly, super-resolution fluorescence imaging (Chudakov et al., 2010). Because of these unprecedented developments, anthozoan PTFPs led to a second revolution in the FP field. They can be classified in three groups: Photo-Activatable Fluorescent Proteins (PAFPs) and Photo-Convertible (PCFPs) exhibit non-reversible photo-transformations, whereas **Photo-Switchable Fluorescent Proteins (RSFPs),** our objet of study, display reversible photoswitching between a fluorescent on state and a non-fluorescent off state.

i. Photo-Activatable FPs (PAFPs)

Photo-Activatable FPs are initially in a non-fluorescent state and are transformed into a fluorescent state upon actinic illumination with violet light (405 nm). The FPs belonging to this group are: PAmRFP1 (Verkhusha and Sorkin, 2005), PA-GFP[c] (Patterson and Lippincott-Schwartz, 2002), PA-mCherry (Subach et al., 2010a), PS-CFP, PS-CFP2 (Chudakov et al., 2004), and PA-TagRFP (Subach et al., 2010b). Typically, PAFPs, before illumination, are in a protonated state and are converted to an anionic state upon relatively strong UV- illumination.

[c] PA-GFP is a variant of the WT-GFP cloned from hydrozoan.

Attenuated photochromatic behavior is also observed in WT-GFP and it is potentialized in PA-GFP with the T203H substitution, that affects the side chain conformation of Glu222 (**Figure 1.9**). Glu222 is rotated away from His203 and occupies a slightly different position than that in WT (Henderson et al., 2009). Both mass spectroscopy and crystallographic data suggest that photo-activation in PA-GFP is caused by oxidative decarboxylation of E222 driven by high-energy UV light (Henderson et al., 2009). This is followed by a reorganization of a H-bond network, resulting in favoring the anionic state of the chromophore. A similar decarboxylation reaction is observed in PA-mCherry (Subach et al., 2010a), and in PS-CFPs (Chudakov et al., 2004). The relative efficiencies of decarboxylation are explained in terms of the Kolbe-type mechanism in which the excited state of the chromophore acts as an oxidant by accepting an electron from E222 (Bell et al., 2003). Thanks to their ability to be irreversibly activated, PAFPs are appropriate for tracking experiments in the cell (Chudakov et al., 2010).

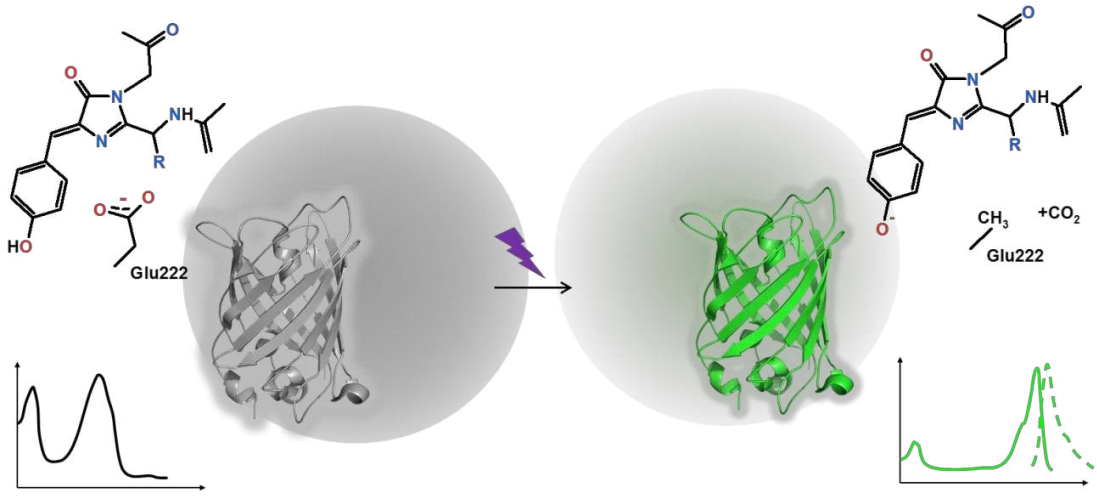

Figure 1.9) Photo-Activatable FPs (PAFPs). Irreversible photo-transformation from the non-fluorescent protonated state to the fluorescent anionic state of chromophore based on oxidative decarboxylation of Glu222 upon illumination with high-energy UV light. Representative spectra of this class are based on PA-GFP photo-activation, excitation (solid lines) and emission (dashed lines).

ii. Photo-Convertible FPs

Photo-Convertible FPs are initially in a first, typically green, fluorescent state and upon actinic illumination are irreversibly converted to another state, typically red, fluorescent state (**Figure 1.10**).

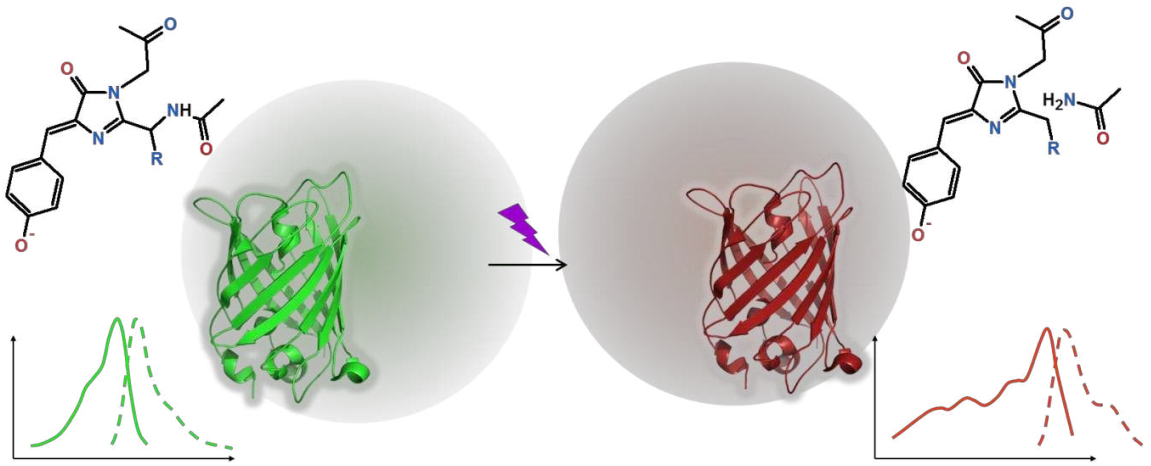

Figure 1.10) Photo-Convertible FPs (PCFPs). Irreversible photo-transformation from the green fluorescent anionic state to the red fluorescent anionic state of chromophore based on backbone cleavage, via a β-elimination reaction, between Nα and Cα of His62 upon illumination with high-energy UV light. Representative spectra of this class are based on Kaede photo-conversion, excitation (solid lines) and emission (dashed lines).

The FPs belonging to this group are: Kaede (Matz et al., 1999), EosFP (Wiedenmann et al., 2004), mEosFP (Gurskaya et al., 2006), mEos2 (Mckinney et al., 2009), KikGR (Tsutsui et al., 2005), Dendra2 (Gurskaya et al., 2006), IrisFP (Adam et al., 2008, 2011), Niji[d] (Adam et al., 2011), PSmOrange (Subach et al., 2011b). Kaede was the first fluorescent protein to exhibit this green to red photo-conversion property upon illumination with UV-violet light (Matz et al., 1999). To date the conversion was observed typically from green to red, but it was observed also from cyan to green (PS-CFP2) (Evrogen, 2007). The mechanism

[d] Iris and Niji FPs are a special characteristic to posses both photo-conversion and photoswitching behavior (Adam et al., 2008, 2011).

accounting for photo-conversion is based on protein backbone cleavage, via a β-elimination reaction, between Nα and Cα of His62 (Mizuno et al., 2003; Wiedenmann and Nienhaus, 2006; Lelimousin et al., 2009), that follows from photon absorption in the protonated state of the chromophore. This irreversible peptide cleavage results in a subsequent extension of the chromophoric conjugated electron system, inducing a red-shifted emission peak.

iii. Reversibly-Photoswitchable Fluorescent Proteins (RSFPs)

Reversibly-Photoswitchable Fluorescent Proteins (RSFPs) are initially in a fluorescent/non-fluorescent state, and upon illumination they are reversibly switched to a non-fluorescent/fluorescent state. The FPs belonging to this group and some of their photo-physical properties are shown in **Table 1.1**.

RSFPs that switch to the non-fluorescent state upon illumination in the absorbance band of the fluorescent state are called "**negatively switchable**": they show a decrease of fluorescence upon excitation. Dronpa is the most well-known representative of this subclass. In contrast, RSFPs that switch to the fluorescent state upon illumination in the absorbance band of the fluorescent state are called "**positively switchable**": they show an increase of fluorescence upon excitation. Well-known members of this subclass are asFP595 and Padron. RSFPs have representative proteins in both Hydrozoan and Anthozoan classes.

Several molecular structures have suggested that the structural mechanism accounting for the photoswitching is a cis-trans isomerization of the chromophore. Spectroscopically, photoswitching manifests itself by a light induced interconversion between the anionic and the protonated absorption bands. However, recently, a completely different mechanism than coupled chromophore isomerization and protonation was observed for a new RSFP, named Dreiklang. In the following, we detail further each RSFP sub-class by reviewing asFP595 and Dronpa.

Table 1.1) Properties of principal RSFPs developed to date.

Protein	(Class) - *Source organism*	Chr. triad	Struct. (*on*)	Strct. (*off*)	λexc/λem	ε ($M^{-1}cm^{-1}$)	Φ_{fluo}	pKa	Φ_{sw} (*on*→*off*)	Φ_{sw} (*off*→*on*)	Actinic Ligh	Ref
Negative swicthing												
mTFP0.7	(A) - *Clavularia sp.*	AYG	2OTB	2OTE	453 / 488	60 000	0.50	4.0	ND	ND	458/405	1
Dronpa	(A) - *Echinophy sp.*	CYG	2Z6Z †	2POX	503 / 517	94 100	0.67	5.3	3.0×10^{-4}	7.0×10^{-1}	458/405	2
rsFastLime	(A) - *Echinophy sp.*	CYG	ND	ND	496 / 518	39 094	0.77	ND	ND	ND	458/405	3
bsDronpa	(A) - *Echinophy sp.*	CYG	ND	ND	460 / 504	45 000	0.50	ND	ND	ND	458/405	4
mEosFP *	(A) - *L. Hemprichii*	HYG	ND	ND	487 / 512	98 600	0.52	4.3	2.6×10^{-3}	1.5×10^{-1}	458/405	5
Iris	(A) - *L. Hemprichii*	HYG	2VVH	2VVI	488 / 516	57 800	0.48	5.7	3.2×10^{-3}	1.5×10^{-1}	458/405	6
mIrisFP	(A) - *L. Hemprichii*	HYG	ND	ND	486 / 516	74 000	0.60	5.7	2.2×10^{-3}	1.5×10^{-1}	458/405	7
NijiFP	(A) - *Dendronephthya sp.*	HYG	ND	ND	469 / 507	41 100	0.64	7.0	1.8×10^{-3}	1.5×10^{-1}	458/405	8
Drenda2 *	(A) - *Dendronephthya sp.*	HYG	ND	ND	471 / 504	51 100	0.55	6.5	1.1×10^{-3}	8.0×10^{-2}	458/405	9
Mut2q	(H) - *A. victoria*	AYG	ND	ND	496 / 507	54 000	0.28	6.0	4.7×10^{-3}	2.6×10^{-2}	478/405	10
rsGFP	(H) - *A. victoria*	TYG	ND	ND	493 / 510	47 000	0.36	6.5	ND	ND	458/405	11
EYQ1	(H) - *A. victoria*	SYG	ND%	ND	510 / 524	73 000	0.72	6.9	1.8×10^{-4}	6.0×10^{-2}	514/405	12
rsCherryRes	(A) - *Dicosoma sp.*	MYG	ND	ND	572 / 608	84 000	0.01	5.5	ND	ND	550/450	13
rsTagRFP	(A) - *E. quadricolor*	MYG	3U8C	3U8A	567 / 585	36 800	0.11	6.6	ND	ND	570/445	14
Iris	(A) - *L. Hemprichii*	HYG	2VVJ	ND	551 / 580	27 000	0.50	6.8	2.0×10^{-3}	5.0×10^{-2}	561/440	15
mIrisFP	(A) - *L. Hemprichii*	HYG	ND	ND	546 / 578	26 000	0.44	7.0	4.0×10^{-4}	1.5×10^{-1}	561/440	16
NijiFP	(A) - *Dendronephthya sp.*	HYG	ND	ND	526 / 569	42 000	0.65	7.3	1.0×10^{-3}	1.5×10^{-1}	561/440	17
Drenda2 *	(A) - *Dendronephthya sp.*	HYG	ND	ND	528 / 562	45 000	0.75	6.8	3.2×10^{-3}	1.0×10^{-2}	561/440	18
Positive swicthing												
Padron	(A) - *Echinophyllia sp.*	CYG	3LS3	3LSA	503 / 522	43 000	0.64	ND	ND	ND	405/488	19
rsCherry	(A) - *Dicosoma sp.*	MYG	ND	ND	572 / 610	80 000	0.02	6.0	ND	ND	450/550	20
asFP595	(A) - *A. sulcata*	MYG	2A56‡	2A53	572 / 595	56 200	0.001	ND	ND	ND	450/568	21
KFP1	(A) - *A. sulcata*	MYG	ND	ND	590 / 600	59 000	0.07	ND	ND	ND	458/532	22
Decoupled swicthing												
Dreiklang	(H) - *A. victoria*	GYG	3ST4 (2)	3ST3	511 / 529	83 000	0.41	7.2	ND	ND	405/365	23

*mutation M159A; †other structures of Dronpa: 2IVO, 2IE2, 2GXO, 2GX2, 2POX, 2Z1O, 2Z6X, 2Z6Z; ‡other structures of asFP595: 2A50, 2A52, 2A53; %not deposited in PDB (see Material and Methods Chapter 4.5.4). Chromophore triad (Chr. triad), excitation and emission wavelengths (λexc/λem), extinction coefficient (ε), fluorescence quantum yield (Φfluo), photoswitching quantum yield (Φsw), References (Ref): (1) (Henderson et al., 2007); (2) (Ando et al., 2004; Andresen et al., 2007); (3, 4) (Stiel et al., 2007); (5, 7, 8, 9, 16, 17, 18) (Adam et al., 2011); (6, 15) (Adam et al., 2008); (7)(Fuchs et al., 2010); (10, 12) (Bizzarri et al., 2010); (11) (Grotjohann et al., 2011); (13, 20) (Bogdanov et al., 2009); (14) (Subach et al., 2010c); (19) (Brakemann et al., 2010); (21) (Lukyanov et al., 2000); (22) (Chudakov et al., 2003a); (23) (Brakemann et al., 2011).

1.3.4 POSITIVE PHOTOSWITCHING: ASFP595

The fluorescent protein asFP595 from Anemonia sulcata was discovered in 2000, in the course of investigations to find homologues of GFP in organisms other than Hydrozoans (Lukyanov et al., 2000; Andresen et al., 2005). Amongst the fluorescent proteins from reef corals, asFP595 was the first observed to exhibit reversible photoswitching (Chudakov et al., 2003b). Upon actinic illumination at 568 nm, asFP595 was observed to dramatically increase its fluorescence (Chudakov et al., 2003b). Due to this property it was called a "kindling

fluorescent protein" (**Figure 1.11**). The kindling phenomenon can be slowly reversed by thermal relaxation or instantly by irradiation with blue-light (Chudakov et al., 2003b).

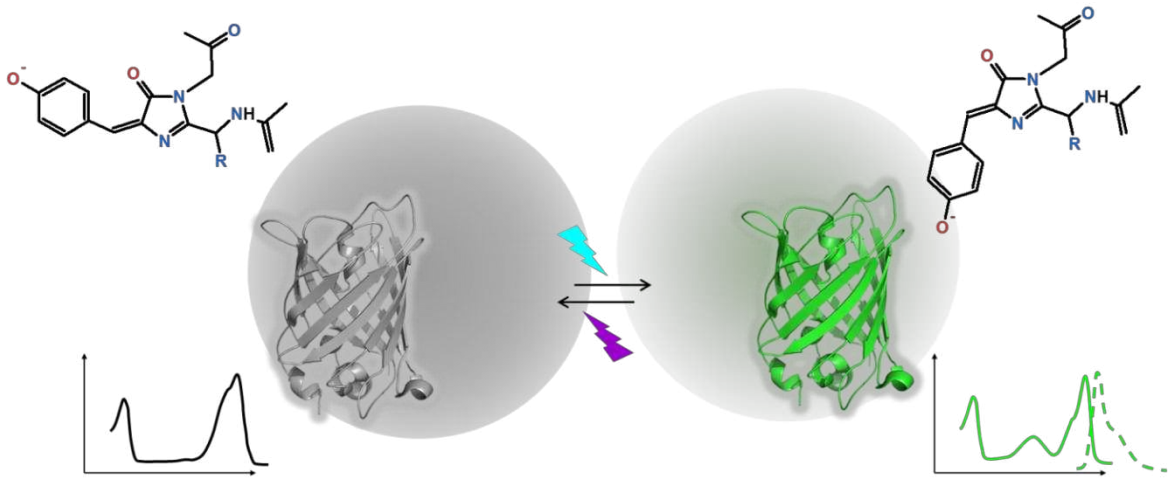

Figure 1.11) Positively photo-switchable FPs. Reversible photo-transformation from the non-fluorescent state to the fluorescent state of chromophore based on trans-cis isomerization of the chromophore upon illumination at 488 nm to switch on and at 405 nm to switch off. Representative spectra of this class are based on Padron photo-switching, excitation (solid lines) and emission (dashed lines).

The first application in fluorescence microscopy taking advantage of reversible switching employed asFP595 to introduce a point-scanning technique relatively similar to STED, and called RESOLFT (REversible Saturable Optical Linear Fluorescence Transitions) (Hofmann et al., 2005). However, asFP595 has a very weak fluorescence quantum yield (<0.001) and it is an obligate tetramer, which considerably limits its practical use for biological applications.

AsFP595 has been subjected to a number of mechanistic investigations. Like for AFPs, a cis-trans isomerization of the chromophore was soon proposed to account for kindling and back-relaxation to the dark state. The cis (fluorescent) to trans (non-fluorescent) isomerization of the chromophore was confirmed by X-ray crystallography for the wild-type

asFP595, as well for the variants asFP595-S158V (Andresen et al., 2005) and asFP595-A143S (designated KFP) (Andresen et al., 2005; Quillin et al., 2005; Wilmann et al., 2005). The single mutation A143S confers to the protein a long-lived bright state and an enhancement of the fluorescence quantum yield, likely because the side chain of Ser143 stabilizes the cis conformation of the chromophore (Quillin et al., 2005).

Based on molecular dynamics calculations, a Hula-Twist motion was suggested as the isomerization mechanism (Andresen et al., 2005). Unfavorable steric clashes were predicted for simple one-bond rotations of the chromophore (Quillin et al., 2005). Contrary to negative RSFPs, only very limited rearrangements of the chromophore pocket were noticed between the trans and the cis configurations, consistent with the observation of kindling at 150 K, below the glass transition temperature of solvent (Schüttrigkeit, 2006).

Schäfer and co-authors have studied how the chromophore protonation state controls photoswitching in asFP595 by performing ab initio calculations and QC/MM molecular dynamics simulations (Schäfer et al., 2007, 2008). It was suggested that cis-trans isomerization occurs in the neutral state of the chromophore, followed by a dark state equilibration to a zwitterionic fluorescent cis state (Schäfer et al., 2008). However, this study did not rule out the possibility that the chromophore may also photo-isomerize in its anionic state.

Other fluorescent proteins exhibit positive photoswitching, for example rsCherry and Padron. RsCherry (and its negative-switching counterpart rsCherryRev) was rationally engineered from the known structure of mCherry (Stiel et al., 2008). It emits at 610 nm and can be switched on/off using blue/yellow illumination, respectively. In contrast with asFP595, rsCherry is monomeric, extending possible applications using red-RSFPs.

i. Padron

Padron was introduced by Andresen et al. in 2008 as being the positive switching counterpart of Dronpa (Andresen et al., 2008). Padron was generated by site-directed saturation mutagenesis of rsFastLime (Dronpa: Val157Gly) at eight positions. Notably, the sole exchange of the Met residue at the position 159 to a Tyr residue is sufficient to confer the positive switching mechanism (Andresen et al., 2008). The scientific interest of this protein stems from the fact that, together with Dronpa, Padron allows the implementation of, multi-label far-field fluorescence nanoscopy (Andresen et al., 2008; Willig et al., 2011). Recently, dual-label monochromatic STED nanoscopy of living cells using Padron and Dronpa reached ~ 70 nm (Padron) and ~ 90 nm (Dronpa) spatial resolution (Willig et al., 2011). The positive photoswitching mechanism of Padron will be extensively studied in the Results Chapter, leading to the central results of this thesis work (see Results and Discussion Chapter 2.2).

1.3.5 NEGATIVE PHOTOSWITCHING: DRONPA

Dronpa is a mutant of fluorescent protein cloned from a coral Pectiniidae. This RSFPs satisfies most requirements for being a suitable dye for imaging applications: it is monomeric, displays a high fluorescence quantum yield (0.67 compared to 0.001 for asFP595), has a high extinction coefficient (94100 $cm^{-1}M^{-1}$ versus 56200 $cm^{-1}M^{-1}$ for asFP595), exhibits a good on-off contrast of the fluorescence (≈ 80%) and shows a moderate photoswitching quantum yield of 10^{-4} [e] (Habuchi et al., 2005). The ensemble of studies carried out with Dronpa forms the basis of our present knowledge of the RSFP's mechanisms (Bourgeois and Adam, 2012).

[e] Photoswitching from on-state to off-state

The absorption spectrum of Dronpa displays a predominant peak at 503 nm at high pH conditions (> 7.5). This peak (called B) is associated to the anionic form of the chromophore. pH titration converts the B peak to a peak at 388 nm (called A) corresponding to the protonated form of the chromophore, while the protein passes from a fluorescent (λ_{em} = 503 nm) to a non-fluorescent state (Ando et al., 2004; Habuchi et al., 2005). Similarly, upon illumination of the anionic absorption band, we observe a decrease of this band, concomitantly with an increase of the protonated band. Dronpa photoswitches from a fluorescent (on-state) to a non-fluorescent state (off-state), obeying the principle of negative-switching (Ando et al., 2004; Habuchi et al., 2005). Thermal relaxation ($t_{1/2}$) occurs in about 840 minutes (Stiel et al., 2007). However, fluorescence emission can be quickly recovered by illuminating the protonated band (**Figure 1.12**). Evidence of ESPT in back-switching has been demonstrated by ultra-fast absorption spectroscopy (Fron et al., 2007). Furthermore, the existence of an intermediate state along the back switching pathway has been proposed (Habuchi et al., 2005; Fron et al., 2007). The photoswitching of Dronpa at the single-molecule level is fast, easy to detect, and in accord with observations in bulk solutions (Habuchi et al., 2005).

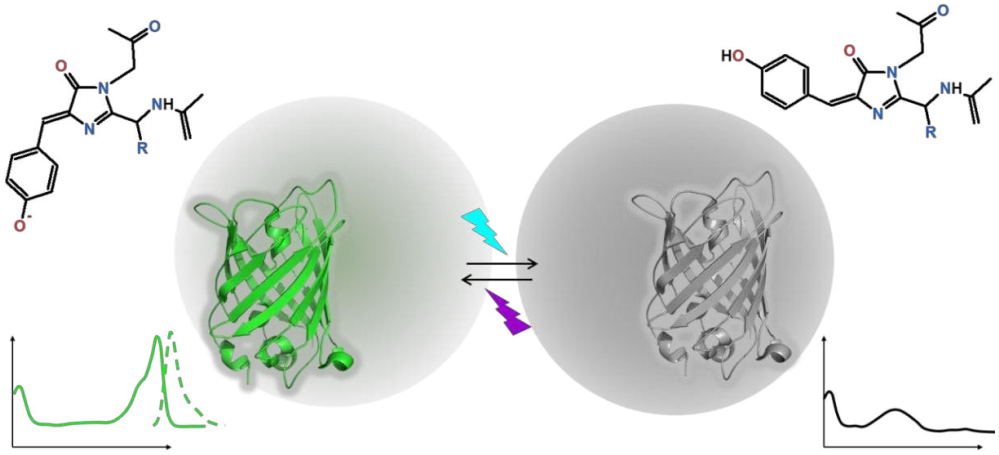

Figure 1.12) Negatively photo-switchable FPs. Reversible photo-transformation from the fluorescent anionic state to the non-fluorescent protonated state of chromophore based on cis-trans isomerization of the chromophore upon illumination at 488 nm to switch off and at 405 nm to switch on. Representative spectra of this class are based on Dronpa photo-switching, excitation (solid lines) and emission (dashed lines).

Several molecular structures of Dronpa have been published (Wilmann et al., 2006; Andresen et al., 2007; Nam et al., 2007; Stiel et al., 2007; Lummer et al., 2011). These structures show that in the fluorescent state the chromophore is in the cis conformation and after actinic illumination the chromophore is non-fluorescent in the trans conformation. Thus, on to off photoswitching involves isomerization of the chromophore. The p-hydroxyphenyl ring of the chromophore loses its interaction with Ser142. Other structural rearrangements in the chromophore surrounding accompany the isomerization. The π−stacking interaction of the p-hydroxyphenyl ring with His193 is replaced by a π−cation interaction with Arg66. Arg66 is relocated to a position beneath the chromophore. Furthermore, the tightly H-bonded triad Glu144-His193-Glu211 in the cis configuration is replaced by the Glu144-Arg66-Glu211 triad in the trans configuration (Andresen et al., 2007).

Photoswitching seems clearly based on the fact that the chromophore is found in a trans conformation in the off state. However, the trans conformation per se cannot be responsible for the lack of fluorescence, since there exist FPs that are fluorescent in their trans isomers (Petersen et al., 2003; Violot et al., 2009). Other investigations based on NMR results have also suggested the importance of the structural flexibility in photoswitching behavior (Mizuno et al., 2008). The non-planarity and the weak attachment of the chromophore to the protein matrix could harm the fluorescence (Andresen et al., 2007). In fact, the flexibility of the chromophore and its protein environment is directly connected to radiationless decays (Li et al., 2010). However, chromophore protonation also plays a key role. Indeed, while isomerization of the chromophore is observed by X-ray crystallography, spectroscopically it is the protonation of the chromophore which is detected. In this context one of the central questions about the mechanism of RSFPs arises. What is the primary event in photoswitching? A hypothesis is that the protonation and deprotonation of the chromophore require minimal structural change of the molecule and could be the primary event triggering

the isomerization (Habuchi et al., 2005). Another hypothesis is that the cis-trans isomerization of the chromophore provides a series of structural rearrangements changing the electrostatic surface potential, and consequently the protonation equilibria at the chromophore (Andresen et al., 2007). Alternatively, another suggestion for the photoswitching mechanism would be the coupling of the protonation and isomerization events by electron delocalization during torsion around the dihedral angle τ (Olsen et al., 2010). The torsion around the dihedral angle τ has also been suggested as the primary event in trans-cis isomerization that may occur or not accompanied of the ESPT process (Li et al., 2010).

Although apparently the products of photo-induced protonation and pH-induced protonation seem identical, the fact that the pH-induced protonated state cannot switch on whatever the intensity or duration of the illumination 405 nm show that they are not (Ando et al., 2004). The difference between the pH-induced protonated state and the photo-induced protonated state was confirmed by ultrafast absorption spectroscopy (Fron et al., 2007). The results show that the photo-induced protonated state has two additional time constants in the photo-conversion pathway, associated to the ESPT and relaxation of the protein environment.

1.3.6 DECOUPLED PHOTOSWITCHING: DREIKLANG

A new fluorescent protein, which exhibits neither positive nor negative reversible photoswitching, was recently published by the Jakobs group (Brakemann et al., 2011). Dreiklang can be activated and inactivated with wavelengths which differ from that used to excite the fluorescence. The photo-switching mechanism was proposed to be based on hydration and dehydration of the chromophore imidazolinone group. Further discussion and structural details can be seen in Results Chapter 2.3.3 iii.

1.3.7 PARTIAL PHOTOSWITCHING FPS OUT OF THE RSFPS GROUP

There are other fluorescent proteins that, although not referred to as RSFPs, exhibit reversible photoswitching. For example, eYFP is not mentioned as a RSFP, but switches between on- and off- states. The main difference is that the achieved photoswitching contrast is much weaker.

Tsien's group has reported (Shaner et al., 2008) partial fluorescence recovery for several FPs: TagRFP, mOrange, mCherry, tdTomato, mKO, mKate, mCerulean , mVenus, EYFP, Citrine , YPet , Topaz, mEGFP. The phenomenon is similar to that previously observed with eYFP (Miyawaki and Tsien, 2000), eBFP, eCFP, Citrine and eGFP (Sinnecker et al., 2005). It is possible that the partial photoswitching observed for these proteins has a common mechanistic origin, but this remains unknown.

1.4 APPLICATIONS OF RSFPS

1.4.1 DATA-STORAGE

The property of RSFPs to switch between on and off states can simulate the binary information 0-1 used in data-storage. The data-storage field aims to encode the largest amount of information in the smallest region. RSFPs constitute molecular switches that can be used as rewritable nano-devices where each molecule could be ascribed to one bit (Dickson et al., 1997). Over the years, the construction of nano-devices based on RSFPs has been suggested by different groups, including Tsien's group (Tsien, 1998), Moerner's group (Dickson et al., 1997) and others investigators (Andresen et al., 2005; Sauer, 2005; Schafer et al., 2008). A practical implementation has been proposed by Adam et al. in a feasibility study using protein crystals as highly-condensed 3D devices (Adam et al., 2010). Recently, the Hell's group showed that, using an efficient RSFP (rs-GFP) and employing the RESOLFT concept allows writing at the nanoscale with focused visible light (Grotjohann et al., 2011).

1.4.2 SUPER-RESOLUTION MICROSCOPY

The spatial resolution in classical fluorescence microscopy is diffraction-limited according to the Abbe-Rayleigh criterion by two factors: the **wavelength of light λ** and the **finite numerical aperture** of the microscope objective (n sinα).

$$\text{Spatial resolution} = \Delta X = \frac{\lambda}{2n\sin\alpha}$$

In optical fluorescence microscopy the used wavelength varies from 400 to 650 nm and advanced objective lenses may have a numerical aperture of up to 1.6. Therefore, images obtained with this technique are limited to a lateral resolution of $\approx$ 200 nm.

In the last two decades, first using point scanning (Hell and Wichmann, 1994) and then using wide-field illumination (Betzig et al., 2006) several techniques of far-field super-resolution imaging have succeeded to overcome the diffraction limit of optical microscopy. In the following, we discuss the two principal classes of super-resolution fluorescence microscopy, STED-like and PALM-like, and we show how RSFPs have contributed to improve these techniques.

i. Stimulated Emission Depletion (STED)

In 1994, Hell and Wichmann described a super-resolution technique based on STimulated Emission Depletion (STED) microscopy, the first far-field imaging technique to overcome the resolution limit (Hell and Wichmann, 1994). The concept of STED is based on two principles: (1) a nonlinear dependence of the fluorescence emission upon illumination and (2) a spatially structured illumination (Klar et al., 2000).

(1) Several physical phenomena respond in a nonlinear way to external input parameters; it is the case of the fluorescence emission rate in the regime of high intensity illumination (MW/cm² - GW/cm²). Upon high intensity illumination, the fluorophores are saturated in the excited state (typically the triplet state) and a higher photon flux does not allow exciting them more. In practice the STED technique induces this effect via rapid switching between two laser sources. The first laser excites the fluorophores (**Figure 1.13 A**) and the second one (called the STED-beam) depletes the excited state by stimulated emission before fluorescence takes place (**Figure 1.13 B**) (Hell and Wichmann, 1994).

(2) The spatially structured illumination is obtained by precisely shaping the laser beams. The pattern of the second laser differs from that of the first one, because it assumes a donut-shaped beam (**Figure 1.13 B**). Thereby only the molecules in the outer region of the

first beam are illuminated and depleted by the second beam, effectively narrowing down the point spread function (**Figure 1.13 C**).

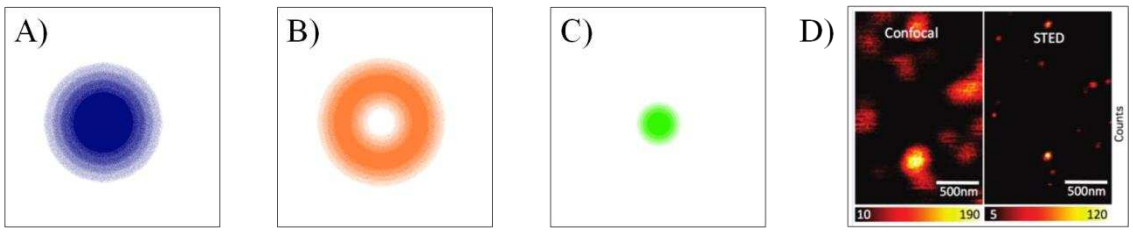

Figure 1.13) STED microscopy. (**A**) Excitation beam (**B**) STED beam (**C**) Effective fluorescence spot (**D**) Comparison between Confocal and STED images of single pTDI molecules, reprinted from (Hotta et al., 2010).

The combination of (1) and (2) results in a small region of molecules that remains fluorescent (**Figure 1.13 C**). The spatial resolution achieved is calculated by:

$$\text{Spatial resolution} = \Delta X = \frac{\lambda}{2n\sin\alpha\sqrt{1+\frac{Imax}{Isat}}}$$

Imax is the maximum intensity used in the STED-beam and Isat is associated to an inherent property of the dye that says how saturable is the fluorophore (Hell and Wichmann, 1994; Klar et al., 2000). Thus, in order to improve spatial resolution, Imax needs to be increased, or Isat needs to be decreased (Fernández-Suárez and Ting, 2008). Assuming that Imax is an instrumentation-limited parameter and that high-intensity illumination is not a suitable condition for in vivo experiments, it is a better choice to reduce Isat. All nonlinear phenomena between two molecular states of the fluorophore are in principle suitable for STED-like super-resolution imaging: reversible photoswitching is a nonlinear process for which Imax is considerably lower. In this context the RSFPs appear as an asset for super-resolution microscopy based on STED experiments.

The RSFP property was used to advantage for the first time in 2005, using asFP595, in a technique called REversible Saturable Optical Linear Fluorescence Transition (RESOLFT) (Hofmann et al., 2005). This technique allows breaking the diffraction barriers with considerable reduction of the light intensity. The same concept of nonlinearity of RSFPs has been explored to enhance the potential of Saturated Structured Illumination Microscopy SSIM (Gustafsson, 2005; Rego et al., 2012).

In practice the RESOLFT set up resembles that of STED: (i) the donut-shaped laser turns off the proteins, that are initially in the on-state, in the peripheral region of the exciting beam (ii) by probing the fluorescence with an unmodified (Gaussian) laser beam fluorescence can be collected from this region (iii) finally, the proteins are reset to their fluorescent state in order to restart the cycle **(Figure 1.14)** (Dedecker et al., 2007).

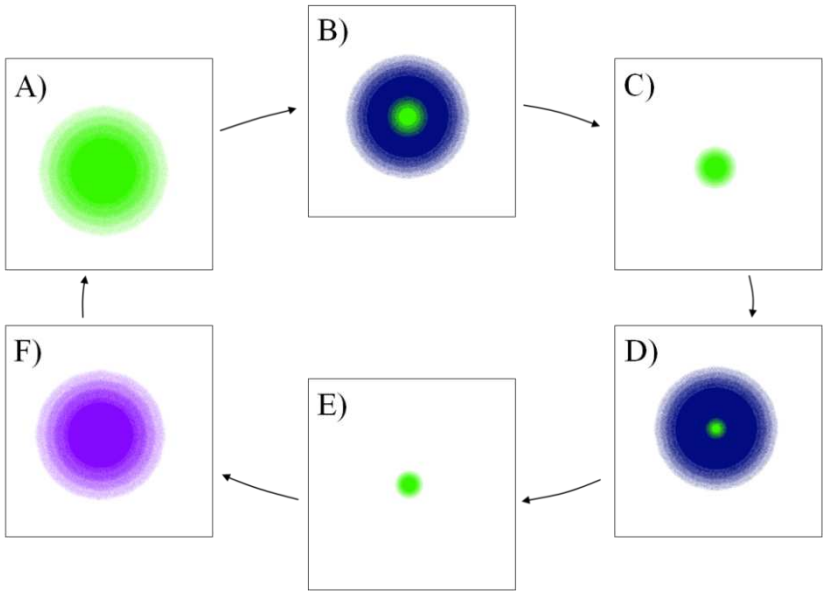

Figure 1.14) STED based on RESOLFT microscopy. (**A**) RSFPs in the fluorescent states (**B**) are illuminated with the donut mode beam (**C**) in order to turn off the proteins in the outer region of the first beam, (**D**) probing the fluorescence with a STED beam (**E**) reduces the effective fluorescent spot. (**F**) The proteins are switched on and this cycle is repeated n times depending on the protein photo-fatigue. Scheme based on (Dedecker et al., 2007).

The achieved resolution depends on the number of switching cycles that the RSFP can withstand before bleaching (Dedecker et al., 2007). For this reason, the RSFP development seeks proteins more resistant to photo-fatigue. The recent discovery of rs-GFP, hundred times more photo-resistant than Dronpa, has allowed super-resolved images in living brain slices with about a million times lower light intensities than before (Grotjohann et al., 2011). In the same line, Dreiklang via decoupled excitation mechanism, presents remarkable reduction of photo-fatigue, being a promising RSFP for future RESOLFT applications (Brakemann et al., 2011). The protein IrisFP, developed in our lab, also displays very strong resistance to photo fatigue (Adam et al., 2008).

The fact of some RSFPs exhibit pairs of negatively and positively photoswitchable proteins, such as Dronpa and Padron, is advantageous for dual-label super-resolution. Information about two different molecules-of-interest can be achieved using a single STED set-up (single excitation, STED wavelength and single detection channel). STED microscopy in microtubules labeled with Dronpa and Padron has demonstrated the applicability of this technique (Willig et al., 2011).

ii. Photo-Activated Localization Microscopy (PALM)

The concept of Photo-Activated Localization Microscopy (or PALM-like techniques) results from the capacity to localize a single emitter with high accuracy if a sufficient number of photons are collected from this emitter (Thompson et al., 2002; Betzig et al., 2006). To isolate single molecules in a densely labeled image, stochastic switching, or activation/conversion followed by bleaching of fluorescence, is performed by proper illumination of PTFPs (Hess et al., 2006) (**Figure 1.15**). The final super-resolved image is reconstructed from the stack of many accurate single-molecule localized images

(**Figure 1.15 Aiii**). To reach a specified resolution, the overall density of labeling should fulfill the Nyquist criterion.

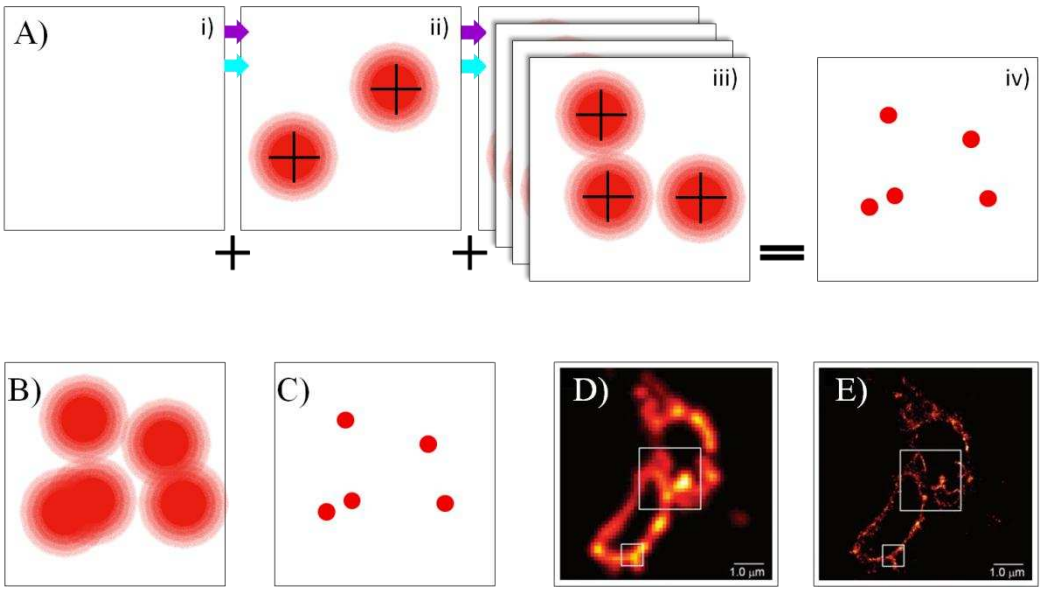

Figure 1.15) PALM microscopy. (**A**) n-step stochastic activation and excitation (ii, iii) of the initially off (i) fluorophores, and image reconstruction (iv) after PSF fitting. Comparison of the limited classic microscopy resolution (**B**) and PALM super resolution (**C**). Comparison between (**D**) TIRF and (**E**) PALM images, reprinted from (Betzig et al., 2006).

Two factors are central to collect high quality PALM data. To enhance the localization of a single molecule, it is important that the background fluorescence be close to zero, and that the photon output from single fluorophores be maximized (Fernández-Suárez and Ting, 2008). Importantly, the use of RSFPs can bias the reconstructed image if the effect of multiple switching is not considered (Flors et al., 2007; Annibale et al., 2011b). Data processing for RSFP-PALM experiments needs to discriminate between bleached and switched molecules, so that molecules that undergo multiple switching events are counted only once (Annibale et al., 2011a). Clustering artifacts in PALM image due to residual reversible switching of mEos2 fluorophores have been described by Annibale and co-authors (Annibale et al., 2010).

However, the use of RSFPs in PALM super-resolution applications can present advantages for some studies. For example, it facilitates two-color experiments (Shroff et al., 2007). Typically, the experiment starts by collecting PALM data on EosFP in the red channel. Once all EosFP molecules are bleached, it continues by collecting another PALM dataset on Dronpa in the green channel (Shroff et al., 2007). Recently, quantitative multicolor super-resolution microscopy, also using Dronpa and EosFP, has aided to understand more about the HIV-1 virus (Lehmann et al., 2011). Notably, the super-resolved images elucidated the interaction between the tetherin protein and the HIV-1 virus.

RSFPs are also attractive dyes for the studies of fast diffusion or transporting of signaling molecules in live cells. In these cases, the switching property represents an alternative control of deactivation, instead of bleaching, in order to ensure the optimal fluorophore density, essential for discrimination between the molecules (Ando et al., 2004; Habuchi et al., 2005). For example, Dronpa made possible the visualization of a single neuron from other neurons in a complex network (Aramaki and Hatta, 2006). The significance of G-actin concentration in the assembly of actin filaments and in the expansion of cells has also been investigated by imaging techniques using Dronpa (Kiuchi et al., 2011). Furthermore, the reversible switching of Dronpa has allowed the characterization of the nucleocytoplasmic transport of RNA in Transgenic Plants (Lummer et al., 2011).

Note that most biological imaging experiments using a RSFP were carried out with Dronpa. This is because until now, this protein has represented the most reliable dye as compared to the others RSFPs. However, with the recent discovery of rs-GFP (Grotjohann et al., 2011), that switches hundred times more than Dronpa, and Dreiklang (Brakemann et al., 2011), with its exceptional decoupled excitation mechanism, it is expected that novel applications using RSFPs will take advantages of these novel proteins.

1.5 GOALS OF THIS THESIS

Fluorescent proteins have been a powerful tool to study living organisms at the microscopic (and nanoscopic) scales. In particular, the reversible switching property of some fluorescent proteins provides remarkable advantages in some imaging applications and even for future biotechnological applications such as the development of high-density data-storage media. To rationally engineer new RSFPs with enhanced properties, it is essential to elucidate how the photo-switching mechanism works. Isomerization accompanied by protonation of the chromophore are the principal structural and spectroscopic manifestations of photoswitching in most RSFPs. However, the mechanistic details of these processes are not completely clear. The aim of this thesis work is to study some of the key questions related to the photo-switching mechanism: How is the isomerization correlated to the protonation of the chromophore? Do these processes necessarily occur together, or is there a temporal order between them? Intermediate states may also exist along the photoswitching pathway, as evidenced in the back switching reaction of Dronpa (Fron et al., 2007). However, so far, intermediate states were not structurally observed. We have addressed these questions by employing a combination of low-temperature X-ray crystallography and in crystallo optical spectroscopy.

1.5.1 METHODOLOGY OF RESEARCH

Optical spectroscopic experiments unveil the kinetic behavior of photo-reactions. However, using this technique, little or no mechanistic information can be obtained. In contrast, standard X-ray crystallography provides an atomic scale description of a single protein state, which is static. However, structural changes along the reaction pathway can be obtained by “kinetic crystallography”, whereby functional activity is directly triggered in the

crystal. Comparison of datasets collected by flash-cooling the sample before or at different time points after triggering allows extracting conformational motions. The technique is mostly suited to photosensitive proteins such as FPs. For such proteins, a dynamical structural view can be obtained by correlating kinetic X-ray crystallography, in crystallo optical spectroscopy and simulation techniques such as molecular dynamics or hybrid quantum mechanics / molecular mechanics approaches (Arcizet et al., 2011). Applying this methodology in different physico-chemical conditions allows walking in the energy landscape of the protein. In particular, experiments performed at low temperature allow to slow down the reaction and facilitate cryo-trapping of intermediate states (Yang et al., 2011).

In our group, the use of coupled kinetic X-ray crystallography and in crystallo spectroscopy has aided in elucidating our understating of fluorescent proteins, such as IrisFP (Adam et al., 2008; Adam et al., 2009), Keima (Violot et al., 2009), or Killer-red (Carpentier et al., 2009). The approach was also applied to other light-activated proteins such as protochlorophyllide oxidoreductase (POR) (Durin et al., 2009).

1.5.2 PHOTOSWITCHING AT CRYO-TEMPERATURE

Finally, in the context of the experiments carried out at low temperature, another interesting question to be asked is about the temperature-dependence of photoswitching. Is it possible to observe photoswitching at cryo-temperature (typically 100 K)? This question pertains to the extension of super-resolution microscopy to cryogenic conditions. This would offer a number of advantages, including the possibility to develop correlated studies with cryo-electron tomography.

Chapter 2

RESULTS AND DISCUSSIONS

2.1 NEW VIEW ABOUT ENHANCED YELLOW FLUORESCENT PROTEIN

2.1.1 OUTLOOK OF EYFP CHAPTER

Reversible photoswitching of Fluorescent Proteins (FPs) consists in the capacity, upon alternate illumination, to turn the fluorescence emission off/on (**Figure 2.1**). This property has been observed in some FPs, such as eGFP, eYFP, Citrine and eCFP. The resemblance between these protein features on the one hand and the reversible photoswitching displayed by the RSFPs group on the other has prompted us to seek a common mechanism for these two groups of proteins. However it has been noted that even the best switcher amongst eYFP, eGFP and eCFP has a very low efficiency when compared to other RSFPs. To compare the properties of these two groups, in particular eYFP, IrisFP and Dronpa, experiments on these proteins and mainly the yellow variant were carried out at room and at low temperature. Our choice to study eYFP is based both on the number of existing publications and on the switch behavior which seems to be more pronounced than on eGFP and eCFP. We will see that at low temperature, in contrast to room temperature, eYFP can switch more efficiently than Dronpa or IrisFP.

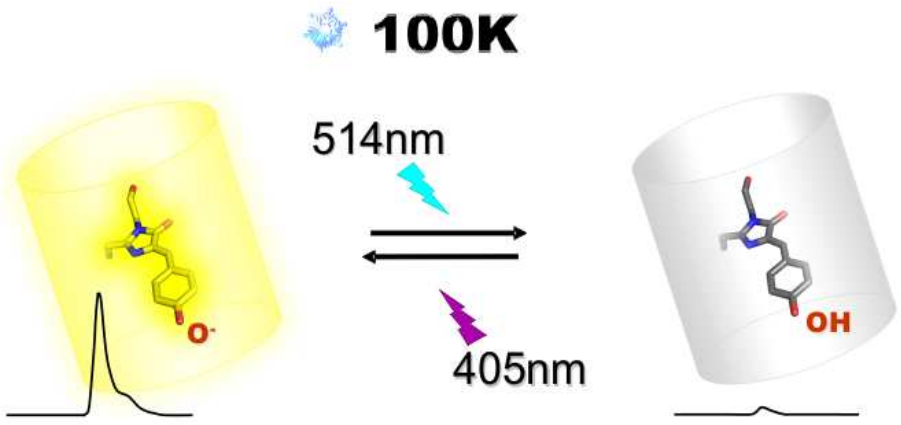

Figure 2.1) Low-temperature reversible photoswitching between anionic and neutral chromophore states is demonstrated in a number of photochromic fluorescent proteins (Faro et al., 2008).

2.1.2 ROOM TEMPERATURE DYNAMICS OF EYFP

At pH 7.5 eYFP exhibits only one fluorescent state with an absorption peak at 514 nm attributed to the anionic form of the chromophore. In analogy to eGFP this state is called B. The excitation of B induces fluorescence emission at 527 nm (**Figure 2.2**). At low pH the protonated form of the chromophore appears exhibiting an absorption peak at 390 nm (called A). A change from basic to acid pH induces interconversion from the B state to the A state with an isosbestic point at 442 nm at room temperature.

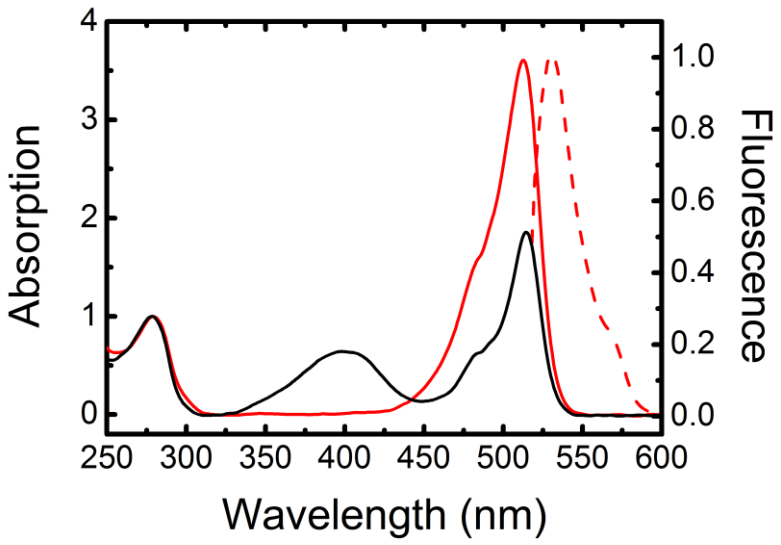

Figure 2.2) Absorbance (red solid line) and fluorescence emission (red dashed line) spectra of eYFP in fluorescent state before illumination at 514 nm (0.2 W/cm²) and after as a mixture of eYFP in fluorescent and photo-induced non-fluorescent state (black solid line). Data collected in solution at 260 K.

The protonated form of the chromophore upon excitation decays in three routes (**Figure 2.3)**: (i) a direct radiationless mode to the A ground state; (ii) a radiative mode via excited state proton transfer (ESPT) from A* to I*, an intermediate state; and (iii) a weak fluorescence emission at 460 nm. In the case of eYFP, unlike GFP, the ESPT has a limited rate constant and for this reason the fluorescence quantum yield of A is weak (McAnaney et al., 2005).

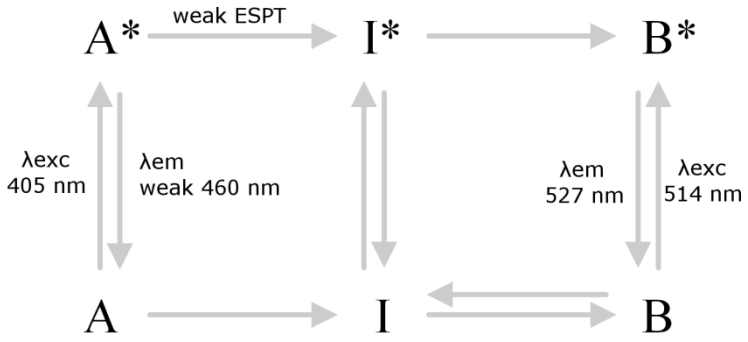

Figure 2.3) Scheme of the protonated and deprotonated states in ground and excited states of EYFP. In contrast with eGFP, fluorescence emission due to ESPT is weak.

The hypothesis considering the isomerization of the chromophore as a central process in photoswitching of Dronpa and IrisFP (Andresen et al., 2007; Stiel et al., 2007; Adam et al., 2008) is accepted within the scientific community (see Chapter Introduction). McAnaney et. al. (McAnaney et al., 2005) by carrying out stopped-flow and pressure-jump experiments have suggested a complete kinetic model for eYFP, according to which the photoswitching occurs in two-steps: a rapid phase of some picoseconds associated to the protonation and a slow phase representing the isomerization of the chromophore. According to them, in the eYFP's case, the term "isomerization" refers to rearrangement of amino acids residues, but not necessarily to cis-trans isomerization of the chromophore as in the case of RSFPs. In regard of the different mechanistic proposals described above, our first experiment is the comparison of all three FPs: eYFP, Dronpa and IrisFP.

All the parameters are set to compare the photoswitching efficiencies of Dronpa, IrisFP and eYFP at room temperature. The power density of the actinic laser (≈ 0.3 - 0.4 W/cm^2) and the concentration of the protein is the same in all three cases. Both Dronpa and IrisFP switch off upon illumination at wavelengths absorbed by the proteins in their fluorescent states (negative photoswitching). Since the deprotonated peak has a maximum at approximately ~ 500 nm, the actinic laser used is 488 nm to turn Dronpa and IrisFP off. Admitting the hypothesis that eYFP exhibits a negative photoswitching, the actinic laser used

is 514 nm. To turn the fluorescence on, the actinic laser used is 405 nm in all three cases because of the similar protonated bands of the three proteins, extending between 385 – 410 nm. We could expect that eYFP will exhibit a photoswitching mechanism similar to Dronpa and IrisFP because of Dickson's observation for this protein in single molecules experiments (Dickson et al., 1997), but we will see below that the result differs from the one expected. The comparison of IrisFP, Dronpa and eYFP photoswitching is shown in **Figure 2.4**.

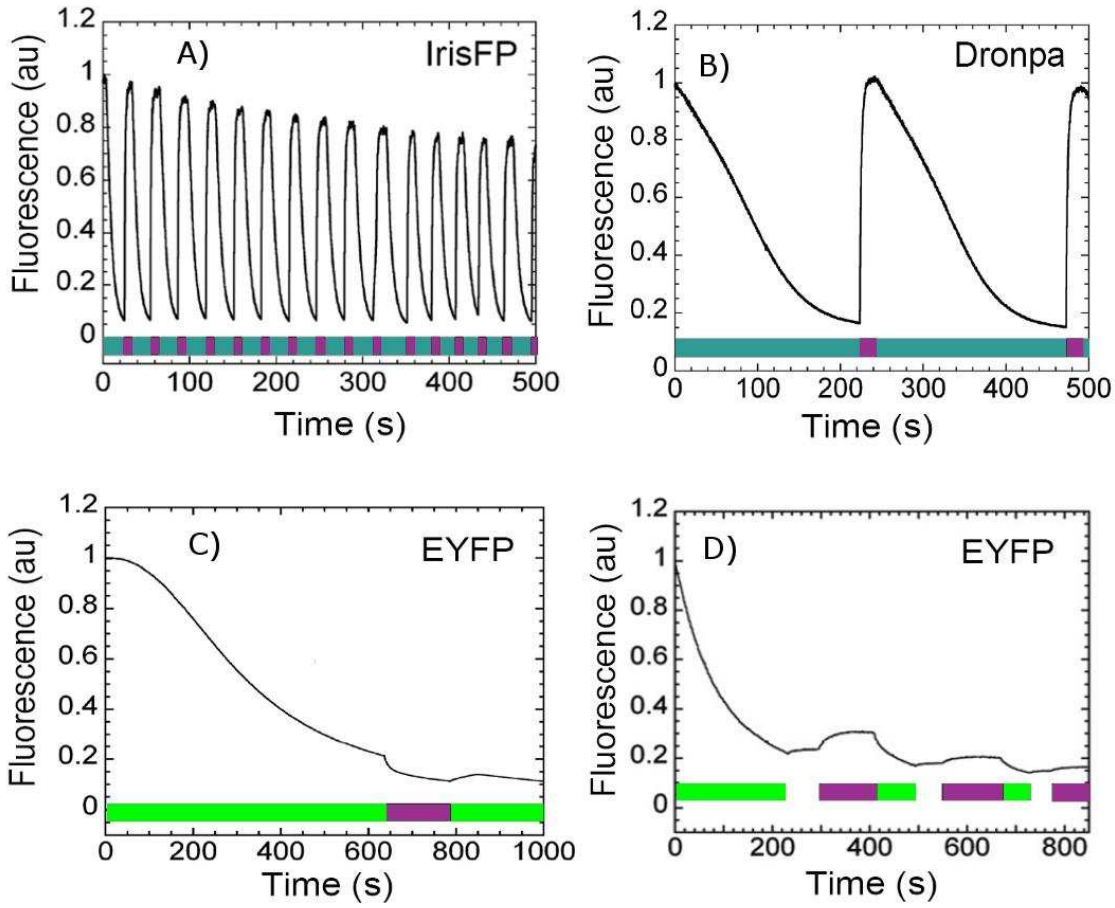

Figure 2.4) Comparison of the photoswitching cycle of IrisFP, Dronpa, eYFP at room temperature. (**A**) IrisFP and (**B**) Dronpa were illuminated with 488 nm laser light to switches off (0.29 W/cm² and 0.39 W/cm², respectively, for IrisFP and Dronpa; teal lines above the x-axis) and with 405 nm laser light (0.3 W/cm², violet lines) to switches on. (**C**) eYFP was alternatively illuminated with 514 nm (0.2 W/cm², green) and 405 nm (0.45 W cm-2, violet lines) light. (**D**) eYFP was alternatively illuminated with 514 nm and 355 nm light for reactivation. A high power density of 0.04 kW/cm² was used to accelerate the reaction. Short delays (white lines) were applied before illuminations at 355 nm to control the absence of fast spontaneous fluorescence recovery. The emission of fluorescence was probed at 474, 494 and 530 nm for IrisFP, Dronpa and eYFP, respectively. Fluorescence excitation wavelengths were the same as those used for actinic illumination.

IrisFP is the most efficient photoswitcher amongst the three proteins, displaying many cycles with a high contrast (90%) within an interval of 500 seconds (**Figure 2.4 A**). The contrast between the fluorescence minima and maxima is a parameter of evaluation of the switching capacities, requesting however the proper method to measure it. In the same time interval, Dronpa switches only twice with a worse contrast than IrisFP, < 90% (**Figure 2.4 B**).

No significant switching is observed in the ensemble average for eYFP with the actinic lasers 514 nm - 405 nm, contrary to the single molecule observation (Dickson et al., 1997). The 405 nm laser does not recover the fluorescence. In fact, it deactivates the fluorescence even more than upon illumination only at 514 nm (**Figure 2.4 C**). The result obtained here, with fluorescence decreasing upon 405 nm is close to the results published by Sinnecker et al, where the laser at 405 nm also switches off instead of activating the fluorescence (Sinnecker et al., 2005). After illumination at 405 nm, a new cycle at 514 nm is applied and we observe that the laser, supposed to deactivate, induces on switching of the fluorescence.

A slight recovery of the eYFP fluorescence is obtained with the laser at 355 nm (**Figure 2.4 D**). This result matches with the action spectrum obtained by McAnaney et al (McAnaney et al., 2005). They provide evidence that this protein can be switched back only with light at wavelengths < 395 nm, with a maximum recovery of 25 %. This property of eYFP seems to be the same effect observed in the new yellow fluorescent protein Dreiklang (Brakemann et al., 2011), which will be discussed in the last chapter (see Results and Discussion Chapter 2.3.3 iii). In this same experiment, we also observe that during the short delays, without illumination, a slight and spontaneous fluorescence recovery takes place.

The discrepancy between the eYFP single molecule and ensemble average results suggests that the back-switching upon illumination at 405 nm is a rare event. Single molecule

experiments allow to identify some properties that cannot be observed in the ensemble experiments. In bulk absorption, the less likely events are hard to detect because the emitted signal is swamped into the averaged ensemble. Dronpa, in contrast to eYFP, has a more efficient photoswitching detected in both bulk measurements and at the single molecule level (Habuchi et al., 2005). For eYFP, upon illumination at 355 nm a slight back-switching is observed, but we do not have the equivalent experiment at the single molecule level. Maybe, single molecule experiments using a 355 nm laser instead of 405 nm would allow to observe a much higher frequency of molecules that return to fluoresce.

The photoswitching observed for the three proteins is coherent with the yields reported in the literature: 10^{-2} for IrisFP (Adam et al., 2008), 10^{-4} for Dronpa (Andresen et al., 2007) and 10^{-6} for eYFP (Dickson et al., 1997). Our data emphasize the differences between the three proteins, but they do not provide evidence about the mechanism that renders eYFP switchable. The same spectroscopic comparison between the proteins can be reproduced at low temperature. We expect that at low temperature protein dynamics will be decelerated and that the reduced thermal energy available will inhibit conformational changes such as isomerization of the chromophore.

2.1.3 LOW TEMPERATURE DYNAMICS OF EYFP

i. Fluorescence emission

The eYFP photoswitching experiment carried out at room temperature (RT) was reproduced at cryo-temperature (100 K). In contrast to RT, a slight photoswitching is observed upon alternating between the actinic lasers 514 nm - 405 nm (**Figure 2.5**).

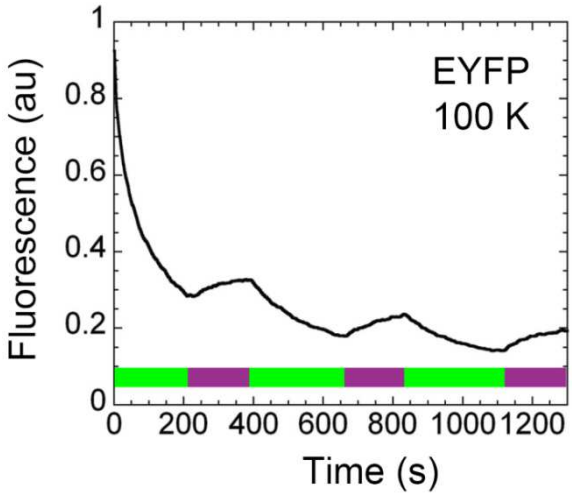

Figure 2.5) Photoswitching cycle of eYFP at 100 K following the fluorescence emission evolution probed at 530 nm. The protein was alternatively illuminated with 514 nm (0.3 kW/cm², green lines above the x-axis) and 405 nm (0.04 kW/cm², violet lines) lasers light.

We highlight two points in this curve: (1) in the first cycle the protein lost about 75 % of its fluorescence upon illumination at 514 nm and recovered only 5 - 10 % after exposure at 405 nm, (2) in the following cycles the ratio between bleached molecules and recovered molecules seems to be much lower and remain about constant.

Two processes can occur during fluorescence decay: photobleaching and a reversible photoswitching. Because the numbers of recovered molecules is about the same for all cycles, we assume the existence of two populations that are not interconvertible at this temperature. One population is susceptible to bleaching and another is susceptible to switching. Once the bleach-sensitive molecules are bleached only the reversible population participates to the reaction. However, the exposure time at 514 nm in the second and third cycle was ≈ 30% longer than the first one, which may this fact be compensated for a decrease in the recovered fraction.

In **Figure 2.6**, we show the spectral changes of the fluorescence emission during the photoswitching process. The actinic lasers used are 514 nm/405 nm (~ 0.3 kW/cm² and

0.04 kW/cm², respectively) for photoswitching and 488 nm and 405 nm for excitation (see Chapter Methods).

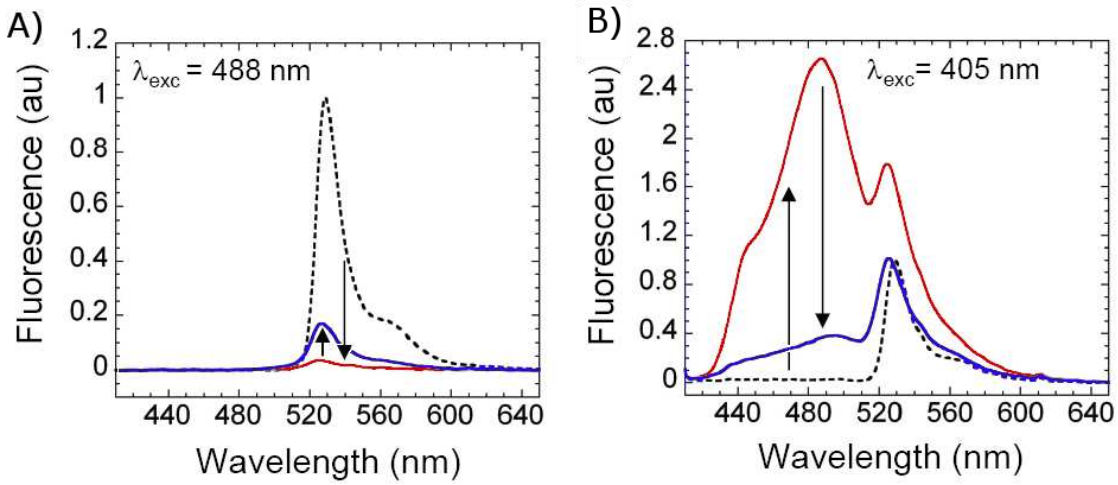

Figure 2.6) Fluorescence emission spectrum during photoswitching cycle of eYFP at 100 K. Excitation at 488 nm (**A**) or 405 nm (**B**) of the starting (black dashed line), switched (red solid line) and backswitched (blue solid line) EYFP. The fluorescence spectra were normalized on the maximum peak of EYFP before illumination. The arrows represent the direction of the photo-transformation.

At the start of the experiment, t_0, at pH 7.5, the protein solution excited at 488 nm produces high fluorescence emission at 527 nm (black dashed line). At t_1, the fluorescence is turned off (red solid line), and then at t_2, it is recovered by illumination at 405 nm, with a contrast of ~ 20% (blue solid line - **Figure 2.6 A**). The same experiment can also be performed exciting the sample at 405 nm. At t_0, the shape of the emission spectrum resembles the one obtained upon exciting at 488 nm (black dashed line). This is reasonable, since there is no protonated species, but the blue shifted part of the anionic band is probably still excited. Another explanation would be that the ESPT process at low temperature is more prominent than at room temperature (McAnaney et al., 2005). After 5 minutes of 514 nm exposure, at t_1, a strong fluorescence at 480 nm is observed overlapped with the emission from the deprotonated state (red solid line). This remarkable blue fluorescence emission must likely originate from the protonated state. Finally, at t_2, after illumination at 405 nm, we still observe

a fluorescence emission with peak maxima at 480 nm, overlapped with the 527 nm peak, from the protonated and deprotonated states respectively (blue solid line - **Figure 2.6 B**). However, a considerable reduction of the fluorescence from the protonated peak is observed.

ii. Absorbance

Analyzing now the absorbance spectra, we observe that the band shape becomes more structured at low temperature, but the absorbance maxima remain almost the same: at 514 nm, associated to the deprotonated state of the chromophore and at 410 - 385 nm, associated to the protonated state of the chromophore (**Figure 2.7**).

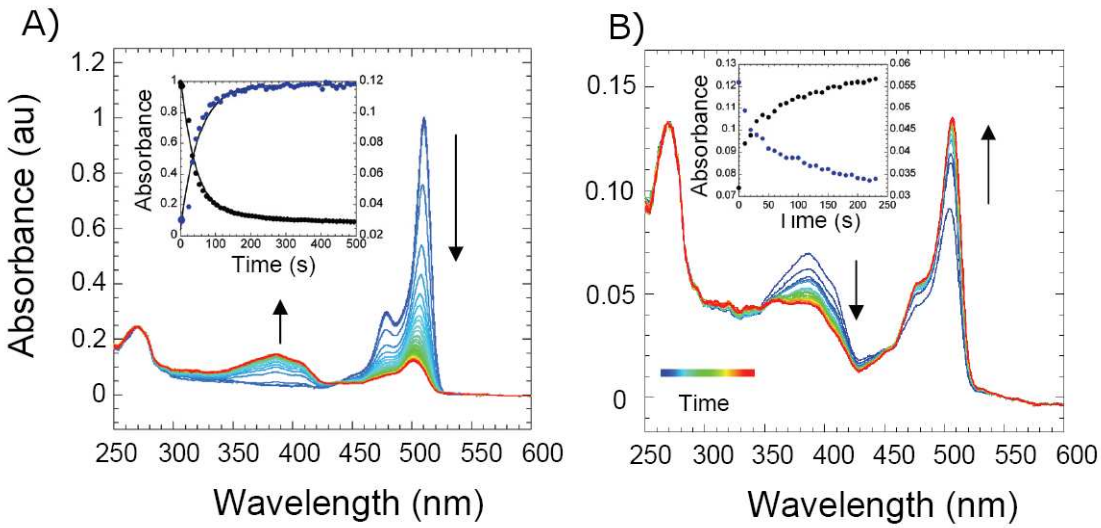

Figure 2.7) Time series of absorption spectra during photoswitching of eYFP flash cooled at 100 K. (**A**) switched by illumination with 514 nm laser light (0.3 kW/cm²). (**Inset**) Kinetic traces of the absorption at 510 nm (black) and 405 nm (blue); solid lines correspond to fitting with a bi-exponential kinetic model. (**B**) Time evolution of the absorption spectra during back-switching with 405 nm laser light (0.04 kW/cm²). (**Inset**) Kinetic traces of the absorption at 510 nm (black) and 405 nm (blue). Spectra were normalized to the EYFP absorption at 510 nm before illumination. They are chronologically plotted according to the color bar (from blue to red). The arrows represent the direction of the photo-transformation.

Figure 2.7 shows the time series of absorption spectra during photoswitching. We observe the decrease of the deprotonated and the increase of the protonated absorption bands

upon actinic illumination at 514 nm and the reverse interconversion upon illumination at 405 nm. Comparing with the spectrum obtained at room temperature the isosbestic point at 100 K is blue-shifted by 5 nm, to 437 nm.

The interconversion between the anionic and the protonated absorption bands is consistent with the fluorescence emission switching described above. However, the observation of increased photoswitching at low temperature is a surprising result especially in view of the fact that at room temperature eYFP photoswitching is negligible. Some quantitative evaluation was performed subsequently to elucidate the phenomenon.

iii. Quantitative evaluation

During switching at 514 nm the disappearance of the anionic form and the appearance of the protonated form are best fitted by a bi-exponential kinetic model (**Figure 2.7 A insert**). The reaction exhibits a fast and a slow phase, maybe associated to the switching and the bleaching of the non interchangeable populations. The rate constants for the fast phase are compatible between them: $k = 0.03\ s^{-1}$ for the protonated band rise and $k = 0.02\ s^{-1}$ for the anionic band decay, respectively. In contrast, during back-switching under 405 nm light, the disappearance of the protonated form and the appearance of the anionic form cannot be adequately fit by either mono-, bi-, or stretched-exponential processes (**Figure 2.7 B insert**).

Quantum yield of photo-transformation are determined as the ratio of the number of molecules transformed by the number of photons absorbed by these molecules before transformation (Braslavsky, 2007). It can be calculated using the fast phase ascribed on-off switching. The final equation is a function of the rate of the reaction $k=1/\tau$, the power density $\left(S/P\right)^{-1}$, where S is the beam cross section (if spot surface is small than sample surface) and

P the effective laser power, the energy of light $\left(hc/\lambda\right)$ with Planck constant, h, speed of light, c, wavelength, λ, the Avogadro constant, N_{Av} and the extinction coefficient, ε.

$$\Phi = \frac{\text{amount of molecules tranformed}}{\text{amount of photons absorbed}} = \frac{S}{\tau \times P} \cdot \frac{hc}{\lambda} \cdot \frac{N_{AV}}{\varepsilon \times \ln 10}$$

The effective laser power P should take the absorption through the sample layer crossed by the beam before reaching the probed volume. Considering the thickness of this layer and the measured optical density of the samples, we estimated that $P \approx P_0/10$, with P_0 the measured laser power.

The quantum yield of the reaction was calculated as 10^{-6} for the switching and 10^{-4} for the back-switching, values considered low compared with other switching quantum yields calculated at room temperature. However, at cryo-temperature the thermal energy available is much reduced as well as other photo-processes, such as photobleaching. Therefore, the measured value for switching corresponds to a significant process.

The linear dependence between the reaction rate and the laser power density indicates that the photo-switching at low temperature seems to be triggered by the absorption of only one photon (**Figure 2.8**). This result suggests that the reaction at low temperature could have the same photo-physical basis as that at room temperature.

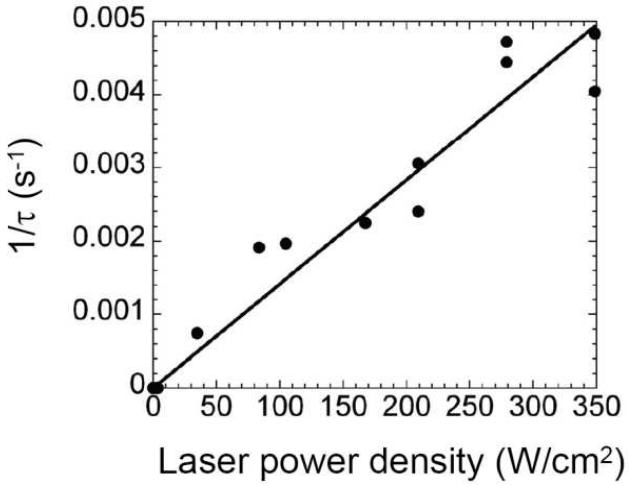

Figure 2.8) Low-temperature photoswitching of EYFP proceeds via a 1-photon absorption process. The rate of photoswitching at 100 K is reported as a function of the 514 nm laser power density. The plotted rates (1/τ) were obtained by fitting the time course of the 510 nm absorbance with a bi-exponential kinetic model. τ corresponds to the rate of the rapid phase. The solid line shows the slope best fitting the data.

iv. Thermal relaxation

Fluorescence recovery is induced by 405 nm illumination and also by thermal relaxation, meaning that the energetic barriers can be overcome in the ground state. Two hours after the photoswitching at low temperature (**Figure 2.9 -** blue solid line and insert), the anionic band is partially recovered by thermal relaxation in the dark at 100 K (**Figure 2.8 -** red solid line). Increasing the temperature above the glass transition relieves another small population able to return to a fluorescent state (**Figure 2.9 -** green dashed line). However, a large fraction of the population seems to be permanently photo-bleached, because increasing the temperature provides only partial recovery of the anionic form, overall.

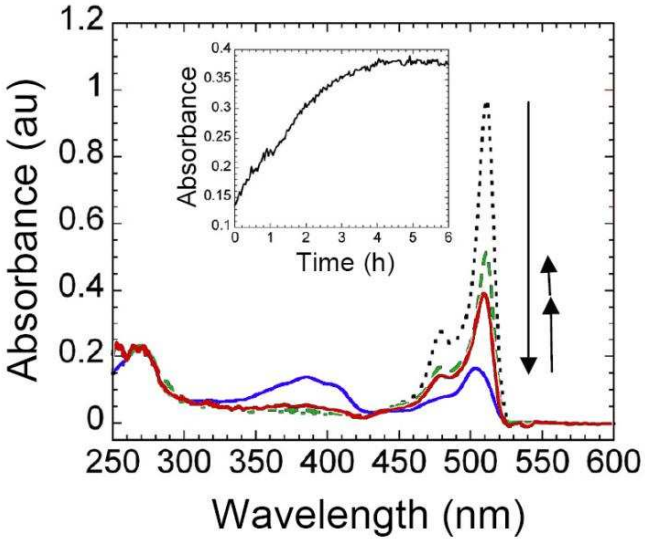

Figure 2.9) Spectral evolution during temperature-driven back-switching of EYFP. EYFP (black dotted line) was illuminated 3 min at 514 nm (0.3 kW/cm², blue solid line) and left in the dark at 100K for 10 hours (red solid line). The resulting product was warmed up to 180K (180K/h) and then cooled down to 100K (green dashed line). (Inset) Kinetic trace of the thermal recovery at 100 K, measured at 510 nm. The arrows represent the direction of the photo-transformation.

The photoswitching mechanism observed in eYFP at low temperature possesses the same spectroscopic features as those observed for RSFPs at room temperature, that is illumination of the deprotonated band induces a non-fluorescent state concomitant with an increase of the protonated band. Likewise, illumination of the protonated band recovers fluorescence emission and populates the deprotonated band. Thus, at low temperature eYFP is a negative photo-switcher. However, the photoswicthing quantum yield is still very weak compared to the values for IrisFP or Dronpa at room temperature. In order to understand further the eYFP photoswitching at low temperature, we addressed the follow questions: (1) Is the phenomenon observed here the same as the photo-induced or pH-induced protonation at RT? (2) Do Dronpa and IrisFP exhibit significant reversible switching at 100 K?

2.1.4 COMPARISON OF PROTONATED STATES OF EYFP.

In **Figure 2.10**, we compare the absorption and the emission spectra obtained upon photo-induced protonation at room and at low temperature and upon pH-induced protonation. The comparison of the different protonated forms of eYFP is done by collecting all spectra at cryo-temperature in order to prevent spectral changes due the temperature difference. Immediately after being acidified at pH 6 or photo-switched at room temperature, the eYFP samples were flash-cooled at 100 K.

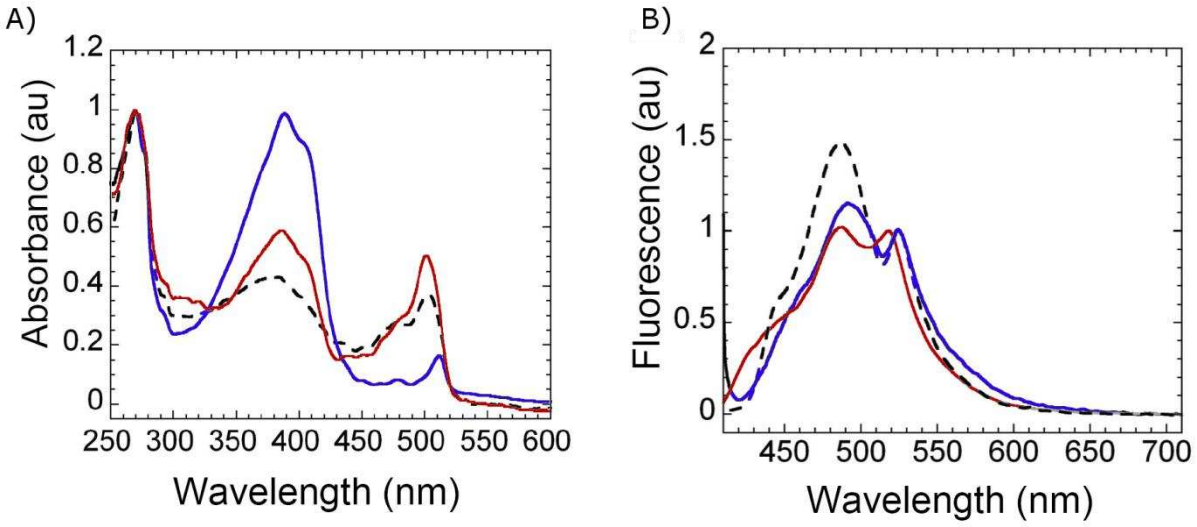

Figure 2.10) Spectral signatures of the different protonated forms of eYFP. (**A**) Absorbance spectra of eYFP at acidic pH (blue line) and at neutral pH after switching with 514 nm laser light at low temperature (red line) and at close to room temperature (black dashed line). (**B**) Fluorescence emission spectra (λ_{exc} = 405 nm) of eYFP at acidic pH (blue line) and at neutral pH after switching with 514 nm laser light at low temperature (red line) and at close to room temperature (black dashed line).

Upon inspection of the absorbance spectra we observe that the population ratio between the protonated and deprotonated forms differs for each protonation pathway. For acid-induced protonation the conversion from the anionic to the protonated form was almost complete. For photo-induced protonation at room temperature, much of the anionic peak was likely bleached during the illumination, which must explain the reduced protonated peak.

Furthermore, the photo-induced protonated peak produced at room temperature is broader and smoother than the others.

The emission spectra are normalized relative to the yellow fluorescence present in all three profiles (527 nm). This peak overlaps with the blue fluorescence from the protonated species. The photo-induced protonated state produced at low temperature exhibits almost similar amount of blue and yellow emission. In the case of pH-induced protonation, the blue emission is slightly stronger. Surprisingly, the photo-induced protonated state at room temperature exhibits a much stronger blue emission at 480 nm. This can be associated to the blue eYFP species that has been described in the literature to produce artefacts in acceptor photobleaching FRET experiments (Valentin et al., 2005; Kirber et al., 2007).

Except for their amplitudes, the pH-induced protonated state and the photo-induced protonated state produced at low temperature display stringing similar spectral shapes. However, upon actinic illumination at 405 nm a clear difference between these states appears (**Figure 2.11**).

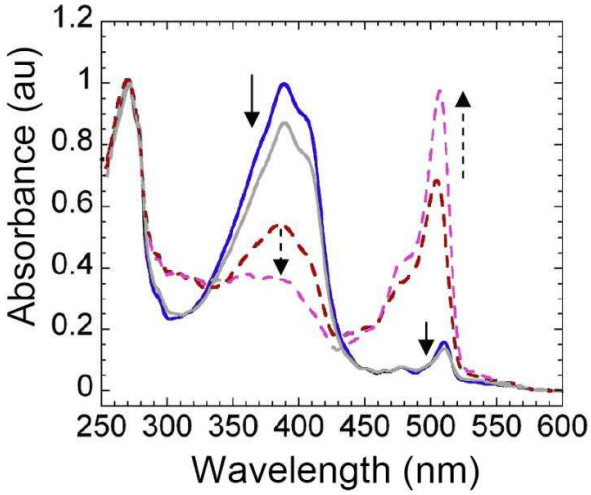

Figure 2.11) Comparison of spectral evolution of protonated state of eYFP. Before (pH-induced protonated form, blue line; photo-induced protonation produced at low temperature, red dashed line) and after 405 nm illumination at 100K (pH-induced protonated form blue line, grey line; photo-induced protonation produced at low temperature, pink dashed line). All spectra were recorded at 100K. The arrows represent the direction of the photo-transformation.

Whereas the pH-induced protonated state can only be bleached, the photo-induced protonated state can be back-switched. The protonated band of the pH-induced protonated state remains with the same profile after illumination. In opposition, after illumination the photo-induced protonated peak gets broader, like the photo-induced protonated species at RT. It is possible that the main difference comes from the structural rearrangements of the chromophore or the close environment that take place in the pH-induced protonation pathway, as suggested by McAnaney et al, and that low temperature prevents the reverse reaction (McAnaney et al., 2005). This works similar to Dronpa for which the pH-induced protonated species cannot be back-switched to a fluorescent form at room temperature, independently of the laser intensity or exposure time (Habuchi et al., 2005).

Overall, the photo-induced protonated state produced at low temperature differs from the other protonated states. We propose that at low temperature small conformational rearrangements are likely to be responsible for the observed photo-induced protonation.

2.1.5 COMPARISON BETWEEN EYFP, DRONPA AND IRISFP AT LOW TEMPERATURE

In **Figure 2.12** we compare the on - off photoswitching of IrisFP, Dronpa and eYFP using the same concentration of the protein and the same laser power density. At room temperature IrisFP is a better switcher than Dronpa and eYFP, the latter one exhibiting a negligible switching at the ensemble level. At 100 K, however, upon illumination, eYFP goes rapidly to a non-fluorescent state and can be back-switched as shown in Figure 2.5. In contrast, Dronpa and IrisFP exhibit the opposite performance at low temperature. The quantum yield for photo-induced protonation at 100 K is 10^{-6} for eYFP, 4×10^{-7} for Dronpa and 9×10^{-8} IrisFP.

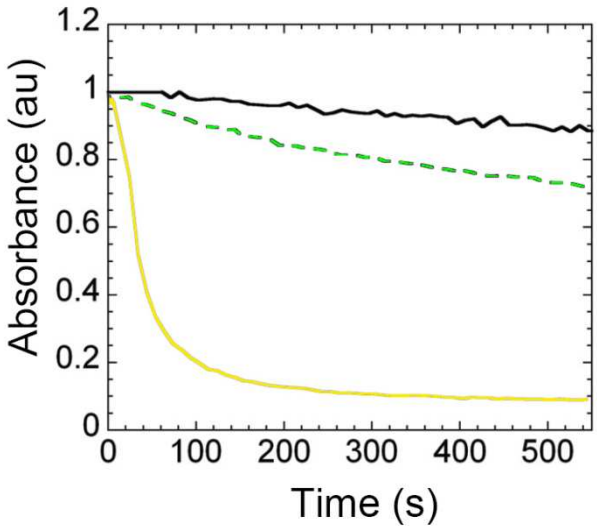

Figure 2.12) Decay of anionic absorption peak of IrisFP (followed at 474 nm black line), Dronpa (at 494 nm; green line) illuminating at 488 nm and eYFP (at 514 nm; yellow line) illuminating at 514 nm at 100 K.

Actinic illumination of Dronpa at 488 nm at 100 K, like in the case of eYFP, induces a slight increase of the protonated band, and illumination at 405 nm induces a small recovery of the anionic band (**Figure 2.13**). The same result can be observed illuminating IrisFP at 100 K (**Figure 2.14**).

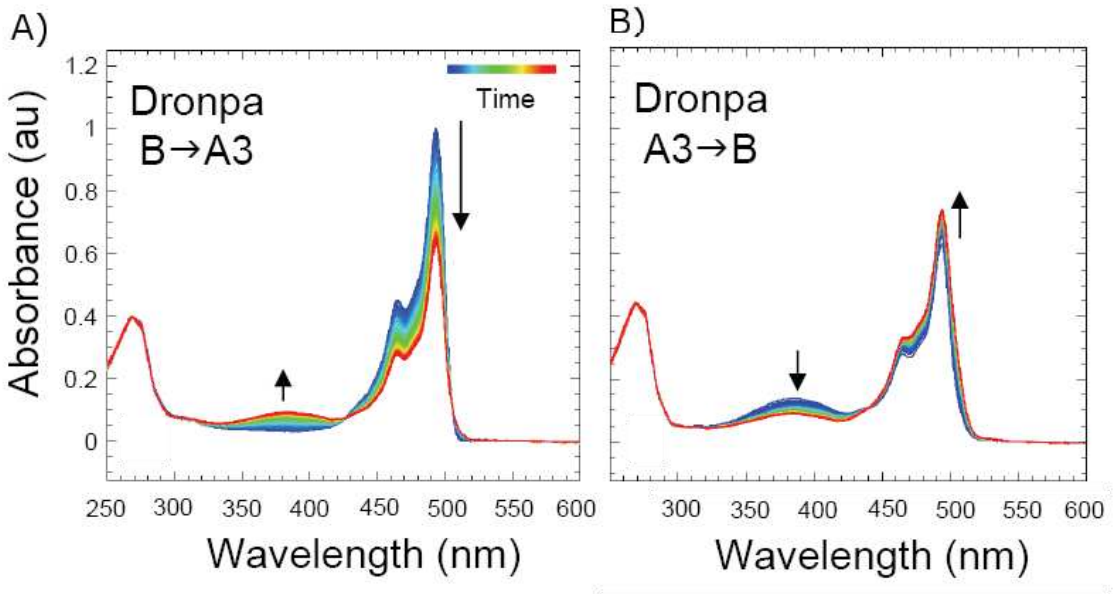

Figure 2.13) Time series of absorption spectra during photoswitching of Dronpa flash cooled at 100 K. (**A**) switched by illumination with 488 nm laser light (0.3 kW/cm²). (**B**) Time evolution of the absorption spectra during back-switching with 405 nm laser light (0.04 W/cm²). They are chronologically plotted according to the color bar (from blue to red).

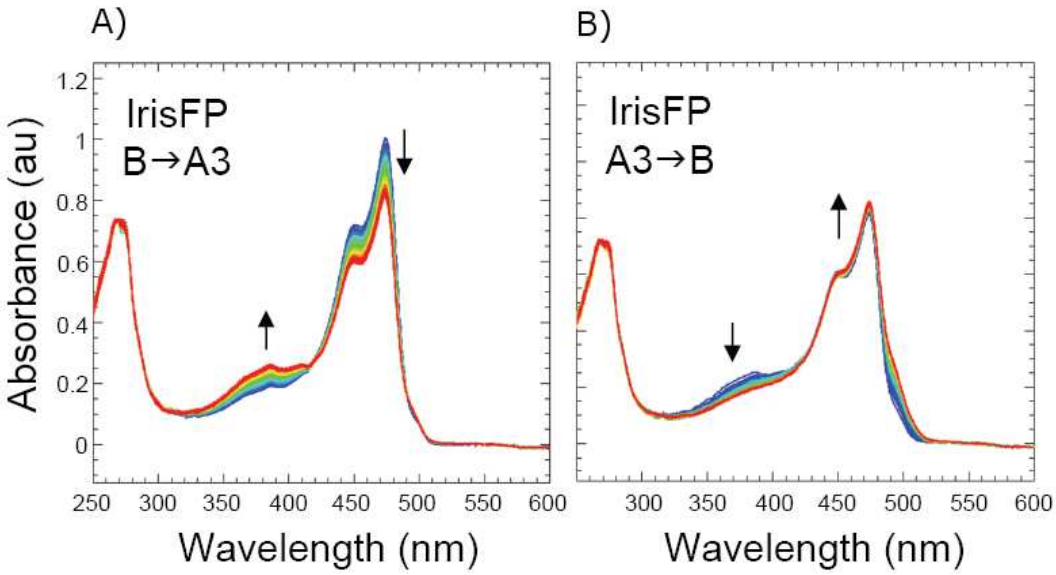

Figure 2.14) Time series of absorption spectra during photoswitching of IrisFP flash cooled at 100 K. (**A**) switched by illumination with 488 nm laser light (0.3 kW/cm²). (**B**) Time evolution of the absorption spectra during back-switching with 405 nm laser light (0.04 W/cm²). They are chronologically plotted according to the color bar (from blue to red).

The photo-induced protonation seems a common feature between Dronpa, IrisFP and eYFP upon actinic illumination at 100 K. We refer to this process as **photo-induced protonation**, because our observations are only based on optical spectroscopic data. However, we know that this reversible protonated long-lived dark-state need to be stabilized by a least some degree of conformational changes, in the chromophore and/or in the close amino acid environment. We observe that ground state relaxation occurs, likely towards the anionic conformation of origin, allowing fluorescence recovery. Therefore in view of the reduced thermal energy available at 100 K, we suggest conformational rearrangements that accompany photo-induced protonation should be of very small amplitude.

The photoswitching mechanisms at room and at low temperature seem to be anti-correlated, since we observed an inversion of relative switching performance of IrisFP, Dronpa and eYFP. It is well known that Dronpa and IrisFP have a photoswitching mechanism based on cis-trans isomerization of the chromophore at room temperature (Andresen et al.,

2007; Adam et al., 2008). Our results therefore suggest that the isomerization of the chromophore is not the structural mechanism responsible for photoswitching at low temperatures. Rather, photo-induced protonation appears to be driving force at these cryo-temperatures

2.1.6 THE FIRST EXPERIMENT WITH PADRON FLUORESCENT PROTEIN

Padron fluorescent protein also shows reversible photoswitching at room temperature. To extend the results obtained with Dronpa and IrisFP, we decided to apply the same protocol for Padron, i.e., actinic illumination after the protein was flash-cooled at 100 K. Unexpectedly, illumination at 514 nm resulted in the appearance of an intriguing blue-shifted absorption peak (**Figure 2.15**).

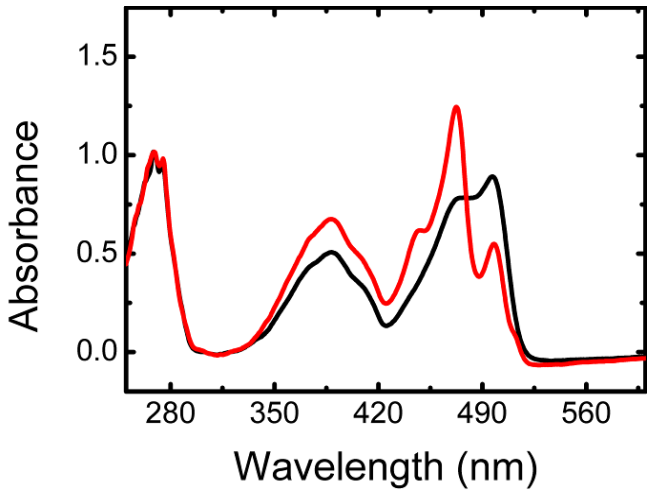

Figure 2.15) Absorbance spectra of Padron. Initial spectrum of the crystal flash cooled at 100 K (black solid line) and after few seconds of irradiation at 514 nm (0.1 kW/cm²) (red line). Uncommon peak observed at 480 nm.

Motivated by this strange result, we decided to study this protein in more details in order to understand the underlying mechanism (see next Chapter 2.2).

2.2 MECHANISTIC INVESTIGATION OF PADRON, AN INTRIGUING PHOTOSWITCHER

2.2.1 OUTLOOK OF PADRON CHAPTER

The study of Padron presented in this subchapter originated from a comparative experiment with the other fluorescent proteins at low temperature, which revealed Padron to be an interesting case to study the photoswitching mechanism. A large series of experiments led us to obtain some answers about essential aspects of the photo-switching mechanism: How is the isomerization correlated to the protonation of the chromophore? Do these processes necessarily occur together, or is there a temporal order between them? Spectroscopic and crystallographic results of Padron at cryo-temperature allowed us to suggest a kinetic model based on cis-trans isomerization decoupled from the protonation of the chromophore, accounting activation of Padron at 100 K (**Figure 2.16**). This subchapter is the most extensive of my thesis and presents original views about reversible photoswitching mechanisms.

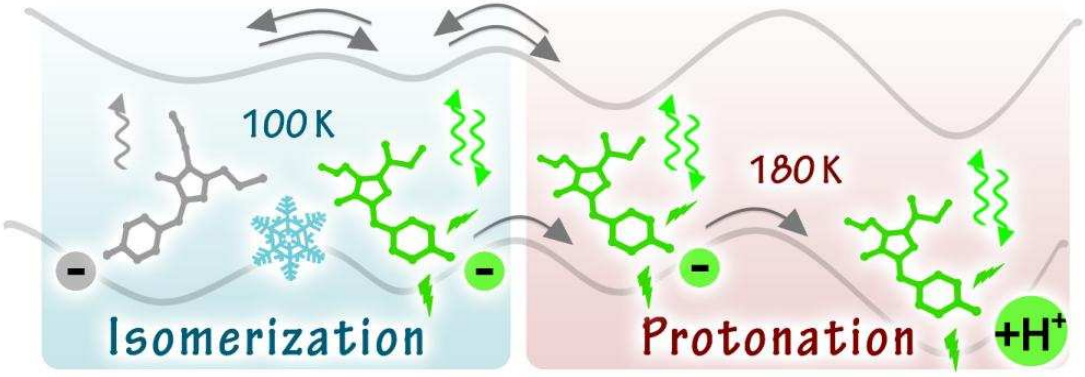

Figure 2.16) Low-Temperature Chromophore Isomerization Reveals the Photoswitching Mechanism of the Fluorescent Protein Padron (FARO ET AL., 2011)**.**

2.2.2 PADRON CHARACTERIZATION

i. Biomolecular sequence of Padron

Andresen et. al. who published the first studies on Padron have described two variants of this protein, Padron and Padron* (Andresen et al., 2008). The first variant possesses the mutations T59M, V60A, N94I, P141L, G155S, V157G, M159Y, and F190S relative to Dronpa and, at low temperature (269 K), 15% of the total population of Padron is a dimer (Andresen et al., 2008). For the second mutant, Padron*, the dimerization tendency is suppressed by exchanging hydrophobic residues with hydrophilic ones outside of the β-barrel interface (mutations T59M, V60A, N94H, I100S, P141R, G155S, V157G, M159Y, F190S, K222N relative to Dronpa FP). In our laboratory, experiments were carried out with the first variant of Padron. These studies include expression, purification, crystallization, spectroscopic and crystallographic analysis. According to Andresen and co-authors, Padron is less stable than Padron* at low temperature, but it possesses better photo physical behaviors such as photoresistance as well as a bigger contrast between the fluorescent and non-fluorescent states. A third variant of Padron (Padron0.9) was also reported recently for structural studies (Brakemann et al., 2010). In contrast with Padron*, the dimerization is intentionally enhanced in Padron0.9 in order to favor the crystallization (Brakemann et al., 2010). The amino acid sequences of Dronpa and all the variants of Padron (Padron, Padron* and Padron0.9) are shown below (**Figure 2.17**).

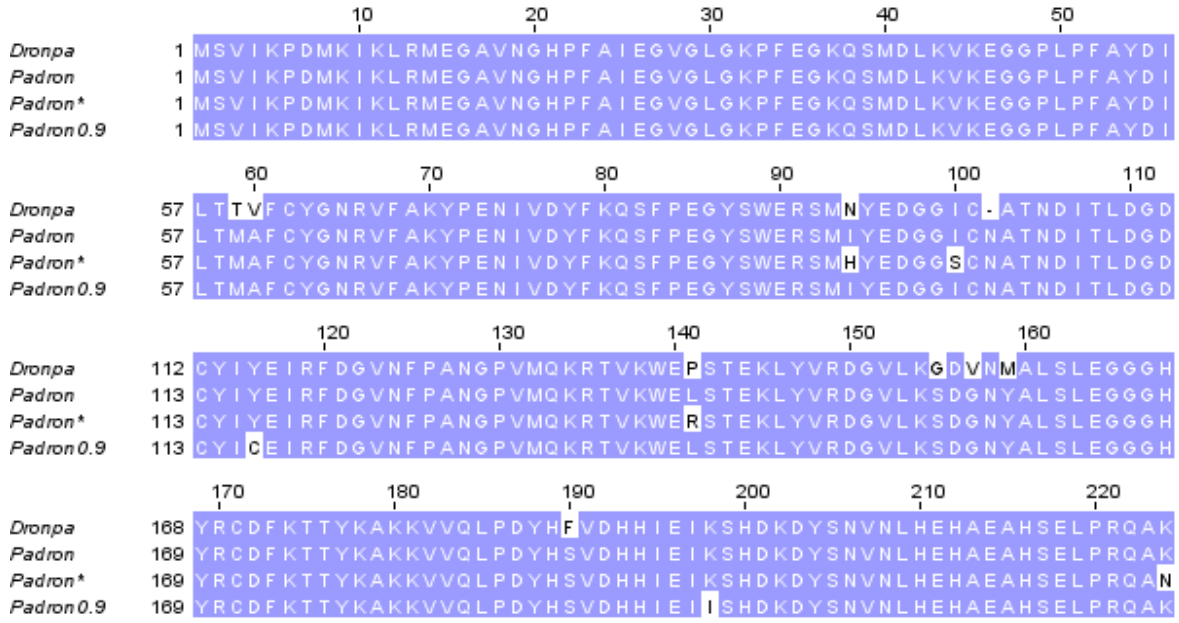

Figure 2.17) Amino acid sequence alignment of Dronpa (Habuchi et al., 2005), Padron (Andresen et al., 2008), Padron*(Andresen et al., 2008) and Padron0.9 (Brakemann et al., 2010). Conserved amino acid residues are highlighted in violet.

ii. Crystalline packing of Padron

The crystal structure of non-fluorescent Padron was solved at 2.2 Å resolution (PDB code 3ZUF) and that of fluorescent Padron at 2.35 Å resolution (PDB code 3ZUJ). In the condition of the experiments, all the crystals of Padron are orthorhombic and belong to the $P2_12_12$ space group. The Matthews coefficient analysis shows that the asymmetric unit contains ~ 48 % of solvent and six monomers (A to F). Each monomer has the conventional 11 β-barrel fold (GFP-like). Monomers are packed in pairs, facing each other with a contact area of ~ 830 Å² (A/B, D/E and C/F interfaces, **Figure 2.18A**). The dimer D/C is packed with the E/F one with a contact area of 1570 Å² (**Figure 2.18B**). Finally, a small contact surface links the last dimer to the others with an area of 322 Å² (C/D/E/F and A/B interfaces, **Figure 2.18C**).

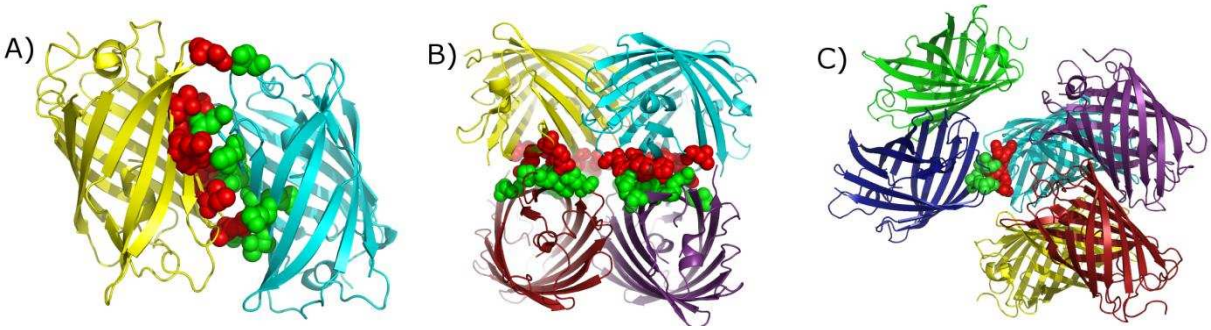

Figure 2.18) Contacts interface between different oligomers of Padron. Spheres represent the principal hydrogen bonds crossing protein interfaces. **(A)** Interface between the monomers A and B (similar for D/E and C/F). **(B)** Interface between the dimers D/C and E/F. **(C)** Interface between F/E/D/C and A/B. This analysis was done with the PISA server at EMI-MSD http://www.ebi.ac.uk/msd/.

In crystals of fluorescent proteins from the Anthozoa class, such as those of IrisFP (Adam et al., 2008) and most crystal structures of Dronpa (Andresen et al., 2007; Nam et al., 2007; Stiel et al., 2007), the monomers are usually grouped in tetramers. In spite of the fact that monomers are packed as hexamers in the Padron asymmetric unit, the same common motif of four monomers can be found when the unit cell is extended (**Figure 2.19**).

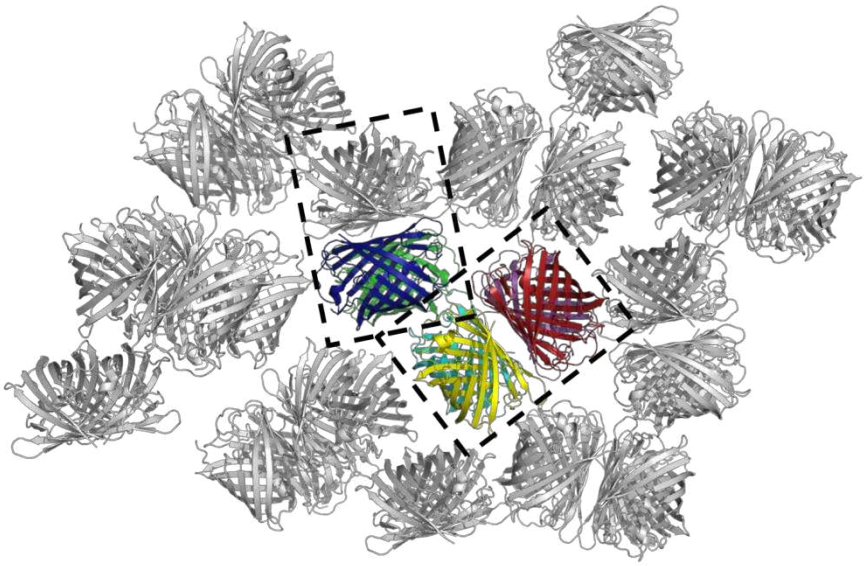

Figure 2.19) Crystalline packing of Padron: the colored structures represent the 6 monomers of the asymmetric unit. The gray structures are the expansion of the crystalline network. Highlighted with black dashed lines are the usual motifs of 4 monomers that can be often found in other crystalline arrangements of FPs from Anthozoa class.

Two crystal structures of Dronpa, PDB code 2Z6Z (Mizuno et al., 2008) and 2IE2 (Wilmann et al., 2006) have similar packing than Padron and their crystallization conditions are also similar, which suggests that this condition favors $P2_12_12$ packing. Details about the crystallographic data processing are found in the Annex 2.

The residues mutated to produce Padron0.9 (Y116C and K198I) are not placed in the chromophore pocket of the protein, which probably corroborates the fact that the spectroscopic behavior of Padron is not modified in Padron0.9 (**Figure 2.20 A, B**).

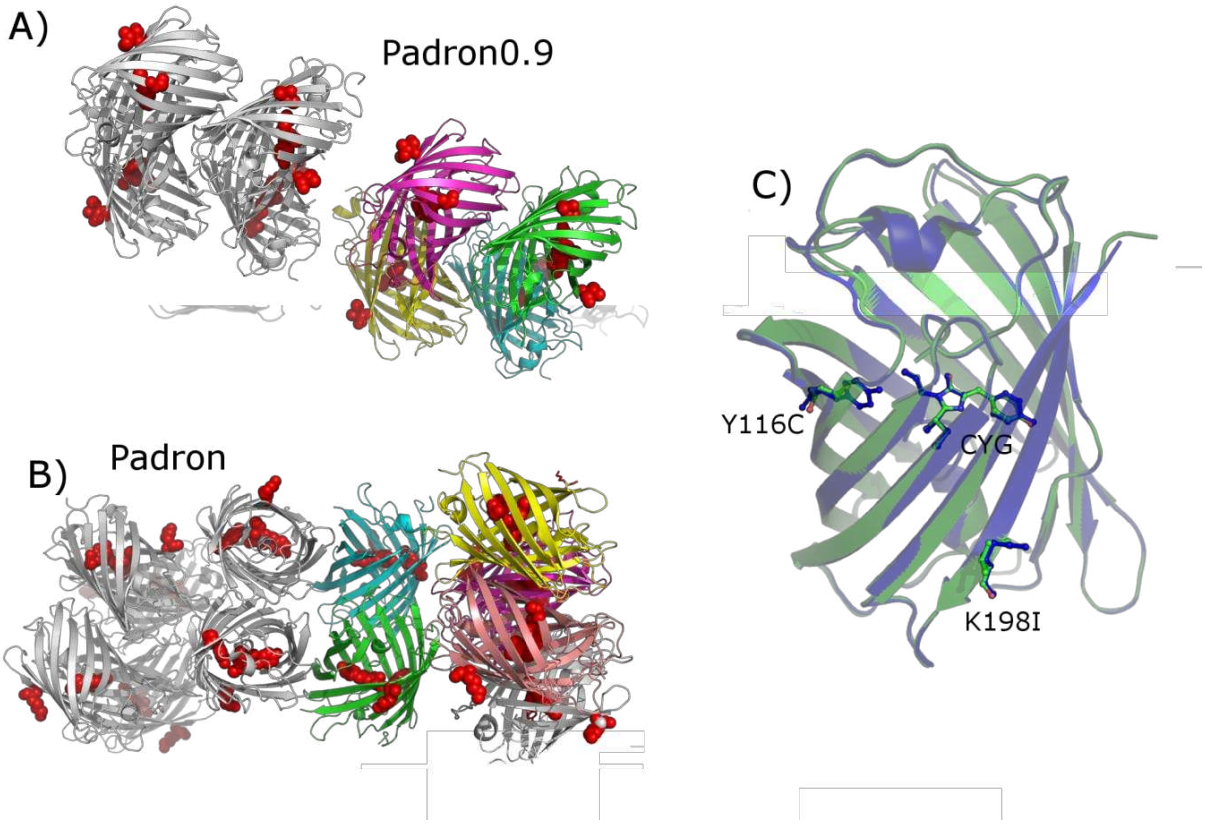

Figure 2.20) Comparison of crystalline packing of **(A)** Padron0.9 (Brakemann et al., 2010) and **(B)** Padron (Faro et al., 2011). In color cartoon the asymmetric unit, in gray cartoon neighbor molecules. The red spheres represent the mutated residues and the chromophore. **(C)** Crystal structures of bright-Padron (blue cartoon) and bright-Padron0.9 (green cartoon) superposed, in sticks the chromophore and mutated residues of Padron and Padron0.9 (Y116C and K198I).

In Padron0.9, exchanging the hydrophobic side-chain of the tyrosine 116 to a cysteine does not seem to directly affect the contact between the monomers because it is placed behind the chromophore inside the β-barrel (**Figure 2.20 C**). In contrast, the lysine 198 mutated to isoleucine is pointed to the exterior of the protein, but it does not participate to the contact interfaces. It is not evident to understand the influence of these mutations in the oligomerization pattern of Padron0.9, although they were claimed by Brakemann to facilitate the crystallization. The crystallization of Padron in our laboratory also might be a result of the dimerization tendency, as observed with Padron0.9. Comparison of the Padron and Padron0.9 structures in their bright and dark states reveal no significant modifications (**Figure 2.20 C**). The root mean square deviation (RMSD) between the two proteins for the chain A (all atoms) is 0.32 Å for the bright state and 0.30 Å for the dark state.

2.2.3 PHOTOSWITCHING MECHANISM OF PADRON AT ROOM TEMPERATURE

i. Fluorescence emission and absorbance of Padron in the equilibrium state at room temperature

At physiological pH (7.5), Padron exists as a mixture of two different states: fluorescent and non fluorescent. A different spectroscopic signature is associated to each of these states. The absorbance spectrum of Padron in its fluorescent state (“bright-Padron”) shows two absorption bands, one band with a maximum at ~ 390 nm corresponding to the neutral form of the chromophore while the other, with a maximum at ~ 503 nm, corresponds to its anionic form (**Figure 2.21, red solid line**). Bright-Padron fluoresces at 518 nm (**Figure 2.21, red dashed line**). In contrast, the spectrum of Padron in its non-fluorescent state (“dark-Padron”) exhibits only one absorption band at 504 nm (**Figure 2.21, black line**) and a very

weak fluorescence at 518 nm. Therefore, dark-Padron is a much weaker emitter than bright-Padron. For this reason and despite the fact that Padron is never completely turned off in its dark conformation, we will use the terminology "non-fluorescent" rather than "weakly fluorescent".

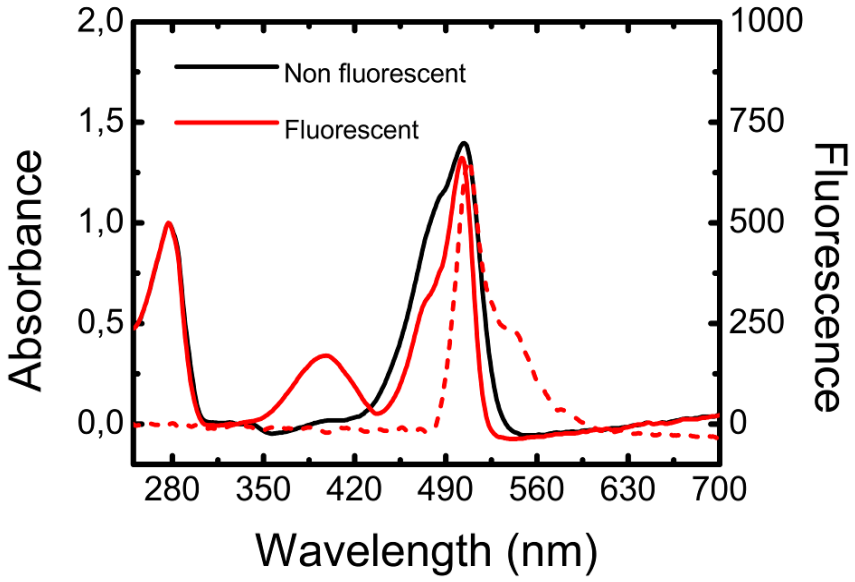

Figure 2.21) Absorbance spectra (solid line) and fluorescence spectrum (dashed line) of a crystalline sample of Padron at room temperature; Bright Padron (red line) and Dark Padron (black line).

Two points need to be emphasized regarding the absorption spectra of Padron. The first point previously described in the introductory chapter (see Chapter Introduction 1.3.3 iii) is that the dark state of FPs is often attributed to the neutral form of the chromophore, which is associated to the absorption band around ~ 400 nm. However, the absorption spectrum of dark-Padron does not display such a neutral band, and this "exotic" behavior will be further discussed in the next subchapter. The second point is that the position of the 500 nm band is very similar for both bright and dark forms, but the anionic band of the bright-Padron is narrower (**Figure 2.21**).

ii. Padron behavior upon photo-activation at room temperature

Spectroscopically, Padron exhibits a positive reversible photoswitching. Illumination into the long-wavelength absorption band (~ 488 nm) increases the population of the on-state protein and therefore enhances fluorescence whereas upon excitation at 405 nm, the protein switches off (**Figure 2.22**). Due to this "kindling" property, Padron is classified as a positive photoswitching protein. This name is in opposition with the properties of the fluorescent protein Dronpa that shows the inverse mechanism (negative photoswitching). Other proteins such as asFP595 (K. Lukyanov et al., 2000) and rsCherry (Stiel et al., 2008) present such kindling mechanisms. Like others RSFPs, the on/off fluorescence cycle of Padron can be repeated several times by alternating the actinic wavelengths.

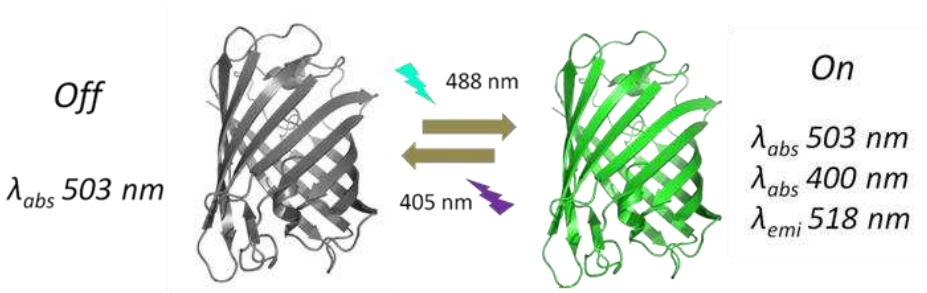

Figure 2.22) Padron positive photoswitching mechanism.

Structurally, photoswitching of Padron is characterized by isomerization of the chromophore. The crystal structure of dark-Padron collected at 100 K shows a chromophore in a trans conformation forming a hydrogen bond (2.63 Å) between its hydroxyl-benzylidene ring and Tyr159 (**Figure 2.23 A**). The crystal structure of bright-Padron, also collected at 100 K, reveals that the chromophore is in its cis configuration and that the chromophoric p-hydroxyphenyl ring is H-bonded (2.86 Å) to Ser142. Apart for the different configuration of the chromophore and significant structural changes in the conformation of the Met59 residue, the two structures are highly similar (**Figure 2.23 B**). Comparison of all the atoms of bright and dark states of Padron affords a RMSD of only 0.54 Å.

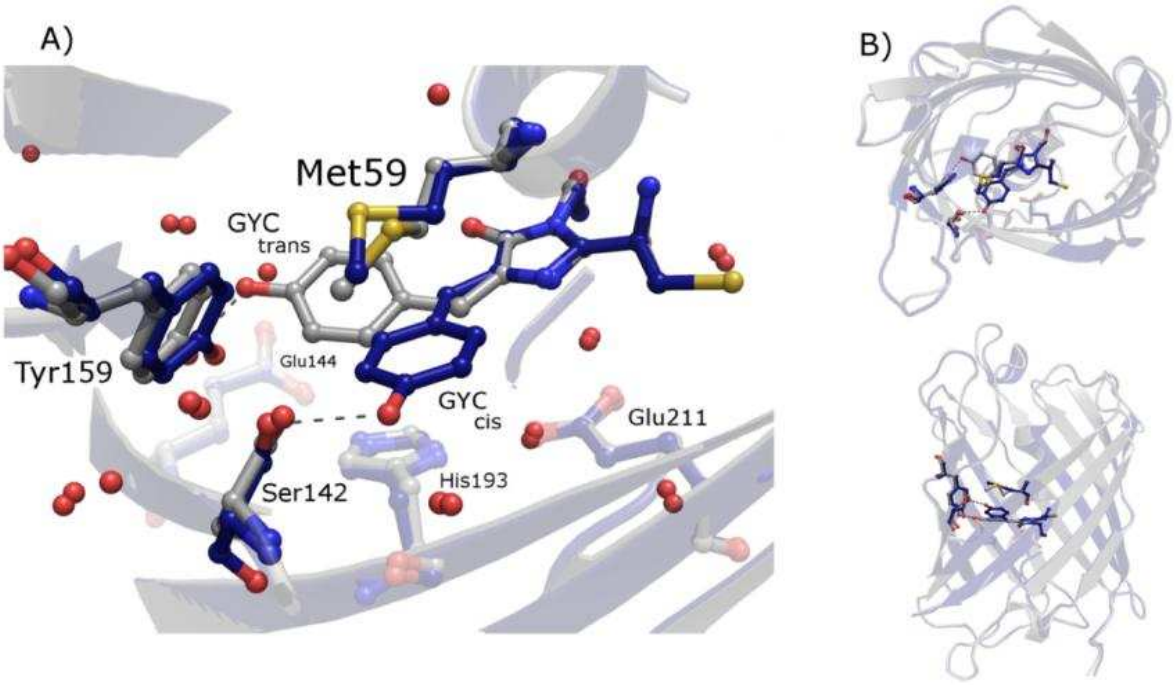

Figure 2.23) Crystal structure of Padron in **(A)** Fluorescent (blue) and non-fluorescent (grey) state, with chromophore and close environment. The structures in cis and in trans conformations of the chromophore display only few differences in surrounding amino acids. **(B)** Overall top and frontal views of the X-ray structures of Padron.

iii. Comparison of Dronpa and Padron

For Dronpa, the cis- anionic configuration of the chromophore is fluorescent and exhibits an absorption band at 503 nm. The trans- neutral conformation of the chromophore is non-fluorescent and exhibits only an absorption band at 405 nm. Thus Dronpa, which shares great sequence and structural homologies with Padron has its photoswitching associated with the cis/trans isomerization of the chromophore and the interconversion between neutral and anionic absorption bands (Ando et al., 2004; Andresen et al., 2005; Stiel et al., 2007). Could the comparison of the spectroscopic and structural data of Dronpa help us to interprete the switching mechanisms of Padron?

Structurally, bright-Dronpa resembles bright-Padron (**Figure 2.24 A**), but in the structures of the dark states the conformations of some residues are different (**Figure 2.24 B**).

In Dronpa, after illumination at 488 nm, the chromophore is isomerized from cis to trans and His193 and Arg66 are displaced, creating a different H-bond network. In Padron, only few structural rearrangements are observed between the cis and trans isomer structures, notably the different orientation of Met59. The position of the amino acid matrix around the protein is, unlike Dronpa, mostly conserved after isomerization.

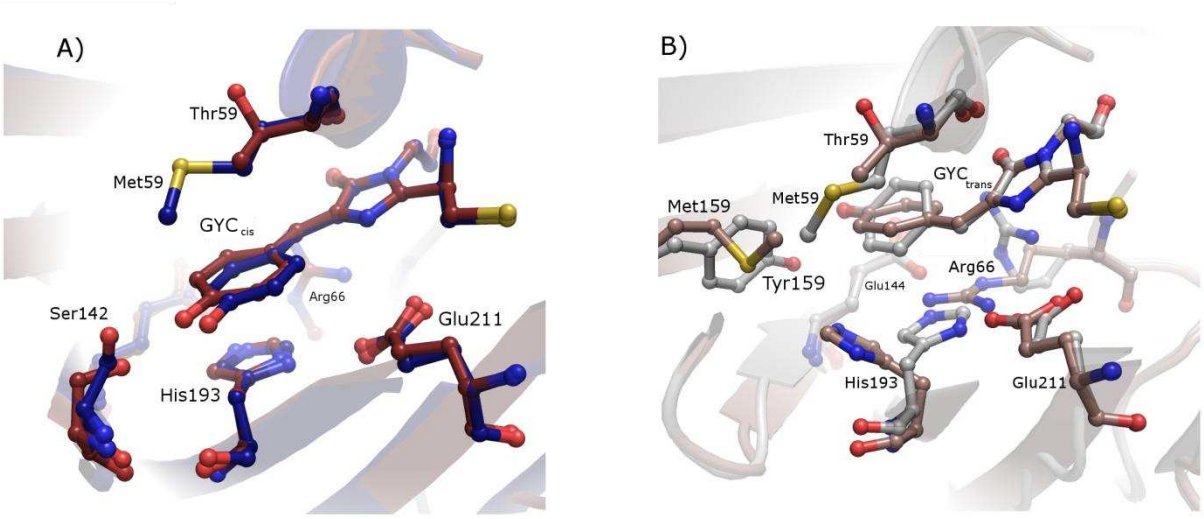

Figure 2.24) Superposition of Padron and Dronpa in **(A)** the bright state (blue- Padron and red- Dronpa) and **(B)** the dark state (white-Padron and pallet pink Dronpa). The main differences are observed in the dark structure residues His193 and Arg66.

The main difficulty in figuring out the photoswitching mechanism of Padron consists in understanding how the chromophore isomerization couples with the UV-vis absorption spectra, in particular the interconversion of the anionic and neutral bands during photoswitching. The model described for Dronpa at physiological pH associated the cis conformation to the anionic bright state and the trans conformation to the neutral dark state. However, for Padron, both bright and dark forms display an anionic band in the absorption spectrum in addition to the neutral band in the cis state. As a consequence three spectroscopic states exist, and we could expect also three different chromophore conformations, but only two were obtained. Depending on the resolution of X-ray structures, some protein

conformations may not be well defined. Probably this is the case for Padron: the two different cis isomer forms of the chromophore probably differ only minimally.

Bizarri et al. have suggested a model where the neutral and anionic states of the chromophore exist in both cis and trans configurations (Bizzarri et al., 2010). This model rationalizes the Padron spectroscopic behavior. Bright-Padron probably has a part of its population in the cis- protonated conformation and another part in the cis- anionic conformation, while dark-Padron's population is in a fully trans deprotonated conformation (**Figure 2.25**).

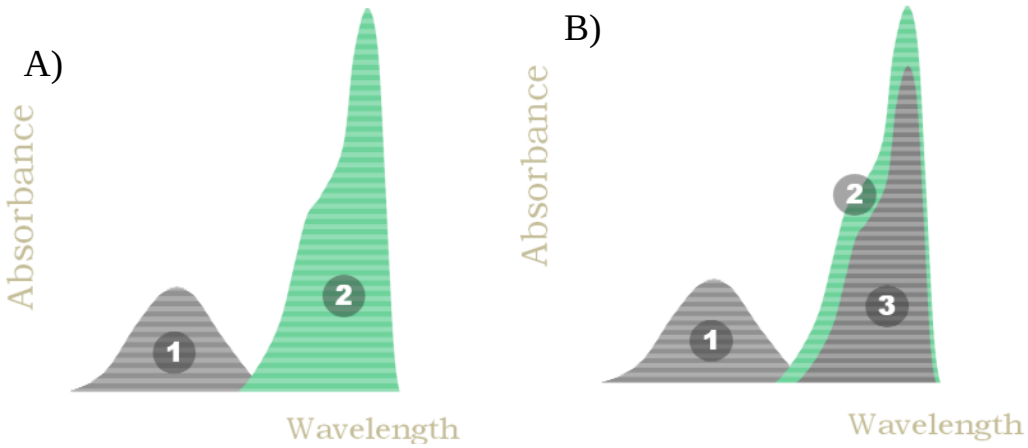

Figure 2.25) Scheme of the hypothetical deconvolution of Dronpa and Padron absorption spectrum. **(A)** Dronpa-like spectrum with two states: trans neutral dark state (1) and cis anionic bright state (2) and **(B)** Padron-like spectrum with three states: cis- protonated state (1) and another part in the cis- anionic state (2), while dark-Padron's population is in a fully trans deprotonated state (3).

Up to now, the spectroscopic and structural results provide the end points of the mechanism, that is, the spectroscopic states and the different conformations of the chromophore before and after switching. However, we have few information about how the photoswitching occurs, notably the order of the isomerization and protonation events. These points will be detailed in the next subchapters based on a cryo-trapping approach.

iv. Padron0.9: Brakemann et al.

In March 2010, Brakemann et al. published the following paper: “Molecular basis of the light-driven switching of photochromic fluorescent protein Padron”, in which they obtained results similar to ours, but using Padron0.9, instead of Padron (Brakemann et al., 2010). Some of the experiments present in this paper had been done in parallel with our work on Padron, for example the crystal structures of Padron0.9. Despite the overlap between the works, the methodological and scientific insights described in Brakemann et al helped us significantly to advance our own work about the photoswitching of Padron.

Depending on pH, Padron can display either several or only one conformation of the chromophore. They interpreted the equilibrium between anionic and protonated states at pH 7.5 based on titration experiments that give a $pK_a \sim 6.0$ for the bright-Padron and a $pK_a \sim 4.5$ for the dark-Padron. This explains why, at physiological pH, bright-Padron displays both absorbance bands, whereas dark-Padron displays only an anionic absorption band. Another insight brought from their paper is the idea to work with a pure state, that is, a homogeneous population of proteins that exhibits a well defined spectroscopic behavior. It is simpler to interpret the evolution of a spectral series, if the initial population is homogeneous. For Padron, a fully trans dark-state can be induced through actinic illumination during some time. Illumination at 405 nm at room temperature during a few seconds leads the protein to a “pure” non-fluorescent state. We will see that it is an important step implemented in my experiments in the following subchapters.

Another issue discussed by the authors is the fact that distinct absorption spectra in the fluorescent and the non-fluorescent state do not constitute an essential requirement for efficient photoswitching in FPs. They obtained a mutant L141P from Padron0.9 that, despite the quite similar absorption spectra in the fluorescent and non-fluorescent states, remains efficiently photo-switchable (comparing the contrast of fluorescence emission between dark

and bright states). We agree that the probabilities of isomerization rather than the distinct absorption spectra in the fluorescent and the non-fluorescent states are the determining factors for switching. However, we diverge from their explanation, concerning the cause of non-fluorescence in the trans state of Padron. They propose that in general the distortion of the chromophore calculated by the modulus of the sum of the τ and φ angles is an indication for the non-fluorescence. In fact for, the structures of Padron obtained in this work, the values of $|\tau + \varphi|$ are 8.0 (1.2) and 18.11 (2.4) for the fluorescent and non-fluorescent states, respectively. But, in our point of view, the trans conformation of the chromophore is non-fluorescent mainly because the energy of an absorbed photon is spent in the attempt to twist the chromophore (see Next Subchapter). The ensemble of results obtained for Padron0.9 suggests that a light-driven cis-trans isomerization of the chromophore can be the fundamental switching mechanism of Padron, but experimental evidence is still lacking.

Despite the broad overlap between works on Padron and Padron0.9 by our two laboratories, the publication of Brakemann et al. was positively received by us. We used their good ideas, such as to start each experiment with a pure non-fluorescent state and we could explore more points that remained unclear, such as the relation between protonation and isomerization in Padron mechanism.

2.2.4 PHOTOSWITCHING MECHANISM OF PADRON AT LOW TEMPERATURE

i. Motivation to continue Padron's study at low temperature

Experiments with Padron have also been carried out at low temperature in order to better understand the photoswitching mechanism. We have described previously in Chapter eYFP 2.1 that crystalline samples of Padron excited at 514 nm [f] at 100 K generate an intriguing absorption spectrum displayed by the red line in **Figure 2.26** [g]. More specifically we observe that (i) a small increase in the neutral band with a maximum at ~ 390 nm has occurred (ii) a strong and unexpected peak is detected with a maximum at 483 nm with a slight shoulder band at 450 nm (iii) a little peak at 500 nm remains. Note that for this experiment the absorption spectrum before illumination (in black) displays already a mixture of states because the Padron sample was not previously illuminated at 405 nm. The appearance of the absorbance band at 483 nm, never observed at room temperature, motivated us to further investigate the photoswitching mechanism of Padron.

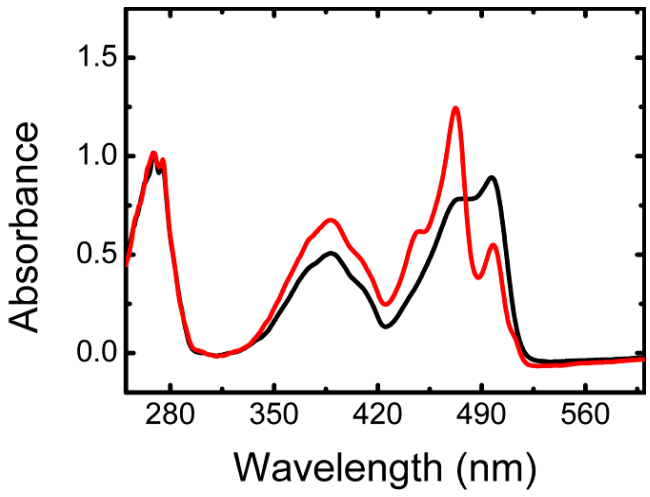

Figure 2.26) Absorbance spectra of Padron at 100 K. Initial spectrum of a crystal flash cooled at 100 K, without previous illumination at 405 nm (black line). Spectrum after few seconds of illumination at 514 nm (0.1 kW/cm²) (red line).

[f] At the beginning of the Padron investigation, the use of the 514 nm laser, instead of 488 nm, was a procedure adopted in order to facilitate eYFP experiments that use this wavelength.
[g] The Figure 2.26 is the same as the Figure 2.15, I put it here again to facilitate the reading.

ii. Walking in the energy landscape and scrutinizing Padron mechanism

Spectroscopically, Padron displays different states during reversible photo-switching. We have seen that the excitation of the crystalline samples of Padron at 514 nm and at 100 K results in the appearance of an intriguing absorption band at 483 nm and the nature of this peak has yet to be determined. The major difference between the experiment described earlier and the one shown below is the preliminary sample illumination at 405 nm at room temperature to ensure a single optical off state of the protein.

At the beginning of the experiment, the absorption signature of crystalline samples of dark-Padron ($\mathbf{B_{trans}}$)[h] is similar with the ones determined previously at room temperature, because a change in temperature alone is not sufficient to alter the absorption spectrum (**Figure 2.27 A, black line**). The excitation of the red edge of the anionic absorption band (514 - 532 nm) of dark-Padron at 100 K induces fluorescence (**Figure 2.27 D, green line**) and increases the absorption at 483 nm as shown in the previous experiment (**Figure 2.27 A, green line**). There is no appearance of the protonated band as observed before (Figure 2.26). We therefore conclude that the 483 nm peak corresponds to an intermediate species which is blue-shifted relative to B_{trans} and appears to have a long absorption tail. We call this intermediate state $\mathbf{I_{cis}}$. By analogy with the absorption shape of other deprotonated bands, we suggest that I_{cis} is also an anionic form of the chromophore. Therefore, our results suggest that this reaction $B_{trans} \rightarrow I_{cis}$ occurs only between deprotonated species. This is clearly different from the reaction observed at room temperature, where after activation part of the chromophore also exists in the protonated state.

In the conditions of the experiment, the intermediate I_{cis} is not very stable and without illumination, it relaxes in a few minutes to another state named $B_{cis,LT}$ (**Figure 2.27 B, blue**

[h] The reasons for the indices of the states denoted in this part will be clear in the following

line). This final state $B_{cis,LT}$ exhibits a very similar fluorescence emission as I_{cis} (**Figure 2.27 E, blue line**). The absorption spectrum of $B_{cis,LT}$ resembles that of B_{trans}, but the anionic band of $B_{cis,LT}$ is narrower and its extinction coefficient bigger. An important point in Figure 2.27 A is that the peak at 504 nm is higher than the initial absorption band, corresponding to the B_{trans} state. This is consistent with the formation of a fraction of $B_{cis,LT}$ species already during illumination with 532 nm light, which it is probably not the result of thermal relaxation from I_{cis} because the duration of the excitation is not long enough to allow a substantial relaxation. An explanation for this observation would be that $B_{cis,LT}$ is also generated by light and not only by thermal relaxation. The entire reaction at 100 K can be represented by this kinetic model:

$$B_{trans} \underset{k_{-1}}{\overset{k_1}{\Leftrightarrow}} I_{cis} \underset{k_{-2}}{\overset{k_2}{\Leftrightarrow}} B_{cis,LT}$$

where k_1, k_2, k_{-1}, k_{-2}, are the rate constants of the reaction which are potentially all dependent on light and temperature conditions. The illumination of Padron samples at 532 nm, therefore may increase all rate constants. Consequently, the absorption spectra can display a mixture of B_{trans}, $B_{cis,LT}$ and I_{cis} species. This last observation will be important in the next chapters.

Heating the crystal for a few seconds (annealing), after the relaxation process by interrupting the nitrogen flux that keeps the protein crystal frozen after $B_{cis,LT}$ production, results in the instantaneous recovery of the protonated state (**Figure 2.27 C, red line**). In addition, after the annealing procedure, the crystalline samples of Padron continue to fluoresce, but the spectral emission is shifted to the blue by 10 nm (**Figure 2.27 F, red line**).

The complete kinetic reaction described during this subchapter and the respective optical properties of the different states are summarized below. The quantitative results about this model will be discussed in the next subchapter 2.2.4.

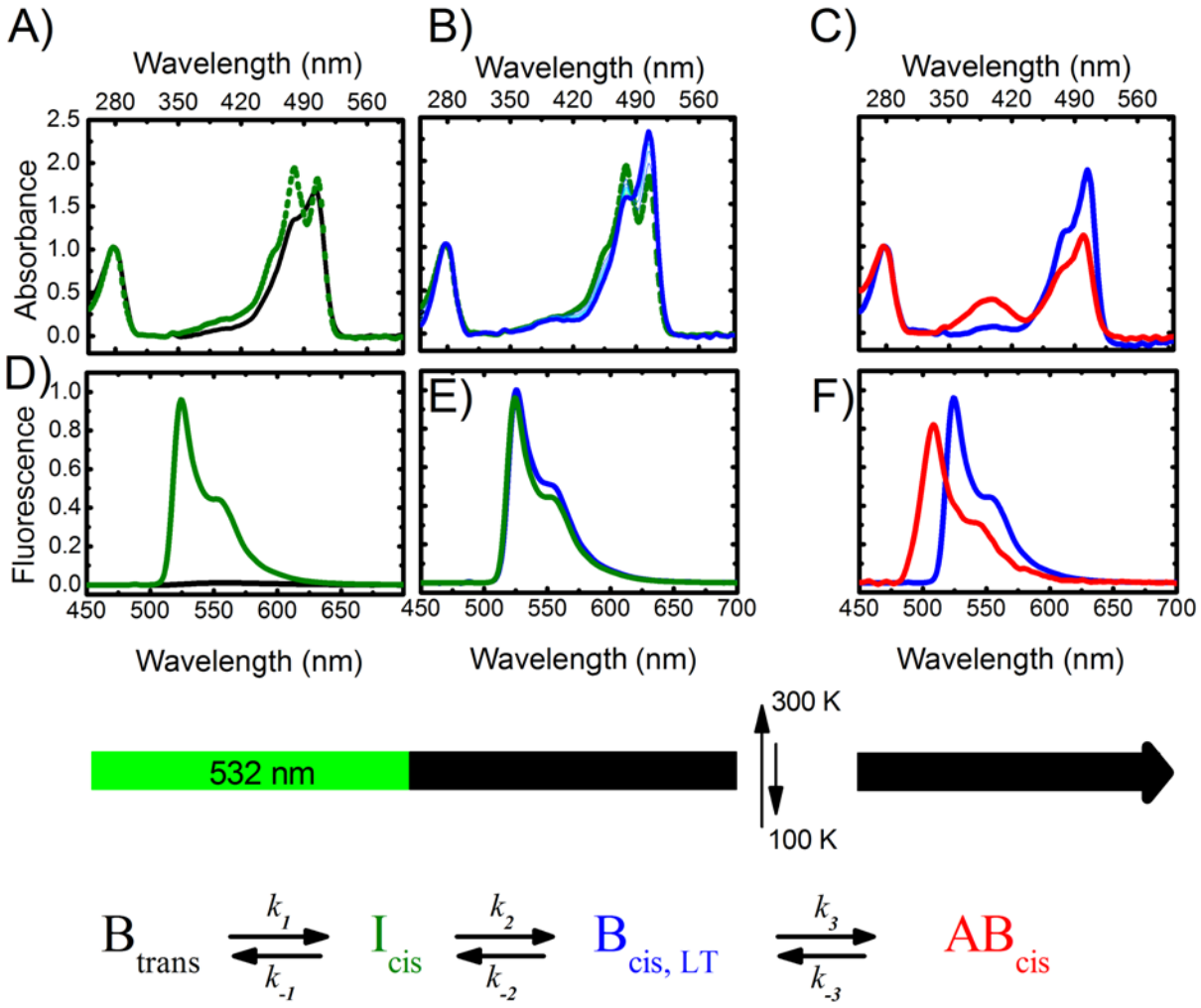

Figure 2.27) Spectroscopic signature of Padron along with its off-on photoswitching pathway, recorded in crystallo with previous illumination at 405 nm at RT. **(A, B, C)** Absorbance spectra (in top) and (**A**) Illumination at 532 nm (0.5 kW/cm^2) at 100 K of the Padron off state (B_{trans}, black line) yields a first intermediate (I_{cis}, blue line). **(B)** Spontaneous relaxation of I_{cis} in the dark at 100 K yields a second intermediate ($B_{cis,LT}$, blue line) (intermediate spectra shown in thin lines). **(C)** Subsequent increase of the temperature (100 K → 240 K) transforms $B_{cis,LT}$ into AB_{cis} (mixture of $A_{cis,RT}$ and $B_{cis,RT}$, red line). **(D, E, F)** the corresponding emission spectra (in bottom) to each step is shown in absorption (in top). B_{trans} (black line), I_{cis} (green line), $B_{cis,LT}$ (blue line) and AB_{cis} (red line). Excitation at 488 nm (2.5 mW/cm^2).

The results shown here provide valuable information about the mechanism of Padron. Firstly, the off to on photo-activation can take place at low temperature. Secondly, the activation mechanism is associated to an intermediate that relaxes in a few minutes to another more stable state at low temperature. Finally, at room temperature, the fluorescent state exhibits a protonated band which is absent at low temperature. These results suggest that the

protonation is completely decoupled from activation at low temperature. Would the isomerization be the key to the mechanism of photoswitching?

Structurally, at 100 K, photoswitching of Padron involves chromophore isomerization. The crystallographic experiments described below request the assistance of a complementary spectroscopic set-up to probe the spectroscopic states of Padron's chromophore during the reaction. The absorption spectra of the crystals are measured before and after excitation at the same position as where they are exposed to X-rays at 100 K (**Figure 2.28**).

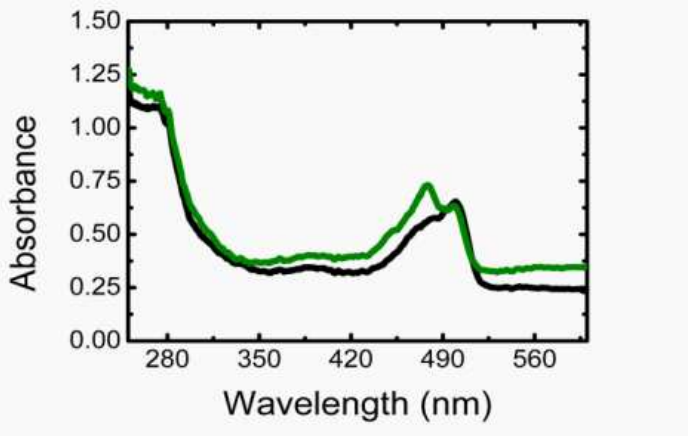

Figure 2.28) Absorbance spectra before (black line) and after (green line) illumination at 532 nm and at 100 K.

We have seen in the last subchapter that Padron does not exist as one isolated state, but as a mixture of the three different states (B_{trans}, I_{cis} and $B_{cis,LT}$) and this fact needs to be taken into account for those crystallography experiments.

Three crystal structures of the $I_{cis}/B_{cis,LT}$ states were obtained in different conditions: for two data-collections the crystal was first illuminated and X-ray data-sets were collected afterwards; for the third data-collection the crystal was illuminated during the X-ray exposure. All results show the chromophore in its cis conformation, suggesting that the same isomerization mechanism "from trans to cis" occurs at 100 K, as it is observed in the experiments carried out at room temperature.

Since the actinic laser and X-ray radiation are used on the same crystal, it is important to consider that the isomerization of the chromophore might be induced either by the one or the other. Based on control experiments, we have concluded that X-rays do not interfere with photoswitching. Indeed, no electron density in the conformation of the chromophore is observed when the crystal is not exposed to the actinic laser and no difference density is observed between two data-sets collected consecutively on a crystal kept in the dark. Therefore, the hypothesis of isomerization of the chromophore generated by the X-ray radiation has been discarded.

Collection of a data-set for one crystal of Padron takes eighteen minutes at the ID14-1 beamline of the European Synchrotron Radiation Facility (ESRF). It is longer than the time of protein relaxation from I_{cis} to $B_{cis,LT,}$ which occurs in about fifteen minutes. Is it possible that the I_{cis} state be actually a trans isomer of the chromophore that has relaxed to the cis configuration during data collection? The answer will depend on the proportions of I_{cis} and $B_{cis,LT}$ generated during the excitation and the X-ray data collection. However, it is not easy to determine ratios between different states, since the best crystals for X-ray measurements are not well suited for spectroscopy, because of their high optical density. As a conclusion, the time resolution of this experiment is not sufficient to ensure that the first intermediate after illumination is entirely in its cis conformation. A time-resolved crystallographic experiment has been set-up in order to solve this problem.

A new experiment was carried out at the Swiss Light Source (SLS) in the expectation to increase the structural contrast between the I_{cis} and $B_{cis,LT}$ states. The beamline X10SA also comprises a spectrophotometer set-up and it has the advantage of having a high-speed PILATUS pixel detector (see Annex 2). Three data-sets have been collected on a unique crystal to ensure that the results would not be altered by the non-homogeneity of different

crystals. Owing to the better time resolution of this detector (1-2 minutes/collect), we can propose that the highest population during the reaction is obtained for (i) B_{trans} state in the first data-set collected prior to illumination, (ii) I_{cis} state immediately after actinic illumination at 100 K at 523 nm for one minute (2 kW/cm2) and (iii) $B_{cis,LT}$ state in the data-set collected 40 minutes after relaxation in the dark. In the next chapter we will estimate the real proportion between these states, but from now on, for simplicity, the terms "B_{trans}", "I_{cis}" and "$B_{cis,LT}$" will be used to refer to the precise instant of the photoswitching reaction.

The new experiment at the SLS has allowed to obtain differences between electron density maps (F_{obs} - F_{obs}) of the forms (I_{cis} - B_{trans}) and ($B_{cis,LT}$ - I_{cis}) (see Material and Methods Chapter 4.5.3). The "I_{cis} - B_{trans}" map shows strong evidence that the off-on mechanism for Padron is associated with the trans to cis chromophore isomerization. The photoisomerization at 100 K occurs with weak conformational changes of the matrix, as it has also been observed at room temperature. The electron density of the sulfur atom from the flexible methionine (Met59) is displaced in opposition with the movement of the chromophore (**Figure 2.29**). This structural rearrangement is probably required for the isomerization to occur. Other smaller motions of Met93 and Ile195 flanking Met59 are most likely associated to a slight distortion of the β-barrel (**Figure 2.30**). The analysis of the differences observed between the electron density maps of I_{cis} and $B_{cis,LT}$ will be discussed in the following.

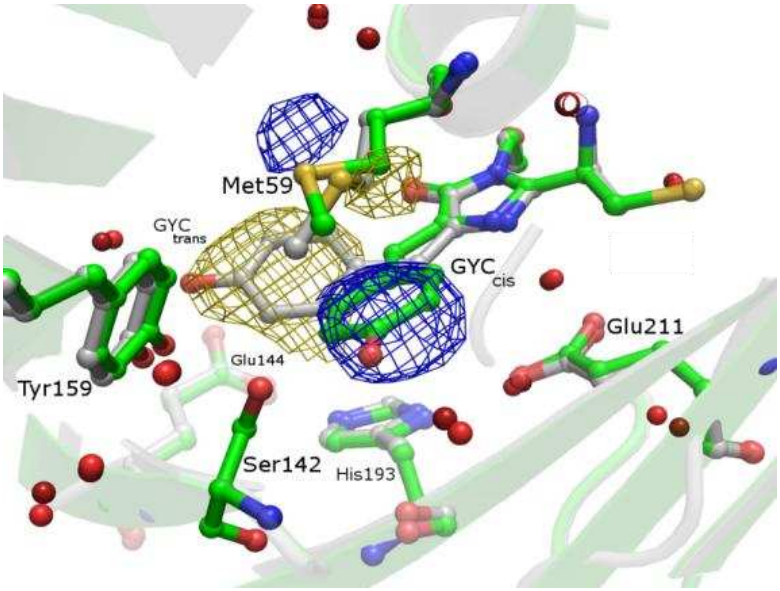

Figure 2.29) Crystal structures in states B_{trans} (non-fluorescent - white cartoon) and I_{cis} (fluorescent – green cartoon) are shown, with the chromophore and key residues of the chromophore pocket (except Arg66, omitted for clarity) represented in ball and stick mode, and the protein matrix in cartoon mode. Isomerization is evident from the experimental difference electron density map (yellow, -4.5σ; blue, +4.5σ) computed from data sets recorded on the same crystal before and after actinic illumination at 532 nm at 100 K.

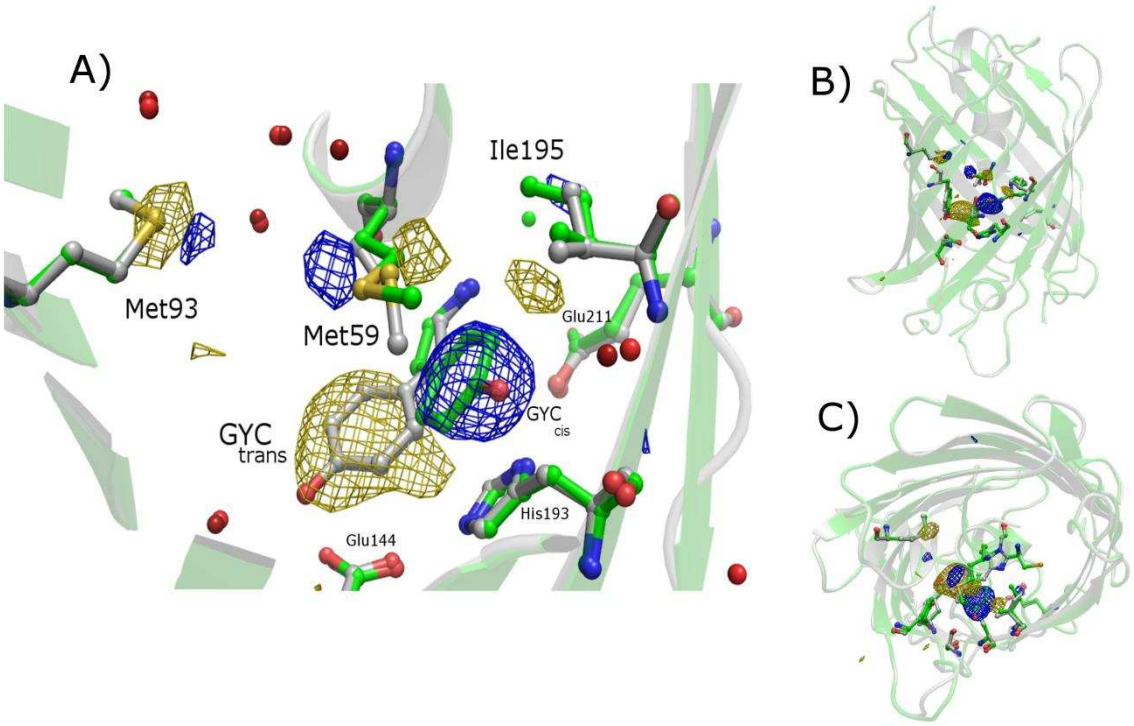

Figure 2.30) (A) Other residues that show a difference in the electron density maps before (B_{trans}) and after (I_{cis}) actinic illumination at 532 nm at 100 K including small movements of Met93 and Ile195 (yellow, -4.5σ; blue, +4.5σ). **(B, C)** Frontal and bottom views of the monomer of Padron, showing the overall difference electron density maps.

There are other indications about the chromophore isomerization mechanism at 100 K. Isabelle Demachy (Laboratoire de Chimie Physique – Paris, FRANCE) and her team (Gabriella Jonasson, Jacqueline Ridard and Bernard Lévy) are also interested in the isomerization mechanism of Padron (Faro et al., 2011). They carried out an experiment about the trans to cis isomerization at room and low temperature via molecular dynamics simulations. Their approach is based on the analytical equations of the force field that describe the chromophore CYG of Padron in its first exited state S1. These equations allow to simulate during a few pico to nanoseconds the chromophore dynamics considering potential energy calculated by taking into account protein constraints (Jonasson et al., 2011). Two parameters are monitored during the system evolution, the dihedral angles φ and τ (**Figure 2.31**) of the imidazolinone-benzylidene bridge bond in the chromophore. The effects of adding/removing H-bonds in the chromophore surrounding are also evaluated. The average between several simulations, with different initial positions, gives the statistics about the probability of the trajectories taken by the chromophore.

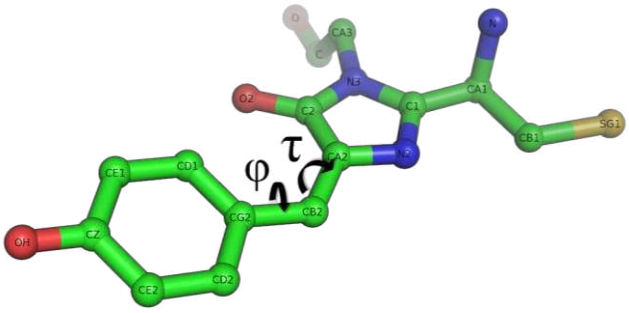

Figure 2.31) Chromophore of Padron CYG and the dihedral angles φ and τ, the arrows show the rotations involved.

The planar chromophore is stabilized in the local minimum region in the energy landscape at the initial time in the ground state. In the excited state S_1, it can escape from this position via tilt and twist distortion in φ and τ angles in some picoseconds, with most of the trajectories occurring in the upper half of the chromophore pocket by the twist in the τ angle, as it was also seen in Dronpa (Li et al., 2010). However, in the conditions of the experiments

(100 K) no more than a partial torsion of the chromophore ($|\tau| \sim 75°$) is observed, accompanied by a slight imidazolinone ring movement and the conservation of hydrogen bonds that support the phenolate ring. Thus, no complete isomerization could be observed. However, the energetic barrier could be overcome when these hydrogen bonds between the phenolate oxygen atom and Tyr159 and Wat9 are forced to be ruptured. At room temperature, without these hydrogen bonds, 2% of the chromophore population exceeds the threshold angle (90°), from which it is easier to go to the cis conformation than to return to trans. By analogy with the result at room temperature, at 100 K we can think that isomerization may occur as well although with a much reduced quantum yield. This hypothesis is reinforced by the idea that photon absorption induces a transient heating of the chromophore for a few picoseconds (Garman and McSweeney, 2007). Our collaborators also showed that a clash occurs between the chromophore and Met59 during the isomerization, and this explains the displacing of the methionine visualized in the crystallographic data. According to their result the anionic chromophore of Padron in the trans configuration does not fluoresce because the energy is rapidly dissipated through non-radiative ground state recovery from the twisted to the planar trans configuration. Their results, therefore, support our experimental observations. Further information about this work can be found in Faro et al. (Faro et al., 2011) (Annex 2).

A similar experiment with Dronpa showed that isomerization at 100 K is not common for all RSFPs. The chromophore isomerization at low temperature is possible for Padron, but it is unclear if this property is common to all reversibly switching fluorescent proteins. To answer this question, an experiment similar to that performed with Padron has been carried out with its parent Dronpa. However, despite the high similarities between the two proteins, Dronpa displays negative photoswitching, that is, upon illumination at wavelengths absorbed by the protein in its fluorescent state the protein switches off, contrarily

to Padron. For this reason, it is not possible to reproduce the exact same experiment: either we focus onto the on to off mechanism, which is different from Padron (off to on) or we illuminate the protonated band, exciting the anionic chromophore, which is also different from Padron for which the anionic band is excited. We decided to focus on the on to off mechanism. Two data-sets were collected before (F_o^B) and after (F_o^A) illumination at 521 nm for 3 minutes at 16 kW/cm^2 and at cryotemperature. The differences in the electron density maps F_o^A - F_o^B do not reveal any chromophore isomerization at cryo-temperature (**Figure 2.32**). It shows only the absence of electron around the residue Glu211, likely due to the radiation damage as was observed in IrisFP (Adam et al., 2009).

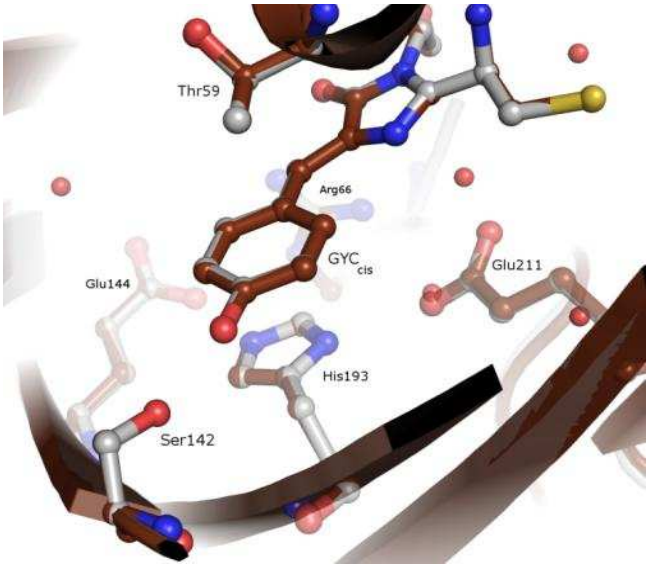

Figure 2.32) Crystal structure of Dronpa recorded under similar experimental conditions as that yielding I_{cis} in Padron. The structure of Dronpa in its fluorescent on-state is shown in white and the structure obtained upon actinic illumination at 100 K with a 521 nm laser light is shown in brown.

Maybe a better choice to perform this experiment would have been to attempt switching from off to on, instead of on to off, because in the off state the fluorescence quantum yield is smaller. Indeed, one reason that contributes to a low quantum yield is that the

absorbed energy which could otherwise be spent radiatively is channeled in attempts to twist the chromophore, possibly favoring isomerization (Li et al., 2010), as in Padron's case.

In chapter eYFP 2.1, we have shown that Dronpa crystalline samples display a slight photochromism at low temperature, and we suggested that this effect was due to a photo-induced protonation of the chromophore. The structural results obtained here corroborate this interpretation, since the chromophore isomerization does not occur at 100 K. This absence of isomerization is likely due to the much larger conformational change of the protein matrix observed upon chromophore isomerization in Dronpa at room temperature as compared to Padron, notably the complete reorganization of the H-bond network involving His194 and Arg66.

The subtle structural difference between I_{cis} and $B_{cis,LT}$ states could be meaningful and the experiment should be reproduced in the future. One of the aims for collecting data at the SLS was to check whether the spectroscopic difference between I_{cis} and $B_{cis,LT}$ correlates with a structural modification. In the first analysis of the difference in the electron density maps, there were no remarkable results. However, averaging the difference electron density map over the six monomers present in the asymmetric unit filters the noise and amplifies the signal, revealing a difference electron density map that can be associated to structural movements occurring during I_{cis} to $B_{cis,,LT}$ relaxation. Then, should this averaged difference electron density maps be considered as a meaningful result? It is important to distinguish between possible experimental artifacts and the actual consequence of the relaxation from I_{cis} to $B_{cis,,LT}$. There are pros and cons arguments related to each of these hypotheses.

First, critics can be formulated by noting that the main features in the non averaged electron difference density map differ among the monomers. It was necessary to average the

data in order to visualize some difference electron densities that made sense. In our first data-sets "I_{cis} - B_{trans}", the chromophore's movement originating from the light action was obvious in the difference density maps without any need for averaging. The lack of sufficient signal-to-noise ratio can result from the limited resolution and quality of the data. We also have observed in previous difference electron density maps a clear correlation between negative and positive densities, revealing a relocalization of the electrons between the two structures. However, for the present data, most of the difference densities were "single" (either positive or negative) without any strong counterpart. In addition, the negative density around Asp192 is a possible evidence that some radiation damage occurred.

In contrast to the previous arguments suggesting that the result should be interpreted as noise or damage, there are also some positive evidences appearing in our data that are a strong justification for repeating this experiment with better quality crystals. The set of difference electron densities features is superimposed to specific H-bond network located mostly on the β-barrel. In Dronpa, this region was described previously as the opening in the β-barrel, connecting the chromophore with the bulk solvent (Stiel et al., 2007). Indeed for Padron, the network is directly linked to the cis (fluorescent) configuration of the chromophore (**Figure 2.33**) in which the $I_{cis} \rightarrow B_{cis,LT}$ relaxation occurs. Furthermore, Agmon et al. (Shinobu et al., 2010) have shown with a high resolution structure of GFP that the residue Asn146 is an important pathway for protons exit, when the crystal is photoactivated. A structural superposition of the GFP and the $I_{cis}/B_{cis,LT}$ structure of Padron shows that Glu140 of Padron is the equivalent Asn146 for GFP. A strong positive electron density is localized between the Glu140 and Ala160 residues (**Figure 2.33**).

One explanation for the presence of positive electron density, while negative density is absent, is the global ordering of H-bonds. The electron excess (positive density) could be

explained by H-bonds rigidifying upon the $I_{cis} \rightarrow B_{cis,LT}$ relaxation due to a decrease in B-factors. Mizuno et al (Mizuno et al., 2008) have suggested through NMR analysis that the same flexible region in the β-barrel is involved during the photoswitching reaction in Dronpa. They noticed the influence of the residue Glu140 and others in the protein distortion, exactly in the region where we observed stronger difference densities. Therefore, the absorption shift between I_{cis} and the relaxed $B_{cis,LT}$ state could be associated to a β-barrel contraction.

In conclusion, we decided not to consider these results for publication due the lack of sufficient signal-to-noise ratio. However, these results merit to be discussed here because they are in accordance with previous results found in the literature (Stiel et al., 2007; Mizuno et al., 2008; Shinobu et al., 2010) and because they open perspectives for future experiments.

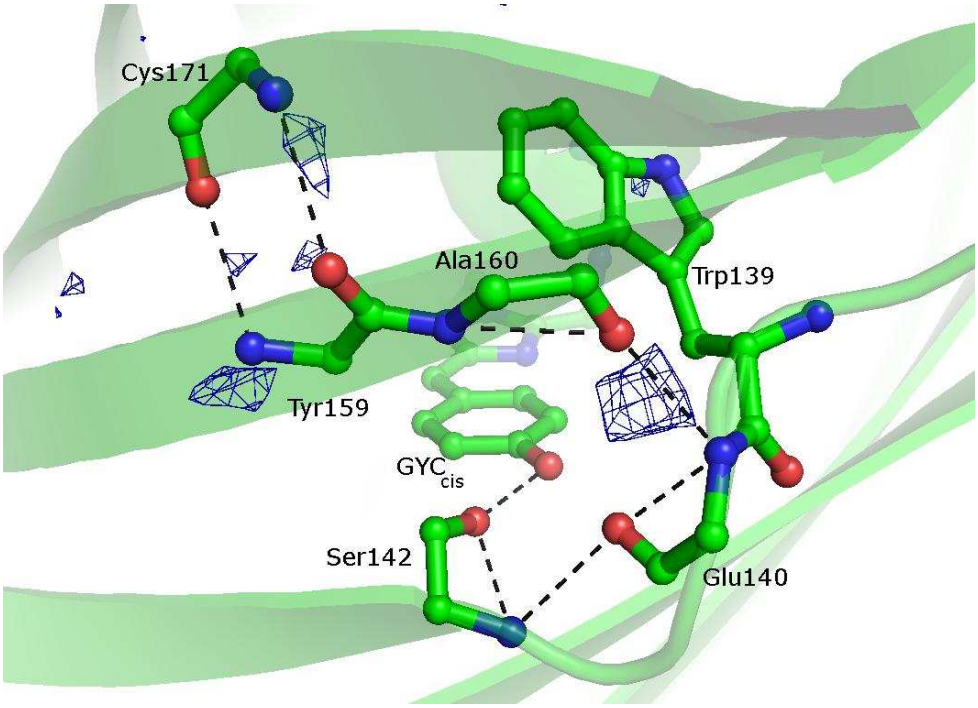

Figure 2.33) Crystal structures in states I_{cis} (green cartoon) with the chromophore CYG and key residues represented in ball and stick mode. The average difference electron density map (blue mesh, 7.5σ) between the data set collected after relaxation ($B_{cis,LT}$) and the data set collected before actinic illumination (I_{cis}) is superposed over the structure. The H-bond networks between the key residues are represented in dashed black lines.

Spectroscopic difference between I_{cis} and $B_{cis,LT}$ states. How to explain almost identical fluorescence emission spectra from two different absorbance spectra? To discuss this question it is important to first consider the arguments that allow us to conclude that I_{cis} is fluorescent. In the absorption evolution during thermal relaxation, we observe the interconversion between I_{cis} and $B_{cis,LT}$. The same relaxation observed via fluorescence evolution shows no change in the fluorescence emission spectra. If $B_{cis,LT}$ was fluorescent and I_{cis} non-fluorescent, during relaxation ($I_{cis} \rightarrow B_{cis,LT}$) we should have observed an increase of the fluorescence, depending on the ratio between the population of I_{cis} and $B_{cis,LT}$. We therefore conclude that I_{cis} and $B_{cis,LT}$ exhibit the same fluorescence. We do not know how to explain the reason for this similarity between the fluorescence spectra of I_{cis} to $B_{cis,LT}$. We can speculate about a possible excited state reaction that rapidly converts I_{cis} to $B_{cis,LT}$ and for this reason, when I_{cis} is excited we observe the fluorescence emission of $B_{cis,LT}$, a process similar to ESPT in GFP for example. In line with this hypothesis I_{cis} state would not be fluorescent. Further investigation needs to be done in order to elucidate the exact nature of the intermediate state I_{cis}.

2.2.5 THE PHYSICAL MODEL OF PADRON PHOTOSWITCHING

A photo-physical model that rationalizes all experimental findings on Padron can be proposed **(Figure 2.34)**. **(1)** In the beginning, the protein is in the B_{trans} deprotonated non-fluorescent form, and upon actinic illumination this species goes to the S_1 excited state that relaxes to the $I_{cis,LT}$ metastable intermediate state**(2)**. Depending on the experimental conditions the $I_{cis,LT}$ intermediate goes to the stable deprotonated bright state $B_{cis,LT}$ via excited state or thermal relaxation in the ground state **(3)** Another energetic barrier forbids the protonation equilibrium AB_{cis} state to be reached at 100 K **(4)**. Equilibration becomes possible around 180 K **(5)**.

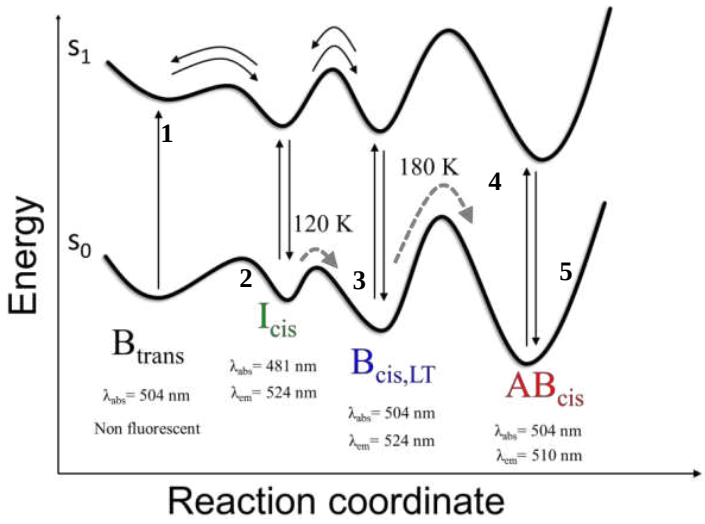

Figure 2.34) Photo-physical model of Padron photoswitching

2.2.6 QUANTITATIVE EVALUATION OF PADRON MECHANISM

The obtained results have revealed the mechanism of photoactivation of Padron at low temperature, but no quantitative evaluation has been performed so far. Based on qualitative observations, we have proposed a kinetic model that induces interconversion of three states at low temperature. In order to validate this model, the aim of this subchapter is to submit it to quantitative evaluation. Recapitulating, the model describes the off to on mechanism of Padron photoswitching at low temperature by:

$$B_{trans} \underset{k_{-1}}{\overset{k_1}{\Leftrightarrow}} I_{cis} \underset{k_{-2}}{\overset{k_2}{\Leftrightarrow}} B_{cis,LT}$$

According to the structural evidences, we assume that the rate constant k_{-1} is negligible ($k_{-1} = 0$). Indeed, the fact that all the crystallographic results obtained from different crystals, exhibit the chromophore in cis configuration after actinic illumination at 532 nm suggests that the B_{trans} population completely disappears upon activation at 100 K. If a significant

population of B_{trans} would remain, we would expect to observe part of the chromophore in trans configuration in density maps, but this is not the case.

The appearance of I_{cis} necessitates light. For this reason, we consider thermal activation of k_1 negligible. In contrast, the rate constant k_2 has both thermal and light sensitive contributions.

$$k_1 = \underbrace{A_1 \cdot P_{laser} \cdot \varepsilon}_{\text{light sensitive}}, \qquad k_2 = \underbrace{A_0' \cdot e^{\frac{-\Delta E_1}{kT}}}_{\text{thermic}} + \underbrace{A_1' \cdot P_{laser} \cdot \varepsilon}_{\text{light sensitive}}$$

$$k_{-1} = 0 \qquad k_{-2} = \underbrace{A_1'' \cdot P_{laser} \cdot \varepsilon}_{\text{light sensitive}}$$

and

where A_1, A_0 are constants, P_{laser} is the laser power , ε is the extinction coefficient , ΔE is the activation energy, k is the Boltzmann constant and T is the temperature.

i. Spectral deconvolution of B_{trans}, I_{cis} and $B_{cis,LT}$

All collected absorption spectra showing the I_{cis} state also exhibit a non-negligible remaining peak at 500 nm, that is, a significant population of B_{trans} and/or $B_{cis,LT}$. We discuss now the procedure for the estimation of the real proportion between the B_{trans}, I_{cis} and $B_{cis,LT}$ states for a record spectra, obtained through spectral deconvolution. However, we note that this analysis is not highly accurate, since the spectrum of B_{trans} is very similar to that of $B_{cis,LT}$.

Data collection is performed in two phases. In a first phase, a crystalline sample of Padron is illuminated during a few seconds, and in a second phase the reaction is let to equilibrate. Both phases are carried out at a temperature of 100 K. Spectral deconvolution requires some considerations to be applied: the first one is that the total population of molecules remains constant during the experiment. The second consideration is that we assume that after illuminating at 405 nm at room temperature and before the actinic

illumination at 532 nm, at instant t_0, the absorption spectrum corresponds to the signature of the pure state B_{trans}:

$$[B_{trans}](t) + [B_{cis,LT}](t) + [I_{cis}](t) = [B_{trans}](t_0)$$

In addition, we assume that after illumination and relaxation, the system reaches equilibrium and the final population is the $B_{cis,LT}$ state. As described previously, $B_{cis,LT}$ exhibits a higher extinction coefficient as compared to B_{trans}. Furthermore, according to the previous considerations the pure spectra of B_{trans} and $B_{cis,LT}$ are available, but not that of I_{cis}.

To calculate the pure absorption spectrum of I_{cis}, we need to subtract the total spectrum obtained in the instant t_1, right after actinic laser illumination at 532 nm (300 s; 0.5 kW/cm^2) where Icis is maximum, with the spectra $S_{Btrans}(t_1)$ and $S_{Bcis,LT}(t_1)$ with accurate proportions. It is very difficult to determinate the exact proportions, because the B_{trans} and the $B_{cis,LT}$ peaks are too similar. However, based on the crystallographic results, the population of B_{trans} is negligible at t_1 and we chose to subtract only $S_{Bcis,LT}(t_1)$.

$$S_{I\,cis}(t_1) = S_{Total}(t_1) - \gamma \cdot S_{B\,cis,LT}(t_0)$$

Figure 2.35 shows the proportion between the populations, for one specific spectrum coming from a successful experiment. The criterion used to chose the γ factor is to obtain no negative values for the spectrum of $I_{cis.}$ The absorption peak at 278 nm has been taken as a reference to normalize the spectra. Assuming that at t_1 $[B_{trans}] = 0$, we obtain $\gamma = 0.61$, that is, there is 61% of $B_{cis,LT}$ and 39% of I_{cis}.

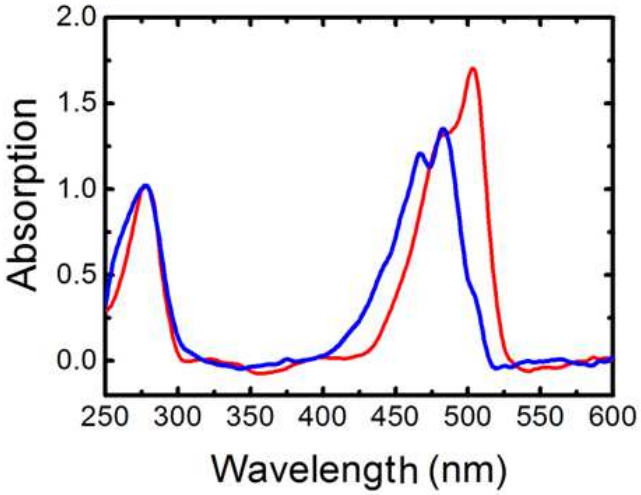

Figure 2.35) Absorption spectra for the states I_{cis} (blue line) and $B_{cis,LT}$ (red line).

The modest amount of I_{cis} produced is consistent with our unsuccessful attempts to obtain a pure state. In addition, this result also explains the weak signal-to-noise obtained in the difference electron density maps between I_{cis} and $B_{cis,LT}$: even for successful experiments such as that performed at SLS only a small part of the collected data represent the true difference between I_{cis} and $B_{cis,LT}$.

ii. Rates of off to on transformations at low temperature

We stored all time-series of absorption spectra in a new experiment similar to the previous one: we carried out actinic illumination at 532 nm in a first phase, followed by relaxation at cryo-temperature in a second phase. To analyze these data, we extracted the rate constants by monitoring the peak evolutions at maxima 504 nm and 488 nm (**method 1**). Both curves were fitted by a monoexponential model, with rate constants 0.028 (0.004) s^{-1} and 0.033 (0.003) s^{-1} respectively. When the actinic light is stopped, in the second phase of the experiment, we observe the relaxation process by monitoring the 483 nm band disappearance and the recovery of the 504 nm band, which this time is most likely associated with the increase of $B_{cis,LT}$. Both the decrease of the 483 nm band and the increase of the 504 nm band

were fitted with a monoexponential kinetic model with k = 0.0020 (0.0001) s^{-1} and k = 0.0014 (0.0001) s^{-1} (**Figure 2.36**).

This analysis by Method 1 involves errors due to absorption band overlaps, which were not taken into account. Moreover, we have noticed that during the first phase, the photoswitching of Padron reaction is more complex than simply B_{trans} to $I_{cis.}$ During illumination, the 483 nm peak increase and the 504 nm peak decay are associated to the transformation from B_{trans} to I_{cis}, but also to the transformation to $B_{cis,LT}$. Method 1 was applied in the publication of the results (Faro et al., 2011). The inaccuracy of method 1 affects mostly the first phase of the experiment, as in the second phase without illumination, the model involves only the transformation between I_{cis} and $B_{cis,RT}$. An rigorous extraction of the rate constants will require the deconvolution of the absorption spectra, so as, to obtain the contribution of the individual species.

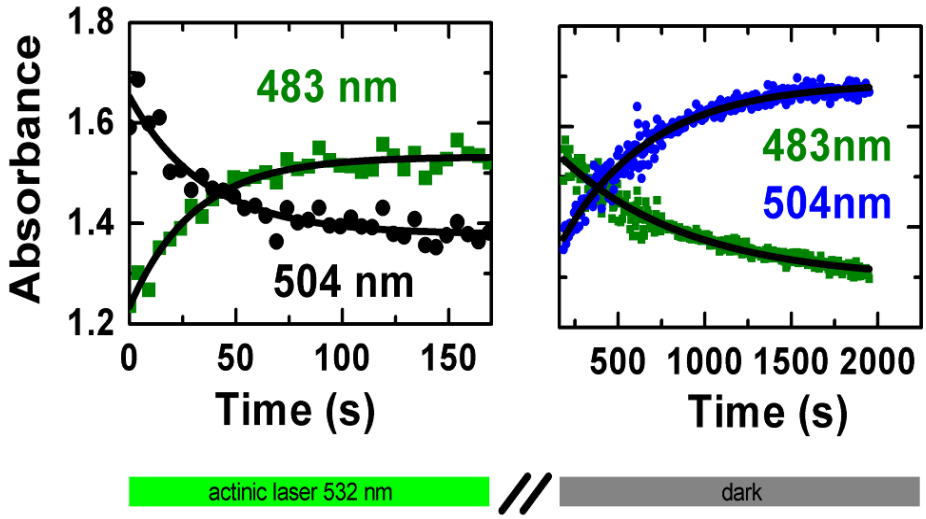

Figure 2.36) Evolution of the peak absorbance of B_{trans} (504 nm, black dots) and I_{cis} (483 nm, green squares) during illumination at 523 nm (0.15 kW/cm²) at 100K. Fitting with monoexponential kinetic models are also shown in black.

Up to now, we have described Padron photo-activation by analyzing absorbance time-series. In our laboratory, because of the experimental set-up, it is easier to record fluorescence

emission spectra than absorbance spectra. However, the rates extracted from the fluorescence data are subject to a numbers of artefacts, since at high laser power the response of the photo-reaction is not linear. In the case of Padron, a considerable disadvantage of fluorescence data compared to absorbance data is that the information about the thermal relaxation phase of the reaction is not discernible. Indeed, the fact that I_{cis} and $B_{cis,LT}$ seek to have the same fluorescence emission spectra prevents to easily distinguish them, resulting in a flat fluorescence trace during the dark phase of the reaction **(Figure 2.37)**.

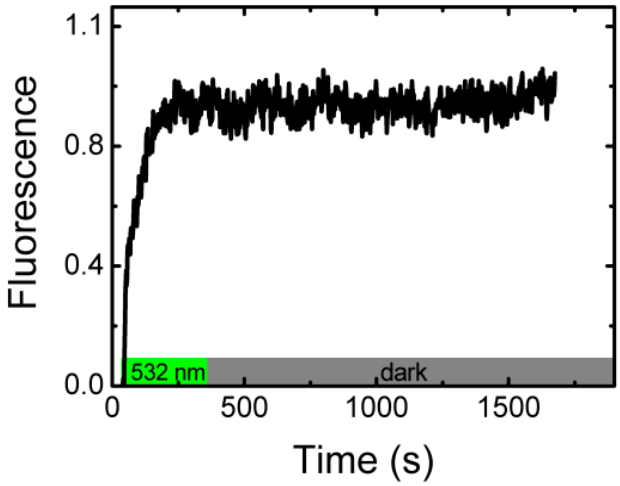

Figure 2.37) Evolution of the peak emission band width at 514 - 530 nm during photoactivation at 532 nm of the crystalline sample of Padron at 100 K.

iii. Quantum yield of photoactivation

We have described in Chapter 2.1.3 iii the quantum yield of photo-transformation that was calculated considering an irreversible photoreaction A→ B. However, if concomitantly with this process the inverse reaction occurs (B → A), the measured quantum yield will not be an effective quantum yield, but an apparent quantum yield.

Indeed, let us consider now the photoreaction A ↔ B with rate constants k_1 and k_{-1}. The concentration of A decays with:

$$\frac{d[A]}{dt} = -k_1[A] + k_{-1}[B]$$

If only A is present initially, then [A] + [B] = $[A]_0$. The solution for this differential equation is:

$$[A] = [A]_0 \frac{k_{-1} + k_1 e^{-(k_1 + k_{-1})t}}{k_{-1} + k_1}$$

Therefore, the apparent rate of decay of A is $k_1 + k_{-1}$ and an apparenrent yield is obtained

$$\phi_{app} = (k_1 + k_{-1}) \cdot \frac{hc \cdot N \cdot V}{\lambda \cdot P \cdot \varepsilon L \cdot \ln 10}$$

The quantum yield is related to the apparent one by:

$$\phi_{eff} = \frac{k_1}{(k_{-1} + k_1)} \cdot \phi_{app}$$

Note that the photoactivation of the reversible reaction displays an apparent quantum yield bigger than the effective quantum yield. It is interesting to emphasize that the effective quantum yield of activation, does not normally depend on the wavelength. However, as the interconversion rates depend on the wavelength, the apparent quantum yield will also depend on it. For example, Padron photoactivation significantly differs upon illumination at 532 nm or 488 nm.

The Padron photoactivation quantum yield was calculated by analyzing the 504 nm absorption peak decay, upon illumination at 532 nm at low temperature, and upon illumination at 488 nm at room temperature. The obtained values are ~5 x 10^{-6} at low temperature and ~2 x 10^{-4} at room temperature assuming non reversible reaction. We cannot compare directly these two values, because at room temperature the overall reaction to $B_{cis,LT}$ is involved, while at cryo-temperature only the first step of the reaction $B_{trans} \rightarrow I_{cis}$ is involved. Also, as described above for the case of a reversible AB reaction, effective quantum yields may quite strongly differ from the apparent values, depending on the exact reaction

pathway. However, we can propose qualitatively that the chromophore isomerization occurs much more easily at room temperature than at 100 K, in agreement with the simulation results discussed in subchapter 2.2.4 iii.

iv. Watching the protonation of Padron

In Figure 2.27 C, we have shown that when the $B_{cis,LT}$ state is heated to room temperature for a few seconds, its absorption spectrum, with only the anionic band, becomes instantly a spectrum displaying two bands. We suppose that this new absorption spectrum corresponds to the AB_{cis} state, a mixture of $A_{cis,RT}$ (protonated) and $B_{cis,RT}$ (deprotonated), the same states produced upon photoswitching at room temperature. This hypothesis is based on the resemblance between the spectrum obtained in this way and the spectrum shape obtained upon photoswitching at room temperature. Another argument that supports this hypothesis is the fact that low temperature induces a slow down, rather than a change, in the reaction (Moffat and Henderson, 1995; Yang et al., 2011). If, instead of the annealing procedure, a gradual increase of the temperature (6 K/min) is applied in the dark, it is possible to watch the protonation process occurring (**Figure 2.38 A, B**).

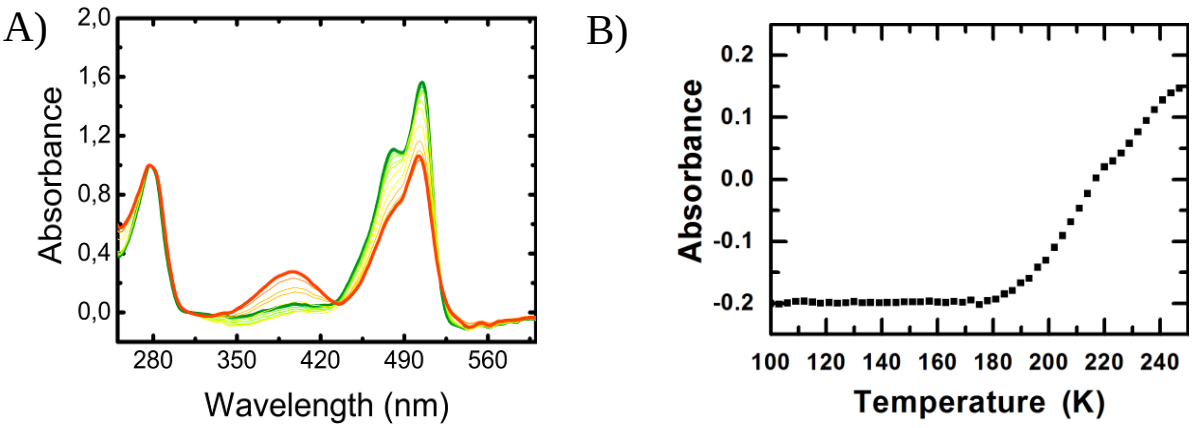

Figure 2.38) (A) Evolution of Padron absorption spectrum during temperature increase (100 K → 240 K), transformation from $B_{cis,LT}$ (green line) into AB_{cis} (mixture of $A_{cis,RT}$ and $B_{cis,RT}$, red line) at ~180K (intermediate spectra shown in thin lines). **(B)** Rise of the absorbance band of the neutral chromophore (at 390 nm) during temperature elevation. The curves are corrected in accordance with the variation of the isosbestic point at 445 nm.

Below 180 K a weak variation in the deprotonated peak is observed. Above this temperature the protonated species appears. This can be associated to the global change of the protein dynamics that occurs at the glass transition temperature (Durin et al., 2009). This is a strong result, because it connects the chromophore protonation step with the release of the bulk solvent freedom at this temperature, also associated with unlocking of protein dynamics.

Agmon and coauthors have described a temperature transition of GFP fluorescence (Leiderman et al., 2006). In their model, the chromophore phenolate proton moves along an unidimensional proton wire inside the protein during the ESPT process (towards Glu222). This behavior is observed at low temperature until a temperature around 230 K. Above this temperature, the proton escapes to the exterior and then moves free in three dimensions. They have attributed this transition to a conformational change in the GFP structure. These effects described by Agmon and coauthors could be linked with our observations. However, the temperature transition measured in their work is 230 K. This may be due to the fact that the transition temperature depends also on the solvent in which the crystal is soaked.

v. Spectroscopic results on solution samples.

The experiments described so far were carried out with crystalline samples. The principal results obtained in crystallo, showed in Figure 2.27, were reproduced in solution samples of Padron (**Figure 2.39**). We could identify the same spectroscopic states along the photoswitching reaction at 100 K, one non-fluorescent state and three fluorescents states (**Figure 2.39 D**). This demonstrates that these states are not specific to the crystalline phase. Overall, the results of the two experiments are consistent with each other. However, there is an exception for the relaxation from I_{cis} to $B_{cis,RT}$ that we will discuss in the following. Considering the model that we applied to crystalline data, we have: B_{trans} undergoes isomerization to I_{cis} and $B_{cis,LT}$ states upon actinic illumination (**Figure 2.39 A**). This is

followed by I_{cis} relaxation to $B_{cis,LT}$ in the ground state (**Figure 2.39 B**). Finally, the AB_{cis} state is obtained by an annealing procedure or by slowly rising the temperature (**Figure 2.39 C**).

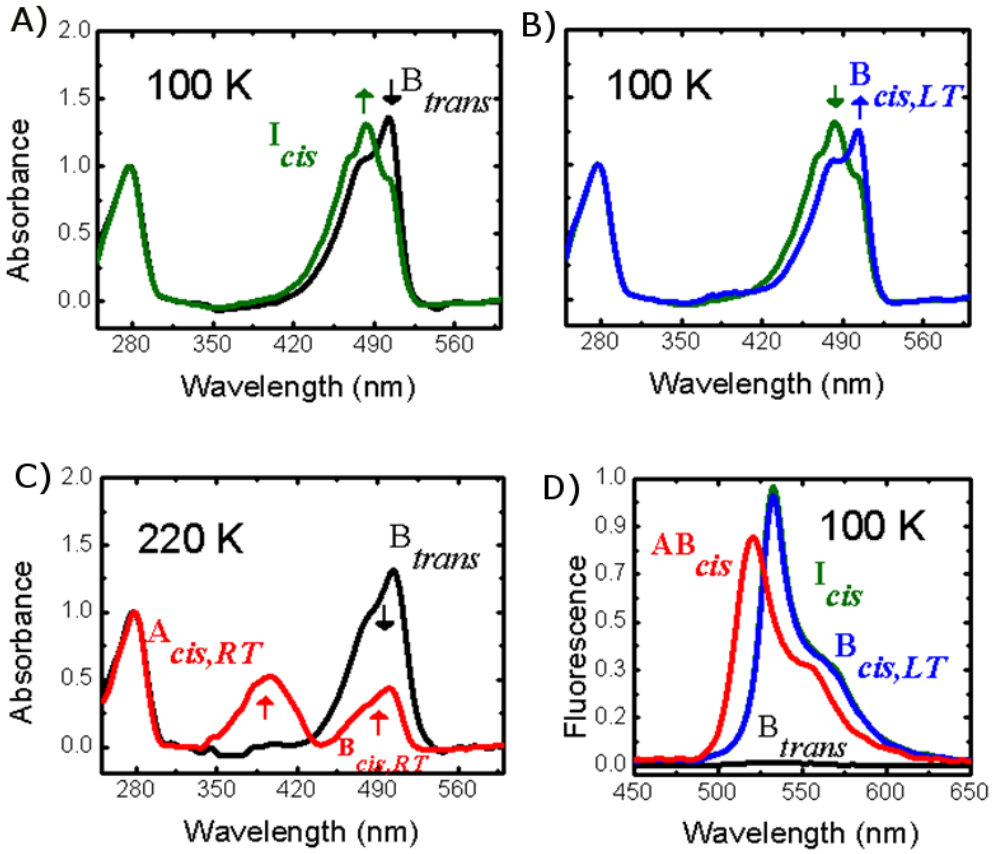

Figure 2.39) (A) Spectroscopic signature of Padron along its off-on photoswitching pathway, recorded in solution samples. **(A, B, C)** Absorbance spectra (**A**) Illumination at 532 nm (1.6 kW/cm^2) at 100 K of the Padron off state (B_{trans}, black line) yields a first intermediate (I_{cis}, green line). **(B)** Spontaneous relaxation of I_{cis} in the dark at 100 K yields a second intermediate ($B_{cis,LT}$, blue line) **(C)** Subsequent annealing procedure (100 K → 240 K) transforms $B_{cis,LT}$ into AB_{cis} (mixture of $A_{cis,RT}$ and $B_{cis,RT}$, red line) **(D)** Corresponding fluorescence emission spectra: B_{trans} (black line), I_{cis} (green line), $B_{cis,LT}$ (blue line) and AB_{cis} (red line). Excitation at 488 nm (2.5 mW/cm^2).

Comparison of I_{cis} relaxation, upon gradual increase of temperature in solution and crystal samples, show a difference in energetic barrier. At 100 K, it was observed that in crystallo the relaxation occurs in about 15 - 30 minutes, while in solution the relaxation is much longer (3 hours). Therefore, one possible explanation is that the activation barrier for this step measured in solution is higher than in crystals. A gradual increase of temperature

(6 K/min) during the relaxation of I_{cis} further highlights this difference between solution and crystalline samples. The experiment consists in following the 390 nm and 504 nm absorption peaks, right after I_{cis} has been produced, upon rising the temperature from 100 K to 230 K. We observe that the protonated band remained almost constant until 200 K, and increases only at the glass transition temperature, as was observed in the crystal experiments (**Figure 2.40**, red squares). Concerning the evolution of the 504 nm absorption peak, we can distinguish three phases (**Figure 2.40**, black cycles): The first one, between 100 – 120 K, where the $B_{cis,LT}$ absorption peak remains practically constant. The second phase, at temperatures above 120 K, where the I_{cis} to $B_{cis,LT}$ transformation occurs, until 200 K. Finally, a third phase above 200 K when this 504 nm peak decays, as a result of the establishment of equilibrium between $B_{cis,RT}$ and $A_{cis,RT}$.

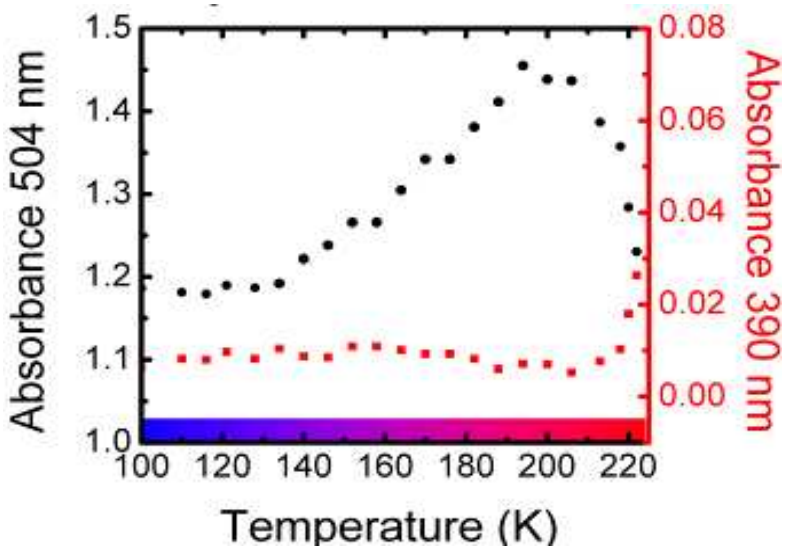

Figure 2.40) Evolution of I_{cis} to $B_{cis,LT}$ and $AB_{cis,LT}$ thermally-induced by a temperature ramp from 100 K to 220 K in solution.

The first phase between 100 K and 120 K is only observed in solution experiments as in crystal, I_{cis} relaxes quite rapidly to $B_{cis,LT}$ at 100 K. This could result from the solvent composition and/or from the difference in viscosity, or even from a conformational selection process occurring in the crystal (see Chapter Material and Methods).

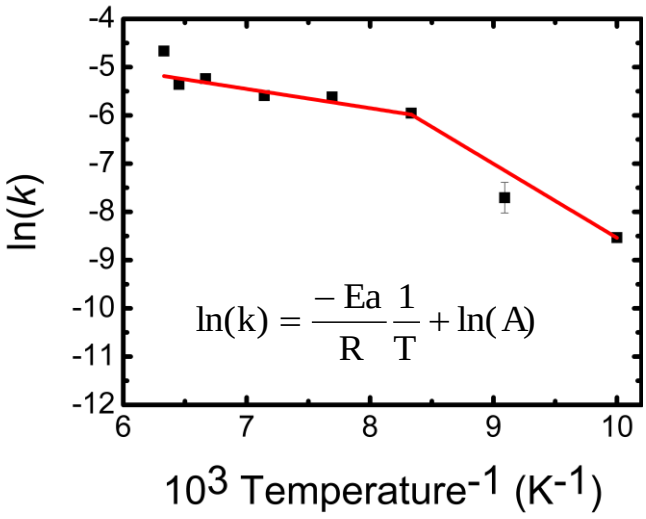

Figure 2.41) Arrhenius representation of the thermally-induced relaxation of I_{cis} to $B_{cis,LT}$ in solution. The logarithm of the relaxation rate $I_{cis} \rightarrow B_{cis,LT}$ is reported as a function of the inverse temperature. The plotted rates k were obtained by fitting the decay of I_{cis} (500 - 507 nm absorbance band) during relaxation in the dark by a mono exponential model. The solid red lines show the slope best fitting the data for two temperature windows where the reaction appears to show a linear behavior.

To estimate the activation free energy barrier separating I_{cis} from $B_{cis,LT}$, we measured the absorption spectral series of spontaneous relaxation from I_{cis} to $B_{cis,LT}$, in the dark at different temperatures using solution samples. For each time-series, the 483 nm absorption decay was fitted by a monoexponential decay model, in order to obtain the value of the rate constant k_2 its thermally activated part. An Arrhenius plot is then produced by the logarithm of k_2 as a function of the inverse temperature (**Figure 2.41**).

According to these measurements, two phases for the relaxation I_{cis} to $B_{cis,LT}$ are observed. The value for the free energy barrier is ~3.8 kJ/mol for temperatures between 120 K - 170 K. That means that above 120 K, the thermally activated term of k_2 becomes influent in the reaction process. We note that this experiment is very difficult to perform because it requires highly reproducible solution sample.

vi. One-photon process

It is important to verify that the reaction presents the same behavior at room and at low temperature, to support the hypothesis that it is the same process. Activation could indeed arise from absorption of one or several sequential photons. If the phenomenon is generated by the absorption of one photon only, the activation rate changes linearly with the applied power density. On the contrary, in the case of two sequential photons, the activation rate will change quadratically as a function of the power density. Therefore, we measured the power dependence of the observed rates at low and at room temperature. Both results show a linear behavior, suggesting one photon process (**Figure 2.42 A** and **B**, respectively). This can be interpreted as an evidence that the photoswitching mechanism in not altered at cryo-temperature, but only slowed down. This result supports the validity of our low temperature approach.

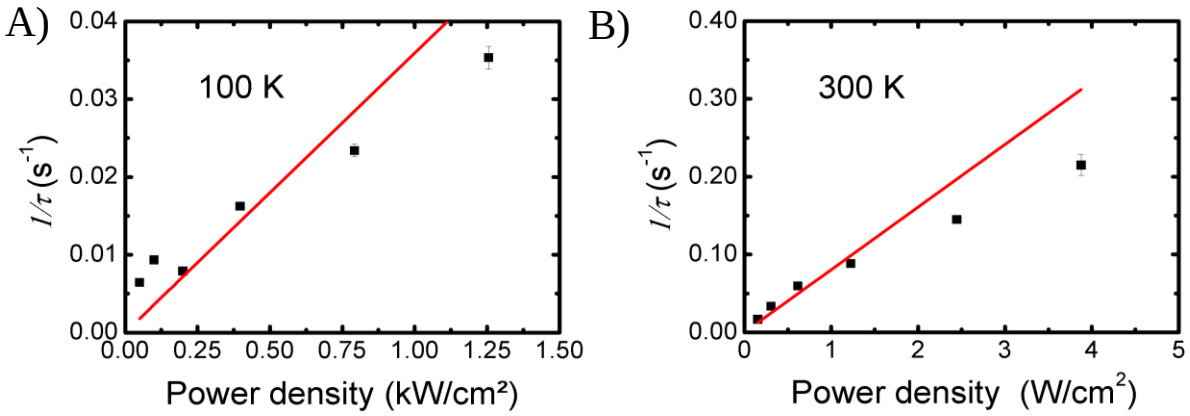

Figure 2.42) Photoactivation of Padron occurs via a 1-photon absorption process at low to room temperature. **(A)** At 100 K, the photoactivation rate reports on the buildup of I_{cis} (actinic laser at 532 nm). **(B)** At room temperature, the rate reports on the buildup of AB_{cis} (actinic laser at 488 nm).

2.2.7 EXPLORING THE PADRON MECHANISM

After having established a possible kinetic model accounting for the photoswitching mechanism of Padron, we will study the influence of some external parameters on photoswitching. In this subchapter, we present how the complexity of the kinetic model results in unexpected behaviors under specific conditions.

i. Effects of the laser power on Padron photoactivation.

We noted that depending on the power of the actinic laser, the intermediate state (I_{cis}) was or was not observed. During photo-activation at low-temperature, the absorbance peak at 483 nm, associated to I_{cis}, can only be seen when the power of the laser is sufficiently high. However, illumination at 532 nm also transforms I_{cis} to $B_{cis,LT}$ and for very high laser powers, again we do not observe the intermediate state anymore. Therefore, the value of the laser power used, in the experiment at 100 K, should be restricted to a specific range of values to visualize I_{cis} in the absorbance spectrum. In the condition of our experimental set-up, the laser power varied between 2 - 20 mW at the focus.

At laser powers below the inferior limit, the result is interpreted by the fact that k_1 becomes < k_2. In order to observe I_{cis}, the laser power should be strong enough to populate the intermediate faster than it relaxes to $B_{cis,LT}$, that is $k_1 > k_2$. At laser powers above the superior limit, the situation is more complex. Both k_1 and k_2 have a photo induced term that rises with the laser power, and k_2 has also a thermally activated term that rises with temperature. It is possible that k_2 rises more than $k_1$due to laser induced heating of the sample (see Annex 2 - SI).

ii. Effects of the temperature on Padron photoactivation.

Upon photoactivation at 532 nm, depending on the temperature, we could observe or not the I_{cis} intermediate state (**Figure 2.43**). The I_{cis} absorption band decreases with the increase of the temperature, to the rise of the thermally activated term in k_2.

This results in $k_1 < k_2$ and the first step of the reaction is not rate limiting. At high temperature, it is thus more difficult to visualize the spectrum of I_{cis}. This is consistent with the fact that at room temperature I_{cis} cannot be observed at all (with our set-up), since $k_2 >> k_1$.

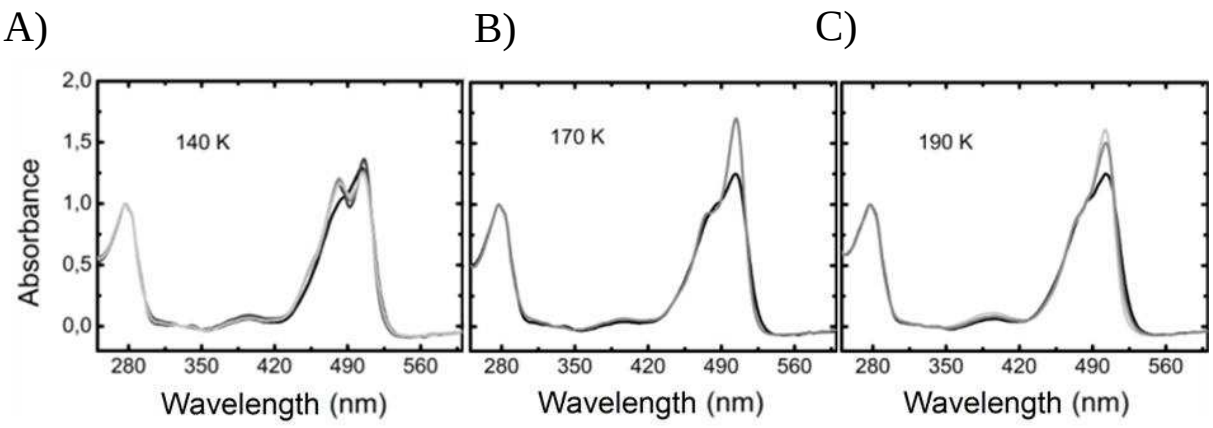

Figure 2.43) Padron photo-activation from B_{trans} (black line) to $I_{cis}/B_{cis,LT}$ (gray lines) **(A)** at 140 K only a little 483 nm band appears **(B)** at 170 K after illumination at 532 nm the band of the intermediate-form increases, note that band produced is thinner than the first one **(C)** at 190 K the deprotonated band increase was observed as well, note that the protonated band starts to grow-up.

By increasing the temperature, the lifetime of I_{cis} becomes shorter. For example at 170 K, the temperature is not sufficiently high to allow protonation, but it is already too high for I_{cis} to be observed. Therefore, the absorption spectral time series displays only the increase of the deprotonated band, which is measurable because the extinction coefficient of $B_{cis,LT}$ is higher than that of B_{trans}. At first glance, this result appeared very strange to us.

iii. Effects of the wavelength on Padron photoactivation.

The usual wavelength used in the microscopy experiments to switch on Padron or switch off Dronpa is 488 nm (Willig et al., 2011), because of the high extinction coefficients at this wavelength. Thus, we expected also an efficient activation of Padron using the 488 nm laser at low temperature this is indeed the case (**Figure 2.44**). However, comparing with the experiment performed at 532 nm, at 488 nm it was impossible to visualize the intermediate state. In fact, Padron activation at cryo-temperature was observed with 532, 523, 514, 488 and 473 nm lasers and I_{cis} appeared only with the less energetic wavelengths 532, 523, and 514 nm.

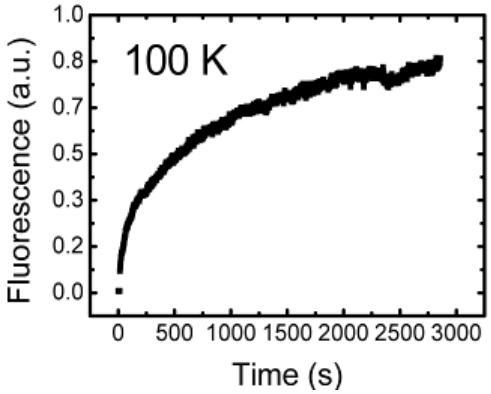

Figure 2.44) Fluorescence emission spectrum of Padron photoactivation at 488 nm at low temperature..

These results are reasonable, regarding the fact that the light-activated parts of the rate constants depend on extinction coefficients. Thus the choice of the actinic wavelength may change the rates, so as to afford $k_1 >> k_2$, so that it is possible observe I_{cis}. However, if the wavelength is chosen so that $k_2 >> k_1$, the observation of I_{cis} is impaired. The spectral overlap between the different states also will critically influence this effect. For Padron's case, the separation between B_{trans} and I_{cis} absorption peaks is relatively small (with maxima at 503 nm and 483 nm). At 473 nm or 488 nm, I_{cis} has a high extinction coefficient, resulting in its fast transformation to $B_{cis,LT}$ (**Figure 2.45**). Therefore, $k_2 > k_1$, and I_{cis} is not observed.

Conversely, at 514 - 532 nm I_{cis} is only weakly light sensitive, whereas B_{trans} and $B_{cis,LT}$ are strongly light sensitive. Thus, $k_2 < (k_1, k_{-2})$ and I_{cis} can be observed. Overall, the wavelength should be chosen according to the goal of the experiment.

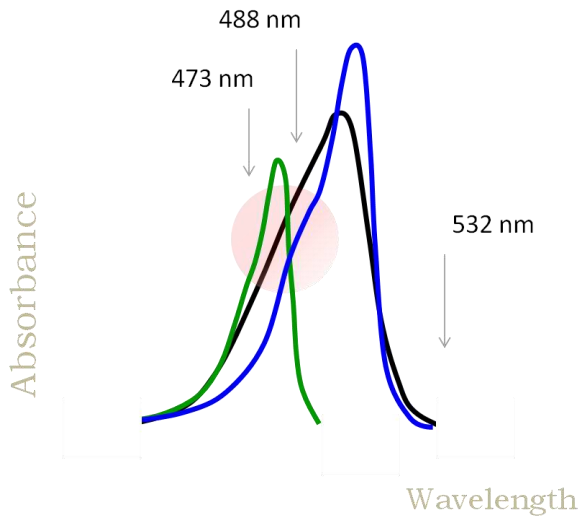

Figure 2.45) Scheme example of the overlapped spectra in Padron's case. Highlighted in the red circle the region where the extinction coefficients of the three states are closer.

2.2.8 PADRON BACK-PHOTOSWITCHING AT 100 K

We are interested to study now the vanishing of the fluorescence emission process, and not only to the first kindling. Careful study of the back-switching reaction at 100 K is needed to complete the photoswitching understanding. The results of the back reaction described below reveal an interesting aspect of Padron properties.

At room temperature, the Padron chromophore thermally switches off in the dark by cis-trans isomerization in 150 minutes, whereas this is almost an instantaneous process, when illumination with 405 nm laser is used (Andresen et al., 2008). Similarly, we could expect that the back-switching is also possible at cryo-temperature, obviously at a lower frequency. In line with this hypothesis, we analyzed how the Padron kinetic model may lead to fluorescence

deactivation. Considering the states B_{trans}, I_{cis} and $B_{cis,LT}$, the two only ways to turn the fluorescence off are: for a particular condition k_{-1} is not negligible; and/or for a particular condition there exists a pathway that directly links $B_{cis,LT}$ to B_{trans} with a rate constant k_{-3} (**Figure 2.46**).

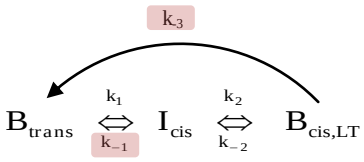

Figure 2.46) Padron kinetic model emphasizing possible back-switching rates to B_{trans} highlighted with red squares.

Evaluating the photo-activated part of k_{-3} is difficult because of the close overlap between $B_{cis,LT}$ and B_{trans} spectra. Evaluating, the thermally-activated part of k_{-3} is also problematic: in view of the relaxation time taken to back-switching Padron at room temperature. Probably at low temperature it would take much more time, if it happens at all, and the unsuitability of the experimental design would not allow to confidently monitor the effect. Thus, our first attempt to switch back the reaction was to evaluate k_{-1} by illuminating I_{cis} at 473 nm.

A crystalline sample of Padron was activated at 532 nm at 100 K to produce the I_{cis} state, followed by illumination at 473 nm to switch back to B_{trans}. The 532/473 nm actinic lasers are alternated and the fluorescence evolution is probed by exciting at 473 nm, a wavelength at which the fluorescence of I_{cis} is enhanced comparatively to $B_{cis,LT}$ due to its higher extinction coefficient at this wavelength (**Figure 2.47**).

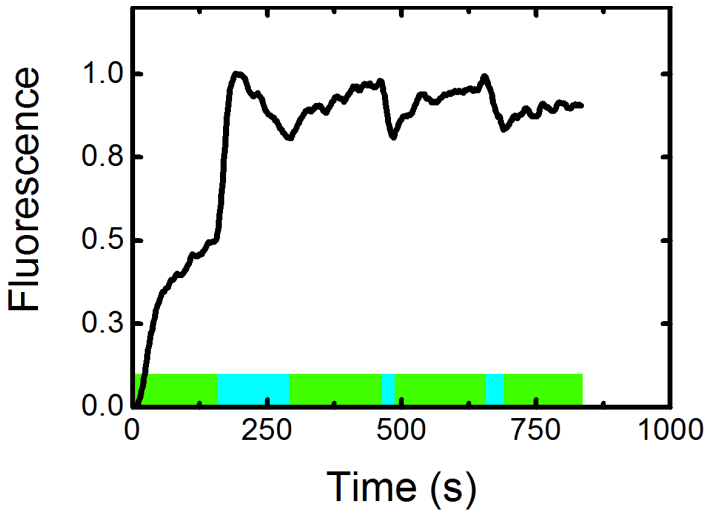

Figure 2.47) Low temperature on and off photoswitching. Activation of the protein is performed at 532 nm (green lines) and back-switching at 473 nm (cyan lines).

Upon 532 nm actinic illumination, the fluorescence increases with the k_1, k_2 and k_{-2} rate constants, following the model $B_{trans} \leftrightarrow I_{cis} \leftrightarrow B_{cis,LT}$. When the laser is changed to 473 nm, the fluorescence evolves with the k_1', k_2', k_{-2}' and k_{-1}' rate constants. The first time 473 nm laser is switched on, we observe a fluorescence rise, followed by a subsequent decrease. This behavior is not reproduced during the subsequent cycles. However, a small fraction of the molecules seem to undergo photoswitching.

Assuming that, after the first illumination at 532 nm, $B_{trans} = 0$ according to our crystallographic results, we do not know how to interpret the fluorescence rise induced by the first illumination at 473 nm. It could however be due to a residual population of B_{trans} chromophore that is efficiently activated by this laser. During the following cycles, the fluorescence oscillation can be explained by a reversible change in the population of I_{cis} and $B_{cis,LT}$. In summary, this experiment does not allow to conclude for a significant value of k_{-1} at 473 nm. In a second experiment, we tried to stimulate back photoswitching by employing further blue shifted light at 405 nm.

Indeed, the photoswitching of Padron was observed by alternating actinic illumination 532/405 nm, even without the protonated band (**Figure 2.48**).

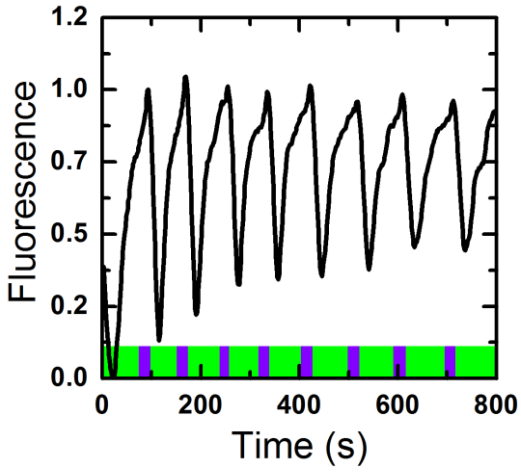

Figure 2.48) In crystallo Padron photoswitching at cryo–temperature (100 K). Activation of the protein is performed at 532 nm (green lines) and back-switching at 405 nm (violet lines) (10 points FFT smoothing).

Upon 532 nm the fluorescence increases and it decreases upon illumination at 405 nm at 100 K in crystallo. Thus, the photoswitching can be performed at low temperatures. However, the profile that the fluorescence emission assumes during laser alternation is quite peculiar. The contrast between fluorescent and non-fluorescent forms is reduced along the cycles. Our model with three states can explain this profile, considering that upon illumination at 405 nm I_{cis} could reversible switching to non-fluorescent state B_{trans}, and concomitantly I_{cis} would be able to undergo to $B_{cis,LT.}$

The model confidence is tested by simulating Padron photoswitching with a Matlab homemade program that takes the rate constants as input. In order to populate I_{cis} during activation phase, we took k_1, $k_{-2} > k_2$, as we have described previously. Because of the fluorescence emission extinction we suggest that B_{trans} needs to be produced during the back-switching, so k_{-1} should be relevant as well as $k_{2.}$ Simulation of Padron photoswitching is shown in **Figure 2.49** and the used rate constants on **Table 2.1**.

Table 2.1) Rate constants used in simulation of Padron photoswitching shown in Figure 4.49

	k_1	k_{-1}	k_2	k_{-2}
switching	0.002	0.000	0.0001	0.001
back- switching	0.010	0.100	0.0150	0.000

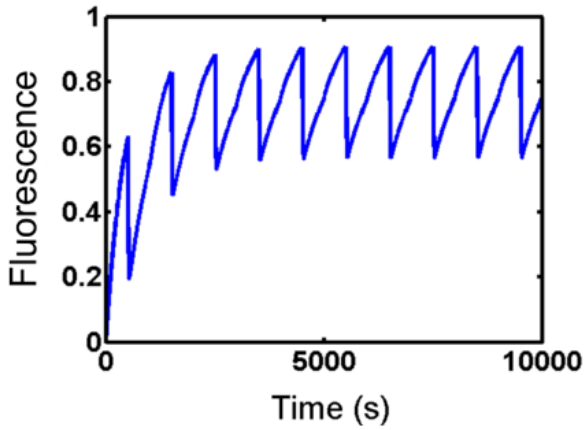

Figure 2.49) Simulation of Padron photoswitching, based on the model $B_{trans} \leftrightarrow I_{cis} \leftrightarrow B_{cis,LT}$ The rate constants are shown on Table 2.1.

The photoswitching was observed for solution samples only above 120 K with attenuated efficiency (**Figure 2.50**). Indeed, we have described that protein energy landscape should differ between solutions and crystalline samples.

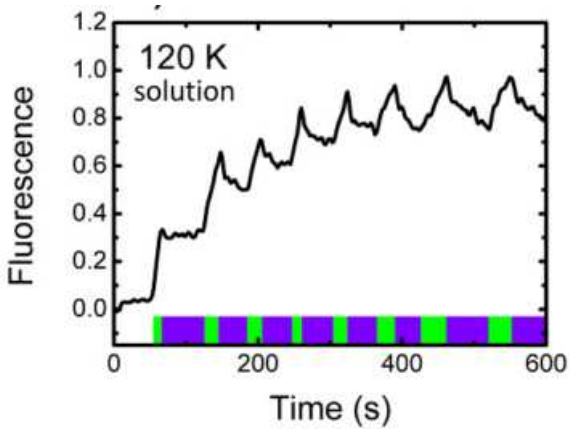

Figure 2.50) Padron photoswitching at 120 K in solution sample. Activation of the protein is performed at 532 nm and back-switching at 405 nm

One possible explanation for the diminished efficiency obtained in solution samples would be that I_{cis} to $B_{cis,LT}$ are fast relative to the conversion of I_{cis} to B_{trans} during the back-switching. That is, in solution experiment k_2 should be higher than that of in crystal. We have simulated this hypothesis and the result is shown in **Figure 2.50** and the rate constants on **Table 2.2**.

Table 2.2) Rate constants used in simulation of Padron photoswitching shown in Figure 4.48

	k_1	k_{-1}	k_2	k_{-2}
switching	0.001	0.000	0.0005	0.001
back- switching	0.010	0.100	0.0200	0.000

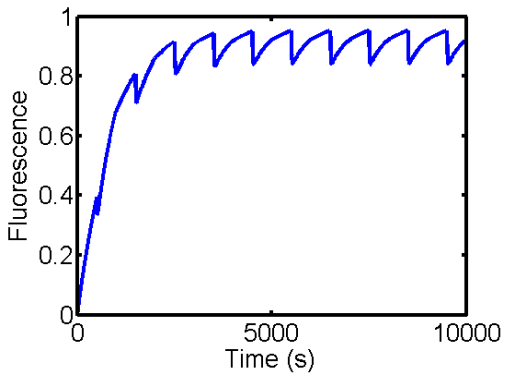

Figure 2.51) Simulation of Padron photoswitching, based on the model $B_{trans} \leftrightarrow I_{cis} \leftrightarrow B_{cis,RT}$ The rate constants are shown on Table 2.2.

2.3 EITHER PHOTOISOMERIZATION, PHOTOPROTONATION OR DEHYDRATION ARE IMPLICATED IN THE SWITCHING

2.3.1 SUBCHAPTER OUTLOOK

The photoswitching behavior in fluorescent proteins has allowed to go beyond the classical microscopy limit. Recent advances in understanding the photoswitching mechanisms have shown potential aspects that can be explored to develop more performant variants in the future. In this chapter, reversible photoswitching is discussed, first focusing on structural aspects and then on kinetic features. Some preliminary experiments are shown in order to illustrate the dissertation. The framework presented here may be of interest to fluorescent protein imaging applications and also for fundamental research about dynamics of proteins.

2.3.2 PHOTOSWITCHING MECHANISMS

Understanding the fundamental mechanism that allows a fluorescent protein to be reversibly photoswitchable could give the key to further control this property. However, there is not a single one but various mechanisms that may confer photoswitching to a fluorescent protein. The essential features involved are: cis-trans isomerization of the chromophore, protonation of the chromophore hydroxybenzylidene moiety, and dehydration/hydration of the chromophore imidazolinone ring. Although various mechanisms are known to exist, there are similarities between them. Structurally, they all involve a temporary distortion of the chromophore to a non-fluorescent conformation. Kinetically, the achievable photoswitching speed and contrast depend on the intrinsic on/off switching quantum yields and on the presence of putative intermediate states along the photo-pathway. They also depend on extrinsic parameters such as laser power, laser wavelength, temperature or pH.

2.3.3 STRUCTURAL POINT OF VIEW

i. Isomerization of the chromophore

Reversible cis-trans isomerization of the chromophore is the most prominently observed structural manifestation of photoswitching in RFSPs. In solution, the p-HBI synthetic chromophore undergoes rapid cis-trans isomerization that requires low energy to occur (Voliani et al., 2008). This mechanism works as an efficient radiationless deactivation pathway to release absorbed energy, resulting in very low fluorescence yield (Mandal, Tahara, & Meech, 2004; Weber et al., 1999). Although chromophore isomerization is an intrinsic mechanism, the tendency to isomerize inside the β-barrel is generally considerably lower due to a much reduced conformational freedom of the chromophore (Maddalo & Zimmer, 2006). However, under certain configurations, the tendency to isomerize remains high and competes with the ability to fluoresce (Olsen and McKenzie, 2009). This can explain the weak or strong fluorescence in various isomer conformations of a single FP.

To date, whenever cis-trans isomerization has been invoked to account for photoswitching, the trans isomer has been found to be associated to the non-fluorescent form and the cis isomer to the fluorescent form. Although the two isomeric states (cis and trans) provide two completely different networks of electrostatic interactions for the chromophore, this is usually not sufficient to account for the difference in fluorescence brightness between these two states. There is an ensemble of conditions that is able to affect the fluorescence emission: chromophore planarity, rigidity, protonation state, potential ESPT pathways, and tendency to isomerize. Empirical proposals were made to quantify the ability of an anionic chromophore to fluoresce, depending on the tilt and twist angles between the cyclic moieties (Brakemann et al., 2010). Excited-state molecular dynamics can be a useful tool to monitor

chromophore torsion upon photon-excitation, which directly relates to fluorescence quantum yield.

Many mutations in the amino acid residues close to the chromophore can be rationally designed to assist the isomerization of the chromophore. Bizzari et al. have shown that a single mutation of glutamate E222 by a glutamine residue turns some GFP derivatives into RSFPs (Bizzarri et al., 2010). E222 is the final acceptor in the ESPT pathway in GFP. Altering this pathway may promote isomerization to become an important channel for deactivation. In these E222Q GFP-variants, as in other RSFPs, both switching and back-switching can be photo-induced. Back-switching can also occur via thermal relaxation. In turn, back and forth switching can be induced in the ground state via pH titration (Bizzarri et al., 2010). Despite the structural and spectral similarities between the photo-induced and pH-induced non-fluorescent forms, these species differ, similar to what was shown with Dronpa using ultrafast spectroscopy (Fron et al., 2007). The results of the experiments carried out with E222Q variants allowed to propose that the chromophore populates both isomeric conformations: cis and trans and that it also exhibits an anionic and a protonated state for each conformation (Bizzarri et al., 2010). In collaboration with the Prof. Ranieri Bizzarri, we solved the molecular structure of the photo-switchable yellow variant EYQ1, containing the E222Q mutation (see Material and Methods Chapter 4.5.4). Although we have obtained the chromophore in cis configuration at high resolution (**Figure 2.52**), a detailed structural analysis was not pursued since we could not obtain the trans structure in similar crystallization conditions.

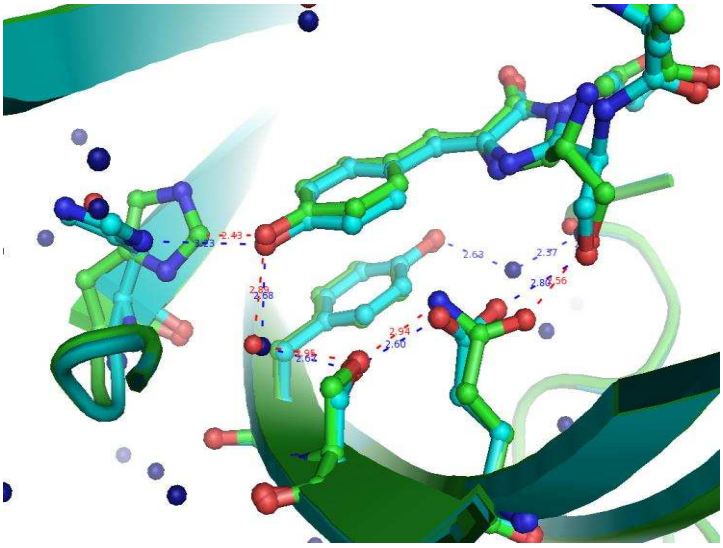

Figure 2.52) Comparison of crystal structures of EYQ1 (E222 – cyan) and the variant Q222 (green). The H-bonds are represented with dashed lines (E222 – blue) and (Q222 –red). The reduced amount of water molecules in the variant Q222 could be due to the lower resolution.

We can emphasize two structural points about crystalline EYQ1. First, we could not efficiently photoswitch the crystal, and we observed the chromophore in the cis configuration after actinic illumination. However, the crystallization conditions resulted in halides molecules docking into the β-barrel close to the chromophore, similar to what was observed with YFP (Wachter, Yarbrough, Kallio, & Remington, 2000). The presence of halide molecules positioned in the region normally occupied by the chromophore in its trans conformation reduces the efficacy of EYQ1 photoswitching. This strongly suggests, although indirectly, that cis-trans isomerization is indeed involved in EYQ1 switching. Second, in our structure, His148 appears to populate two conformations that may hint at the structural rearrangement that allows the switching. Nevertheless, further structural studies need to be done to understand EYQ1 photoswitching structurally, preferably with crystals grown in the absence of halides molecules.

Recently, Grotjohann et al. introduced to the scientific community a new RSFP named rsEGFP (Grotjohann et al., 2011). It is a GFP variant carrying five mutations, although only one mutation (Q69L) seems to be essential to confer photoswitching. The crystal structure is

not yet published, but based on the GFP structure (Shinobu et al., 2010) the region where the glutamate is located seems to be a strategic position to modulate chromophore twisting. Mutating the long side chain of a glutamine by the shorter side chain of a leucine release some space for easy cis-trans isomerization of the chromophore (**Figure 2.53**). Of course, the interactions between the chromophore and the other mutated amino acids also play important roles in making rsGFP efficiently photoswitchable.

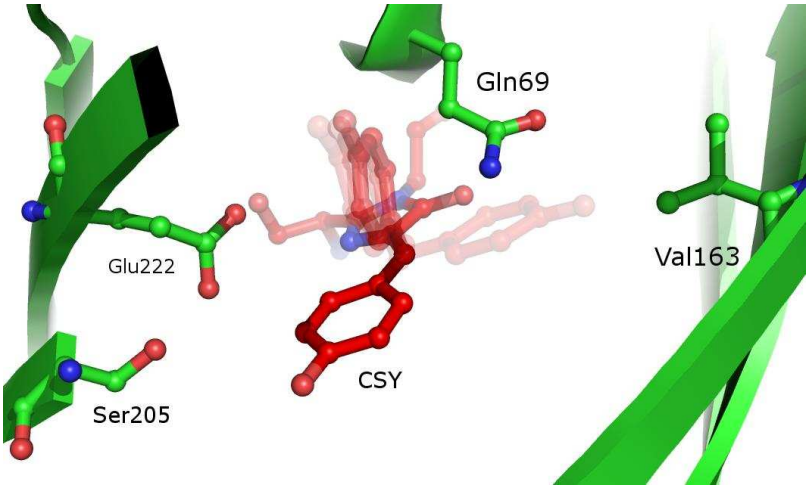

Figure 2.53) Illustration of the hypothetic chromophore twisting into GFP cavity, where the Gln69 residue can probably disfavor the isomerization mechanism. The Glu222 and Ser205 are put as reference and the Val163 is another mutated residue to Ser in the rsGFP. GFP structure from PDB 2WUR (Shinobu et al., 2010).

The common point between EYQ1 and rsGFP is that they extend cis-trans isomerization of the chromophore as a photoswitching mechanism to the Hydrozoan FPs (Bizzarri et al., 2010; Grotjohann et al., 2011). This mechanism so far had only been observed in Anthozoan FPs (Ando et al., 2004) to the Hydrozoan FPs (Bizzarri et al., 2010; Grotjohann et al., 2011). However, we note that so far a direct structural proof of cis trans isomerization is lacking in these two proteins.

Chromophore isomerization has generally been observed coupled with chromophore protonation (Andresen et al., 2005, 2007; Subach et al., 2010c). Our work on Padron suggested that isomerization may be the driving event leading in a second step to

chromophore protonation. However, photoswitching may also result from the process of direct photo-induced protonation.

ii. Photo induced protonation

Shaner et al. have shown that several fluorescent proteins exhibit a partial switching behavior induced by illumination (Shaner, Lin, McKeown, et al., 2008). These results were obtained in cells expressing the proteins or directly in protein solutions by laser scanning confocal microscopy. The fluorescence decays upon actinic illumination and a partial recovery occurs after a period without illumination. These results resemble those obtained by Sinnecker et al. (Sinnecker et al., 2005) in experiments carried out with eYFP, Citrine, eCFP and eGFP. Although cis-trans isomerization has been suggested to explain the partial photoswitching (Weber et al., 1999), there are some observations that go against this hypothesis. First, this group of proteins exhibits weak switching contrast compared with the RSFPs. Second, in the Protein Data Bank, no structure of trans isomers is found for these proteins. We can analyze further the eYFP case because it has been extensively studied in the literature and also because we worked with this protein (see Chapter Results and Discussion 2.1).

We have suggested that the mechanism of eYFP photoswitching involves only a small structural rearrangement, because the cryo-temperature does not prevent switching, but on the contrary enhances it. However, a clear protonation of the chromophore is observed spectroscopically, and thus we call this mechanism photo-induced protonation. In contrast, in RSFPs for which chromophore isomerization has been confirmed, such as Dronpa, IrisFP or even Padron, the switching efficiency is considerably reduced at low temperature. We obtained structural hints that photoswitching in eYFP is probably not associated to chromophore isomerization. Two crystal structures were solved for eYFP, one after

illumination and another at low pH, at resolutions of 1.8 Å and 2.3 Å, respectively. After 5 minutes of illumination at 523 nm (100 mW/cm^2) at room temperature, the crystal was flash-cooled. The molecular structure shows that the chromophore is in cis conformation and that the residue Glu222 does not interact directly with the imidazolinone ring. A similar eYFP conformation is obtained also at low pH condition (3.6) (see Material and Methods Chapter 4.5.4). This rearrangement of Glu222 as compared to the structure at physiological pH is consistent with the reorganization of the hydrogen bond network linking the hydroxybenzylidene moiety of the chromophore to the glutamate, suggesting the formation of a neutral (protonated) chromophore. Therefore, our data suggest that chromophore isomerization is not the mechanism responsible for eYFP photoswitching. However, it cannot be excluded that cis-trans isomerization events occur, but are too rare to be detected structurally (**Figure 2.54**).

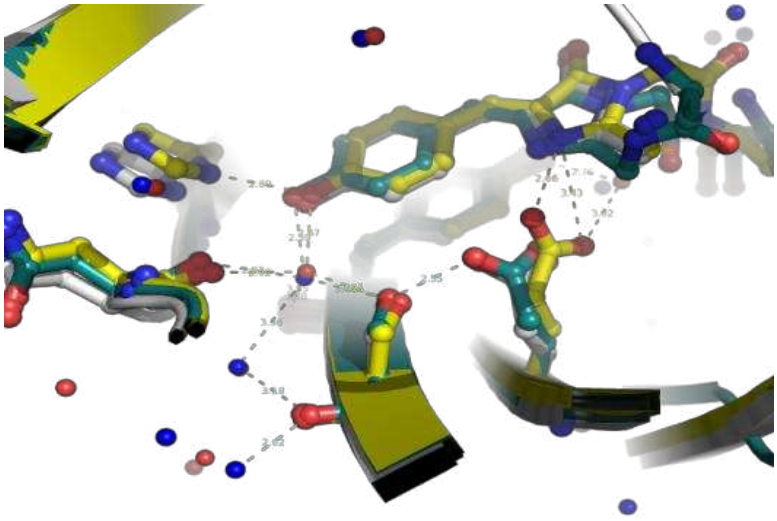

Figure 2.54) Comparison of crystal structures of EYFP: 1YFP from PDB (Wachter et al., 1998) at pH 7.5 (yellow); low pH-protonated at 3.6 (A1 - white) and photo-induced protonated (A2 - blue). The H-bonds are represented with dashed lines for A1 and A2 (blue) and for 1YFP (yellow).

Following in the text, we describe the RSFP Dreiklang, a variant from Citrine that in turn is an eYFP variant. Dreiklang photoswitching is based on photo-induced dehydration and

hydration of the chromophore. To the small differences between these proteins, there is the possibility that the photoswitching mechanism detected in eYFP is similar to that of Dreiklang.

In conclusion, we speculate that the mechanism responsible for partial photoswitching in eYFP involves protonation of the chromophore followed by a structural rearrangement that is not chromophore isomerization, and is small in amplitude. Some implications of a partial photoswitching behavior can be predicted by a kinetic model discussed in the next chapter.

iii. Imidazolinone-ring hydration ("Dreiklang mechanism")

Brakemann et al. (Brakemann et al., 2011) engineered a new fluorescent protein, called Dreiklang. This innovative protein exhibits on and off-switching with alternated actinic light completely decoupled from the excitation light. This protein is a variant of Citrine obtained by the following mutations: V61L, F64I, Y145H, N146D. The design of Dreiklang started with extensive random mutagenesis, in order to enhance this "decoupled" behavior, which was somewhat already exhibited by eYFP and Citrine (McAnaney et al., 2005). Dreiklang switches off efficiently upon illumination at 405 nm and switches on upon illumination at 365 nm. Fluorescence emission is excited at 515 nm, at a much lower energy wavelength. Upon 405 nm illumination, an absorption band develops at 340 nm, allowing back switching to the fluorescent state upon illumination of this band. The proposed photoswitching mechanism is based on the chromophore distortion caused by the hydration and dehydration of the C_{65} atom of the imidazolinone ring (Dreiklang numbering). In its bright form, the protein adopts a structure similar to that of other yellow fluorescent proteins. There is a water molecule (Wat_a) that stabilizes the C65 and consequently the imidazolinone in the fluorescent form of the chromophore is planar. Upon 405 nm illumination, this water

molecule is used to hydrate the imidazolinone, inducing a non-planar tetrahedral geometry (**Figure 2.55**).

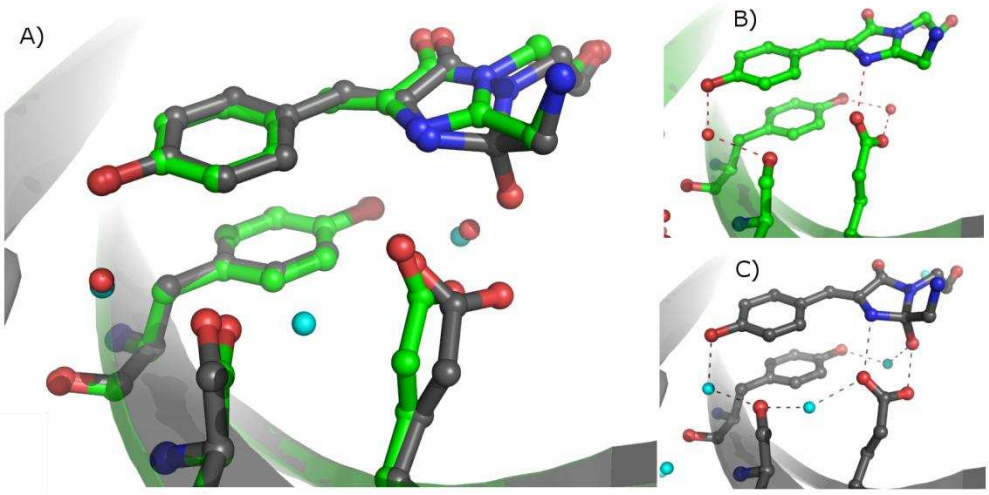

Figure 2.55) (**A**) Dreiklang structure PDB 3ST2 and 3ST3 (Brakemann et al., 2011), fluorescent state in green cartoon and non fluorescent state with the tetrahedral geometry of the imidazolinone ring (gray cartoon) (**B**) fluorescent state and the interaction between the residues (**C**) non fluorescent state and the interaction between the residues.

The Dreiklang behavior offers several advantages for imaging applications. The decoupling of excitation and actinic wavelengths allows to maximize the photon-output during image acquisition, since the readout laser does not induce switching prematurely like in other negative RSFPs. Dreiklang is therefore a promising prototype of a new generation of RSFPs.

2.3.4 KINETIC POINT OF VIEW

It has been demonstrated in the literature that several "standard" fluorescent proteins are subject to partial photoswitching (Shaner, Lin, Mckeown, et al., 2008).

Photoswitching behaviors have also been noticed in PCFPs, which typically exhibit an irreversible green to red photo-conversion. For example, this is the case of mEos2 (Annibale et al., 2010) and of proteins derived from IrisFP. In the case of mEos2, single molecules

experiments by Annibale et al have shown that a non-negligible fraction of supposedly bleached molecules recover their fluorescence upon illumination at 405 nm or thermal relaxation, like RSFPs. This effect can be the cause of clustering artifacts in PALM experiment. Alternatively, residual photoswitching (or long lasting blinking) can be used to advantage, such as in the case of dark state shelving strategies proposed by Moerner and co-authors (Lew et al., 2011)

Based on our learned experience with photoswitching of eYFP and Padron, we discuss below some consequences of partial photoswitching in FP behavior, with a kinetic point of view. This residual photoswitching can be the cause the artifacts, such as in the case of mEoS2, but it can be used as advantage, such as the case of Moerner and co-authors described following.

i. Power- dependent active intermittency

Moerner and co-authors (Lew et al., 2011) have used partial fluorescence recovery after illumination of eYFP to improve the resolution of fluorescence microscopy. They call the technique "super-resolution by power-dependent active intermittency" (SPRAI). Partial photoswitching provides sufficient active control to reduce the concentration of fluorophores, as needed to achieve super-resolution imaging. In addition, the molecules temporarily shelved into a reversible dark state are protected against photobleaching. The population of shelved molecules increases with high intensity laser pumping. The authors characterized the eYFP behavior through bulk solvent experiments, which allowed them to choose the appropriate laser power to perform photoswitching at the single molecule level. In their experiment, the fluorescence emission decreases during 0.5 seconds of illumination at 480 nm and a partial population of the molecules recovers its fluorescence during 1 second without illumination. This eYFP behavior is similar to that first observed by Miyawaki (Miyawaki & Tsien, 2000)

and Sinnecker et al (Sinnecker et al., 2005) and further described by Shaner (Shaner, Lin, Mckeown, et al., 2008). The mechanism responsible for this eYFP partial switching is accurately fitted by a three-states model. The long-lived dark state has a lifetime which is longer than most triplet lifetimes and, for this reason, cannot be considered a common triplet state. Rather, it could be the photo-induced protonated state described earlier in this thesis.

Based on Moerner's experiment, let's create a hypothetic kinetic scheme to illustrate the influence of power-dependent active intermittency. The simulated experiment consists in following the evolution of eYFP emission upon alternating periods with illumination at 488 nm and periods without illumination, at room temperature. Our model is only valid at the ensemble level. We assume a system with three states: a fluorescent state B that can be converted to a reversible dark state A, but that can also bleach to an irreversible dark state D. The rate constants of the reaction are k_1, k_{-1} and k_2.

$$D \xleftarrow{k_2} B \underset{k_{-1}}{\overset{k_1}{\rightleftharpoons}} A$$

Assuming first-order kinetics, the evolution of B is described by the following differential equation:

$$\frac{dB}{dt} = k_{-1} \cdot [A] - (k_2 + k_1) \cdot [B]$$

At physiological pH, we assume that B represents the fluorescent anionic state, and that the initial concentrations are [B] = 100%, [D] = 0% and [A] = 0%. Consequently in the absence of illumination k_1 and k_2 are equal to zero. Moreover, we suppose that in the absence of illumination the rate constant k_{-1} is 0.05 s^{-1}, based on the relaxation rate constant after partial switching observed in eYFP (Sinnecker et al., 2005) and in our observations.

Upon illumination, the rate constants k_1 and k_2 depend on actinic illumination:

$$k_{1,2} = \Phi_{1,2} \cdot P_D \cdot \frac{\lambda}{hc} \frac{\varepsilon_\lambda \cdot \ln 10}{N_{AV}}$$

where ϕ is the quantum yield, P_D is the power density, λ is the actinic wavelength, h is the Planck constant, c the velocity of light, N_{AV} the Avogadro's number, and ε_λ is the extinction coefficient at wavelength, λ.

The extinction coefficient of A at 488 nm is very close to zero. For this reason, we consider that k_1 is light independent. The extinction coefficient of B at 488 nm is approximately 42000 $M^{-1}cm^{-1}$. We suppose that the photobleaching quantum yield is equal to 10^{-6}, based on typical bleaching yields of fluorescent proteins (Dickson et al., 1997). The off-switching quantum yield is taken to be $1.5x10^{-6}$, based on our calculus at room temperature (see Results and Discussion Chapter 2.1.3 iii). It is known that for very high intensity of illumination, rate constants may change in a non-linear way. Our model is thus only valid for moderate intensities, at which reaction rates change linearly. The laser power and the final rate constants used in the simulation are shown in **Table 2.3**. We observe different levels of partial switching depending on the laser power used for actinic intermittent illumination (**Figure 2.56**).

Table 2.3) Rate constants values of a hypothetic experiment performed with eYFP

	P(W/cm²)	**$k_1(s^{-1})$**	**$k_{-1}(s^{-1})$**	**$k_2(s^{-1})$**	**$N_{DARK}/N_{UNBLEACHED}$**
(i)	25	0.015	0 .05	0.009	0.001
(ii)	500	0.296	0.05	0.197	0.033
(iii)	3000	1.777	0 .05	1.185	0.470

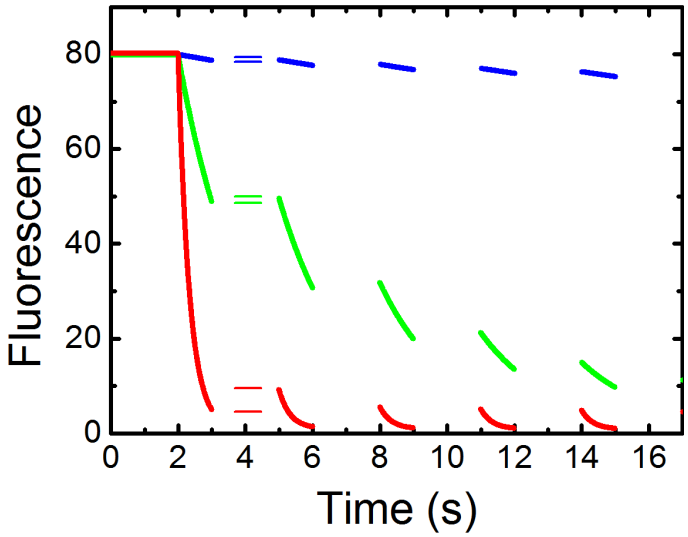

Figure 2.56) Simulation of eYFP switch alternating between with and without illumination **(i)** fluorescence evolution associated to weak power intensity illumination (25 W/cm² - blue) **(ii)** fluorescence evolution associated to medium power intensity illumination (500 W/cm² - green) and **(iii)** fluorescence evolution associated to high power intensity illumination (3 kW/cm² - red). The reversible fraction recovered from the dark state during the first cycle is denoted by horizontal lines.

We note that both photoswitching and photobleaching increase with laser power. To conclude, the laser intensity used in spectroscopy experiments at the single molecule or at the ensemble level needs to be carefully chosen, because it can alter the FP behavior if the latter is able to switch. To prevent artifacts due the partial photoswitching, it is recommend to reduce the used power density. In contrast, if the aim of the experiment is to take advantage of photoswitching, it is recommended to increase the laser power.

ii. Time- dependent active intermittency

For long imaging experiments, photo-stability is a crucial characteristic (Shaner, Steinbach, & Tsien, 2005). **Figure 2.57 A** shows a simulated photo-bleaching experiment with a non photo-switchable fluorescent protein, where the gray area is proportional to the number of photons collected. To increase the imaging time, it is possible to insert intervals

without illumination (**Figure 2.57 B)**. However, the temporal resolution is damaged because no information can be collected during the blind periods.

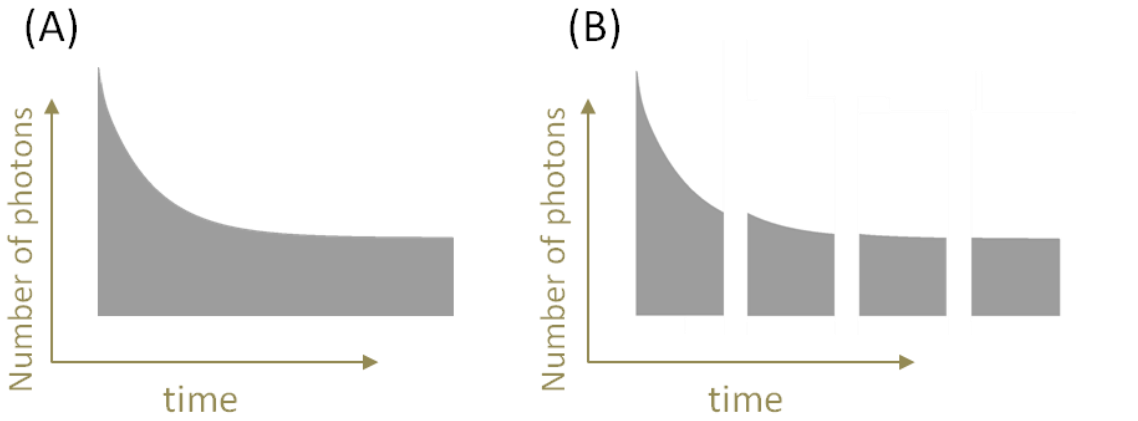

Figure 2.57) Scheme about the fluorescence emission collected during the time **(A)** Upon continuous illumination and (**B**) with interval without illumination.

However, if the same experiment is performed with a photo-switchable protein, there can be an advantage in spreading data collection time in this way. The intervals between illumination periods can be used to recover molecules that are shelved (but not irreversibly bleached).

In **Figure 2.58,** we simulate the effects obtained with 1 s of illumination alternate with different time intervals without illumination (continuous, 2 s; 4 s; 8 s; 16 s; 32 s and 64 s). We use the same kinetic model as in the last paragraph: a bright state (B) interconverts to a reversible dark state (A) or to an irreversible dark state (D). The reactions were simulated with the same inputs as those used in Figure 2.56 (green line: k_1 = 0.296 s^{-1}; k_2= 0.197s^{-1}; k_{-1} = 0.05 s^{-1}). Total time of actinic illumination is 5 s for all experiments, only the period without illumination changes. The area upon actinic illumination is measured and plotted in function of the period without illumination. It can be seen that when the interval without illumination is long, the area measured is bigger. The optimal situation is obtained when the interval without illumination is close to the dark-state relaxation time.

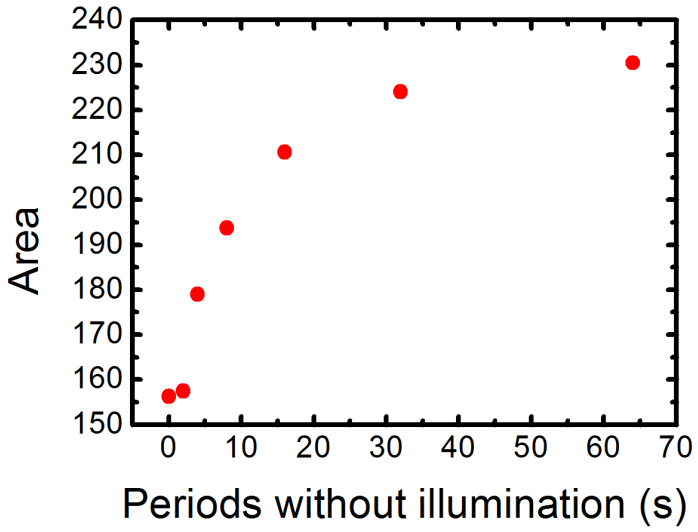

Figure 2.58) Total area measured as a function of different periods without illumination. Illumination pulse is equal 1 second applied five times.

Experimentally, the rate of relaxation of the dark state can be measured by first switching off the sample and then collecting the fluorescence increase after different dark time intervals. We carried out this experiment with Citrine (**Figure 2.59**).

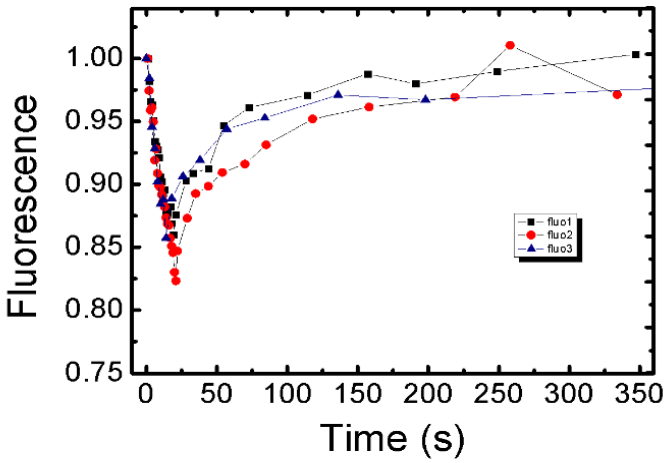

Figure 2.59) Exposure of Citrine sample at 405 nm followed by thermal relaxation recovery at room temperature. Similar experiment reproduced three times with different samples.

In this experiment, the sample was illuminated during 20 seconds with a 405 nm laser (1 W/cm²) and the amount of recovered fluorescence was measured at different times. We obtained consistent results using three different samples. Fitting by a kinetic monoexponential

model yields $\tau = 45$ s in conformity with the value found by Sinnecker, eYFP and Citrine $\tau = 54$ s and $\tau = 25$ s respectively (Sinnecker et al., 2005). The experimental reproducibility suggests that the collected data are not property of a particular sample.

Indeed the photoswitching can aid to improve the number of photons collected per unit time is shown in **Figure 2.60**, using the same conditions as those of Figure 2.56 (red line: $k_1 = 1.777\ s^{-1}$; $k_2 = 1.185\ s^{-1}$, $k_{-1} = 0.05\ s^{-1}$). It can be seen that higher number of photons can be collected per unit time than when alternate illumination is used. The photons missed during the intervals without illumination (**Figure 2.60 area gray, a**) are more than compensated by the fluorescence recovered (**Figure 2.60 hatched transparent area, b**).

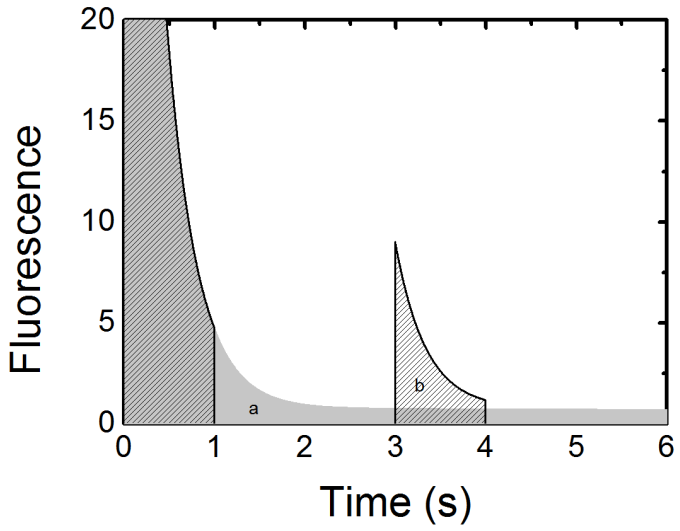

Figure 2.60) Simulation of eYFP photobleaching upon continuous illumination (gray area) and with periods (2 s) without illumination (hatched area).The gray area **a** represent the photons missed during dark period (2.84) and the hatched transparent area **b** represent the photons gained with the fluorescence recovery (2.98).

Furthermore, the observed behavior depends not only on of intervals without illumination, but also on the intervals upon actinic illumination. In the next simulation, we show the effects of changing the alternation time from 1:1 s to 2:1 s (**Figure 2.61**).

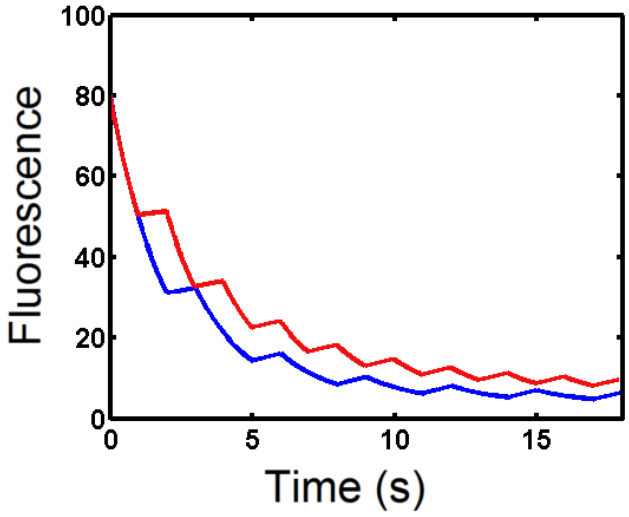

Figure 2.61) Simulation of eYFP photobleaching using as input the same rate constants for both reactions (similar to Figure 2.56 laser power ii), changing only the time interval with and without illumination from 1 s and 1 s (red line) to 2 s and 1 s (blue line).

Shaner et al. in their partial photoswitching experiment have observed nearly 100% recovery after very short periods of bleaching, and whereas less recovery could be achieved after longer periods (Shaner, Lin, Mckeown, et al., 2008). Our hypothesis about the influence of time interval with and without illumination on the recovered fraction is consistent with their findings. To properly use the described strategy, it is recommended to precisely evaluate the photobleaching and the photoswitching kinetics of the reaction.

To conclude, power-dependent active intermittency can be employed together with time-dependent active intermittency to alter the photo-physical behavior of reversibly photoswitchable fluorescent proteins.

2.3.5 ENDPOINTS

i. Cryo-nanoscopy

In the two Results chapters, eYFP (2.1) and Padron (2.2), we have detailed the behavior of two fluorescent proteins that are able to photoswitch at low temperature. Although their cryo-photoswitching quantum yield is low compared to the typical switching yield of RSFPs at room temperature, our findings are a first step forwards a new super-resolution branch: **cryo-nanoscopy**.

The cryo-nanoscopy consists in super-resolution imaging microscopy, which is optical imaging at a resolution of a few tens of nanometers, and at a temperature of 80-100 K via liquid or nitrogen gas. In this aim the development of fluorophores photo-activated at cryo-temperatures, such as Padron and eYFP, is essential. Despite of the implementation of cryo-nanoscopy requires more sophisticated set-up than conventional microscopes, several expected advantages (described below) have prompted us to investigate cryo-photoactivated FPs in order to make this technique available.

Remarkable numbers of experiments in PALM imaging are performed using fixed cells (Betzig et al., 2006; Lee et al., 2011; Kopek et al., 2012). Several factors, such as chemical composition of fixation products and time of fixation, can induce harmful effects on the structural organization of cells during cell fixation, especially at the scale of a few tens of nanometers. In contrast, the cryo-fixation is a less offensive technique, based on the rapid water vitrification into crystalline state, **preserving the structural integrality of cells** (Hurbain and Sachse, 2011). In addition, the cryo-fixation of cells can allow to cryo-trapping a specific biologic state of the cell dynamic, similar as in the crystallography experiments.

The vitrified samples can be used both for fluorescence and cryo-electron microscopy, which is the aim of correlative microscopy (Carlson and Evans, 2011). Another advantage of the cryo-nanoscopy is that at low temperature, both photo-bleaching and cellular damage are reduced (Bouchet-Marquis and Hoenger, 2011). Improving the photo-stability of the fluorophore leads a higher number N of collected photons per fluorophore, which results in better single molecule localization (localization error proportional to $1/\sqrt{N}$). Thus, it is expected an **improvement of the spatial resolution** due the low temperature experiment.

Furthermore, reduction of conformational dynamics of the fluorophore by lowering the temperature has been shown to improve the quantum yield (Abbyad et al., 2007). The cryo-nanoscopy can also take advantage of the quantum yield improvement **to extend the number of the chromophores available to the imaging experiments**.

ii. Parameter- dependent active intermittency

Many parameters induce alterations in the photoswitching behavior, such as pH, viscosity, or, as we have seen before, temperature or photo excitation pattern. Understanding how photoswitching is influenced by all these parameters is important to characterize the FP behavior, to prevent artifacts or to enhance imaging experiments. In this chapter, we have presented some cases where the laser power density, and/or the on- and off- exposure time have allowed to modify the photoswitching pattern. The influences of the physical parameters discussed here could be combined together, as well as with other parameters not discussed here, for example pH (Bizzarri et al., 2010; Hendrix, Flors, Dedecker, Hofkens, & Engelborghs, 2008; McAnaney, Shi, et al., 2005). Together with fluorescent protein engineering, the approach described here could aid to improve the super-resolution microscopy field.

Chapter 3

CONCLUSION AND PERSPECTIVE

3.1 GENERAL CONCLUSION

We have presented the study of switching mechanisms focused on the photo-physical behavior of two fluorescent proteins, eYFP and Padron. The experiments were performed using kinetic X-ray crystallography combined with optical spectroscopy, methodology previously developed in our laboratory. Here, we have introduced an innovation in this method, working with fast detection, in order to obtain a short-time-averaged molecular structure. Experiments performed at cryotemperatures (≈100 K) were an important feature of this work. This approach has proven to be a good strategy to slow down the photo-reaction, and to trap states of interest useful for understanding the photo-switching mechanism.

While most publications about RSFPs claim that the protonation combined with the isomerization of the chromophore is the principle manifestation of photoswitching, our findings show that protonation and isomerization are not necessarily coupled. In the case of eYFP, the photo-switching mechanism seems to be associated with large structural rearrangements and, mostly, a photo-induced protonation of the chromophore without isomerization. In the case of Padron, the photoswitching at 100 K involves the isomerization between anionic forms of the chromophore. Understanding more about the switching mechanism of the FPs can lead to rational development of new dyes, as well as to enhancement of available imaging techniques. In particular, our results contribute to the development of a new and promising branch of the super-resolution microscopy, the cryo-nanoscopy.

i. eYFP and the photo-induced protonation

The photo-switching behavior of eYFP was first observed through single molecule experiments by Dickson et al. at room temperature (Dickson et al., 1997). At the ensemble

level, a partial photoswitching takes places via thermal relaxation after actinic illumination (Sinnecker et al., 2005). In concordance with others groups (McAnaney et al., 2005), we have presented here that the fluorescence emission recovery is possible only with 355 nm actinic lasers, and that the contrast between bright and dark states is negligible compared to Dronpa and IrisFP. In contrast, at 100 K, eYFP switches remarkably by altering 514 nm and 405 nm lasers; whereas Dronpa and IrisFP show only low switchable behavior. We have presented that the photo-induced protonation at 100 K is a common process for eYFP, Dronpa and IrisFP. Because of the opposite photo-switching behavior of these fluorescent proteins at low temperature and at room temperature, we deduce that structural mechanisms responsible for the switching are not the same at both temperatures. In view of the reduced thermal energy available at 100 K, we suggest that the conformational rearrangements that accompany photo-induced protonation involve only the very small amplitude fluctuations possible at low temperatures. As evidence, we have obtained two crystal structures of eYFP: one at low pH, and another after actinic illumination at 523 nm switched the protein to dark state. Both structures show the chromophore in cis conformation, similar to the structure obtained by the protein at basic pH (Wachter et al., 1998).

ii. Padron and the photo-induced isomerization

The positive-switching FP, Padron, was able to switch at room temperature and, surprisingly, at 100 K as well. Our structural results suggest that the mechanism of switching at cryo-temperature is also based on the chromophore isomerization from trans to cis. Already with Dronpa, no chromophore isomerization was observed upon illumination at low temperature. Probably, the particularity of the Padron behavior at 100 K comes from the fact that minor structural rearrangements are needed to accomplish the isomerization. Salient for

Padron is Met59, which limits the isomerization of the chromophore; whereas for Dronpa it is Arg66 and His193 which need to be relocated.

Spectroscopically, we have observed that during actinic illumination, the non-fluorescent anionic absorption peak at 504 nm, B_{trans}, is converted to a fluorescent anionic peak at 481 nm, I_{cis}; and to another fluorescent anionic peak, $B_{cis,LT}$, also at 504 nm. $B_{cis,LT}$ differs from B_{trans} by a bigger extinction coefficient and a thinner band. The protonated peak at 396 nm remains unaltered during the anionic peak conversion. Concomitantly with this photo-reaction and even after illumination, a thermal relaxation occurs from I_{cis} to $B_{cis,LT}$. In spite of differing spectroscopic observations of these three states, structural differences between I_{cis} and $B_{cis,LT}$ are not observed. The crystal structures collected instantly and 40 minutes after actinic illumination are very similar. Each showed positive electron densities when averaging over the six monomers present in the asymmetric unit. We could therefore not conclude if this result is involved in the relaxation of I_{cis} to $B_{cis,LT,}$ or if it is only an artifact. In perspective, it will be interesting to reproduce and enhance this experiment, since it can reveal the structural mechanism which transforms I_{cis} to $B_{cis,LT}$.

After photo-conversion, increasing the temperature allows the protein to assume structural conformations previously unavailable. This results in an augmentation of the protonated band ($A_{cis,RT}$), and a small blue-shift of the anionic band ($B_{cis,RT}$). We have suggested a kinetic model in order to account for the behavior of Padron at these different temperatures, laser powers and wavelengths. The back-switching was achieved less efficiently with 473 nm lasers, and more efficiently with 405 nm lasers, despite the absence of a protonated band.

3.2 PERSPECTIVES

We describe below possible future directions for the study about photoswitching mechanism, based on the results and discussion presented in this work.

i. Partial photoswitching of fluorescent proteins

Several fluorescent proteins seem to exhibit some degree of photoswitching, such as eYFP (see Introduction Chapter 1.3.7). Certainly, it will be interesting to investigate further the origin of this phenomenon. Is it associated with the isomerization of the chromophore? We have shown in Chapter 2.3.4 that even without structural details about the mechanism, it is possible to profit from this feature in order to enhance the spectroscopic experiments.

ii. The intermediate state of Padron

Some questions about the intermediate state of Padron remain open. **1)** Is I_{cis} really fluorescent (chapter 2.2.4)? **2)** What are the structural changes that allow the conversion from I_{cis} to $B_{cis,LT}$ (chapter 2.2.4)? **3)** How does the back-switching at 405 nm affect I_{cis} state? **4**) Is it possible to obtain more efficient back-switching illuminating at red-shifted wavelengths (405 nm < λ < 473 nm)? Further experiments are needed to answer these questions.

iii. Olsen's insight

After the publication of our results with Padron (Faro et al., 2011), we had the pleasure of receiving an e-mail from Dr. Olsen, of University of Queensland, Australia, commenting on our work. Dr. Olsen has published several theoretical studies of fluorescent proteins, using quantum chemistry calculations to characterize the relevant electronic states which mediate

the photoswitching mechanism. We consider it appropriate to present the email (**Figure 3.1** below**),** as a perspective of our work.

Dear Prof. Bourgeois,

I read with very much interest your recent article "Low Temperature Chromophore Isomerization Reveals the Photoswitching Mechanism of the Fluorescent Protein Padron" (JACS 133 16362 (2011)). This work raises some very interesting questions about a very interesting protein. In particular, I note that the intermediate state I_cis, apparently an anionic chromophore in the cis state, can be switched back to B_trans (also an anion) by excitation at 405nm. As you point out in the supplement, this excitation would normally be attributed to a neutral chromophore, but there is no evidence for protonation of the chromophore in I_cis.

I may be able to shed some insight into this issue. In the attached CPL paper, my colleague and I argue that theories of color in arylmethane dyes predict that the anionic GFP chromophore should have a higher excited state associated with its charge-resonant electronic structure. We also show that the excitation energy of this state, calculated by a CASPT2 quantum chemistry model, lies at similar wavelengths to the lowest-lying excitation of the neutral chromophore. I have also attached a JCP paper that shows that this excited state plays a crucial role in the description of the photoisomerization reaction in the anion.

It may be that the higher excited state of the anion is responsible for the 405nm switching of I_cis. This could be experimentally tested, because the transition to the higher excited state of the anion should have polarized orthogonal to the low-lying transition (see paper). If the photoreaction could be observed in the crystalline state, then the dependence of the switching on the excitation polarization could test this idea.

Many thanks again for a very enjoyable and enlightening paper.

Best Regards,

Seth Olsen

Figure 3.1) Digital letter (e-mail) written by Olsen sent for us. The articles cited for him refer to CPL (Olsen and McKenzie, 2010) and JPC (Olsen and McKenzie, 2009).

It would be interesting in the future to perform the experiment suggested by Olsen, in order to verify his hypothesis and perhaps to extend to other FPs a similar behavior observed with Padron. This would present a good opportunity to gather theoretical and experimental investigations, and to advance the research about fluorescent proteins.

iv. asFP595

The molecular structures of asFP595 were solved in bright and dark states (Andresen et al., 2005). Similarly to Padron, there is little difference between the bright and dark structures, except by the chromophore isomerization. It would be interesting to perform similar experiments to those described in Chapter 2.2.4 with asFP595, in order to verify our hypothesis that the photo-switching is able to occur at 100 K to minor structural rearrangements. Another experiment to be performed with Padron and asFP595 will be their characterization at single molecule level at cryo-temperature, in order to verify our results of cryo-activation.

Chapter 4

MATERIAL AND METHODS

4.1 OUTLOOK OF MATERIAL AND METHODS

This chapter describes the experimental procedures used along this thesis period (**Figure 4.1)**. We put emphasis on particular cases for which specific procedures were required. We also describe some problems that occurred during our investigation or that could occur in similar studies, expecting that these informations will be useful for future researches. Details about the experimental protocols used in the eYFP and Padron's experiments can be found in the Annex 2 and 1, respectively (Faro et al., 2011; Faro et al., 2008).

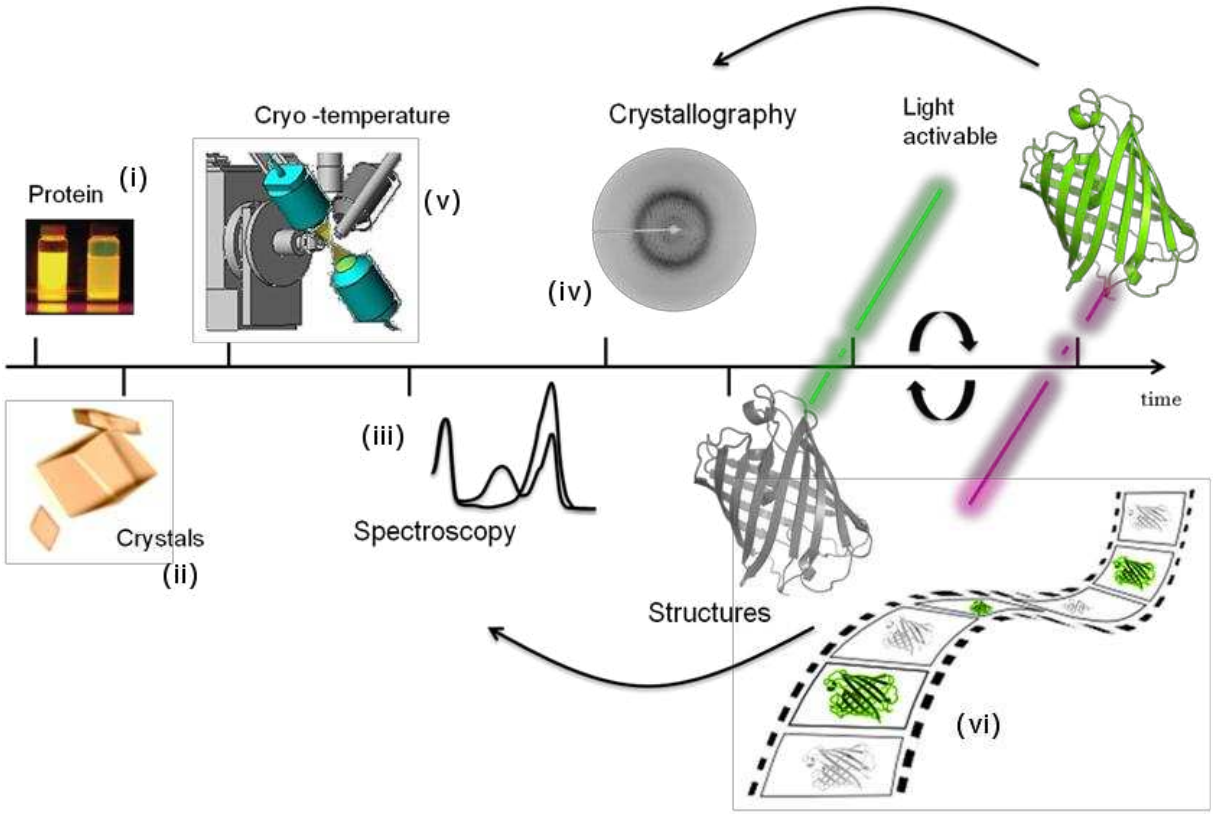

Figure 4.1) Scheme about the typical procedure used during this thesis: (i) Expression of the fluorescent protein; (ii) Crystallization of fluorescent protein; (iii) Spectroscopic characterization of fluorescent protein; (iv) X-ray crystallographic experiments and (v and vi) low temperature X-ray crystallography and in crystallo optical.

4.2 MOLECULAR BIOLOGY

4.2.1 THE EYFP GENE

For convenience, fluorescent proteins are expressed in prokaryotic cells (E. coli). In this purpose the eYFP gene (peYFP) is inserted in the expression vector plasmid pET15b. This vector includes the DNA sequence of: T7 phage promoter inducible by IPTG, ampicilline resistance, polyhistidine-tag (that is added at the N-terminal protein sequence), two restriction sites, NdeI and BamHI, etc (**Figure 4.2**).

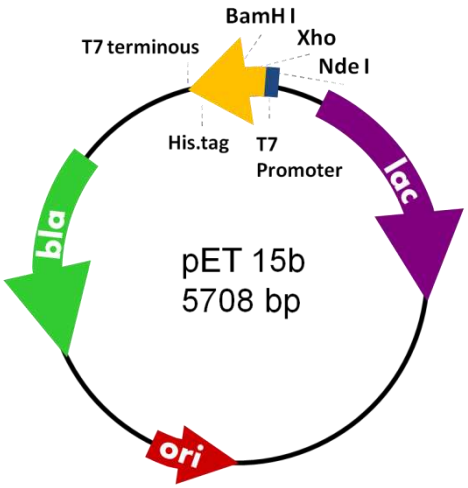

Figure 4.2) pET-15b vector (Novagen Vector, Darmstadt, Allemagne) simplified representation.

For the cloning, the initial peYFP plasmid of 3000 bp (**Figure 4.3a**) that included the eYFP gene of 700 bp (**Figure 4.3b**) was provided to by François Parcy from iRTSV (Institut de Biologie Structurale – FRANCE). eYFP gene is extracted by PCR and inserted into the pET15b vector (**Figure 4.3**). To this aim, we designed two oligonucleotides primers which include the restriction sites specific to NdeI and BamHI enzymes respectively. The final DNA product from the PCR amplification and digestion (with NdeI and BamHI enzymes) is inserted into the pET15b thanks to the T4DNA ligase.

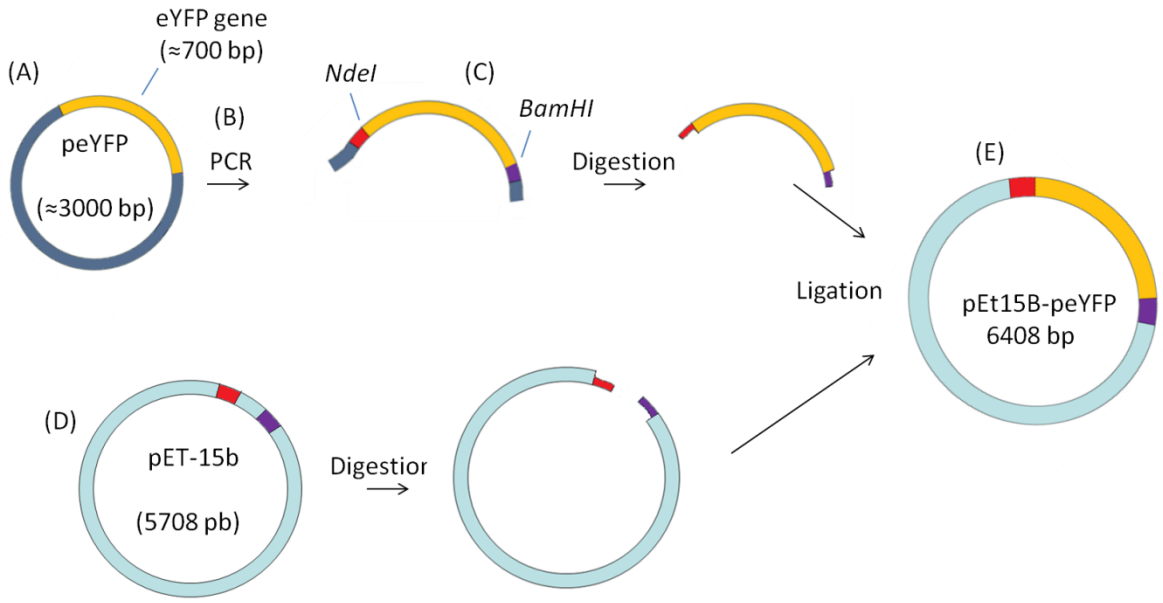

Figure 4.3) Scheme about the eYFP insertion into pET-15b. (A) peYFP plasmid and eYFP gene (yellow) (B) PCR amplification (C) peYFP plasmid including the restriction sites of the NdeI (red) and BamHI enzymes (violet) (D) pET15b and (E) final plasmid of eYFP gene inserted into pET15b.

4.2.2 DRONPA, PADRON AND EYQ1 GENES

The gene of Dronpa (Dronpa 2 and Dronpa 3) and Padron were provided by our collaborator Peter Dedecker (Katholieke Universiteit Leuven - BELGIUM). They are cloned and expressed into pRSET vector (Ando et al., 2004). The gene of EYQ1 was provided by our collaborator Ranieri Bizzarri (Scuola Normale Superiore - ITALY). It is cloned and expressed into IBA vector (IBA GmbH, Göttingen, Germany) (Bizzarri et al., 2010).

4.3 BIOCHEMISTRY TO PRODUCE FPS

4.3.1 EYFP HETEROLOGOUS TRANSFORMATION OF ESCHERICHIA COLI BACTERIA

Once the gene is inserted in the pET15b vector, the next step is the heterologous transformation of the bacteria Escherichia coli host with the plasmid (BL21-DE3). In this transformation process, 100 - 200 µL of bacterial competent cells treated with $CaCl_2$ to be porous to DNA and 3 - 1 µL (at ≈ 50ng/µL) of recombinant plasmids are mixed together. Then, the pET15-eYFP plasmid is introduced in the bacteria by heat shock: 90 s at 42° C followed by 90 s in ice. After that, Lysogeny Broth culture medium (LB) is added (1 mL), in order to induce the cells to express the antibiotic gene resistance. The bacterial culture (100 µL) is plated on agar petri dishes (20 mL) with the antibiotic ampicilline (50 µg/mL), in order to induce a genetic selection. Only, the transformed bacteria survive in this antibiotic condition. All the fluorescent proteins IrisFP, Dronpa, Padron and EYQ1 were also transformed in BL21 (DE3) using the same protocol that was used for eYFP transformation.

We have noticed that when the plates are illuminated with UV-light green fluorescence is observed indicating that despite the absence of expression inductor IPTG some FPs are expressed. It is associated to the phenomenon called leak.

4.3.2 WORKING IN THE DARK

Our goal of working with fluorescent proteins is to understand its behaviors upon illumination. Hence, to obtain a reliable and reproducible result, we performed the following steps of the fluorescent protein expression and purification without light exposure. We have

adopted a procedure to envellope all chemical apparatus with a tin foil, in order to block the light and to avoid unsuitable phototranformations.

4.3.3 EXPRESSION OF FLUORESCENT PROTEINS

To over-express fluorescent proteins, the recombinant bacteria are grown in the culture medium LB with the selection antibiotic to select the colonies that contain the plasmid. Typically, a large volume of culture medium (~ 4 L) is inoculated with a small volume of an over-night preculture (50 mL). The culture medium is incubated in optimal conditions for bacterial reproduction (37 °C, 200 rpm). The cells growth until to the beginning of the exponential phase corresponding to the optimal population density, measured through sample optical density equal to 0.6 probed at 600 nm. At this stage, the over-expression of the gene is induced by adding 1mM of IPTG or Anhydrotetracycline in the case of EYQ1. The expression time and temperature of induction depends on the fluorescent protein, because during this step, chromophore maturation occurs concomitantly with protein folding in the (see Chapter Introduction 1.2.1). In eYFP's case, the protein induction takes over-night at 37 °C. For IrisFP, because of the slow chromophore maturation the induction step takes few days and requires low temperatures (around 4 °C). The expression protocol of Padron and Dronpa are described in the Annex 2.

After induction, the bacteria are pelleted by centrifugation (4 °C, 4000 rpm) and diluted in lysis buffer (50 mM Hepes pH7.5, 300 mM NaCl, 15 mM imidazole). Fluorescent protein as eYFP (Wachter et al., 2000) and even IrisFP[i] exhibit alteration in its photochromic behavior in presence of the halides ions. For this reason, we recommend, when necessary, to exchange the typical hydrochloric acid (HCl) used to adjust the pH of the buffer by acetic

[i] Experiment carried out in our laboratory, result not shown.

acid. The cell pellet can be stored at -20 ºC or immediately submitted to the next step of process: the protein purification.

4.3.4 PROTEIN PURIFICATION

The procedure to obtain a pure protein starts with the lysis of the bacterial wall via ultrasound pulses (10 pulses of 30 s with 30 s interval). The cell lysis reduces the viscosity of the solution, causing a change of color from opaque to translucent and then to bright. The cell membrane and organelle pellet are separated from the soluble part, via centrifugation (4 °C, 15000 rpm). This fraction is mostly made of a mixture of soluble proteins, including the fluorescent protein of interest (crude extract). Because the fluorescent proteins have a strong color (yellow for eYFP, green for Dronpa and IrisFP and red for Padron) no clear increase of the brightness of the color sample strongly suggest that the lysis was not efficient or the protein was not expressed.

We have used two steps to purify the protein, first immobilized metal affinity chromatography (IMAC) followed by molecular size exclusion chromatography. In both purifications steps, the protein track is controlled by the high-pressure chromatography systems monitoring the absorbance at 280 nm. Other wavelengths can be used in order to avoid the photobleaching or to discriminate the FP from the other proteins. The selected fractions can be collected manually or automatically.

i. Immobilized metal affinity chromatography (IMAC)

IMAC technique consists in adding a charged metal, cobalt (Co^{2+}) in our case, to the resin of the column (Clontech Laboratories, California, USA). The His-tag N-terminal of the protein carries electron lone pairs that coordinate the cobalt. Therefore the protein binds to the

column. It is eluted by competition with imidazole that mimics the side chain of the His. To reduce unspecific binding of the proteins the crude extract sample is loaded and washed in presence of 15 mM of Imidazole. The fluorescent protein is eluted using a gradient of imidazole (15 – 300 mM). At some point, the imidazole concentration is sufficiently high to compete with the protein, resulting in its release from the column. We have noticed that after several purifications, the color resin remains fluorescent even after elution. To avoid this problem we recommend to filter (0.4 µm porous) the crude extract before to start the purification, or to add DNAse to the crude extract in order to reduce the viscosity, by cleaving the remaining DNA.

Despite the fact that the protein obtained in this experimental step is diluted, the sample can be tested by spectroscopic analysis. A second purification step is applied, using the molecular size exclusion chromatography method.

ii. Molecular size exclusion Chromatography (gel filtration)

This purification method is based on protein separation by molecular size. This purification step, together with the previous steps, ensures to obtain the protein's purity needed for crystallization trials. The columns used is High Load 16/60 Superdex 75 gel-filtration and Hiload 16/60 Superdex 200 gel-filtration (GE healthcare, Pennsylvania, USA).

Using this purification method, the imidazole is removed from the protein solution, so no dialysis method is needed.

4.3.5 FLUORESCENT PROTEIN STORAGE

The condition of storage depends on the Fluorescent Protein produced and its finality. There is not one general rule for fluorescent protein storage, but most of them posseses a good

stability, even at room temperature. Generally, the protein that will be used for spectroscopy experiments can be stored during a long period in the dark (several months, at 4 °C). In principle for crystallization, technique that requires higher protein integrity, the protein can be stored for months as well. However, if the crystallization results are negatives it is not possible to identify if the problem comes from the storage time or because the crystallization condition is not accurate. One recommendation is to centrifuge the protein, during 10 minutes 13000 g, before preparing the crystallization assay. We note that sometimes, when using old proteins (8 months) in well established crystallization protocol, the crystal does not appear. In this case, the sample is loaded on gel filtration to obtain more homogeneous protein.

4.4 CRYSTAL GROWTH

4.4.1 PROTEIN CRYSTALLIZATION

The crystallization process consists in a phase transition from the disordered to the ordered state of the protein molecules. In the ordered state the molecules are periodically positioned in the space, in all 3 dimensions. This transition occurs typically with the gradual increase of the protein saturation level. It must occur sufficiently slowly, so that the system adopts the most periodic configuration among other energetically favorable ones. During the crystallization process, the sample overtakes the supersaturation state (a metastable state) close to the liquid-solid transition, promoting the appearance of a small group of ordered molecules (nucleation). The nucleation is the origin of the crystalline network. In the following step of the crystallization, other molecules come around the nucleus and the crystal grows in non super saturated solution.

The protein crystallization depends on several physico-chemical parameters. A slight change in the crystallization conditions can decide on the appearance or not of the crystal. Crystallization trials are based on the study of the protein solubility as a function of the physico-chemical parameters (phase diagram). The principal parameters which influence the protein solubility are the temperature, the pH value and the precipitant agent (salt or organic solvent). In the crystallization attempts a common (unsuccessful) result is protein precipitation (or aggregation), that is, a solid state in which the protein molecules are disarranged **(Figure 4.4 A)**. Another result frequently obtained from crystallization attempts is the formation of multi-crystals that grow attached **(Figure 4.4 B)**. In most of the cases, these multi-crystals are inappropriate for X-ray crystallographic experiments. Some

techniques take advantage of multi-crystals to enhance the crystallization conditions. This was the case for Padron crystallization, as that will be described below.

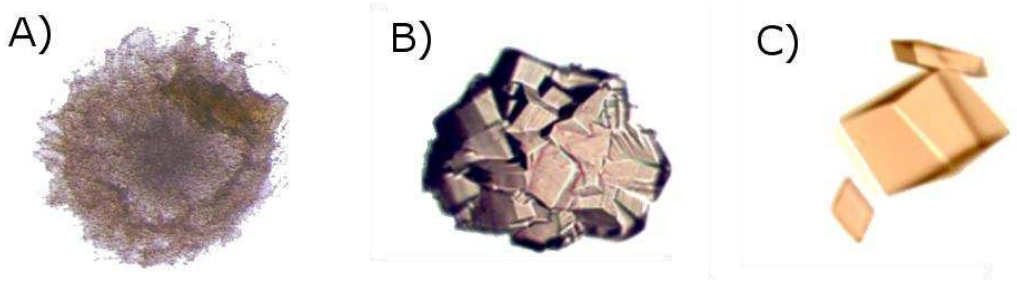

Figure 4.4) Protein crystallization. (**A**) Protein precipitates (**B**) Multi-crystal of Dronpa (**C**) Crystal of Padron

4.4.2 OPTIMIZING PADRON CRYSTALLIZATION BY SEEDING

Seeding techniques consist in using crystal germs to induce the crystal growth into another drop than the original one. There are three main procedures to seed: streakseeding, which uses a streakseeder (whisker); microseeding, which uses diluted crushed crystals; and macroseeding, which uses small macro-crystals as a seed. The crystallization sample of the new drop is similar to the one in which the seed crystal has been grown or frequently it has a lower concentration of the precipitant agent in order to slow down crystallization.

The first crystals of Padron were grown in solution of 500 mM of $Mg(NO_3)_2$, 50 mM of Hepes and 26% PEG 3350. We have used the streakseeding procedure to optimize the quality of crystals. In practice, we pull germs by touching smoothly crystal clusters of Padron with a clean whisker, which next is put in contact with the pre-equilibrated drops prepared on the previous day. Optimized crystals grow in lower PEG concentration 16% PEG 3350. The crystals take one day to grow up and start to degrade after 2 - 10 weak **(Figure 4.4 C).**

4.4.3 CRYSTALLIZATION CONDITIONS

Despite the high structural homology between fluorescent proteins, the crystallization process is not restricted to a limited small group of crystallization conditions. We noted that sometimes, for a fluorescent protein variant with a single or few mutations, a different crystallization condition is required. The crystallization conditions that allowed us to obtain crystals are shown on **Table 4.1**.

We obtained several crystallization conditions for EYQ1. Most of them contain Polyethylene glycol (PEG) as precipitant agent and all of them contain halide molecules. Our hypothesis is that the halide atoms help to stabilize one conformation of the protein. Indeed, in the EYQ1 structure the halide atom is placed close to the chromophore, similarly to what was found for YFP (Wachter et al., 2000) .

Table 4.1) Table of the crystallization conditions of the protein used during this thesis

Protein	Temp.	Method	Reprod.	Optimization	Crystallization buffer
eYFP	20 °C	hanging drop	non	low pH	0.2 M Sodium fluoride 20% PEG 3350
EYQ1	20 °C	hanging drop	yes	Non	0.2 M Magnesium chloride, 20% PEG 3350
Padron	20 °C	hanging drop	yes	streakseeding	500 mM $Mg(NO_3)_2$, 50 mM Hepes (pH 7.5), 16* - 26% PEG 3350
Dronpa	20 °C	hanging drop	yes	streakseeding	80 mM $Mg(NO_3)_2$, 100 mM Tris (pH 7.2), 18% PEG 3350

* The low concentration of precipitant agents required for streakseeding optimization.

The crystallization can be considered as a method of purification, where only the similar molecules are selected to constitute the protein network. However, the crystallization can generally not discriminate between different conformations of a single FPs. For example, a single crystal can be constituted of both dark-Dronpa with the chromophore in trans and bright-Dronpa with the chromophore in cis.

The obtained crystallization conditions have often PEG as precipitant agents. Depending on the PEG concentration and mass, it also provides cryo-protection, saving from additional manipulations (soaking in the cryoprotectant) that may damage the crystal.

4.4.4 SPONTANEOUS CRYSTAL BLEACHING OVER TIME

We have observed that some protein crystals become transparent during long time storage. The explanation found is the acidification of the crystallization medium. Indeed, measuring the crystallization pH after long storage time, we have noticed a lower value than in the initial condition. Concerning the fluorescent proteins studied here, at low pH the protonated state of the chromophore is favored, which can explain the crystal transparency. This hypothesis was confirmed when adding a small amount of Sodium hydroxide (1 µL, weakly concentrated) into the crystal drop. We have observed that the crystal recovers its color almost instantly after the addition of NaOH. The cause of acidification is yet unknown, since the phenomenon is generally not reproducible. It could be due to bacterial contamination. As the sample acidification is a spontaneous and slow process, the chances to damage the crystal are smaller. We could take advantage of this to solve the crystal structure of eYFP in the protonated state at pH 3.6 (see Results and Discussion Chapter 2.3.3). The appearance of a transparent crystal was noticed only six months after the drop preparation. In spite of being a good way to obtain the protonated crystal, it is a hard task to reproduce such experiment because of the long crystallization time.

4.5 CRYSTALLOGRAPHY

4.5.1 SOME CRYSTALLOGRAPHY CONCEPTS

The next step after obtaining the protein crystal is to collect X-ray diffraction data in order to solve the molecular structure of the protein. The crystal is exposed to X-ray beam that has appropriate wavelength "to see" interatomic distances (0.7-1.5 Å). The use of a crystal rather than an amorphous solid for X-ray measurements originates from the necessity to obtain coherent interferences of the scattered beam in order to potentiate the collected signal.

If a single molecule is irradiated, the diffraction pattern observed is the Fourier transform of the molecular structure. However, the diffraction pattern of a protein crystal lattice is also a lattice in reciprocal space, which defines restricted spatial positions where the scattered beam can be observed. The diffraction by a molecule in a crystal lattice is given by the structure factor equation.

$$\mathbf{F}(\mathrm{hkl}) = \sum_{j=1}^{N} f_j e^{2\pi i(hx_j + ky_j + lz_j)} = F(\mathrm{hkl})\, e^{i\alpha(\mathrm{hkl})}$$

where N is the number of atoms, f_j is the scatter factor associated to the j^{th} atom at the position, x_j, y_j, z_j and h, k, l are the integers associated to the reciprocal lattice considered.

The electron density, $\rho(xyz)$, can be calculated from the Fourier transform of the diffraction pattern.

$$\rho(xyz) = \frac{1}{V} \sum_{h=-\infty}^{\infty} \sum_{k=-\infty}^{\infty} \sum_{l=-\infty}^{\infty} \mathbf{F}(\mathrm{hkl}) e^{-2\pi i(hx_j + ky_j + lz_j)}$$

In order to calculate the electron density, the structure factor vectors are needed. However, the physical observable is not the vetorial structure factor, but the scattered intensities $I(\mathrm{hkl}) = \mathbf{F}(\mathrm{hkl})\, \mathbf{F}(\mathrm{hkl})^*$. Thus, all the information on the phase is lost. There are

several methods to solve the phase problem: molecular replacement is one of the most common and most appropriate for FPs.

4.5.2 MODEL BUILDING AND MODEL REFINEMENT OF FPS

Molecular replacement uses as input a model of a structure homologue to the structure to be solved and structure factor amplitudes of the observed diffraction pattern (F_{obs}). The closer is the homologue structure to the real structure, the better will be the statistics of the molecular replacement. Due the high structural homology between all fluorescent proteins, molecular replacement is sufficient to solve the phase problem. However, the fact that highly homologous models are used as input can bias the calculated coordinates of the new model.

Model bias results from using an atomic model to calculate crystallographic phases, in which case the resulting electron density map will tend to have the features present in the model even if they are not actually present in the structure (Terwilliger et al., 2008). For FPs, in order to reduce the model bias in important regions such as the chromophore or mutated residues, we have removed these parts in the input model. Refinement from a model omitting incorrectly placed atoms should reduce this bias, but a memory of their positions can still remain and the resulting map may retain incorrect features. To reduce this memory effect, we have included in the refinement strategy a simulated annealing step.

Simulated annealing works by computationally increasing the temperature at which the model is “shaken”, so that it can escape local energy minima (Brunger and Adams, 2002b) and converge to the correct structure. The same principle is used to calculate “omit maps” as way to validate the specific molecular structure of special importance modeling of a local.

The strategy performed to obtain the structures, and the programs used for model building and refinement are shown in **Figure 4.5**.

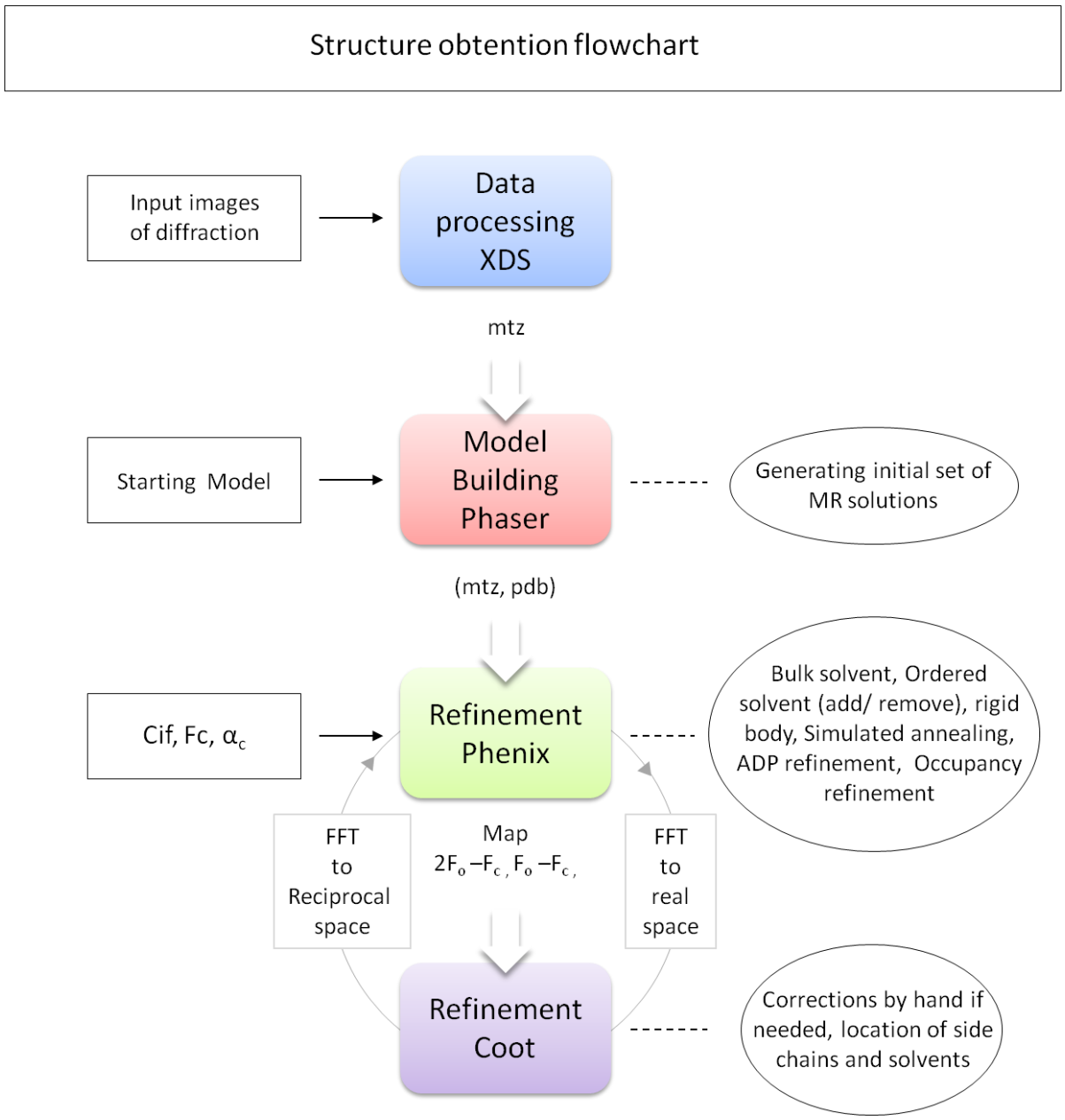

Figure 4.5) Strategy and the programs used in model building and refinement. All crystallographic data sets were integrated and scaled with XDS (Kabsch, 1988). The starting model phases depend on the protein (see text), molecular replacement was performed with PHASER (Mccoy, 2007). Model refinements were performed with PHENIX (Afonine, P.V., Grosse-Kunstleve, 2005) using simulated annealed maps (Brunger and Adams, 2002a) to avoid introducing model bias.

4.5.3 KINETIC X-RAY CRYSTALLOGRAPHY

Kinetic X-ray crystallography consists in triggering functional activity directly in the crystalline state and in collecting two (or more) crystallographic data-sets at different instants along the protein reaction pathway to access their differences. We can watch the movements performed by the protein by gathering several static structures in different states. Trapping of a particular state is achieved by rapidly cooling the crystal in order to stop large conformational movements (freeze-trapping). This approach is suited for photosensitive proteins, such as FPs, because the triggering source is light and it can be operated even at low-temperatures contrary to subtract diffusion for example. Model bias in kinetic X-ray crystallography is avoided by comparing only experimental data that is by calculating difference electron density maps of the form F_{obs} (t_1) – F_{obs} (t_2). It is preferable to use the same crystal to minimize systematic errors and facilitate the interpretation of difference electron density maps.

i. F_{obs} - F_{obs} difference electron density maps

F_{obs} - F_{obs} difference maps were calculated using Bayesian q-weighting (Ursby and Bourgeois, 1997). Using a CCP4 script the difference map can be calculated by first merging the mtz files from two different data-sets using the program CAD and a third containing the calculated phases form the model. Next, the structure factor amplitudes are scaled using the program RSTATS. For experiment with low signal-to-noise due to subtle structural differences it is advantageous to use Bayesian q-weighting to provide better estimations of difference amplitudes (Ursby and Bourgeois, 1997). Finally, the difference positions in reciprocal space (HKL) are calculated using the program FFT.

4.5.4 X-RAY DATA COLLECTION

i. eYFP

X-ray diffraction data sets from eYFP were collected at the European Synchrotron Radiation Facility (ESRF) on beamline ID14-1 (Wed Mar 31, 8–9 p.m., 2010), with an ADSC Q4 detector (ADSC, California, USA). Two crystals of eYFP were collected: (1) The structure of the pH-induced protonated form of eYFP (**A1)** was obtained by flash-cooling a crystal that grew at pH 3.6 by spontaneous acidification of the crystallization medium. (2) That of the photo-induced protonated form of eYFP (**A2**) was obtained by soaking a crystal (like A1) in a crystallization medium at pH 8 and illuminating at 514 nm (20 min; 0.3 W/cm²) at room temperature prior to flash-cooling. Due to the needs for further investigations and eventually reproduction of the X-ray experiments, the structural data were not deposited in the Protein Data Bank (PDB). Data collection statistics and refinement parameters are summarized in **Table 4.2** and in **Table 4.3**.

Table 4.2) Crystallographic data collection statistics of eYFP

	eYFP (A1)	**eYFP (A2)**
Space group	$P\ 2_1 2_1 2_1$	
Cell dimension, (Å)	a=51.66 b=62.85 c=69.32 α=90.00 β=90.00 γ=90.00	
	a=51.58 b=62.23 c=69.22 α=90.00 β=90.00 γ=90.00	
Wavelength, (Å)	0.933	0.933
Resolution, (Å)	2.3	1.8
No. uniq. reflections	10235	27008
Completeness, (%)	97.39	89.86
R_{sym}, (%)	26.3	nd ¶
Mean I/σ(I)	6.94	nd ¶
Wilson B_{factor}, (Å²)	33.21	18.54

‡ $\mathrm{Rsym} = \sum_j \sum_h \left| I_{h,j} - \langle I_h \rangle \right| \Big/ \sum_j \sum_h I_{h,j}$

¶ Preliminary data that need to be processed again.

Table 4.3) Model refinement statistics of eYFP

	eYFP (A1)	eYFP (A2)
R_{work} , (%) #	0.2406	0.1869
R_{free} , (%) Δ	0.3005	0.2252
RMSD bond length, (Å)	0.008	0.006
RMSD bond angles, (°)	1.191	1.287

$R_{work} = \sum_h |F_{obs} - F_{cal}| / \sum_h F_{obs}$

Δ R_{free} is calculate is calculated with a small fraction (5 %) of reflections chosen to be part of a test group.

ii. EYQ1

X-ray diffraction data sets from EYQ1 were collected at the European Synchrotron Radiation Facility (ESRF) also on beamline ID14-1 (Thu Jul 01, 3 – 4 a.m., 2010). This protein was crystallized in a medium that contains halide atoms, which likely inhibits the photoswitching efficiency. The reproduction of the X-ray experiment with a crystal grown in a different crystallization medium is required. This is one of the reasons for which this crystal structure was not deposited in the PDB. Data collection statistics and refinement parameters are summarized in **Table 4.4** and in **Table 4.5**.

Table 4.4) Crystallographic data collection statistics of EYQ1

	EYQ1
Space group	P 1
Cell dimensions	a=45.27 Å b=56.550 Å c=56.560 Å α=71.76 β=75.32 γ=75.19
Wavelength, (Å)	0.933
Resolution, (Å)	1.36
No. uniq. reflections	101382
Completeness, (%)	93.28
R_{sym}, (%)	4.3
Mean I/σ(I)	14
Wilson B_{factor} , (Å²)	8.31

Table 4.5) Model refinement statistics of EYQ1

	EYQ1
R_{work} , (%) #	0.1677
R_{free} , (%) Δ	0.1839
RMSD bond length, (Å)	0.006
RMSD bond angles, (°)	1.362

iii. Padron and Dronpa

Details about the X-ray data collections of Padron and Dronpa are described in the Annex 2 (Supporting information).

4.6 SPECTROSCOPY

4.6.1 SPECTROSCOPIC SETUP

i. Spectroscopic setup: microspectrophotometry

Absorption and fluorescence spectra from crystals and thin films solution samples were recorded using a microspectrophotometry set-up in the Cryobench laboratory of the IBS/ESRF (Grenoble, France) (Royant et al., 2007) for eYFP experiments and in the Pixel laboratory IBS/iRTSV (Grenoble, France) (Arcizet et al., 2011 in French) for Padron experiments.

The microspectrophotometry setup allows studying macromolecular crystals at cryogenic temperatures and offers the opportunity to study nano-volumes of solution samples, which can be easily flash-cooled to the glassy state with only a moderate amount of cryo-protectant. In practice, this device is constituted by: two mirror objectives face-to-face and the third one at 90° from the others (magnification ratio 1:4 for Cryobench and Pixel laboratories); one goniometer with a magnetized support to mount the standard cryoloops in objectives focus; one HR2000+ CCD-based spectrometer (Ocean Optics, Dunedin, FL, USA) in Cryobench lab and AvaSpec-ULS2048 (Avantes, Eerbeek, the Netherlands) in Pixel lab; one microscope to visualize the sample; and one cryocooling device to control the temperature samples varying between 100 K and 300 K, Oxford Series 700 in Cryobench and 600 in Pixel lab (Oxford, UK) (**Figure 4.6**).

The light sources, such as white lamp and lasers, and the spectrometer can be connected to the objectives using optical fibers (100 – 600 µm of diameter) and a pulse generator allows controlling the exposure time for measurements as a function of time. The spectrometer readout can also be controlled by a computer (**Figure 4.7**). For a typical

experiment using the microspectrophotometry setup, the sample, crystal or solution, is fished using a cryoloops, and rapidly put on the goniometer support being so that the sample is instantly flash-cooled in the flux of gaseous nitrogen at 100 K. Using the goniometer, the samples are manually centered in the Pixel lab and in an automated way in the Cryobench, which facilitates the alignment.

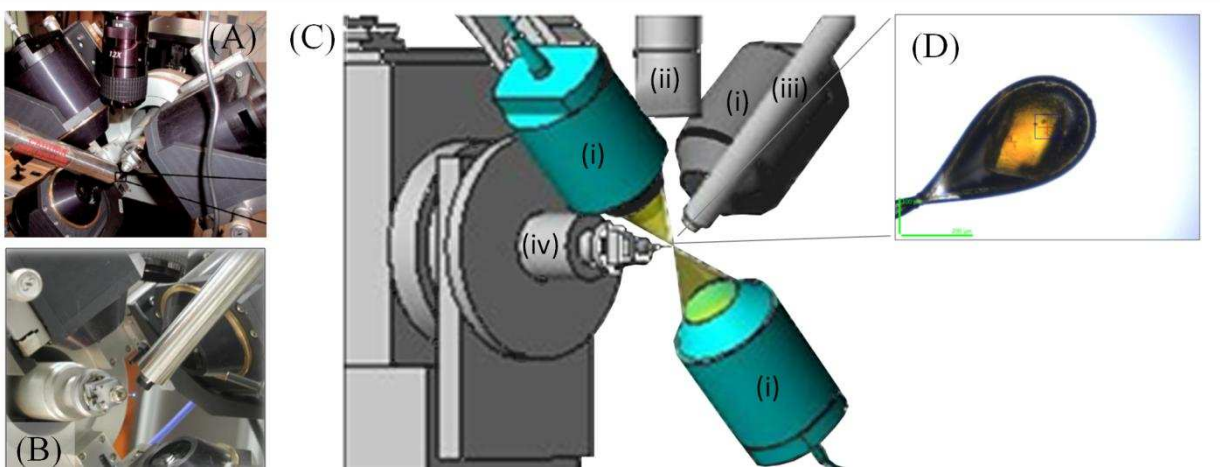

Figure 4.6) Microspectrophotometry setup: (**A**) in the Pixel laboratory (**B**) in the Cryobench laboratory (**C**) three mirror objectives (**i**), microscope objective to visualize the sample (**ii**), cryocooling device (**iii**) and goniometer (**iv**); (D) cryoloop with a crystal of EQY1.

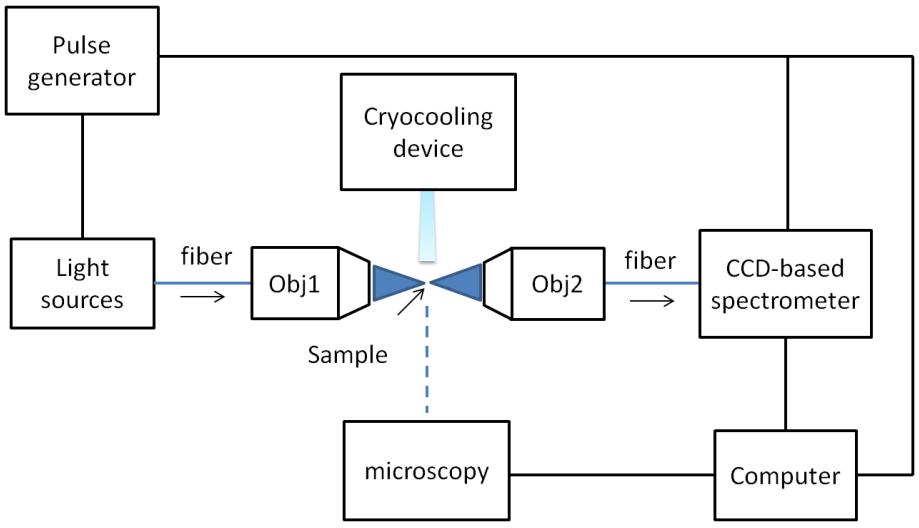

Figure 4.7) Scheme of microspectrophotometry components. The computer is connected with the microscope, with the photospectrometer and with the pulse generator (in the Cryobench laboratory, the cryocooling device can also be controlled by a computer). The sample is centered in focus between the objectives (Obj) that are connected to the light sources and to the spectrophotometer by optical fibers. The microscope allows visualizing the sample, which is essential for the alignment. One objective (Obj) and the goniometer are omitted to facilitate the visualization.

ii. Light source set-up

In the Cryobench laboratory, the laser is directly coupled into the fiber and some filters can be inserted in the light pathway inside the objective. In the Pixel laboratory, an ensemble of mirrors (flip-mounted), beam splitters, dichroic filters and collimators allow the coupling of all lasers at 405, 523 532 nm (DPSS lasers, Changchun New Industries Optoeletronics Tech, Changchun, China) and 488 nm (Argon ion laser, Melles Griot, Albuquerque, USA) and/or a broadband halogen-deuterium source (AvaLight-DH-S-BAL, Avantes, Eerbeek, the Netherlands) into a 100 - 200 µm diameter optical fiber (**Figure 4.8**).

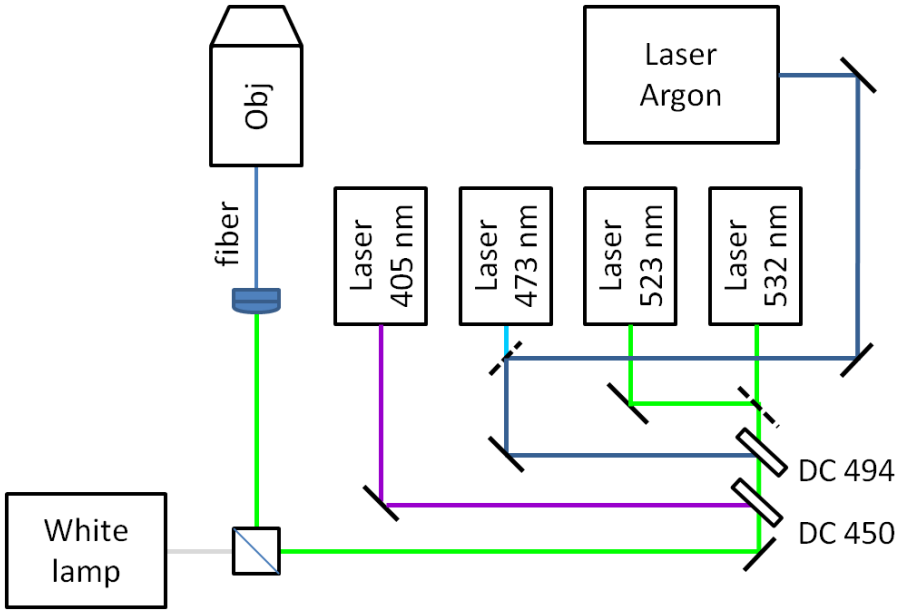

Figure 4.8) Scheme of the light source in the Pixel laboratory. DC450(494): dichroic mirrors with a cut-off at the wavelength 450 nm (494 nm), Objective (Obj), ⋱ flip-mounted mirror, ⧅ beam splitter cube (50/50), collimators.

The advantage of this optical setup is that all the lasers and the white lamp are coupled into a single optical fiber, which ensures the illuminations of the same sample region for all spectroscopic experiments. Both absorption and fluorescence emission measurements were performed by direct transmission from the objective connected to the light sources (Obj1) to the objective connected to the spectrophotometer (Obj2), positioned face-to-face. In direct

transmission mode, we expected an easier observation of the same sample region than when using the perpendicular objective (Obj3). To prevent a spectrophotometer damage caused by high power laser emitted from the Obj1, we used notch filters mounted on a mobile holder before the Obj2. The notch system is put and removed manually, for this reason it is easier to measure the fluorescence emission than the absorbance spectra, when the experiment requires alternation with the actinic laser (**Figure 4.9**).

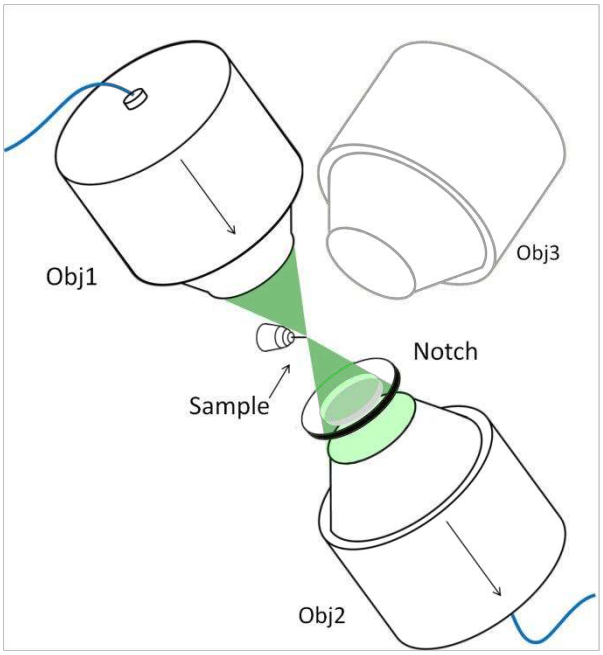

Figure 4.9) Scheme of illumination setup. The sample is positioned in focus on axis of two objectives (Obj1, Ob2j). Absorption and fluorescence emission are measured by direct light transmission, the last one using a notch filter to block the laser wavelength.

References

Abbyad, P., Childs, W., Shi, X., and Boxer, S.G. (2007). Dynamic Stokes shift in green fluorescent protein variants. Proceedings of the National Academy of Sciences of the United States of America 104, 20189–20194.

Adam, V., Carpentier, P., Violot, S., Lelimousin, M., Darnault, C., Nienhaus, G.U., and Bourgeois, D. (2009). Structural basis of X-ray-induced transient photobleaching in a Photoactivatable Green Fluorescent Protein. Journal of the American Chemical Society 131, 18063–18065.

Adam, V., Lelimousin, M., Boehme, S., Desfonds, G., Nienhaus, K., Field, M.J., Wiedenmann, J., McSweeney, S., Nienhaus, G.U., and Bourgeois, D. (2008). Structural characterization of IrisFP, an optical highlighter undergoing multiple photo-induced transformations. Proceedings of the National Academy of Sciences of the United States of America 105, 18343–18348.

Adam, V., Mizuno, H., Grichine, A., Hotta, J., Yamagata, Y., Moeyaert, B., Nienhaus, G.U., Miyawaki, A., Bourgeois, D., and Hofkens, J. (2010). Data storage based on photochromic and photoconvertible fluorescent proteins. Journal of Biotechnology 149, 289–298.

Adam, V., Moeyaert, B., David, C.C., Mizuno, H., Lelimousin, M., Dedecker, P., Ando, R., Miyawaki, A., Michiels, J., Engelborghs, Y., et al. (2011). Rational design of photoconvertible and biphotochromic fluorescent proteins for advanced microscopy applications. Chemistry & Biology 18, 1241–1251.

Afonine, P.V., Grosse-Kunstleve, R.W.& A. (2005). The Phenix refinement framework. CCP4 Newsletter Contribuit, 1–7.

Alieva, N.O., Konzen, K.A., Field, S.F., Meleshkevitch, E.A., Hunt, M.E., Beltran-Ramirez, V., Miller, D.J., Wiedenmann, J., Salih, A., and Matz, M.V. (2008). Diversity and evolution of coral fluorescent proteins. PloS One 3, e2680.

Ando, R., Mizuno, H., and Miyawaki, A. (2004). Regulated fast nucleocytoplasmic shuttling observed by reversible protein highlighting. Science 306, 1370–1373.

Andresen, M., Stiel, A.C., Fölling, J., Wenzel, D., Schönle, A., Egner, A., Eggeling, C., Hell, S.W., and Jakobs, S. (2008). Photoswitchable fluorescent proteins enable monochromatic multilabel imaging and dual color fluorescence nanoscopy. Nature Biotechnology 26, 1035–1040.

Andresen, M., Stiel, A.C., Trowitzsch, S., Weber, G., Eggeling, C., Wahl, M.C., Hell, S.W., and Jakobs, S. (2007). Structural basis for reversible photoswitching in Dronpa. Proceedings of the National Academy of Sciences of the United States of America 104, 13005–13009.

Andresen, M., Wahl, M.C., Stiel, A.C., Gräter, F., Schäfer, L.V., Trowitzsch, S., Weber, G., Eggeling, C., Grubmüller, H., Hell, S.W., et al. (2005). Structure and mechanism of the reversible photoswitch of a fluorescent protein. Proceedings of the National Academy of Sciences of the United States of America 102, 13070–13074.

Annibale, P., Scarselli, M., Kodiyan, A., and Radenovic, A. (2010). Photoactivatable Fluorescent Protein mEos2 displays repeated photoactivation after a long-lived dark state in the red photoconverted form. Journal of Physical Chemistry Letters 1, 1506–1510.

Annibale, P., Vanni, S., Scarselli, M., Rothlisberger, U., and Radenovic, A. (2011a). Identification of clustering artifacts in photoactivated localization microscopy. Nature Methods 8, 527–528.

Annibale, P., Vanni, S., Scarselli, M., Rothlisberger, U., and Radenovic, A. (2011b). Quantitative photo activated localization microscopy: unraveling the effects of photoblinking. PloS One 6, e22678.

Aramaki, S., and Hatta, K. (2006). Visualizing neurons one-by-one in vivo: optical dissection and reconstruction of neural networks with reversible fluorescent proteins. Developmental Dynamics 235, 2192–2199.

Arcizet, D., Adam, V., Carpentier, P., Faro, A., and Bourgeois, D. (2011). Combiner cristallographie cinétique et spectroscopie optique Application à l'étude des protéines fluorescentes (in french). 78–83.

Bell, A.F., Stoner-Ma, D., Wachter, R.M., and Tonge, P.J. (2003). Light-driven decarboxylation of wild-type green fluorescent protein. Journal of the American Chemical Society 125, 6919–6926.

Betzig, E., Patterson, G.H., Sougrat, R., Lindwasser, O.W., Olenych, S., Bonifacino, J.S., Davidson, M.W., Lippincott-Schwartz, J., and Hess, H.F. (2006). Imaging intracellular fluorescent proteins at nanometer resolution. Science 313, 1642–1645.

Bizzarri, R., Serresi, M., Cardarelli, F., Abbruzzetti, S., Campanini, B., Viappiani, C., and Beltram, F. (2010). Single amino acid replacement makes Aequorea victoria fluorescent proteins reversibly photoswitchable. Journal of the American Chemical Society 132, 85–95.

Bogdanov, A.M., Mishin, A.S., Yampolsky, I.V., Belousov, V.V., Chudakov, D.M., Subach, F.V., Verkhusha, V.V., Lukyanov, S., and Lukyanov, K.A. (2009). Green fluorescent proteins are light-induced electron donors. Nature Chemical Biology 5, 459–461.

Bouchet-Marquis, C., and Hoenger, A. (2011). Cryo-electron tomography on vitrified sections: A critical analysis of benefits and limitations for structural cell biology. Micron 42, 152–162.

Bourgeois, D., and Adam, V. (2012). Reversible photoswitching in fluorescent proteins: A mechanistic view. IUBMB Life 64, 482–491.

Brakemann, T., Stiel, A.C., Weber, G., Andresen, M., Testa, I., Grotjohann, T., Leutenegger, M., Plessmann, U., Urlaub, H., Eggeling, C., et al. (2011). A reversibly photoswitchable GFP-like protein with fluorescence excitation decoupled from switching. Nature Biotechnology 29, 942–947.

Brakemann, T., Weber, G., Andresen, M., Groenhof, G., Stiel, A.C., Trowitzsch, S., Eggeling, C., Grubmüller, H., Hell, S.W., Wahl, M.C., et al. (2010). Molecular basis of the light-driven switching of the photochromic fluorescent protein Padron. The Journal of Biological Chemistry 285, 14603–14609.

Braslavsky, S.E. (2007). Glossary of terms used in photochemistry, 3rd edition (IUPAC Recommendations 2006). Pure and Applied Chemistry 79, 293–465.

Bravaya, K.B., Subach, O.M., Korovina, N., Verkhusha, V.V., and Krylov, A.I. (2012). Insight into the Common Mechanism of the Chromophore Formation in the Red Fluorescent Proteins: The Elusive Blue Intermediate Revealed. Journal of the American Chemical Society 134, 2807–2814.

Brunger, A.T., and Adams, P.D. (2002a). Molecular Dynamics Applied to X-Ray Structure Refinement. ChemInform 33,.

Brunger, A.T., and Adams, P.D. (2002b). Molecular dynamics applied to X-ray structure refinement. Accounts of Chemical Research 35, 404–412.

Carlson, D.B., and Evans, J.E. (2011). Low-Cost Cryo-Light Microscopy Stage Fabrication for Correlated Light/Electron Microscopy. Journal of Visualized Experiments 52, 2–5.

Carpentier, P., Violot, S., Blanchoin, L., and Bourgeois, D. (2009). Structural basis for the phototoxicity of the fluorescent protein KillerRed. FEBS Letters 583, 2839–2842.

Chattoraj, M., King, B.A., Bublitz, G.U., and Boxer, S.G. (1996). Ultra-fast excited state dynamics in green fluorescent protein: multiple states and proton transfer. Proceedings of the National Academy of Sciences of the United States of America 93, 8362–8367.

Chudakov, D.M., Belousov, V.V., Zaraisky, A.G., Novoselov, V.V., Staroverov, D.B., Zorov, D.B., Lukyanov, S., and Lukyanov, K. a (2003a). Kindling fluorescent proteins for precise in vivo photolabeling. Nature Biotechnology 21, 191–194.

Chudakov, D.M., Feofanov, A.V., Mudrik, N.N., Lukyanov, S., and Lukyanov, K.A. (2003b). Chromophore environment provides clue to “kindling fluorescent protein” riddle. The Journal of Biological Chemistry 278, 7215–7219.

Chudakov, D.M., Matz, M.V., Lukyanov, S., and Lukyanov, K.A. (2010). Fluorescent Proteins and their applications in imaging living cells and tissues. Physiological Reviews 1103–1163.

Chudakov, D.M., Verkhusha, V.V., Staroverov, D.B., Souslova, E. a, Lukyanov, S., and Lukyanov, K.A. (2004). Photoswitchable cyan fluorescent protein for protein tracking. Nature Biotechnology 22, 1435–1439.

Cormack, B.P., Valdivia, R.H., and Falkow, S. (1996). FACS-optimized mutants of the green fluorescent protein (GFP). Gene 173, 33–38.

Creemers, T.M., Lock, a J., Subramaniam, V., Jovin, T.M., and Völker, S. (2000). Photophysics and optical switching in green fluorescent protein mutants. Proceedings of the National Academy of Sciences of the United States of America 97, 2974–2978.

Creemers, T.M.H., Lock, A.J., and Subramaniam, V. (1999). Three photoconvertible forms of green fluorescent protein identified by spectral hole-burning. Nature 557–560.

Creemers, TM H Lock, A.J., Subramaniam, V., and Jovin, T.M. (2002). Red-shifted mutants of green fluorescent protein : reversible photoconversions studied by hole-burning and high-resolution spectroscopy. Science 275, 109–121.

Dedecker, P., Hotta, J., Flors, C., Sliwa, M., Uji-i, H., Roeffaers, M.B.J., Ando, R., Mizuno, H., and Miyawaki, A. (2007). Subdiffraction imaging through the selective donut-mode depletion of thermally stable photoswitchable fluorophores : numerical analysis and application to the Fluorescent Protein Dronpa. 16132–16141.

Deheyn, D.D., Kubokawa, K., McCarthy, J.K., Murakami, A., Porrachia, M., Rouse, G.W., and Holland, N.D. (2007). Endogenous green fluorescent protein (GFP) in amphioxus. The Biological Bulletin 213, 95–100.

Delagrave, S., Hawtin, R.E., Silva, C.M., Yang, M.M., and Youvan, D.C. (1995). Red-Shifted Excitation Mutants of the Green Fluorescent Protein. Nature Biotechnology 13, 151–154.

Dickson, R.M., Cubitt, a B., Tsien, R.Y., and Moerner, W.E. (1997). On/off blinking and switching behaviour of single molecules of green fluorescent protein. Nature 388, 355–358.

Durin, G., Delaunay, A., Darnault, C., Heyes, D.J., Royant, A., Vernede, X., Hunter, C.N., Weik, M., and Bourgeois, D. (2009). Simultaneous measurements of solvent dynamics and functional kinetics in a light-activated enzyme. Biophysical Journal 96, 1902–1910.

Ehrenberg, M. (2008). The green fluorescent protein : discovery, expression and development. In Scientific Background on the Nobel Prize in Chemistry 2008, pp. 0–17.

Evrogen (2007). Cyan-to-green photoswitchable fluorescent protein. 2–5.

Fang, C., Frontiera, R.R., Tran, R., and Mathies, R.A. (2009). Mapping GFP structure evolution during proton transfer with femtosecond Raman spectroscopy. Nature 462, 200–204.

Faro, A.R., Adam, V., Carpentier, P., Darnault, C., and Rosny, E.D. (2008). Low-temperature photoinduced protonation in photochromic fluorescent proteins . Photochemical & Photobiological Sciences 1–7.

Faro, A.R., Carpentier, P., Jonasson, G., Pompidor, G., Arcizet, D., Demachy, I., and Bourgeois, D. (2011). Low-temperature chromophore isomerization reveals the photoswitching mechanism of the fluorescent protein Padron. Journal of the American Chemical Society 133, 16362–16365.

Fernández-Suárez, M., and Ting, A.Y. (2008). Fluorescent probes for super-resolution imaging in living cells. Nature Reviews. 9, 929–943.

Field, S., Bulina, M., Kelmanson, I., Bielawski, J., and Matz, M. (2006). Adaptive evolution of multicolored Fluorescent Proteins in reef-building corals. Journal of Molecular Evolution 62, 332–339.

Flors, C., Hotta, J., Uji-i, H., Dedecker, P., Ando, R., Mizuno, H., Miyawaki, A., and Hofkens, J. (2007). A Stroboscopic approach for fast photoactivation−localization microscopy with Dronpa mutants. Journal of the American Chemical Society 129, 13970–13977.

Follenius-Wund, A., Bourotte, M., Schmitt, M., Iyice, F., Lami, H., Bourguignon, J.-J., Haiech, J., and Pigault, C. (2003). Fluorescent derivatives of the GFP chromophore give a new insight into the GFP fluorescence process. Biophysical Journal 85, 1839–1850.

Fron, E., Flors, C., Schweitzer, G., Habuchi, S., Mizuno, H., Ando, R., Schryver, F.C.D., Miyawaki, A., and Hofkens, J. (2007). Ultrafast excited-state dynamics of the photoswitchable protein Dronpa. Journal of the American Chemical Society 129, 4870–4871.

Fuchs, J., Bohme, S., Oswald, F., Hedde, P.N., Krause, M., Wiedenmann, J., and Nienhaus, G.U. (2010). A photoactivatable marker protein for pulse-chase imaging with superresolution. Nature Methods 7, 627–630.

Garman, E.F., and McSweeney, S.M. (2007). Progress in research into radiation damage in cryo-cooled macromolecular crystals. Journal of Synchrotron Radiation 14, 1–3.

Grotjohann, T., Testa, I., Leutenegger, M., Bock, H., Urban, N.T., Lavoie-Cardinal, F., Willig, K.I., Eggeling, C., Jakobs, S., and Hell, S.W. (2011). Diffraction-unlimited all-optical imaging and writing with a photochromic GFP. Nature 1–5.

Gurskaya, N.G., Fradkov, A.F., Pounkova, N.I., Staroverov, D.B., Bulina, M.E., Yanushevich, Y.G., Labas, Y.A., Lukyanov, S., and Lukyanov, K. a (2003). A colourless green fluorescent protein homologue from the non-fluorescent hydromedusa Aequorea coerulescens and its fluorescent mutants. The Biochemical Journal 373, 403–408.

Gurskaya, N.G., Verkhusha, V.V., Shcheglov, A.S., Staroverov, D.B., Chepurnykh, T.V., Fradkov, A.F., Lukyanov, S., and Lukyanov, K. a (2006). Engineering of a monomeric green-to-red photoactivatable fluorescent protein induced by blue light. Nature Biotechnology 24, 461–465.

Gustafsson, M.G.L. (2005). Nonlinear structured-illumination microscopy: wide-field fluorescence imaging with theoretically unlimited resolution. Proceedings of the National Academy of Sciences of the United States of America 102, 13081–13086.

Habuchi, S., Ando, R., Dedecker, P., Verheijen, W., Mizuno, H., Miyawaki, A., and Hofkens, J. (2005). Reversible single-molecule photoswitching in the GFP-like fluorescent protein Dronpa. Proceedings of the National Academy of Sciences of the United States of America 102, 9511–9516.

Haddock, S.H.D., Mastroianni, N., and Christianson, L.M. (2010). A photoactivatable green-fluorescent protein from the phylum Ctenophora. Proceedings of the Royal Society B: Biological Sciences 277, 1155–1160.

Heim, R., Cubitt, A.B., and Tsien, R.Y. (1995). Improved green fluorescence. Nature 373, 663–664.

Heim, R., Prasher, D.C., and Tsien, R.Y. (1994). Wavelength mutations and posttranslational autoxidation of green fluorescent protein. Proceedings of the National Academy of Sciences of the United States of America 91, 12501–12504.

Hell, S.W., and Wichmann, J. (1994). Breaking the diffraction resolution limit by stimulated emission: stimulated-emission-depletion fluorescence microscopy. Optics Letters 19, 780–782.

Henderson, J.N., Ai, H.-W., Campbell, R.E., and Remington, S.J. (2007). Structural basis for reversible photobleaching of a green fluorescent protein homologue. Proceedings of the National Academy of Sciences of the United States of America 104, 6672–6677.

Henderson, J.N., Gepshtein, R., Heenan, J.R., Kallio, K., Huppert, D., and Remington, S.J. (2009). Structure and mechanism of the photoactivatable Green Fluorescent Protein. Journal of the American Chemical Society 131, 4176–4177.

Hess, S.T., Girirajan, T.P.K., and Mason, M.D. (2006). Ultra-high resolution imaging by fluorescence photoactivation localization microscopy. Biophysical Journal 91, 4258–4272.

Hofmann, M., Eggeling, C., Jakobs, S., and Hell, S.W. (2005). Breaking the diffraction barrier in fluorescence microscopy at low light intensities by using reversibly photoswitchable proteins. Proceedings of the National Academy of Sciences of the United States of America 102, 17565–17569.

Hotta, J., Fron, E., Dedecker, P., Janssen, K.P.F., Li, C., Mu, K., Harke, B., Bu, J., Hell, S.W., and Hofkens, J. (2010). Spectroscopic rationale for efficient stimulated-emission depletion microscopy fluorophores. Journal of the American Chemical Society 5021–5023.

Hurbain, I., and Sachse, M. (2011). The future is cold: cryo-preparation methods for transmission electron microscopy of cells. Biology of the Cell 103, 405–420.

Jonasson, G., Teuler, J.-M., Vallverdu, G., Mérola, F., Ridard, J., Lévy, B., and Demachy, I. (2011). Excited state dynamics of the Green Fluorescent Protein on the nanosecond time scale. Journal of Chemical Theory and Computation 7, 1990–1997.

Kabsch, W. (1988). Automatic indexing of rotation diffraction patterns. Journal of Applied Crystallography 21, 67–72.

Kirber, M.T., Chen, K., and Keaney, J.F. (2007). YFP photoconversion revisited: confirmation of the CFP-like species. Nature Methods 4, 767–768.

Kiuchi, T., Nagai, T., Ohashi, K., and Mizuno, K. (2011). Measurements of spatiotemporal changes in G-actin concentration reveal its effect on stimulus-induced actin assembly and lamellipodium extension. The Journal of Cell Biology 193, 365–380.

Klar, T.A., Jakobs, S., Dyba, M., Egner, A., and Hell, S.W. (2000). Fluorescence microscopy with diffraction resolution barrier broken by stimulated emission. Proceedings of the National Academy of Sciences of the United States of America 97, 8206–8210.

Kopek, B.G., Shtengel, G., Xu, C.S., Clayton, D.A., and Hess, H.F. (2012). Correlative 3D superresolution fluorescence and electron microscopy reveal the relationship of mitochondrial nucleoids to membranes. Proceedings of the National Academy of Sciences of the United States of America 109, 6136–6141.

Labas, Y.A., Gurskaya, N.G., Yanushevich, Y.G., Fradkov, A.F., Lukyanov, K.A., Lukyanov, S.A., and Matz, M.V. (2002). Diversity and evolution of the green fluorescent protein family. Proceedings of the National Academy of Sciences of the United States of America 99, 4256–4261.

Lee, S.F., Thompson, M.A., Schwartz, M.A., Shapiro, L., and Moerner, W.E. (2011). Super-resolution imaging of the nucleoid-associated protein HU in Caulobacter crescentus. Biophysical Journal 100, L31–3.

Lehmann, M., Rocha, S., Mangeat, B., Blanchet, F., Uji-I, H., Hofkens, J., and Piguet, V. (2011). Quantitative multicolor super-resolution microscopy reveals tetherin HIV-1 interaction. PLoS Pathogens 7, e1002456.

Leiderman, P., Huppert, D., and Agmon, N. (2006). Transition in the temperature-dependence of GFP fluorescence: from proton wires to proton exit. Biophysical Journal 90, 1009–1018.

Lelimousin, M., Adam, V., Nienhaus, G.U., Bourgeois, D., and Field, M.J. (2009). Photoconversion of the fluorescent protein EosFP: a hybrid potential simulation study reveals intersystem crossings. Journal of the American Chemical Society 131, 16814–16823.

Lew, M.D., Lee, S.F., Ptacin, J.L., Lee, M.K., Twieg, R.J., Shapiro, L., and Moerner, W.E. (2011). Three-dimensional superresolution colocalization of intracellular protein superstructures and the cell surface in live Caulobacter crescentus. Proceedings of the National Academy of Sciences of the United States of America.

Li, G., Zhang, Q.-J., Zhong, J., and Wang, Y.-Q. (2009). Evolutionary and functional diversity of green fluorescent proteins in cephalochordates. Gene 446, 41–49.

Li, X., Chung, L.W., Mizuno, H., Miyawaki, A., and Morokuma, K. (2010). Primary events of photodynamics in reversible photoswitching Fluorescent Protein Dronpa. The Journal of Physical Chemistry Letters 1, 3328–3333.

Livet, J., Weissman, T. a, Kang, H., Draft, R.W., Lu, J., Bennis, R. a, Sanes, J.R., and Lichtman, J.W. (2007). Transgenic strategies for combinatorial expression of fluorescent proteins in the nervous system. Nature 450, 56–62.

Lu, H.P., and Xie, X.S. (1997). Single-molecule spectral fluctuations at room temperature. Nature 385, 143–146.

Luin, S., Voliani, V., Lanza, G., Bizzarri, R., Amat, P., Tozzini, V., Serresi, M., and Beltram, F. (2009). Raman study of chromophore states in photochromic fluorescent proteins. Journal of the American Chemical Society 131, 96–103.

Lukyanov, K.A., Fradkov, A.F., Gurskaya, N.G., Matz, M.V., Labas, Y.A., Savitsky, A.P., Markelov, M.L., Zaraisky, A.G., Zhao, X., Fang, Y., et al. (2000). Natural animal coloration can Be determined by a nonfluorescent green fluorescent protein homolog. The Journal of Biological Chemistry 275, 25879–25882.

Lummer, M., Humpert, F., Steuwe, C., Caesar, K., Schüttpelz, M., Sauer, M., and Staiger, D. (2011). Reversible Photoswitchable DRONPA-s Monitors Nucleocytoplasmic Transport of an RNA-Binding Protein in Transgenic Plants. Traffic 12, 693–702.

Maddalo, S.L., and Zimmer, M. (2006). The role of the protein matrix in green fluorescent protein fluorescence. Photochemical & Photobiological 82, 367–372.

Matz, M.V., Fradkov, A.F., Labas, Y.A., Savitsky, A.P., Zaraisky, A.G., Markelov, M.L., and Lukyanov, S.A. (1999). Fluorescent proteins from nonbioluminescent Anthozoa species. Nature Biotechnology 17, 969–973.

McAnaney, T.B., Zeng, W., Doe, C.F.E., Bhanji, N., Wakelin, S., Pearson, D.S., Abbyad, P., Shi, X., Boxer, S.G., and Bagshaw, C.R. (2005). Protonation, photobleaching, and photoactivation of yellow fluorescent protein (YFP 10C): a unifying mechanism. Biochemistry 44, 5510–5524.

Mccoy, A.J. (2007). Structures of protein complexes by molecular replacement with Phaser. Acta Crystallographica Section D D63, 32–41.

Mckinney, S.A., Murphy, C.S., Hazelwood, K.L., Michael, W., and Looger, L.L. (2009). A bright and photostable photoconvertible fluorescent protein for fusion tags. Nature Methods 6, 131–133.

Miyawaki, A., and Tsien, R.Y. (2000). Monitoring protein conformations and interactions by fluorescence resonance energy transfer between mutants of green fluorescent protein. Methods in Enzymology 327, 472–500.

Mizuno, H., Mal, T.K., Tong, K.I., Ando, R., Furuta, T., Ikura, M., and Miyawaki, A. (2003). Photo-induced peptide cleavage in the green-to-red conversion of a fluorescent protein. Molecular Cell 12, 1051–1058.

Mizuno, H., Mal, T.K., Wälchli, M., Kikuchi, A., Fukano, T., Ando, R., Jeyakanthan, J., Taka, J., Shiro, Y., Ikura, M., et al. (2008). Light-dependent regulation of structural flexibility

in a photochromic fluorescent protein. Proceedings of the National Academy of Sciences of the United States of America 105, 9227–9232.

Moffat, K., and Henderson, R. (1995). Freeze trapping of reaction intermediates. Current Opinion in Structural Biology 5, 656–663.

Nam, K.-H., Kwon, O.Y., Sugiyama, K., Lee, W.-H., Kim, Y.K., Song, H.K., Kim, E.E., Park, S.-Y., Jeon, H., and Hwang, K.Y. (2007). Structural characterization of the photoswitchable fluorescent protein Dronpa-C62S. Biochemical and Biophysical Research Cmmunications 354, 962–967.

Nifosı, R., Ferrari, A., Arcangeli, C., Tozzini, V., and Pellegrini, V. (2003). Photoreversible dark state in a tristable Green Fluorescent Protein variant. Journal of Physical Chemistry B 107, 1679–1684.

Niwa, H., Inouye, S., Hirano, T., Matsuno, T., Kojima, S., Kubota, M., Ohashi, M., and Tsuji, F.I. (1996). Chemical nature of the light emitter of the Aequorea green fluorescent protein. Proceedings of the National Academy of Sciences of the United States of America 93, 13617–13622.

Nobelprize.org (2008). "The Nobel Prize in Chemistry 2008."

Olsen, S., Lamothe, K., and Martínez, T.J. (2010). Protonic gating of excited-state twisting and charge localization in GFP Chromophores: a mechanistic hypothesis for reversible photoswitching. Journal of the American Chemical Society 132, 1192–1193.

Olsen, S., and McKenzie, R.H. (2009). A diabatic three-state representation of photoisomerization in the green fluorescent protein chromophore. The Journal of Chemical Physics 130, 184302.

Olsen, S., and McKenzie, R.H. (2010). A dark excited state of fluorescent protein chromophores, considered as Brooker dyes. Chemical Physics Letters 492, 150–156.

Ormo, M. (1996). Crystal structure of the Aequorea victoria green fluorescent protein. Science 273, 1392–1395.

Patterson, G.H., and Lippincott-Schwartz, J. (2002). A Photoactivatable GFP for selective photolabeling of proteins and cells. Science 297, 1873–1877.

Petersen, J., Wilmann, P.G., Beddoe, T., Oakley, A.J., Devenish, R.J., Prescott, M., and Rossjohn, J. (2003). The 2.0-A crystal structure of eqFP611, a far red fluorescent protein from the sea anemone Entacmaea quadricolor. The Journal of Biological Chemistry 278, 44626–44631.

Pouwels, L.J., Zhang, L., Chan, N.H., Dorrestein, P.C., and Wachter, R.M. (2008). Kinetic isotope effect studies on the de novo rate of chromophore formation in fast- and slow-maturing GFP variants. Biochemistry 47, 10111–10122.

Quillin, M.L., Anstrom, D.M., Shu, X., O'Leary, S., Kallio, K., Chudakov, D.M., and Remington, S.J. (2005). Kindling fluorescent protein from Anemonia sulcata: dark-state structure at 1.38 A resolution. Biochemistry 44, 5774–5787.

Rego, E.H., Shao, L., Macklin, J.J., Winoto, L., Johansson, G.A., Kamps-Hughes, N., Davidson, M.W., and Gustafsson, M.G.L. (2012). Nonlinear structured-illumination microscopy with a photoswitchable protein reveals cellular structures at 50-nm resolution. Proceedings of the National Academy of Sciences of the United States of America 109, E135–43.

Royant, A., Carpentier, P., Ohana, J., McGeehan, J., Paetzold, B., Noirclerc-Savoye, M., Vernède, X., Adam, V., and Bourgeois, D. (2007). Advances in spectroscopic methods for biological crystals. Journal of Applied Crystallography 40, 1105–1112.

Schäfer, L.V., Groenhof, G., Boggio-Pasqua, M., Robb, M. a, and Grubmüller, H. (2008). Chromophore protonation state controls photoswitching of the fluoroprotein asFP595. PLoS Computational Biology 4, e1000034.

Schäfer, L.V., Groenhof, G., Klingen, A.R., Ullmann, G.M., Boggio-Pasqua, M., Robb, M. a, and Grubmüller, H. (2007). Photoswitching of the fluorescent protein asFP595: mechanism, proton pathways, and absorption spectra. Angewandte Chemie 46, 530–536.

Shagin, D.A., Barsova, E.V., Yanushevich, Y.G., Fradkov, A.F., Lukyanov, K.A., Labas, Y.A., Semenova, T.N., Ugalde, J.A., Meyers, A., Nunez, J.M., et al. (2004). GFP-like proteins as ubiquitous metazoan superfamily: evolution of functional features and structural complexity. Molecular Biology and Evolution 21, 841–850.

Shaner, N.C., Lin, M.Z., McKeown, M.R., Steinbach, P.A., Hazelwood, K.L., Davidson, M.W., and Tsien, R.Y. (2008). Improving the photostability of bright monomeric orange and red fluorescent proteins. Nature Methods 5, 545–551.

Shimomura, O. (1995). A short story of aequorin. The Biological Bulletin 189, 1–5.

Shimomura, O., Johnson, F.H., and Saiga, Y. (1962). Extraction, purification and properties of aequorin, a bioluminescent protein from the luminous hydromedusan, Aequorea. Journal of Cellular and Comparative Physiology 59, 223–239.

Shinobu, A., Palm, G.J., Schierbeek, A.J., and Agmon, N. (2010). Visualizing Proton Antenna in a High-Resolution Green Fluorescent Protein Structure. Journal of the American Chemical Society 132, 11093–11102.

Shroff, H., Galbraith, C.G., Galbraith, J.A., White, H., Gillette, J., Olenych, S., Davidson, M.W., and Betzig, E. (2007). Dual-color superresolution imaging of genetically expressed probes within individual adhesion complexes. Proceedings of the National Academy of Sciences of the United States of America 104, 20308–20313.

Sinnecker, D., Voigt, P., Hellwig, N., and Schaefer, M. (2005). Reversible photobleaching of enhanced green fluorescent proteins. Biochemistry 44, 7085–7094.

Stiel, A.C., Andresen, M., Bock, H., Hilbert, M., Schilde, J., Schönle, A., Eggeling, C., Egner, A., Hell, S.W., and Jakobs, S. (2008). Generation of monomeric reversibly switchable red fluorescent proteins for far-field fluorescence nanoscopy. Biophysical Journal 95, 2989–2997.

Stiel, A.C., Trowitzsch, S., Weber, G., Andresen, M., Eggeling, C., Hell, S.W., Jakobs, S., and Wahl, M.C. (2007). 1.8 A bright-state structure of the reversibly switchable fluorescent protein Dronpa guides the generation of fast switching variants. Biochemical Journal 402, 35–42.

Subach, F.V., Patterson, G.H., Manley, S., Gillette, J.M., and Verkhusha, V.V. (2010a). Photoactivatable mCherry for high-resolution two-color fluorescence microscopy. Nature Methods 6, 153–159.

Subach, F.V., Patterson, G.H., Renz, M., Lippincott-Schwartz, J., and Verkhusha, V.V. (2010b). Bright monomeric photoactivatable Red Fluorescent Protein for two-color super-resolution sptPALM of live cells. Journal of the American Chemical Society 132, 6481–6491.

Subach, F.V., Piatkevich, K.D., and Verkhusha, V.V. (2011a). Directed molecular evolution to design advanced red fluorescent proteins. Nature Methods 8, 1019–1026.

Subach, F.V., Zhang, L., Gadella, T.W.J., Gurskaya, N.G., Lukyanov, K.A., and Verkhusha, V.V. (2010c). Red fluorescent protein with reversibly photoswitchable absorbance for photochromic FRET. Chemistry & Biology 17, 745–755.

Subach, O.M., Patterson, G.H., Ting, L.-M., Wang, Y., Condeelis, J.S., and Verkhusha, V.V. (2011b). A photoswitchable orange-to-far-red fluorescent protein, PSmOrange. Nature Methods 8, 771–777.

Terwilliger, T.C., Grosse-Kunstleve, R.W., Afonine, P.V., Moriarty, N.W., Adams, P.D., Read, R.J., Zwart, P.H., and Hung, L.-W. (2008). Iterative-build OMIT maps: map improvement by iterative model building and refinement without model bias. Acta Crystallographica Section D 64, 515–524.

Thompson, R.E., Larson, D.R., and Webb, W.W. (2002). Precise nanometer localization analysis for individual fluorescent probes. Biophysical Journal 82, 2775–2783.

Tsien, R.Y. (1998). The green fluorescent protein. Annual Review of Biochemistry 67, 509–544.

Tsutsui, H., Karasawa, S., Shimizu, H., Nukina, N., and Miyawaki, A. (2005). Semi-rational engineering of a coral fluorescent protein into an efficient highlighter. EMBO Reports 6, 233–238.

Ursby, T., and Bourgeois, D. (1997). Improved estimation of structure-factor difference amplitudesfrom poorly accurate data. Acta Crystallographica Section A 53, 564–575.

Valentin, G., Verheggen, C., Piolot, T., Neel, H., Coppey-Moisan, M., and Bertrand, E. (2005). Photoconversion of YFP into a CFP-like species during acceptor photobleaching FRET experiments. Nature Methods 2, 801.

Verkhusha, V.V., and Sorkin, A. (2005). Conversion of the monomeric red fluorescent protein into a photoactivatable probe. Chemistry & Biology 12, 279–285.

Violot, S., Carpentier, P., Blanchoin, L., and Bourgeois, D. (2009). Reverse pH-dependence of chromophore protonation explains the large Stokes shift of the red fluorescent protein mKeima. Journal of the American Chemical Society 131, 10356–10357.

Wachter, R.M., Elsliger, M. a, Kallio, K., Hanson, G.T., and Remington, S.J. (1998). Structural basis of spectral shifts in the yellow-emission variants of green fluorescent protein. Structure 6, 1267–1277.

Wachter, R.M., Yarbrough, D., Kallio, K., and Remington, S.J. (2000). Crystallographic and energetic analysis of binding of selected anions to the yellow variants of green fluorescent protein. Journal of Molecular Biology 301, 157–171.

Ward, W.W., and Bokman, S.H. (1982). Reversible denaturation of Aequorea green-fluorescent protein: physical separation and characterization of the renatured protein. Biochemistry 21, 4535–4540.

Weber, W., Helms, V., McCammon, J.A., and Langhoff, P.W. (1999). Shedding light on the dark and weakly fluorescent states of green fluorescent proteins. Proceedings of the National Academy of Sciences of the United States of America 96, 6177–6182.

Wiedenmann, J., Ivanchenko, S., Oswald, F., Schmitt, F., Röcker, C., Salih, A., Spindler, K.-D., and Nienhaus, G.U. (2004). EosFP, a fluorescent marker protein with UV-inducible green-to-red fluorescence conversion. Proceedings of the National Academy of Sciences of the United States of America 101, 15905–15910.

Wiedenmann, J., and Nienhaus, G.U. (2006). Live-cell imaging with EosFP and other photoactivatable marker proteins of the GFP family. Proteomics 1–14.

Willig, K.I., Stiel, A.C., Brakemann, T., Jakobs, S., and Hell, S.W. (2011). Dual-Label STED nanoscopy of living cells using photochromism. Nano Letters 11, 3970–3973.

Wilmann, P.G., Petersen, J., Devenish, R.J., Prescott, M., and Rossjohn, J. (2005). Variations on the GFP chromophore: A polypeptide fragmentation within the chromophore revealed in the 2.1 A crystal structure of a nonfluorescent chromoprotein from Anemonia sulcata. Journal of Biological Chemistry 280, 2401–2404.

Wilmann, P.G., Turcic, K., Battad, J.M., Wilce, M.C.J., Devenish, R.J., Prescott, M., and Rossjohn, J. (2006). The 1.7 A crystal structure of Dronpa: a photoswitchable Green Fluorescent Protein. Journal of Molecular Biology 364, 213–224.

Yang, F., Moss, L.G., and Phillips, G.N. (1996). The molecular structure of Green Fluorescent Protein. Nature Biotechnology 14, 1246–1251.

Yang, X., Ren, Z., Kuk, J., and Moffat, K. (2011). Temperature-scan cryocrystallography reveals reaction intermediates in bacteriophytochrome. Nature 479, 428–432.

Zhang, L., Patel, H.N., Lappe, J.W., and Wachter, R.M. (2006). Reaction progress of chromophore biogenesis in green fluorescent protein. Journal of the American Chemical Society 128, 4766–4772.

Annex 1

LOW-TEMPERATURE PHOTOINDUCED PROTONATION IN PHOTOCHROMIC FLUORESCENT PROTEINS. FARO, ALINE REGIS; ADAM, VIRGILE; CARPENTIER, PHILIPPE; DARNAULT, CLAUDINE; BOURGEOIS, DOMINIQUE; DE ROSNY, EVE. **PHOTOCHEMICAL & PHOTOBIOLOGICAL SCIENCES, 2008.**

This article is published as part of a themed issue of ***Photochemical & Photobiological Sciences*** on

Synthetic and natural photoswitches

Guest edited by **Dario Bassani**, **Johan Hofkens** and **Jean Luc Pozzo**

Published in **issue 2, 2010**

Other articles in this issue include:

Low-temperature switching by photoinduced protonation in photochromic fluorescent proteins†

Aline Regis Faro,[a] Virgile Adam,[b] Philippe Carpentier,[a] Claudine Darnault,[a] Dominique Bourgeois*[a] and Eve de Rosny*[a]

Received 2nd October 2009, Accepted 23rd November 2009
First published as an Advance Article on the web 19th January 2010
DOI: 10.1039/b9pp00121b

We have studied the photoswitching behaviour of a number of photochromic fluorescent proteins at cryo-temperature. Spectroscopic investigations at the ensemble level showed that EYFP, Dronpa and IrisFP all exhibit reversible photoswitching at 100 K, albeit with a low quantum yield. The photophysics of the process were studied in more details in the case of EYFP. The data suggest that photoinduced protonation of the chromophore is responsible for off-switching at cryo-temperature, and thus is possible in the absence of significant conformational freedom. This finding is consistent with the hypothesis that chromophore protonation may precede large amplitude conformational changes such as *cis–trans* isomerisation during off-photoswitching at room temperature. However, our data suggest that low-barrier photoinduced protonation pathways may in fact compete with room-temperature off-switching reactions in photochromic fluorescent proteins. The occurrence of reversible photoswitching at low-temperature is of interest to envisage cryo-nanoscopy experiments using genetically encoded fluorophores.

Introduction

Photochromism in fluorescent proteins (FPs) was discovered more than 10 years ago in a seminal work by Dickson *et al.*,[1] who showed that the fluorescence properties of yellow fluorescent proteins (YFPs) could be reversibly modified upon illumination at specific wavelengths. In the last few years, an impressive number of photochromic FPs (also called reversibly switchable FPs (RSFPs)), have been discovered or engineered, including Dronpa,[2,3] variants thereof,[4,5] mTFP0.7,[6] rsCherryRev,[7] and, recently, cerFP505 from a deep-sea ceriantharian.[8] Most RSFPs display negative photoswitching, that is, fluorescence off-switching resulting from illumination at wavelengths absorbed by the protein in its fluorescent state. However, the palette of RSFPs also includes asFP595,[9] Padron[10] and rsCherry,[7] which, in contrast, display positive switching. RSFPs, switching reversibly between a dark and a fluorescent state, are distinguished from photoconvertible fluorescent proteins (PCFPs), such as Kaede[11] or EosFP,[12] which undergo an irreversible colour change from green to red upon illumination with violet light. Recently, a single mutant of EosFP, named IrisFP, has been shown to be an efficient photoswitcher combining the properties of RSFPs and PCFPs.[13] Interestingly, the combination of off-switching and intramolecular Förster energy transfer (FRET) promotes reversible switching in tetrameric IrisFP between red and green colours.[13]

RSFPs offer interesting perspectives as biotechnological tools, for example as potential high-density optical data storage media.[14] However, their major impact, together with PCFPs, has concerned the development of super-resolution microscopy through PALM/STORM approaches.[15] RESOLFT point scanning nanoscopy schemes, which allow utilizing reduced laser power density as compared to STED microscopy, have also been developed based on RSFPs.[16,17]

Despite the widespread interest of photochromic fluorescent proteins, the exact photophysical mechanisms leading to the light-induced reversible but thermally stable loss of fluorescence remains poorly understood. *Cis–trans* isomerisation of the chromophore has been directly observed in a number of crystallographic structures[6,9,13,18] and was evidenced by Raman experiments.[19] However, chromophore isomerisation need not be a common feature of all RSFPs. Mizuno *et al.* proposed in a recent NMR experiment that off-switching in Dronpa involves a disordering of the chromophore following light-induced protonation of its phenol moiety.[20] In fact, a common property of all RSFPs appears to be that the chromophore in the photoswitched state is protonated.[21] This is corroborated by the blue-shifted absorbance of the switched-state, which in all cases closely resembles that of the acid-induced state, although the two states actually differ.[19,22]

What is the primary event in on-off photoswitching, therefore, remains an open question. This is in contrast to back photoswitching, which can be explained by excited state proton transfer (ESPT). ESPT is a well known process by which the pK_a of the chromophore phenol group decreases dramatically in the excited state.[23] In back photoswitching, light induced deprotonation of the chromophore by ESPT may facilitate subsequent conformational relaxation (such as *trans–cis* isomerisation), leading back to the stable fluorescent state.[6] The high quantum yield of this process (>0.1) is consistent with efficient ESPT in the singlet excited state

[a]*IBS, Institut de Biologie Structurale Jean-Pierre Ebel, CEA, CNRS, Université Joseph Fourier, 41 rue Jules Horowitz, F-38027, Grenoble, France. E-mail: dominique.bourgeois@ibs.fr, eve.derosny@ibs.fr; Fax: +33-4-38785122; Tel: +33-4-38789644*
[b]*ESRF, 6 rue Jules Horowitz, BP 220, F-38043, Grenoble Cedex, France*
† This paper is part of a themed issue on synthetic and natural photoswitches.

S_1. It is interesting to envisage a symmetrical mechanism for on-off switching, that is, a light-induced protonation of the chromophore followed by structural changes. In this case, a significant rise of the chromophore pK_a in the excited state would be required as a first reaction step, a mechanism opposed to standard ESPT. The much lower yield observed experimentally for off-switching as compared to on-switching, typically $<10^{-3}$, is consistent with the idea that such "paradoxical" ESPT could take place in the triplet state T_1.[20] Indeed, molecules excited in the triplet state are less acidic than in the singlet state (see note added in proof).[24]

In order to decipher the mechanisms of photoswitching in RSFPs, it is useful to work at low-temperatures (LT). Photoswitching of organic dyes at temperatures as low as 1.4 K has been described at the single-molecule level, highlighting *e.g.* spectral diffusion processes.[25] Evidence for LT reversible photoswitching in GFP mutants between anionic and neutral states of the chromophore has also been provided by hole-burning experiments.[26,27] In the case of EYFP, it was proposed that reversible conversion occurs from the anionic B-state or from the neutral A-state to an anionic intermediate-like I-state absorbing at a maximum of ~460 nm.[28]

In the present work, we have used UV-vis spectroscopy at the ensemble level to demonstrate that reversible photoswitching can be achieved at 100 K between A and B states in a number of RSFPs, as a result of a light-induced protonation of the chromophore, in agreement with the previous hole-burning experiments.[27,28] At this temperature, due to the glassy state of the solvent, no large structural rearrangement of the chromophore and protein matrix is possible, indicating that significant conformational freedom is not required to achieve light-induced chromophore protonation. We show results from three different RSFPs, but we elaborate on EYFP to evaluate the mechanism of LT switching in more detail. EYFP is the first FP for which photoswitching was observed,[1] has been studied in great detail[27–34] and has been recently used in PALM nanoscopy.[35] We provide evidence that the nature of the light-induced protonated off-state at 100 K differs from that achieved upon illumination or acidification at room temperature (RT). Although our results are consistent with photoinduced protonation being the driving step in the RT switching pathway of RSFPs, we suggest that low-barrier photoinduced protonation pathways rather compete with RT off-switching reactions in these fluorescent proteins

Experimental

Expression and purification of the proteins

EYFP (Clontech, Mountainview, CA, USA) was cloned in a pET-15b vector using the appropriate restriction sites and expressed in *E. coli* BL21(DE3). It corresponds to the EGFP mutant S65G, V68L, S72A and T203Y[36] and contains the N terminal sequence (M)GSSHHHHHHSSGLVPRGSHM. Cells were grown in LB medium, to an absorbance ($A_{600\,nm}$) of 0.5–0.8 prior to induction for 15 h at 30 °C by the addition of 1 mM IPTG. After centrifugation, the cell pellet was re-suspended in 50 mM Tris-HCl pH 8.0, 300 mM NaCl, 15 mM imidazole plus Complete EDTA-free antiprotease (Roche Applied Sciences) and lysed by sonication. The protein was purified by chromatography on a cobalt affinity column (Clontech) followed by gel filtration on a High Load 16/60 superdex 75 column (Amersham Biosciences) in 50 mM Tris-HCl pH 8.0 and 300 mM NaCl. To remove Cl^- ions (which are known to alter the EYFP properties[37]), and to adjust the pH, buffer exchanges were performed using ultrafiltration (Microcon YM-10). The deprotonated form of EYFP was prepared in 50 mM Hepes pH 7.5 and the protonated form in 50 mM MES pH 6.0. Final pH values were adjusted with acetic acid.

Dronpa and IrisFP were kindly provided by Atsushi Miyawaki (RIKEN BSI, Japan) and Gerd Ulrich Nienhaus (Karlsruhe University, Germany), respectively, and were prepared as previously described.[13,20]

Absorption and fluorescence spectroscopy

Experiments were carried out at the Cryobench laboratory of the IBS/ESRF (Grenoble, France). For a detailed description of the setup used, see Royant *et al.*[38] and Durin *et al.*[39] Briefly, absorption and fluorescence emission spectra were recorded at 100 K or 295 K (RT) using a CCD-based spectrometer (HR2000+, Ocean Optics, Dunedin, FL, USA). Absorption measurements were realized using light from a broad band halogen–deuterium source (Mikropack DH2000-BAL, Ocean Optics) and optical fibers of 100 μm diameter connected to the two face-to-face objectives of the microspectrophotometer. Fluorescence excitation, as well as actinic illumination, were performed using an argon ion laser (514 nm or 488 nm, 532-MAP-A01, Melles-Griot, Carlsbad, CA, USA), a solid state diode laser (405 nm, OZ-1000, OZ optics, Ottawa, Canada) or a YAG laser (355 nm, NV-10210-110, JDS Uniphase, Milpitas, CA, USA).

For the low-temperature experiments, samples consisted of thin films (~20 μm optical path) of amorphous solutions, flash-frozen in cryo-loops typically used as sample holders in macromolecular crystallography experiments. Flash-cooling was realized with a nitrogen gas stream maintained at 100 K (Oxford cryostream, Series 700, Oxford, UK). Temperature ramps at a rate of 180 K h^{-1} were generated with this device. Solutions of EYFP, IrisFP and Dronpa were used at 1.7 mM, 1.4 mM and 0.9 mM concentrations, respectively. Such concentrations were necessary to ensure sufficient optical density considering the very thin samples. Moreover, these concentrations are relevant because they are in the same range as those in cells expressing fluorescent proteins used for cell imaging.[40] We verified in the case of EYFP that a three-fold reduced protein concentration did not measurably change the kinetics of LT switching (not shown). Glycerol (30 to 50%) was used as a cryo-protectant to prevent crystalline ice formation, which would interfere with spectroscopic measurements. In this setup, 200 μm-diameter fibres from the lasers were connected to the third objective of the microspectrophotometer, achieving a 90° geometry and a laser spot size on the sample of ~50 μm diameter.

For room temperature experiments, a 0.2 μL droplet of protein was mounted in a cell made of two cover slips sealed together with silicon grease, especially designed for the microspectrophotometer.[41] In this setup, laser illumination of the sample was achieved through a 200 μm-diameter fibre brought in close contact to the sample *via* a fibre holder. This allowed to achieve a laser spot size at the sample of ~0.4 mm diameter, *i.e.* larger than the sample diameter. Thus, the entire sample could be illuminated, an important consideration at RT when diffusion occurs in the liquid state.

Data analysis

Data were processed using a home-made routine based on the IDL software (Boulder, CO). Absorption spectra were corrected for background using a straight-slope baseline subtraction. Areas of overlapping absorbance peaks in Fig. 7 were calculated by non-linear least-square Gaussian fitting.

Quantum yield calculations

Quantum yields for LT switching were calculated based on time course experiments. Decay kinetics were fitted with mono- or biexponential models. In the latter case, only the fast phase was considered representative of the reversible protonation process (the slow phase is associated to non reversible bleaching processes).[42] The quantum yields Φ were obtained from the following formula:

$$\Phi = \frac{hc \times S \times N_{Av}}{\tau \times P \times \lambda \times \varepsilon \times \ln 10} \quad (1)$$

with Planck constant, h, speed of light, c, sample cross section, S, Avogadro's constant, N_{Av}, inverse rate constant τ, effective laser power, P, wavelength, λ, and extinction coefficient, ε. The effective laser power P was obtained from the laser power P_0 measured at the sample surface by taking into account absorption through the sample layer crossed by the beam before reaching the probed volume. Considering the thickness of this layer and the measured optical density of the samples, we estimated that $P \approx P_0/10$.

Results and discussion

Photochromic fluorescent proteins were investigated at the ensemble level using the microspectrophotometer of the Cryobench laboratory.[43] This device, normally dedicated to the study of macromolecular crystals at cryogenic temperatures, offers the opportunity to study nano-volume solution samples, which can be easily flash-cooled to the glassy state with only a moderate amount of cryo-protectant. Three different RSFPs exhibiting vastly different photoswitching capabilities where investigated: IrisFP, a very efficient photoswitcher ($\Phi_{on\text{-}off} \approx 10^{-2}$),[13] Dronpa, a moderately efficient photoswitcher ($\Phi_{on\text{-}off} \approx 10^{-4}$),[3] and EYFP, a weak photoswitcher ($\Phi_{on\text{-}off} \approx 10^{-6}$).[1]

Photoswitching at RT

First, the photoswitching efficiencies of the three proteins were compared at room temperature. Using similar illumination power density (≈0.4 W cm^{-2}), strong differences between the proteins were immediately apparent (Fig. 1). Whereas IrisFP could be reversibly photoswitched multiple times within a time window of ~500 s, with a contrast between the on and off states > 90%, Dronpa could only be switched twice with a lower contrast (~85%), and EYFP could not be reversibly switched at all using 514 nm and 405 nm light. In fact, illumination of EYFP with 405 nm light induced even more pronounced off-switching than with 514 nm light alone. This additional loss of fluorescence was spontaneously recovered by thermal relaxation (Fig. 1C). The lack of back-switching of EYFP at the ensemble level with 405 nm light differs from observations made at the single molecule level,[1,35] but is consistent with previous findings by Sinnecker *et al.*,[30] and by McAnaney *et al.*[29] who provided evidence that this protein can be reversibly switched only to a limited extent (≈25%), with back-switching requiring light at wavelengths <390 nm. In fact, when applying 355 nm laser light instead of 405 nm for

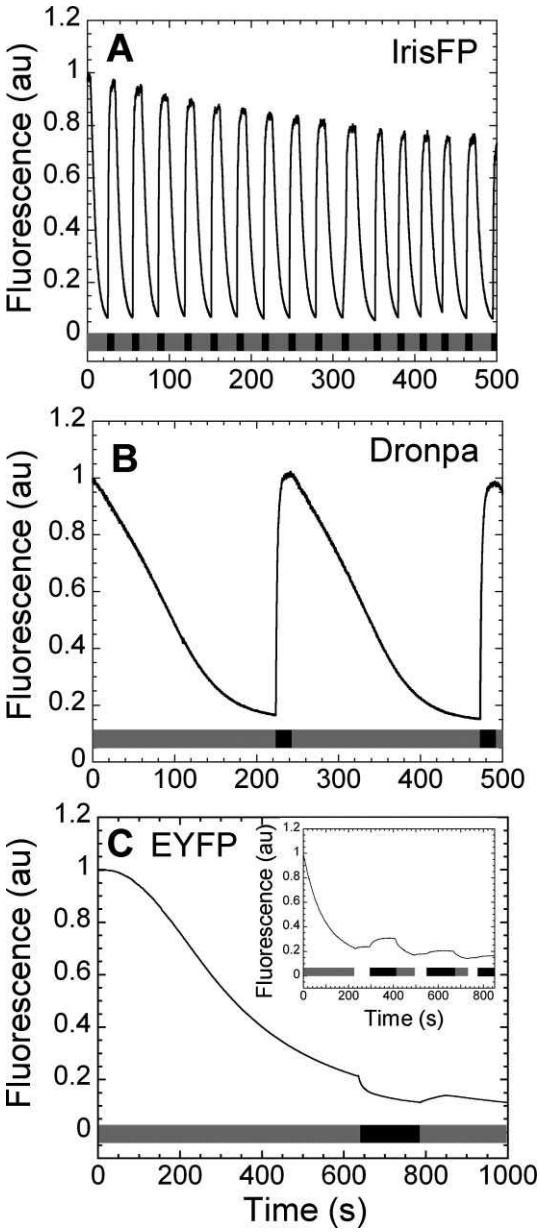

Fig. 1 Room temperature photoswitching of IrisFP, Dronpa and EYFP. (A) IrisFP and (B) Dronpa were illuminated with 488 nm laser light (0.29 W cm^{-2} and 0.39 W cm^{-2}, respectively, for IrisFP and Dronpa; grey lines above the *x*-axis) while 405 nm laser light (0.3 W cm^{-2}, black lines) was switched on and off. (C) EYFP was alternatively illuminated with 514 nm (0.2 W cm^{-2}, grey) and 405 nm (0.45 W cm^{-2}, black lines) light. (Inset) Similar experiment with 355 nm light for reactivation. A high power density of 0.04 kW cm^{-2} was used to accelerate the reaction. Short delays (white lines) were applied before illuminations at 355 nm to control the absence of fast spontaneous fluorescence recovery. The emission of fluorescence was measured at 474, 494 and 530 nm for IrisFP, Dronpa and EYFP, respectively. Fluorescence excitation wavelengths were the same as those used for actinic illumination.

back switching, EYFP fluorescence could be partly recovered, as expected (Fig. 1C, inset). The discrepancy between the behaviour of EYFP at the ensemble and single molecule levels might originate from an intrinsic bias in the selection of fluorescent molecules in single molecule experiments. It is possible that back switching by 405 nm light be only effective in some rare conformational states of the protein slowly interconverting with highly populated states that rather undergo irreversible bleaching or follow different switching pathways. Other factors, such as the level of oxygenation, the cellular environment,[35] the presence of a polymer matrix,[1] the salt content,[37] or the used light intensities may also play a role.

Photoswitching at 100 K of EYFP

A very different switching behaviour of EYFP was obtained at cryogenic temperature: when a nano droplet of a concentrated solution of EYFP was flash-cooled to 100 K and submitted to a sequence of illumination at 514 nm (~0.3 kW cm^{-2}) and 405 nm (~0.04 kW cm^{-2}), a minor but significant fraction (about 5%) of the molecules underwent multiple reversible switching (Fig. 2). Interestingly, this fraction was apparently resistant to photobleaching and did not interconvert to other proteins states during the experimental time, as the amount of fluorescence recovery in each cycle stayed approximately constant (see arrows on Fig. 2). This can be explained by the lack of major conformational fluctuations at 100 K.

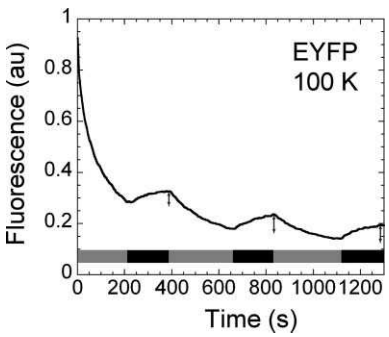

Fig. 2 Photoswitching of EYFP at 100 K. The protein was alternatively illuminated with 514 nm (0.3 kW cm^{-2}, grey lines above the *x*-axis) and 405 nm (0.06 kW cm^{-2}, black lines) laser light. At each cycle, an arrow shows the amount of fluorescence recovery during 405 nm illumination.

Next, the low-temperature photoswitching of EYFP was characterized in more detail. A time series of absorption spectra was recorded during illumination with 514 nm light at 100 K (Fig. 3A). A clear phototransformation was observed, from the anionic, deprotonated state of the chromophore (state B), to a presumably neutral state characterized by a broad absorbance band featuring maxima at 385 nm and 410 nm, and extending to the UV range. We refer to this absorption band as A3 (by reference to A1 and A2, which are common notations for acid-induced and RT switched states, respectively). The absorbance data exhibit a crisp isosbestic point at 437 nm, consistent with a single step interconversion process. The phototransformation kinetics, extracted at the peak absorption of the B-band and at 405 nm for the A3-band are shown in the inset of Fig. 3A. The decay of the anionic band is essentially biphasic, with a rapid phase followed by a slower phase. The build-up of A3 is also best described with a bi-exponential process, with the rate of the rapid phase (k = 0.03 s^{-1}) matching that of the fast decay of B (k = 0.02 s^{-1}). Based on these kinetics, the quantum yield of the rapid interconversion process was estimated to be $\Phi_{\text{on-off, 100 K}} \approx 10^{-6}$. Although this quantum yield is very small, it has to be considered in view of the considerably reduced rate of photobleaching at the used temperature, and is therefore significant. The neutral states photoinduced at 100 K are essentially non-fluorescent when excited at 488 nm, but exhibit blue fluorescence upon excitation in cryo-conditions with 405 nm light (Fig. 3C, D). Upon actinic illumination of A3 with 405 nm light at 100 K, back photoswitching occurs rapidly, although to a limited extent (Fig. 3B). The decay of the 405 nm component and the rise of the peak absorption of the B-band (Fig. 3B, inset) cannot be adequately fit by either mono-, bi-, or stretched-exponential processes. Nevertheless, the quantum yield for back photoswitching could be estimated to be $\Phi_{\text{off-on, 100 K}} \approx 10^{-4}$. Recovery of the fluorescent state B also slowly occurs in the dark at 100 K ($t_{1/2} \approx 2$ h, Fig. 4). The recovery is more pronounced and strongly accelerated upon temperature increase. These results suggest that different pathways may lead from A3 to B, which are thermally activated to a different extent and may involve intermediate species. In total, ~40% of the molecules are eventually able to back convert to the B-state.

Despite the moderate laser power density used in the described experiments, we verified that the B to A3 low temperature photoswitching results from a ground-state (one-photon) absorption process. This is demonstrated in Fig. 5, in which the rate of photoswitching is shown to be proportional to the used laser power density. Therefore, a two-step absorption process, which could be expected from the increase at low temperature of excited states lifetimes (such as that of the triplet state T_1), and which has been shown to trigger photoconversion in other fluorescent proteins,[44,45] can be ruled out.

States A1, A2′ and A3 differ

To further characterize the EYFP A3 band, we compared it to two other absorbance states corresponding to a neutral chromophore, A1 and A2′. A1 was obtained by buffer acidification, whereas A2′ was achieved by illumination at 514 nm at close to ambient temperature (in conditions similar to those used in Fig. 1; thus it should be noted that A2′ here refers to a mostly non-reversibly switched state and therefore is not called A2 as for other RSFPs). Samples of EYFP in those states were brought to 100 K and absorption and fluorescence emission spectra were recorded. Superpositions of the normalised spectra from A1, A2′ and A3 are shown in Fig. 6. It is seen that A1 and A3 share similar vibronic structures, clearly resolved at low-temperature (Fig. 6A). In contrast, A2′ exhibits a broader, smoother and blue shifted absorption profile. Similar fluorescence emission originate from all three species upon excitation by 405 nm light (Fig. 6B). The emission spectra display a double-humped blue fluorescence, accompanied by residual yellow fluorescence possibly due to direct excitation of molecules left in the B-state, or to limited excited state proton transfer (ESPT). Interestingly, we note that the blue fluorescence by A2′, which is largely composed of irreversibly switched molecules in a neutral state (Fig. 1), might relate to the spurious "blue species" previously noticed in EYFP and corrupting FRET experiments through contamination of the ECFP channel.[33,34,46] Whereas A1 and A3

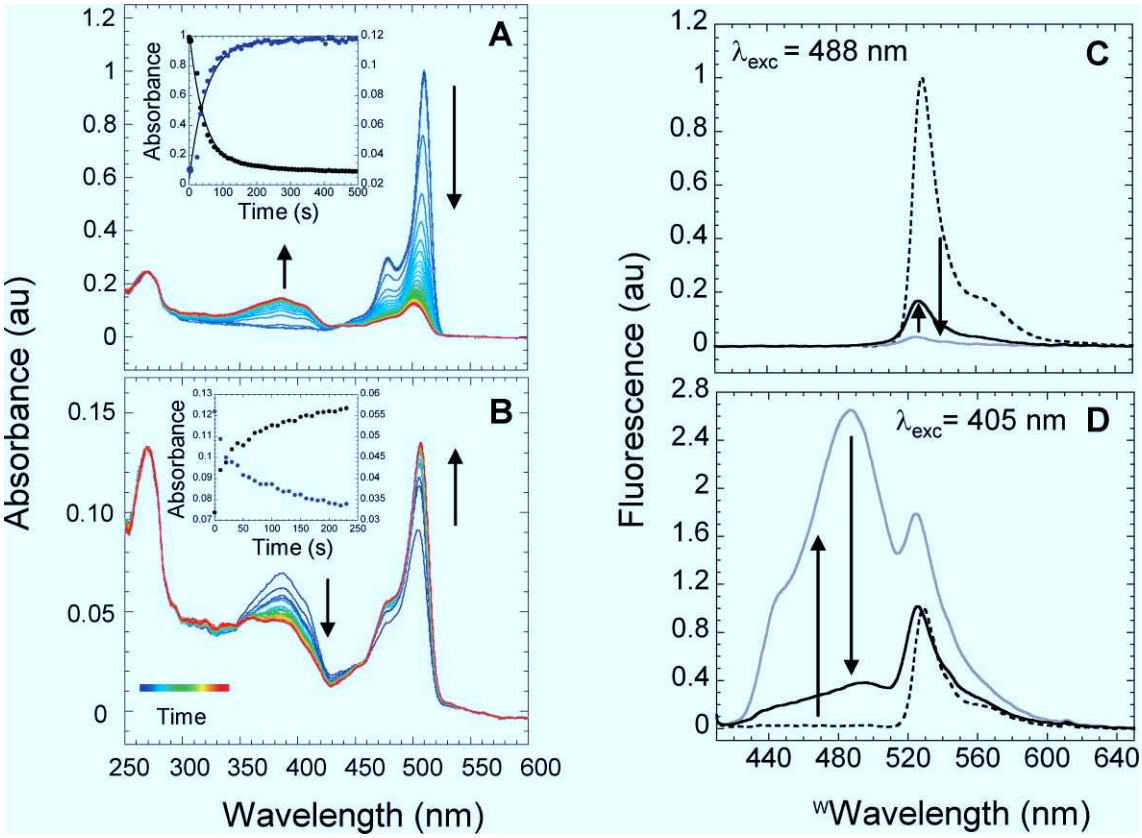

Fig. 3 Spectral evolution of EYFP during photoswitching at 100 K. (A) Time evolution of the absorption spectra of EYFP switched by illumination with 514 nm laser light (0.3 kW cm^{-2}). (Inset) Kinetic traces of the absorption at 510 nm (black) and 405 nm (blue); solid lines correspond to fitting with a bi-exponential kinetic model. (B) Time evolution of the absorption spectra during backswitching with 405 nm laser light (0.04 kW cm^{-2}). (Inset) Kinetic traces of the absorption at 510 nm (black) and 405 nm (blue). Spectra were normalized to the EYFP absorption at 510 nm before illumination. They are chronologically plotted according to the colour bar (from blue to red). (C,D) Fluorescence spectra upon excitation at 488 nm (C) or 405 nm (D) of the starting (black dashed line), switched (grey solid line) and backswitched (black solid line) EYFP. The fluorescence spectra were normalized on the maximum peak of EYFP before illumination.

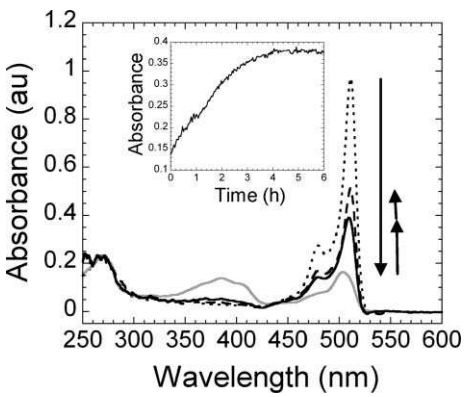

Fig. 4 Spectral evolution during temperature-driven backswitching of EYFP. EYFP (dotted line) was illuminated 3 min at 514 nm (0.3 kW cm^{-2}, grey solid line) and left in the dark at 100 K for 10 h (black solid line). The resulting product was warmed up to 180 K (180 K h^{-1}) and then cooled down to 100 K (dashed line). (Inset) Kinetic trace of the thermal recovery at 100 K, measured at 510 nm.

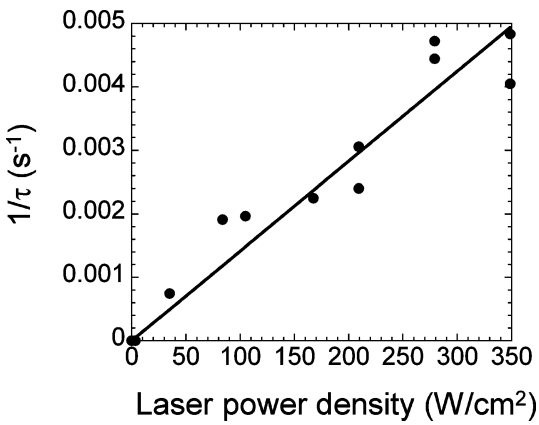

Fig. 5 Low-temperature photoswitching of EYFP proceeds *via* a 1-photon absorption process. The rate of photoswitching at 100 K is reported as a function of the 514 nm laser power density. The plotted rates ($1/\tau$) were obtained by fitting the time course of the 510 nm absorbance with a biexponential kinetic model. τ corresponds to the rate of the rapid phase. The solid line shows the slope best fitting the data.

may not be easily distinguished based on the LT absorption or fluorescence spectra, a strong difference exists between them. Indeed, contrary to A3, A1 cannot be back-converted to the B-state upon excitation at 405 nm at 100 K (Fig. 6C). Excitation of this species at cryo- temperature only results in photobleaching.

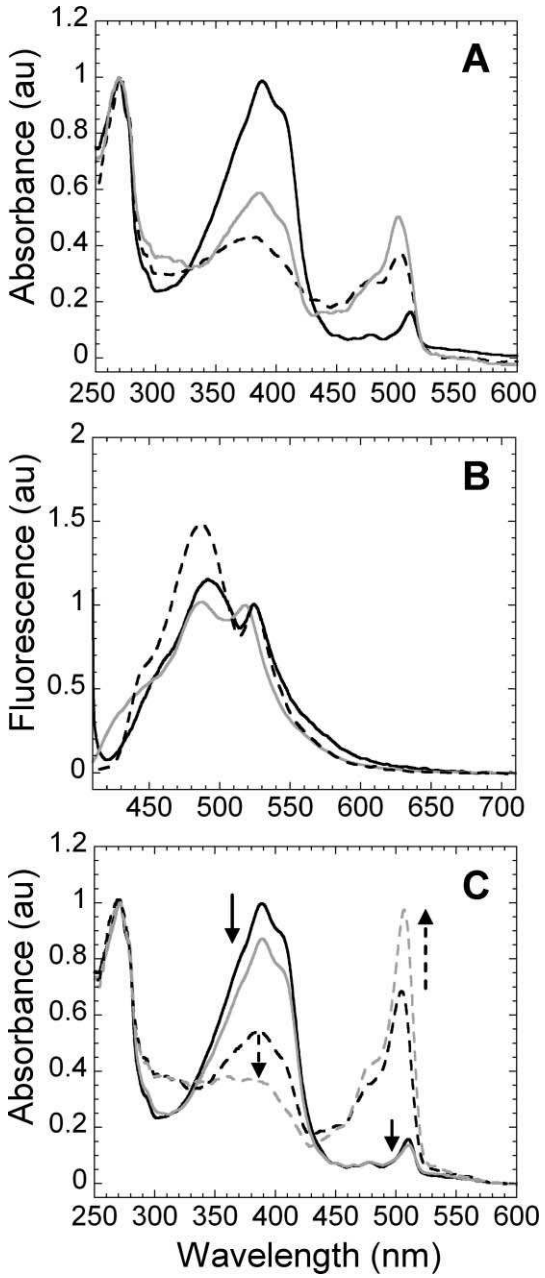

Fig. 6 Spectral signatures of the different protonated forms of EYFP. (A) Absorbance spectra of EYFP at acidic pH (A1, black line) and at neutral pH after switching with 514 nm laser light at low temperature (A3, grey line) and at close to room temperature (A2′, dashed line). (B) Fluorescence emission spectra (λ_{exc} = 405 nm) of EYFP at acidic pH (black line) and at neutral pH after switching with 514 nm laser light at low temperature (grey line) and at close to room temperature (dashed line). (C) Spectral evolution of EYFP before (A1, black line; A3 black dashed line) and after 405 nm illumination at 100 K (A1, grey line; A3 grey dashed line). All spectra were recorded at 100 K.

Taken together, these results suggest that pronounced structural differences exist between states A1/A2′ and B, whereas structural differences between states A3 and B are small. In the case of A1, this finding is fully consistent with pH jump experiments carried out at room temperature which showed that EYFP protonation occurs in two steps with a fast intermediate occurring first, followed by some slower step involving larger conformational rearrangements.[29] In summary, our data demonstrate that the A1, A2′ and A3 absorbance bands are essentially made of distinct EYFP species.

Is A3 involved in the reaction path from B to A2′?

In order to investigate whether A3 could be an intermediate on the pathway leading from B to A2′, a temperature dependent absorption microspectrophotometry (TDAM) experiment was conducted.[39] After a nano-droplet of EYFP was flash cooled to 100 K, a series of absorption spectra were recorded continuously while a temperature ramp from 100 to 260 K was applied at 180 K h^{-1}, under continuous illumination with 514 nm light (Fig. 7). Although these data only allow a qualitative assessment of the phototransformations involved, they suggest the following evolution of the sample. At cryo-temperatures (from 100 K to ~110 K), a buildup of A3 is clearly observed. However, from 110 K onwards, back conversion from A3 to B takes place, possibly driven by thermal activation as observed in Fig. 4. A new intermediate state builds-up, displaying peak absorption at 447 nm, and reaching a maximum at 155 K. Interestingly, this intermediate is reminiscent of the I-intermediate previously identified in low-temperature work and proposed to be involved in the EYFP photoconversion pathways.[28] From ~160 K, the I-like intermediate, as well as residual molecules in the B-state convert into the A2′ state, which reaches full occupancy from ~200 K onwards. A quantitative chemical kinetic model of the B → A2′ phototransformation pathway cannot be easily extracted from these data, notably due to the inherent coupling between time and temperature in TDAM experiments. Importantly, it remains unclear whether the A3 species is involved in this pathway. Although at first glance the data would suggest that A3 is not involved, since it essentially back transforms to B before A2′ starts being produced, this is not necessarily the case, as it may reappear

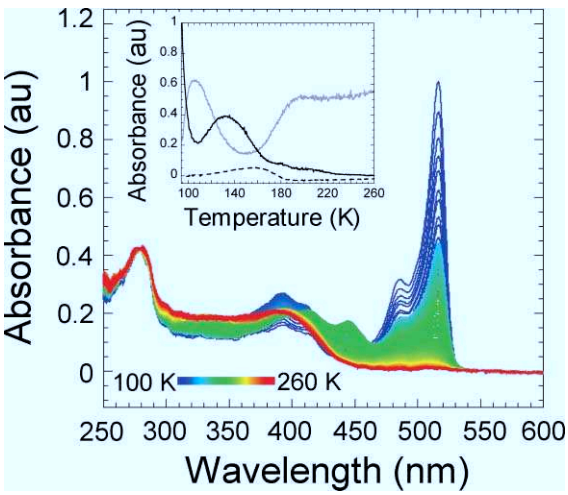

Fig. 7 Temperature dependent absorption microspectrophotometry of EYFP photoswitching. Evolution of the absorption spectra of EYFP submitted to a temperature gradient from 100 to 260 K (180 K h^{-1}, colour bar) during illumination at 514 nm (113 W cm^{-2}). (Inset) Temperature dependant evolution of the area of absorption bands centered at 400 nm (A-states; grey line), 445 nm (I-state; dashed line) and 514 nm (B-state; black line).

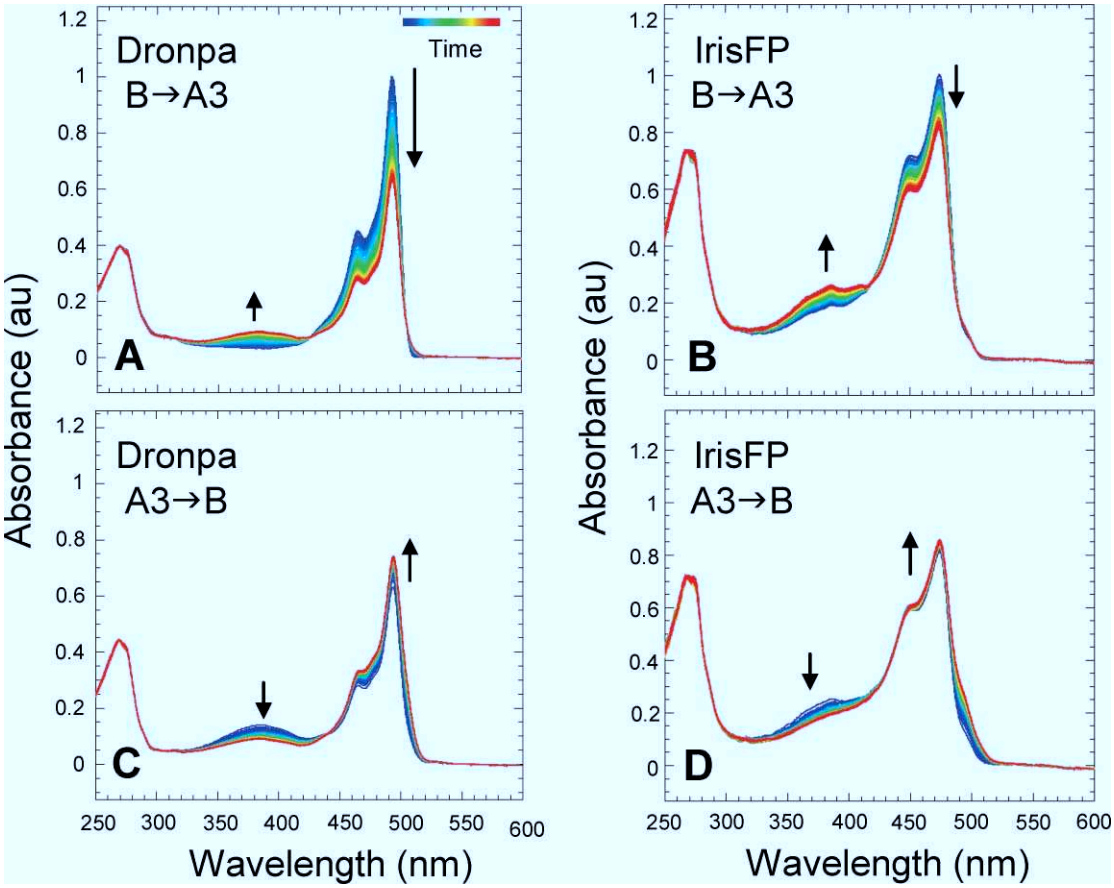

Fig. 8 Spectral evolution during photoswitching of Dronpa and IrisFP at 100 K. Time evolution of the absorption spectra after switching of (A) Dronpa and (B) IrisFP by illumination with 488 nm laser light (356 W cm^{-2}). Backswitching of (C) Dronpa and (D) IrisFP by illumination with 405 nm laser light (40 W cm^{-2}). The spectra are plotted chronologically according to the colour bars (from blue to red).

as a non rate-limiting intermediate (non visible in the TDAM data) at higher temperatures. In contrast, a I-like intermediate is definitively identified along the B to A2′ pathway and its further characterization will be of interest in future studies. Interpretation of the above-described experiment in terms of the mechanism of reversible switching at RT is impaired by the fact that A2′ is mostly composed of non-reversibly switched molecules (possibly the EYFP "blue species"[33,34,46]). Therefore, whether or not A3 is implicated in the switching mechanism of those molecules that can be reversibly switched by 514 nm and 405 nm light, as observed at the single molecule level, cannot be concluded from this experiment. Nevertheless, additional insight can be obtained by comparing different RSFPs, as described below.

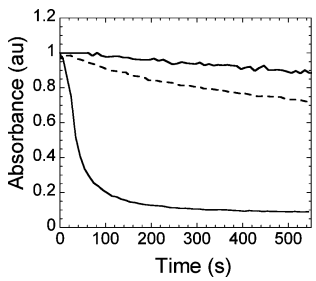

Fig. 9 Comparison of low-temperature photoswitching between EYFP, Dronpa and IrisFP. Absorption time-courses are plotted at 474 nm for Dronpa (dashed line), 494 nm for IrisFP (black line) and 514 nm for EYFP (grey line).

Photoinduced protonation in Dronpa and IrisFP

Low-temperature photoswitching in two other RSFPs, Dronpa and IrisFP, was investigated in a similar manner as that used for EYFP. Remarkably, the two proteins display reversible low-temperature photoswitching attributable to a photoinduced protonation of the chromophore (Fig. 8). The photoswitching kinetics at 100 K, however, are much slower as compared to the case of EYFP (Fig. 9). Whereas the quantum yield for low-temperature photoinduced protonation is ~10^{-6} for EYFP, it is ~4×10^{-7} for Dronpa, and ~9×10^{-8} for IrisFP. Therefore, by comparison with the results shown in Fig. 1, a clear anticorrelation emerges between the photoswitching efficiencies at RT and at 100 K. This suggests that a low activation barrier for photoinduced protonation possibly disfavours efficient photoswitching at room temperature. We hypothesize that photoinduced protonation leading to A_3 may act as a leakage pathway through which RSFPs escape bi-stable RT photoswitching. Further experiments will be needed to verify this assumption. The idea that, in RSFPs, low-temperature photoswitching mechanisms are decoupled from,

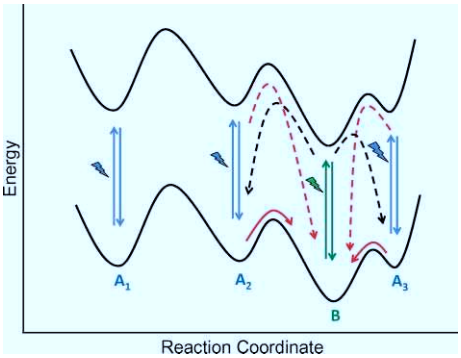

Fig. 10 Schematic diagram of the photoswitching of RSFPs. B, deprotonated form; A1, pH-induced protonated form; A2, reversibly switched protonated form photo-induced at room-temperature; A3 reversibly switched protonated form photo-induced at low-temperature. Photoswitching pathways from B to A2 or A3 are shown by black arrows. The photoswitching pathways from A2 or A3 to B are shown by red arrows.

and compete with those at room temperature, is sketched in Fig. 10. Nevertheless, this tentative conclusion does not exclude the possibility that RT photoswitching could be triggered by another mechanism of photoinduced protonation rather than by *cis–trans* isomerisation, as proposed for Dronpa.[20] Which photophysical event triggers photoswitching in RSFPs, therefore, still remains an open question (see note added in proof).

Conclusions

We have shown that reversible photoswitching occurs to a certain extent in a number of photochromic fluorescent proteins at cryo-temperature. Such photoswitching exhibits a low quantum yield and competes with other non-reversible phototransformations. A feature common to all RSFPs investigated is that low-temperature photoswitching involves a protonation of the chromophore. The occurrence of light-induced protonation at 100 K, a temperature at which conformational dynamics in proteins are largely inhibited, suggests that minor structural changes accompany the charge transfer process. Proton transfer to the hydroxybenzilidene group of the chromophore must therefore arise from nearby proton donors, possibly through proton tunnelling. In the case of GFP, Leiderman *et al.*[47] have shown that hydrogen-bond networks, *e.g.* formed between water molecules and Glu222, Asp82 and Glu5, provide proton wires even at low temperature. In the studied RSFPs, such proton donors are actually available, as judged from previous structural studies. In EYFP, His148 and a water molecule are in direct contact to the chromophore hydroxybenzylidene group.[32] In Dronpa, Ser142 H-bonds this group, and a network of residues may also be involved, including Glu140, His194, Ile195 and a water molecule.[20] In the case of IrisFP, Ser142 also H-bonds the chromophore, as well as a chain of water molecules leading directly into bulk solvent.[13]

We have also shown that LT photoinduced protonation results from a ground state absorption process. It is difficult to envisage the proton transfer in the singlet excited state, due to the drastic increase in the chromophore phenol group acidity known to take place in this excited state. Rather, we suggest that photoinduced protonation takes place in the triplet state, in agreement with previous proposals.[20,27,28] The significant reaction yield at 100 K might be linked to the increase of the triplet state lifetime as the temperature is lowered. Phosphorescence spectroscopy investigations would be useful to confirm the involvement of the triplet state.

The observation that chromophore protonation can occur in the absence of pronounced structural modification, and in particular without chromophore isomerisation, would suggest that protonation might precede further large scale structural relaxation such as *cis–trans* isomerisation during photoswitching at ambient temperature. However, our data hint that photoinduced protonation may rather divert RSFPs from their useful switching pathway. Based on this idea, it would be interesting to test how destabilization of the network of putative proton donors to the chromophore by rational engineering may alter the RT photoswitching properties of RSFPs.

The complexity and variety of the switching mechanisms observed in this work emphasizes the conformational heterogeneity commonly found in RSFPs and PCFPs. The superposition of states with differing photophysical properties has been also highlighted in a number of GFP members[48–51] and probably constitutes a general property of fluorescent proteins. Understanding the mechanisms leading to particular species is greatly facilitated when their molecular structures can be solved at near-atomic resolution. In the case of the various protonated species discussed here, subtle structural differences could be revealed. However it has to be kept in mind that the accuracy of structural models derived from crystallographic studies strongly depends on the achievable occupation of the species of interest relative to other species in the crystal. To this aim, in crystallo-spectroscopy and crystallography must go hand in hand.[52]

Finally, low temperature reversible photoswitching of genetically encoded fluorophores may find applications in cryo-nanoscopy schemes, a potentially useful method for correlative imaging in structural biology.[53–55]

Note added in proof

Recently, two papers provided new insight into the interplay between *cis–trans* isomerization and chromophore protonation in RSFPs.[56,57]

Abbreviations

EYFP	Enhanced Yellow Fluorescent Protein
PAFP	PhotoActivatable Fluorescent Protein
RSFP	Reversibly Switchable Fluorescent Protein
PCFP	PhotoConvertible Fluorescent Protein
PALM	PhotoActivated Localization Microscopy
STORM	STochastic Optical Reconstruction Microscopy
RESOLFT	REversible Saturable OpticaL Fluorescence Transitions
STED	STimulated Emission Depletion (microscopy)
TDAM	Temperature Derivative Absorption Microspectrophotometry
FRET	Förster Resonance Energy Transfer
LT	Low-temperature
RT	Room-temperature

Acknowledgements

The ESRF/PSB is acknowledged for support of the Cryobench laboratory. We thank U. Nienhaus for providing us with IrisFP and EosFP, and A. Miyawaki for providing us with Dronpa. This work was supported by the "Agence Nationale de la Recherche" (ANR-07-BLAN-0107-01). A. R. was supported by the CEA.

References

1 R. M. Dickson, A. B. Cubitt, R. Y. Tsien and W. E. Moerner, *Nature*, 1997, **388**, 355–358.
2 R. Ando, H. Mizuno and A. Miyawaki, *Science*, 2004, **306**, 1370–1373.
3 S. Habuchi, R. Ando, P. Dedecker, W. Verheijen, H. Mizuno, A. Miyawaki and J. Hofkens, *Proc. Natl. Acad. Sci. U. S. A.*, 2005, **102**, 9511–9516.
4 C. Flors, J. Hotta, H. Uji-i, P. Dedecker, R. Ando, H. Mizuno, A. Miyawaki and J. Hofkens, *J. Am. Chem. Soc.*, 2007, **129**, 13970–13977.
5 A. C. Stiel, S. Trowitzsch, G. Weber, M. Andresen, C. Eggeling, S. W. Hell, S. Jakobs and M. C. Wahl, *Biochem. J.*, 2007, **402**, 35–42.
6 J. N. Henderson, H. W. Ai, R. E. Campbell and S. J. Remington, *Proc. Natl. Acad. Sci. U. S. A.*, 2007, **104**, 6672–6677.
7 A. C. Stiel, M. Andresen, H. Bock, M. Hilbert, J. Schilde, A. Schonle, C. Eggeling, A. Egner, S. W. Hell and S. Jakobs, *Biophys. J.*, 2008, **95**, 2989–2997.
8 A. Vogt, C. D'Angelo, F. Oswald, A. Denzel, C. H. Mazel, M. V. Matz, S. Ivanchenko, G. U. Nienhaus and J. Wiedenmann, *PLoS One*, 2008, **3**, e3766.
9 M. Andresen, M. C. Wahl, A. C. Stiel, F. Grater, L. V. Schafer, S. Trowitzsch, G. Weber, C. Eggeling, H. Grubmuller, S. W. Hell and S. Jakobs, *Proc. Natl. Acad. Sci. U. S. A.*, 2005, **102**, 13070–13074.
10 M. Andresen, A. C. Stiel, J. Folling, D. Wenzel, A. Schonle, A. Egner, C. Eggeling, S. W. Hell and S. Jakobs, *Nat. Biotechnol.*, 2008, **26**, 1035–1040.
11 R. Ando, H. Hama, M. Yamamoto-Hino, H. Mizuno and A. Miyawaki, *Proc. Natl. Acad. Sci. U. S. A.*, 2002, **99**, 12651–12656.
12 J. Wiedenmann, S. Ivanchenko, F. Oswald, F. Schmitt, C. Rocker, A. Salih, K. D. Spindler and G. U. Nienhaus, *Proc. Natl. Acad. Sci. U. S. A.*, 2004, **101**, 15905–15910.
13 V. Adam, M. Lelimousin, S. Boehme, G. Desfonds, K. Nienhaus, M. J. Field, J. Wiedenmann, S. McSweeney, G. U. Nienhaus and D. Bourgeois, *Proc. Natl. Acad. Sci. U. S. A.*, 2008, **105**, 18343–18348.
14 M. Sauer, *Proc. Natl. Acad. Sci. U. S. A.*, 2005, **102**, 9433–9434.
15 B. Huang, M. Bates and X. Zhuang, *Annu. Rev. Biochem.*, 2009, **78**, 993–1016.
16 P. Dedecker, J. Hotta, C. Flors, M. Sliwa, H. Uji-i, M. B. Roeffaers, R. Ando, H. Mizuno, A. Miyawaki and J. Hofkens, *J. Am. Chem. Soc.*, 2007, **129**, 16132–16141.
17 M. Hofmann, C. Eggeling, S. Jakobs and S. W. Hell, *Proc. Natl. Acad. Sci. U. S. A.*, 2005, **102**, 17565–17569.
18 M. Andresen, A. C. Stiel, S. Trowitzsch, G. Weber, C. Eggeling, M. C. Wahl, S. W. Hell and S. Jakobs, *Proc. Natl. Acad. Sci. U. S. A.*, 2007, **104**, 13005–13009.
19 S. Luin, V. Voliani, G. Lanza, R. Bizzarri, P. Amat, V. Tozzini, M. Serresi and F. Beltram, *J. Am. Chem. Soc.*, 2009, **131**, 96–103.
20 H. Mizuno, T. K. Mal, M. Walchli, A. Kikuchi, T. Fukano, R. Ando, J. Jeyakanthan, J. Taka, Y. Shiro, M. Ikura and A. Miyawaki, *Proc. Natl. Acad. Sci. U. S. A.*, 2008, **105**, 9227–9232.
21 S. Habuchi, P. Dedecker, J. Hotta, C. Flors, R. Ando, H. Mizuno, A. Miyawaki and J. Hofkens, *Photochem. Photobiol. Sci.*, 2006, **5**, 567–576.
22 E. Fron, C. Flors, G. Schweitzer, S. Habuchi, H. Mizuno, R. Ando, F. C. Schryver, A. Miyawaki and J. Hofkens, *J. Am. Chem. Soc.*, 2007, **129**, 4870–4871.
23 M. Chattoraj, B. A. King, G. U. Bublitz and S. G. Boxer, *Proc. Natl. Acad. Sci. U. S. A.*, 1996, **93**, 8362–8367.
24 N. J. Turro, *Modern Molecular Photochemistry* Mill Valley, CA, 1991.
25 W. E. Moerner, *J. Phys. Chem. B*, 2002, **106**, 910–927.
26 T. M. Creemers, A. J. Lock, V. V. Subramaniam, T. M. Jovin and S. Volker, *Nat. Struct. Biol.*, 1999, **6**, 706.
27 T. M. Creemers, A. J. Lock, V. Subramaniam, T. M. Jovin and S. Volker, *Proc. Natl. Acad. Sci. U. S. A.*, 2000, **97**, 2974–2978.
28 T. M. Creemers, A. J. Locka, V. Subramaniam, T. M. Jovin and S. Volker, *Chem. Phys.*, 2002, **275**, 109–121.
29 T. B. McAnaney, W. Zeng, C. F. Doe, N. Bhanji, S. Wakelin, D. S. Pearson, P. Abbyad, X. Shi, S. G. Boxer and C. R. Bagshaw, *Biochemistry*, 2005, **44**, 5510–5524.
30 D. Sinnecker, P. Voigt, N. Hellwig and M. Schaefer, *Biochemistry*, 2005, **44**, 7085–7094.
31 P. Schwille, S. Kummer, A. A. Heikal, W. E. Moerner and W. W. Webb, *Proc. Natl. Acad. Sci. U. S. A.*, 2000, **97**, 151–156.
32 R. M. Wachter, M. A. Elsliger, K. Kallio, G. T. Hanson and S. J. Remington, *Structure*, 1998, **6**, 1267–1277.
33 M. T. Kirber, K. Chen and J. F. Keaney Jr., *Nat. Methods*, 2007, **4**, 767–768.
34 G. Valentin, C. Verheggen, T. Piolot, H. Neel, M. Coppey-Moisan and E. Bertrand, *Nat. Methods*, 2005, **2**, 801.
35 J. S. Biteen, M. A. Thompson, N. K. Tselentis, G. R. Bowman, L. Shapiro and W. E. Moerner, *Nat. Methods*, 2008, **5**, 947–949.
36 R. Y. Tsien, *Annu. Rev. Biochem.*, 1998, **67**, 509–544.
37 R. M. Wachter, D. Yarbrough, K. Kallio and S. J. Remington, *J. Mol. Biol.*, 2000, **301**, 157–171.
38 A. Royant, P. Carpentier, J. Ohana, J. McGeehan, B. Paetzold, M. Noirclerc-Savoye, X. Vernede, V. Adam and D. Bourgeois, *J. Appl. Crystallogr.*, 2007, **40**, 1105–1112.
39 G. Durin, A. Delaunay, C. Darnault, D. J. Heyes, A. Royant, X. Vernede, C. N. Hunter, M. Weik and D. Bourgeois, *Biophys. J.*, 2009, **96**, 1902–1910.
40 R. Grailhe, F. Merola, J. Ridard, S. Couvignou, C. Le Poupon, J. P. Changeux and H. Laguitton-Pasquier, *ChemPhysChem*, 2006, **7**, 1442–1454.
41 P. Carpentier, A. Royant, J. Ohana and D. Bourgeois, *J. Appl. Crystallogr.*, 2007, **40**, 1113–1122.
42 V. Adam, P. Carpentier, S. Violot, M. Lelimousin, C. Darnault, G. U. Nienhaus and D. Bourgeois, *J. Am. Chem. Soc.*, 2009, **131**, 18063–18065.
43 D. Bourgeois, X. Vernede, V. Adam, E. Fioravanti and T. Ursby, *J. Appl. Crystallogr.*, 2002, **35**, 319–326.
44 G. J. Kremers, K. L. Hazelwood, C. S. Murphy, M. W. Davidson and D. W. Piston, *Nat. Methods*, 2009, **6**, 355–358.
45 S. Habuchi, M. Cotlet, T. Gensch, T. Bednarz, S. Haber-Pohlmeier, J. Rozenski, G. Dirix, J. Michiels, J. Vanderleyden, J. Heberle, F. C. De Schryver and J. Hofkens, *J. Am. Chem. Soc.*, 2005, **127**, 8977–8984.
46 M. K. Raarup, A. W. Fjorback, S. M. Jensen, H. K. Muller, M. M. Kjaergaard, H. Poulsen, O. Wiborg and J. R. Nyengaard, *J. Biomed. Opt.*, 2009, **14**, 034039.
47 P. Leiderman, D. Huppert and N. Agmon, *Biophys. J.*, 2006, **90**, 1009–1018.
48 A. Villoing, M. Ridhoir, B. Cinquin, M. Erard, L. Alvarez, G. Vallverdu, P. Pernot, R. Grailhe, F. Merola and H. Pasquier, *Biochemistry*, 2008, **47**, 12483–12492.
49 M. Lelimousin, M. Noirclerc-Savoye, C. Lazareno-Saez, B. Paetzold, S. Le Vot, R. Chazal, P. Macheboeuf, M. J. Field, D. Bourgeois and A. Royant, *Biochemistry*, 2009, **48**, 10038–10046.
50 M. Cotlet, J. Hofkens, M. Maus, T. Gensch, M. Van Der Auweraer, J. Michiels, G. Dirix, M. Van Guyse, J. Vanderleyden, A. J. W. G. Visser and F. C. De Schryver, *J. Phys. Chem. B*, 2001, **105**, 4999–5006.
51 S. Habuchi, M. Cotlet, J. Hofkens, G. Dirix, J. Michiels, J. Vanderleyden, V. Subramaniam and F. C. De Schryver, *Biophys. J.*, 2002, **83**, 3499–3506.
52 D. Bourgeois and A. Royant, *Curr. Opin. Struct. Biol.*, 2005, **15**, 538–547.
53 C. L. Schwartz, V. I. Sarbash, F. I. Ataullakhanov, J. R. McIntosh and D. Nicastro, *J. Microsc.*, 2007, **227**, 98–109.
54 L. F. van Driel, J. A. Valentijn, K. M. Valentijn, R. I. Koning and A. J. Koster, *Eur. J. Cell Biol.*, 2009, **88**, 669–684.
55 A. Sartori, R. Gatz, F. Beck, A. Rigort, W. Baumeister and J. M. Plitzko, *J. Struct. Biol.*, 2007, **160**, 135–145.
56 R. Bizzari, M. Serresi, F. Cardarelli, S. Abbruzzetti, B. Campanini, C. Viappiani and F. Beltram, *J. Am. Chem. Soc.*, 2010, **132**, 85–95.
57 S. Olsen, K. Lamothe and T. J. Martinez, *J. Am. Chem. Soc.*, 2010, DOI: 10.1021/ja907447k.

Annex 2

LOW-TEMPERATURE CHROMOPHORE ISOMERIZATION REVEALS THE PHOTOSWITCHING MECHANISM OF THE FLUORESCENT PROTEIN PADRON. FARO, ALINE REGIS; CARPENTIER, PHILIPPE; JONASSON, GABRIELLA; POMPIDOR, GUILLAUME; ARCIZET, DELPHINE; DEMACHY, ISABELLE; BOURGEOIS, DOMINIQUE. **JOURNAL OF THE AMERICAN CHEMICAL SOCIETY, 2011.**

JACS
JOURNAL OF THE AMERICAN CHEMICAL SOCIETY

COMMUNICATION

pubs.acs.org/JACS

Low-Temperature Chromophore Isomerization Reveals the Photoswitching Mechanism of the Fluorescent Protein Padron

Aline Regis Faro,[†] Philippe Carpentier,[†,#] Gabriella Jonasson,[‡] Guillaume Pompidor,[§] Delphine Arcizet,[†] Isabelle Demachy,[‡] and Dominique Bourgeois*[,†]

[†]Pixel Team, IBS, Institut de Biologie Structurale Jean-Pierre Ebel, CEA, CNRS, Université Joseph Fourier, 41 rue Jules Horowitz, F-38027 Grenoble, France, and Institut de Recherches en Technologies et Sciences pour le Vivant, iRTSV, Laboratoire de Physiologie Cellulaire et Végétale, CNRS/CEA/INRA/UJF, Grenoble 38054, France

[‡]Laboratoire de Chimie Physique, UMR 8000, CNRS, Université Paris Sud 11, 91405 Orsay, France

[§]Swiss Light Source, Paul Scherrer Institute, CH-5232 Villigen PSI, Switzerland

Supporting Information

ABSTRACT: Photoactivatable fluorescent proteins are essential players in nanoscopy approaches based on the super-localization of single molecules. The subclass of reversibly photoswitchable fluorescent proteins typically activate through isomerization of the chromophore coupled with a change in its protonation state. However, the interplay between these two events, the details of photoswitching pathways, and the role of protein dynamics remain incompletely understood. Here, by using a combination of structural and spectroscopic approaches, we discovered two fluorescent intermediate states along the on-switching pathway of the fluorescent protein Padron. The first intermediate can be populated at temperatures as low as 100 K and results from a remarkable trans−cis isomerization of the anionic chromophore taking place within a protein matrix essentially deprived of conformational flexibility. This intermediate evolves in the dark at cryotemperatures to a second structurally similar but spectroscopically distinct anionic intermediate. The final fluorescent state, which consists of a mixture of anionic and neutral chromophores in the cis configuration, is only reached above the glass transition temperature, suggesting that chromophore protonation involves solvent interactions mediated by pronounced dynamical breathing of the protein scaffold. The possibility of efficiently and reversibly photoactivating Padron at cryotemperatures will facilitate the development of advanced super-resolution imaging modalities such as cryonanoscopy.

Reversibly photoswitchable fluorescent proteins (RSFPs) have received particular attention because of their utility in nanoscopy,[1] contrast-enhancing imaging schemes,[2] and biotechnological applications.[3] RSFPs can be repeatedly photoswitched between a fluorescent on state and a nonfluorescent off state by illumination with visible light of appropriate wavelengths. The molecular mechanisms of the switching processes, however, remain incompletely understood, and no intermediates along the switching reaction pathways have been experimentally identified. Here, by using a combination of low-temperature X-ray crystallography, in crystallo optical spectroscopy, and molecular dynamics simulations, we investigated the on-switching pathway of the fluorescent protein Padron[4] and discovered two fluorescent intermediates along the pathway. Upon illumination at 100 K, the trans anionic chromophore characteristic of the Padron off state, B_{trans}, activates to a first intermediate I_{cis}, which displays a spectroscopically distinct cis anionic configuration. I_{cis} relaxes in the dark to a second intermediate $B_{cis,LT}$, also cis anionic, which upon an increase in temperature above the glass transition temperature (T_g) in turn evolves to AB_{cis}, a mixture of B_{cis}, the fluorescent on state, and A_{cis}, a nonfluorescent protonated form of the chromophore. The observation of I_{cis} reveals that, remarkably, trans−cis chromophore isomerization can take place in Padron at 100 K, a temperature at which protein dynamics is essentially arrested. Furthermore, the data show that trans−cis chromophore isomerization can occur in Padron through a mechanism entirely decoupled from a protonation change of the chromophore benzylidene moiety. Thus, Padron is capable of dramatic fluorescence photoactivation at cryotemperatures.

Whereas most RSFPs display negative photoswitching, that is, fluorescence off-switching results from illumination at wavelengths absorbed by the protein in its fluorescent state, Padron and some other RSFPs[5,6] display positive switching, that is, illumination at such wavelengths enhances fluorescence on-switching. The X-ray structures of Padron in its off and on states [Figure S1 in the Supporting Information (SI)] closely resemble those of Padron0.9 (a mutant of wild-type Padron that favored crystallization)[7] and reveal trans and cis configurations of the chromophore, respectively, with surprisingly little rearrangement of the chromophore pocket between the two states. In its trans configuration and at physiological pH, a nonfluorescent anionic form of the chromophore (B_{trans}; λ_{abs} = 504 nm) is maintained by H-bonding of the benzilidene phenolate to Tyr159 and a water molecule. Upon illumination of B_{trans} at 523−532 nm at 100 K, a blue-shifted absorbance peak grows (λ_{abs} = 481 nm; Figure 1A), reminiscent of low-temperature photoconversion processes that have been described in green fluorescent protein and some mutants.[8] Time-resolved cryocrystallographic data (Tables S1 and S2 in the SI) reveal a concomitant trans−cis isomerization of the chromophore (Figure 2 and Figure S2), with

Received: July 26, 2011

   dx.doi.org/10.1021/ja207001y | J. Am. Chem. Soc. XXXX, XXX, 000–000

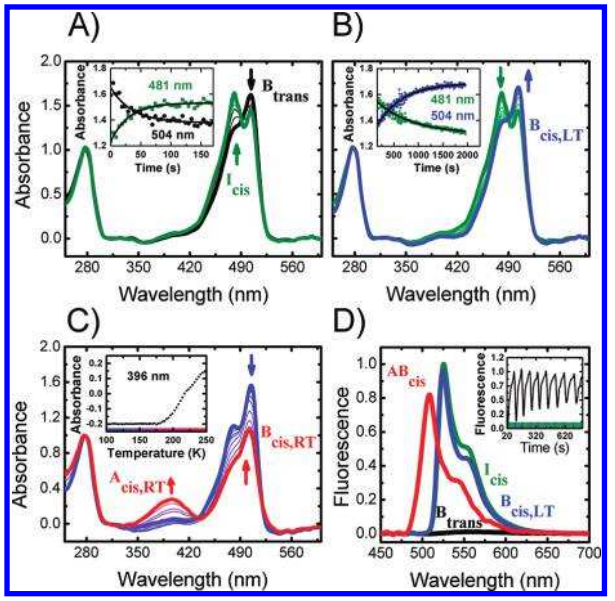

Figure 1. Spectroscopic signature of Padron along its off−on photoswitching pathway, recorded in crystallo. (A, B, C) Absorbance spectra. (A) Illumination of the Padron off state (B_{trans}, black line) at 523 nm (0.15 kW/cm^2) at 100 K yields a (partially populated) first intermediate (I_{cis}, green line). Inset: evolution of the peak absorbances of B_{trans} (black ●) and I_{cis} (green ■). Fits with monoexponential kinetic models are also shown with black lines. (B) Spontaneous relaxation of I_{cis} in the dark at 100 K yields a second intermediate ($B_{cis,LT}$, blue line). Inset: evolution of the peak absorbances of I_{cis} (green ●) and $B_{cis,LT}$ (blue ■). Fits with monoexponential kinetic models are also shown with black lines. (C) A subsequent increase in the temperature (100 K → 240 K) transforms $B_{cis,LT}$ into AB_{cis} (mixture of $A_{cis,RT}$ and $B_{cis,RT}$, red line) at ∼180 K. Inset: rise of the absorbance band of the neutral chromophore during temperature elevation. In panels A-C, intermediate spectra are shown as thin lines. (D) Emission spectra of Padron in B_{trans} (black line), I_{cis} (green line), $B_{cis,LT}$ (blue line), and AB_{cis} (red line). Excitation at 488 nm (2.5 mW/cm^2). Inset: Padron reversible photoswitching at 100 K upon alternate actinic irradiation at 532 nm (1.2 kW/cm^2, green bars) and 405 nm (0.03 kW/cm^2, violet bars) and with excitation at 488 nm (2.5 mW/cm^2). All spectra except intermediate spectra in (C) were collected at 100 K. Absorbance spectra were normalized at 280 nm. Spectra recorded in solution are presented in Figure S4. Fluorescence spectra were normalized according to the results in solution.

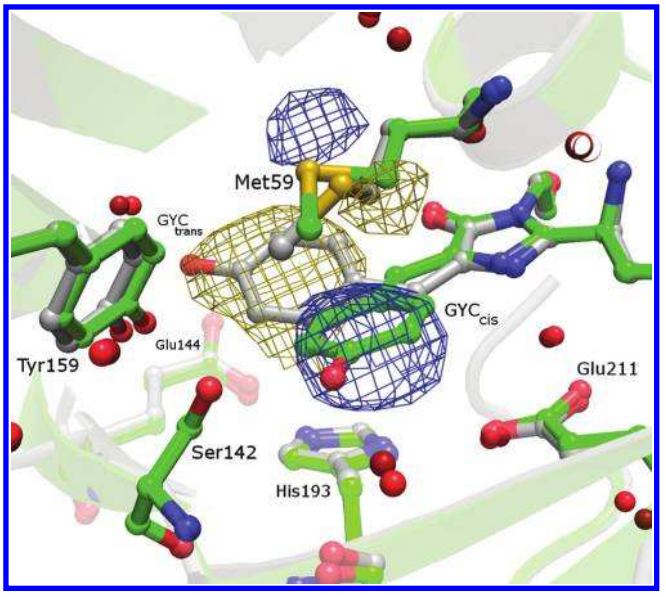

Figure 2. Low-temperature chromophore isomerization in Padron. Crystal structures in states B_{trans} (nonfluorescent, white color) and I_{cis} (fluorescent, green color) are shown, with the chromophore and key residues of the chromophore pocket (except Arg66, omitted for clarity) represented in ball-and-stick mode and the protein matrix in cartoon mode. Isomerization is evident from the experimental difference electron density map (yellow, -4.5σ; blue, $+4.5\sigma$) computed from data sets recorded on the same crystal before and after actinic illumination at 532 nm at 100 K.

only minor structural changes of the protein matrix detectable at the resolution of our data (2.7 Å). A clear displacement of Met59, located above the chromophore, is seen, accompanied by smaller motions of Met93 and Ile195 flanking Met59, which suggests that isomerization might couple with a slight deformation of the β-barrel. Molecular dynamics simulations at 100 K are consistent with these findings. They reveal that upon excitation in the rigid protein matrix, pronounced twisting of the B_{trans} chromophore around the imidazolinone bridge bond occurs, exclusively in the upper half of the chromophore pocket. This also accounts for the nonfluorescence of this anionic chromophoric state. The simulations suggest that residual backbone dynamics are necessary to break the H-bonding of the hydroxybenzilidene moiety to complete the isomerization and that a significant motion of Met59 is required (see Figure S3 and the discussion in the SI).

The formed I_{cis} intermediate is brightly fluorescent at λ_{em} = 524 nm and relaxes in minutes in the dark at 100 K to a second intermediate $B_{cis,LT}$, which has an absorbance signature similar to but narrower than that of B_{trans} (λ_{abs} = 504 nm) and fluoresces like I_{cis} (λ_{em} = 524 nm) (Figure 1B,D and Figure S4).

Crystallographic analysis of $B_{cis,LT}$ shows no detectable structural difference in comparison with I_{cis}, consistent with a low free-energy barrier between the two states that likely involves only minor conformational rearrangements. Altered electrostatics or H-bonding networks in the strained protein matrix following chromophore isomerization are likely to be responsible for the blue-shifted absorption spectrum of I_{cis}. Interestingly, illumination of I_{cis} at 405 nm is able to switch the chromophore back to a nonfluorescent (presumably trans) state. Thus, alternate excitation of Padron at 532 and 405 nm at 100 K results in partially reversible fluorescence photoswitching (Figure 1D). This photocycle apparently involves B_{trans}, I_{cis}, and $B_{cis,LT}$ as the main players (for details, see the SI and Figure S5). We note that illumination of Padron at 100 K at 488 nm (the wavelength typically used for room-temperature microscopy of this protein) still activates fluorescence (Figure S4) but prevents efficient population of I_{cis}, presumably because at this wavelength I_{cis} displays a strong extinction coefficient and thus either converts to $B_{cis,LT}$ or switches back to B_{trans}.

Like the B_{trans} → AB_{cis} process at room temperature (RT), the reaction B_{trans} → I_{cis} at 100 K involves a one-photon absorption process (Figure S6) that displays a quantum yield of $\sim 5 \times 10^{-6}$ instead of $\sim 2 \times 10^{-4}$ at RT. The I_{cis} → $B_{cis,LT}$ relaxation rate increases with temperature, following an Arrhenius law over the temperature range 120−160 K with a low free-energy barrier of ∼3.8 kJ/mol (Figure S7). Above a temperature of ∼180 K, typical of T_g in proteins, the fluorescence emission is blue-shifted to 510 nm (Figure 1D and Figure S4), and the absorbance band at 504 nm decreases concomitantly with a significant rise of a broad absorption band centered at ∼396 nm (Figure 1C). This

dx.doi.org/10.1021/ja207001y |J. Am. Chem. Soc. XXXX, XXX, 000–000

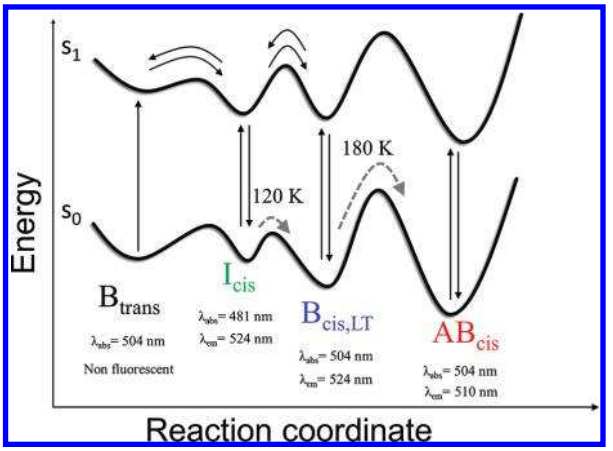

Figure 3. Scheme of the proposed mechanism for off−on Padron photoswitching.

reveals relaxation of $B_{cis,LT}$ to the mixture of the neutral (A_{cis}; λ_{abs} = 396 nm) and anionic (B_{cis}; λ_{abs} = 502 nm) species of the chromophore normally observed at room temperature in the Padron on state. The structural similarity of $B_{cis,LT}$ and the on-state mixture AB_{cis} at the resolution of our diffraction data (2.35 Å) suggests that the relaxation process does not involve pronounced conformational rearrangements, although dynamical breathing must be required for efficient proton transfer (probably from the bulk solvent) following isomerization, in line with recent proposals.[7]

A proposed model for off−on photoswitching in Padron is recapitulated in Figure 3. This model brings new insight into the photoswitching mechanisms in RSFPs. First, photoswitching has to date been described as correlated changes in chromophore protonation and isomerization,[5,9−11] but the interplay between these two changes has remained debated.[12−17] Our data strongly suggest that in the case of Padron, protonation of the benzylidene moiety of the chromophore is not needed in the process of chromophore trans−cis isomerization but rather follows that step. Different scenarios might hold in other RSFPs. Second, the occurrence of chromophore isomerization in Padron at cryotemperatures, which involves a much larger displacement than in other photoreceptors,[18,19] is remarkable in terms of protein dynamics and is unique among RSFPs. In Dronpa (see Figure S8 and the discussion in the SI),[10] mTFP0.7,[9] and IrisFP,[11] cis−trans isomerization involves major conformational rearrangements of residues Glu144, His193, Glu211, and Arg66 (Padron numbering), all situated in the lower half of the chromophore pocket. These structural changes are incompatible with the essentially stalled protein dynamics at 100 K. In contrast, Padron seems to be tuned in such a way that isomerization may occur in the upper half of the pocket, involving only subtle motions of Met59 and the neighboring protein scaffold, compatible with low-temperature protein dynamics. The positively switchable RSFP asFP595 also exhibits only minor conformational rearrangements upon chromophore isomerization,[5] and it will be interesting to investigate the cryoswitching properties of this protein, particularly in view of the anionic-to-zwitterionic activation mechanism suggested by theoretical investigations.[20]

The possibility of photoactivating Padron at cryotemperatures opens the door to the development of cryonanoscopy, which would offer a number of advantages, including reduced photobleaching, sample preservation, freeze-trapping of transient cellular states, and potential correlative light cryoelectron microscopy studies. Furthermore, brighter fluorescence activation is obtained than at ambient temperature, since no fluorescence loss follows from substantial chromophore protonation as observed upon photoswitching at room temperature and at physiological pH.

■ ASSOCIATED CONTENT

Supporting Information. Crystal growth, X-ray data collection and structure determination, spectroscopy setup and methods, molecular dynamics simulations, details of the low-temperature Padron photocycle, and illustrations. This material is available free of charge via the Internet at http://pubs.acs.org.

■ AUTHOR INFORMATION

Corresponding Author
dominique.bourgeois@ibs.fr

Present Address
[#]European Synchrotron Radiation Facility, 6 rue Jules Horowitz, BP 220, 38043 Grenoble Cedex, France

■ ACKNOWLEDGMENT

We thank Peter Dedecker for providing the Padron plasmid. The ESRF and SLS synchrotron facilities are acknowledged for providing beamtime. We thank Laurent Blanchoin, Jérémie Gaillard, Christophe Guérin, Laurent Guyon, Claudine Darnault, Jacqueline Ridard, and Bernard Lévy for fruitful discussions and invaluable help. This work was granted access to the HPC resources of CINES under the alocation 2010-[c2010086318] made by Grand Equipement National de Calcul Intensif (GENCI). A.R.F. was supported by the CEA (Irtelis Grant). D.B. acknowledges financial support by the ANR (ANR-07-BLAN-0107-01).

■ REFERENCES

(1) Lippincott-Schwartz, J.; Patterson, G. H. *Trends Cell. Biol.* **2009**, *19*, 555–565.
(2) Yan, Y.; Marriott, M. E.; Petchprayoon, C.; Marriott, G. *Biochem. J.* **2011**, *433*, 411–422.
(3) Adam, V.; Mizuno, H.; Grichine, A.; Hotta, J.; Yamagata, Y.; Moeyaert, B.; Nienhaus, G. U.; Miyawaki, A.; Bourgeois, D.; Hofkens, J. *J. Biotechnol.* **2010**, *149*, 289–298.
(4) Andresen, M.; Stiel, A. C.; Folling, J.; Wenzel, D.; Schonle, A.; Egner, A.; Eggeling, C.; Hell, S. W.; Jakobs, S. *Nat. Biotechnol.* **2008**, *26*, 1035–1040.
(5) Andresen, M.; Wahl, M. C.; Stiel, A. C.; Grater, F.; Schafer, L. V.; Trowitzsch, S.; Weber, G.; Eggeling, C.; Grubmuller, H.; Hell, S. W.; Jakobs, S. *Proc. Natl. Acad. Sci. U.S.A.* **2005**, *102*, 13070–13074.
(6) Stiel, A. C.; Andresen, M.; Bock, H.; Hilbert, M.; Schilde, J.; Schonle, A.; Eggeling, C.; Egner, A.; Hell, S. W.; Jakobs, S. *Biophys. J.* **2008**, *95*, 2989–2997.
(7) Brakemann, T.; Weber, G.; Andresen, M.; Groenhof, G.; Stiel, A. C.; Trowitzsch, S.; Eggeling, C.; Grubmuller, H.; Hell, S. W.; Wahl, M. C.; Jakobs, S. *J. Biol. Chem.* **2010**, *285*, 14603–14609.
(8) Creemers, T. M.; Lock, A. J.; Subramaniam, V.; Jovin, T. M.; Volker, S. *Proc. Natl. Acad. Sci. U.S.A.* **2000**, *97*, 2974–2978.
(9) Henderson, J. N.; Ai, H. W.; Campbell, R. E.; Remington, S. J. *Proc. Natl. Acad. Sci. U.S.A.* **2007**, *104*, 6672–6677.
(10) Andresen, M.; Stiel, A. C.; Trowitzsch, S.; Weber, G.; Eggeling, C.; Wahl, M. C.; Hell, S. W.; Jakobs, S. *Proc. Natl. Acad. Sci. U.S.A.* **2007**, *104*, 13005–13009.

(11) Adam, V.; Lelimousin, M.; Boehme, S.; Desfonds, G.; Nienhaus, K.; Field, M. J.; Wiedenmann, J.; McSweeney, S.; Nienhaus, G. U.; Bourgeois, D. *Proc. Natl. Acad. Sci. U.S.A.* **2008**, *105*, 18343–18348.
(12) Luin, S.; Voliani, V.; Lanza, G.; Bizzarri, R.; Amat, P.; Tozzini, V.; Serresi, M.; Beltram, F. *J. Am. Chem. Soc.* **2009**, *131*, 96–103.
(13) Mizuno, H.; Mal, T. K.; Walchli, M.; Kikuchi, A.; Fukano, T.; Ando, R.; Jeyakanthan, J.; Taka, J.; Shiro, Y.; Ikura, M.; Miyawaki, A. *Proc. Natl. Acad. Sci. U.S.A.* **2008**, *105*, 9227–9232.
(14) Bizzarri, R.; Serresi, M.; Cardarelli, F.; Abbruzzetti, S.; Campanini, B.; Viappiani, C.; Beltram, F. *J. Am. Chem. Soc.* **2010**, *132*, 85–95.
(15) Li, X.; Chung, L. W.; Mizuno, H.; Miyawaki, A.; Morokuma, K. *J. Phys. Chem. B* **2010**, *114*, 1114–1126.
(16) Olsen, S.; Lamothe, K.; Martinez, T. J. *J. Am. Chem. Soc.* **2010**, *132*, 1192–1193.
(17) Fron, E.; Flors, C.; Schweitzer, G.; Habuchi, S.; Mizuno, H.; Ando, R.; Schryver, F. C.; Miyawaki, A.; Hofkens, J. *J. Am. Chem. Soc.* **2007**, *129*, 4870–4871.
(18) Kort, R.; Hellingwerf, K. J.; Ravelli, R. B. G. *J. Biol. Chem.* **2004**, *279*, 26417–26424.
(19) Edman, K.; Nollert, P.; Royant, A.; Belrhali, H.; Pebay-Peyroula, E.; Hajdu, J.; Neutze, R.; Landau, E. M. *Nature* **1999**, *401*, 822–826.
(20) Schafer, L. V.; Groenhof, G.; Boggio-Pasqua, M.; Robb, M. A.; Grubmuller, H. *PLoS Comput. Biol.* **2008**, *4*, No. e1000034.

Supporting Information

Low-temperature chromophore isomerization reveals the photoswitching mechanism of the fluorescent protein Padron

Aline Regis Faro, Philippe Carpentier, Gabriella Jonasson, Guillaume Pompidor, Delphine Arcizet, Isabelle Demachy and Dominique Bourgeois

Materials and Methods

Expression and purification

Padron was expressed in *Escherichia coli* (strain BL21). The bacterial culture was grown at 310 K to $OD_{600\ nm} = 0.6$. Overexpression was induced by adding 0.1 mM IPTG and incubating overnight at 295 K. After centrifugation, the cell pellet was resuspended in a solution containing 50 mM Hepes (pH 7.5) and 150 mM NaCl, and then lyzed by sonication. The His-tagged recombinant protein was purified in two steps, using a pre-packed Talon metal affinity column (Clontech Laboratories, California, USA) and then a Hiload 16/60 Superdex 200 gel-filtration column (GE healthcare, Pennsylvania, USA). Fractions suitable for spectroscopic characterization and crystallization trials were concentrated to 0.8 mM in 50 mM Hepes (pH 7.5).

Crystallization

Micro-crystals were first grown at 293 K by the hanging drop method, using 500 mM $Mg(NO_3)_2$, 50 mM Hepes (pH 7.5), 26% PEG 3350 as crystallization buffer. Crystallization drops were prepared by mixing 1 µL of protein solution with 2 µL of the crystallization buffer. Optimized crystals were then obtained by micro-seeding in the same buffer, except that a reduced amount of PEG 3350 was used (16%). The orange colored crystals displayed a rhombohedral shape with typical dimensions $30 \times 30 \times 70\ \mu m^3$.

Cryoprotection

For optical spectroscopy, crystals were rapidly transferred to a cryoprotectant solution (20% glycerol, 500 mM $Mg(NO_3)_2$, 50 mM Hepes (pH 7.5), 24% PEG 3350) before being flash-frozen in gaseous nitrogen at 100 K. For X-ray diffraction, crystals were directly frozen in liquid or gaseous N_2, as glycerol was found to deteriorate the quality of diffraction. Residual ice formation did not pose a problem for successful processing of the diffraction data, but had to be completely avoided to record high-quality optical spectra.

For solution spectroscopy, thin films (~20 µm thickness) of Padron solution (0.05 – 5 mM) containing 33% glycerol were rapidly frozen in gaseous N_2 at 100 K.

X-Ray data collection

X-ray diffraction standard data sets were collected at the European Synchrotron Radiation Facility (ESRF) on beamlines ID14-2 and ID23-2, with an ADSC Q4 (ADSC, California, USA) and a MarCCD detector (Rayonix, Illinois, USA), respectively. Time-resolved data-sets were collected at the Swiss Light Source (SLS) at the beamline X10SA, taking advantage of the high-speed PILATUS pixel detector. Diffraction experiments on ID14-2 and X10SA were combined with online microspectrophotometry[1,2] to allow crystal photo-activation and/or spectroscopic monitoring (Figure S2) by UV-vis absorbance measurements.

Atomic coordinates and structure factors amplitudes of Padron in states B_{trans}, AB_{cis} and I_{cis} have been deposited in the Protein Data Bank (www.pdb.org) under the PDB accession codes 3ZUF, 3ZUJ and 3ZUL.

Although Padron is essentially nonfluorescent in its native state, all crystals or solution samples were first illuminated by 405 nm light at room temperature (5 min; 1 W/cm^2) to ensure a reproducible, fully nonfluorescent, starting state ($B_{trans,RT}$). The structure of B_{trans} was obtained upon flash-cooling a crystal some seconds after the illumination at 405 nm. That of AB_{cis} was obtained by illuminating a crystal at 405 nm and then at 514 nm (5 min; 0.3 W/cm^2) at room temperature prior to flash-cooling. Except for the chromophore isomeric state and the conformation of Met59, both structures display a very similar chromophore environment, and show an overall RMSD of 0.54 Å (all atoms) over the 6 monomers in the asymmetric unit. Comparisons of Padron (this work) and Padron0.9 (ref [3]) structures in their

bright and dark states reveal no significant modifications (RMSD of 0.30 Å and 0.32 Å for B_{trans} and AB_{cis} over all atoms, respectively, for chain A).

Several diffraction data sets from I_{cis}, $B_{cis,LT}$ or mixtures thereof were collected at ESRF and reproducibly showed the same structural change of the chromophore. Crystals were first frozen in gaseous nitrogen after 405 nm illumination, and then illuminated at 523 or 532 nm (1 to 12 min; 0.2 to 10 kW/cm^2). In view of the relatively short $I_{cis} \rightarrow B_{cis,LT}$ relaxation time observed in crystals at 100 K by spectroscopy, it is likely that, due to the slower detector readout times, diffraction data sets collected at ESRF corresponded to a mixture of the two states. Thus, we took advantage of the high-speed PILATUS pixel detector available at SLS, achieving the necessary time resolution (2 min / data set), to unambiguously prove that the chromophore in I_{cis} adopts a *cis* configuration. Three data sets were collected on a unique crystal, using the same procedures as described above. A first structure of B_{trans} was collected, and, immediately after actinic illumination at 100 K at 523 nm (1 min; 2 kW/cm^2), a second data set was collected (I_{cis}). A third data set was collected 40 minutes after relaxation in the dark ($B_{cis,LT}$). Experimental difference electron density maps of the form (F_{obs}-F_{obs}) between B_{trans} and I_{cis} and between I_{cis} and $B_{cis,LT}$ were calculated with the CCP4 suite,[4] using phases from the B_{trans} structure and Bayesian q-weighting of the difference structure factor amplitudes.[5]

The absorbed dose per diffraction data set collected at SLS was calculated to be 2.0 MGy using *RADDOSE*.[6] The total dose absorbed during the 3 successive data collections was thus 6.0 MGy, corresponding to ~20 % of the Garman limit.[7] No degradation of the diffraction quality of the crystal could be noticed between the first and the third data set. Similar absorbed doses are typical of data sets collected at ESRF ID14-1. A control experiment performed on the latter beamline showed no structural changes of the *trans* chromophore between two successive data sets collected on the same non-illuminated crystal (not shown). These data unambiguously show that chromophore isomerization is triggered by green light at 100 K in Padron, and that this is not an X-ray induced radiation damage effect.

As no significant difference electron density between I_{cis} and $B_{cis,LT}$ could be observed at the resolution of the data collected at the SLS, we decided to use the higher resolution ESRF data to refine a model of I_{cis}, even though these data might be contaminated by a fraction of $B_{cis,LT}$.

All crystallographic data sets were integrated and scaled with XDS.[8] Data collection statistics are compiled in Table S1. Phases of Dronpa's structure (2Z1O) were used to construct a starting model of Padron, using PHASER.[9] Model refinements were performed with PHENIX,[10] using simulated annealed maps[11] to avoid introducing model bias. Refinement parameters are summarized in Table S2.

Figures 2, S1, S2, S8 were prepared with Pymol.[12]

Microspectrophotometry setup

Absorption and fluorescence emission spectra from Padron crystals and thin films solution samples were recorded using microspectrophotometry setups. All samples were mounted with standard cryoloops, except solution samples at room-temperature which were mounted in a polyacrylamide gel maintained between two cover-slips to minimize protein diffusion effects during the measurements. For *off*-line measurements, spectra were collected using a CCD based spectrometer (AvaSpec-ULS2048, Avantes, Eerbeek, the Netherlands). An ensemble of collimators, mirrors, beam splitters and dichroic filters allowed coupling lasers at 405, 523 532 nm (DPSS lasers, Chagchun New Industries Optoeletronics Tech, Changchun, China) and 488 nm (Argon ion laser, Melles Griot, Albuquerque, USA) and/or a broadband halogen-deuterium source (AvaLight-DH-S-BALL, Avantes, Eerbeek, the Netherlands) into a 200 µm diameter optical fiber which was connected to a reflecting objective of magnification ratio 1:4, yielding an illumination area on the sample of ~50 µm diameter. Transmitted or emitted light was collected by a second identical objective, placed opposite the first relative to the sample position, and connected to a 100 µm diameter optical fiber so as to guide light to the spectrometer.[13] Notch filters were used to filter out transmitted laser light. Samples were cooled by a nitrogen gas cryo-stream (Oxford cryostream, Series 600, Oxford, UK) allowing adjustment of the temperature from 100 to 300 K.

$B_{trans} \rightarrow I_{cis}$ quantum-yield calculation

The quantum yield for the photoactivated step of Padron cryo-switching ($B_{trans} \rightarrow I_{cis}$) was calculated with solution samples based on absorbance timecourses such as reported in the inset of Figure 1A. The buildup kinetics of I_{cis} (absorbance at 483 nm) was fitted with a mono-exponential model. The quantum yields Φ was obtained from:

$$\Phi = \frac{hc \times S \times N_{Av}}{\tau \times P \times \lambda \times \varepsilon \times \ln 10}$$

with Planck constant, h, speed of light, c, sample cross section, S, Avogadro constant, N_{Av}, inverse rate constant τ, effective laser power, P, wavelength, λ, and extinction coefficient, ε.

$I_{cis} \rightarrow B_{cis,LT}$ activation free energy calculation

To estimate the activation free energy barrier separating I_{cis} from $B_{cis,LT}$, I_{cis} was first populated by light in solution samples, and then spectral series were acquired during spontaneous relaxation to $B_{cis,LT}$ in the dark and at different temperatures. The decay of the 483 nm absorbance was fitted by a mono-exponential model, and the activation free energy ΔG^* was obtained from an Arrhenius plot (Figure S6), considering only the linear range between 120 and 160K (see below).

Spectroscopic data analysis

Spectroscopic data were processed using homemade routines based on the IDL software (Boulder, CO). Absorption spectra were corrected for backround using a polynomial baseline subtraction. Model fitting was performed with Origin (OriginLab, Northampton, USA).

Fluorescence emission measured in crystals is difficult to quantitatively assess due to the very high protein concentration which typically results in nonlinear responses due to e.g. inner-filtering effects. Thus, proper normalization of fluorescence spectra in crystals is not reliable (Figure 1D) and we chose to scale them according to solution data.

Spectroscopic results on solution samples

The cryo-photoswitching properties of Padron obtained in crystals (Figure 1) was reproduced in solution samples (Figure S4) so as to show that they are not specific to the crystalline state. However, we noticed a slight difference in the temperature dependence of the $I_{cis} \rightarrow B_{cis,LT}$ step between the two phases. The activation free energy barrier for that step measured in solution appeared somewhat higher than in crystals. The $I_{cis} \rightarrow B_{cis,LT}$ relaxation in solution samples was very slow and only partial at 100 K and started to proceed more efficiently at ~120 K, ie ~20 K higher than in crystals. As a consequence, the I_{cis} intermediate

could be populated at 100 K to a much higher degree than in crystals, and its signature could be better characterized (Figure S4A). This difference might relate to the different solvent composition between the two types of samples, and/or result from some conformational selection occurring in the crystal. Probably due to the subtle protein dynamics involved, relating to the organization of the conformational landscape in tiers,[14] the $I_{cis} \rightarrow B_{cis,LT}$ relaxation did not follow an Arrhenius behaviour over the whole tested temperature range (100 - 180 K). A transition in Padron protein dynamics seems to occur at ~120 K under our experimental conditions (Figure S4E). At temperatures significantly higher than 120 K, I_{cis} decays more rapidly than it is formed and thus cannot be observed anymore (Figure S4C). At 220 K, above the glass transition temperature, chromophore protonation occurs readily and $B_{cis,LT}$ cannot be observed anymore (Figure S4D).

In summary, comparison of spectra collected in crystalline and solution phases strongly suggest that the cryo-photoswitching pathway identified *in crystallo*, also occurs in solution and involves the same intermediate states.

Off-on photoswitching of Padron at room temperature is typically performed by employing actinic light at 488 nm. Instead, we used 523 or 532 nm light in our mechanistic investigations at cryo-temperature. This was justified by the need to uniformly excite the high optical density crystals. Also, the observation of I_{cis} is compromised if 488 nm light is used, due to the photosensitivity of the intermediate at this wavelength. Nevertheless, photoactivation of Padron at 488 nm at 100 K remains possible, although at a slow rate (Figure S4G). We propose that at room temperature, the lifetime of I_{cis} is so short that, at the typical laser powers used, photo-induced back-switching to B_{trans} is unlikely, making the activation process efficient.

Details on the low-temperature Padron photocycle.

In order to better understand the low-temperature Padron photoswitching cycle (inset of Figure 1D), we addressed the following questions: (i) What is the origin of the relatively poor switching contrast ? (ii) Is a protonated species involved in fluorescence back switching ?

(i): A reduced switching contrast would be expected if, in addition to B_{trans} and I_{cis}, $B_{cis,LT}$ would be involved in the photocycle. In the crystalline state, illumination of I_{cis} at 100 K at 405 nm mostly returns the sample to B_{trans} (Figure S5A), but the progressively reduced fluorescence off-switching (Figure 1D, inset) suggests that a fraction of $B_{cis,LT}$ also builds up.

The involvement of $B_{cis,LT}$ appears clearer in solution, where I_{cis} still completely vanishes upon illumination at 405 nm, while fluorescence decays only marginally (Figure S5B and C). Note that, after illumination at 405 nm, the absorption spectrum slightly differs from that of B_{trans}, showing a narrower main band (Figure S5B). This is consistent with a large fraction of I_{cis} being transformed into $B_{cis,LT}$. In addition, $B_{cis,LT}$ can apparently be transformed back into B_{trans} by illumination at 405 nm, maybe via I_{cis}, or directly (Figure S5D). Overall , the data are consistent with a model in which the low-temperature Padron photocycle involves three species, two of which being fluorescent.

$$B_{trans} \leftrightarrow I_{cis} \leftrightarrow B_{cis,LT}$$

Depending on the inter-conversion rates between B_{trans} and I_{cis} on the one hand, and between I_{cis} and $B_{cis,LT}$ on the other hand, at the used wavelengths, this model results in a progressive buildup of $B_{cis,LT}$ along switching cycles, accounting for the observed limited contrast and for the fact that several cycles are needed to establish a steady-state (we verified this by computer simulations). The inter-conversion rates seem to depend on the experimental conditions (solution versus crystalline phase), explaining why substantially superior switching contrast can be achieved in crystals as compared to solution samples.

(ii) The fact that fluorescence back-switching is most efficient by employing 405 nm light (a wavelength typically absorbed by neutral chromophores) could suggest that a protonated chromophore species is involved in the process. However, three arguments argue against this hypothesis: 1/ Absorbance data collected on a thick crystal (Figure S5E) show no sign of a significant protonated band developing along the switching process. 2/ Fluorescence photoswitching can as well be achieved by employing 473 nm instead of 405 nm light, although the switching contrast is lower (Figure S5F). 3/ Illumination at 405 nm at 100 K of the neutral band of AB_{cis} irreversibly depletes this band and results in a fluorescence increase rather than a decrease (not shown).

Strictly speaking, however, we cannot completely exclude the possibility that a neutral species (that would be non-rate limiting and in fast equilibrium with I_{cis}) be involved in the back-switching process. It could be conceived that illumination with 405 nm light depletes I_{cis} to B_{trans} *via* this state. A more detailed study of the cryo-photoswitching cycle of Padron goes beyond the scope of the present paper.

Laser induced temperature elevation

The adiabatic temperature rise of the crystals in the laser beam was estimated to be less than 10 K, assuming that the crystal was made of pure water and based on $\Delta T = E_{abs} / mC$ with E_{abs} the laser energy absorbed by the crystal, m the number of moles of water in the crystal volume and C the molar heat capacity of water ($C = 75.3\ JK^{-1}mol^{-1}$).

Although absorption of a single photon is expected to instantaneously raise the temperature of the chromophore by several hundreds Kelvins, molecular dynamics simulations carried out previously on other light-sensitive proteins[15] suggest that this energy dissipates throughout the protein matrix on the picosecond timescale. Therefore, large-scale conformational motions that, typically, require much longer times to occur at room temperature, are believed to have no chance to take place in the frozen sample. Thus, our low-temperature data are unlikely to be affected by this effect. This is also substantiated by our results on Dronpa (see below).

Comparative studies on Dronpa

For comparative purposes, a similar experimental approach as that yielding I_{cis} in Padron was used on the negatively photoswitchable fluorescent protein Dronpa, except that in this case the crystals were not pre-illuminated at 405 nm and illumination was performed at 521 nm for 3 minutes at 16 kW/cm^2. In agreement with our previous findings by spectroscopy, which suggested only minor photoinduced protonation of the chromophore under such conditions,[16] diffraction data sets collected at ESRF revealed no chromophore isomerization at cryo-temperature (Figure S8).

Molecular dynamics simulations

Trans-cis isomerization of Padron at low temperature

From a molecular point of view, the photoisomerisation process requires three steps: first, a twist about the Imidazolinone (I) bridge bond of ± 90° induced by the S_1 state energy profile; note that τ (I-bond dihedral angle) values equal to ± 90° correspond to S_1 energy minima[17,18] so the rotation should stop there. The second step involves a non-radiative ground state recovery. Then in the third step, the electronic driving force of the S_0 state energy profile

tends to restore a planar geometry either in the *cis* or in the *trans* conformation depending of the I-bond angle value at the non-radiative process.

We examine here if B_{trans} Padron is likely to allow that process by means of molecular dynamics simulations and energy interaction calculations.

Molecular dynamics (MD) details

The starting coordinates were taken from the B_{trans} crystal structure. The different protonation states of the triad Glu211, His193, Glu144 have been considered in MD simulations of the ground state. Only the combination neutral Glu144, neutral His193 (protonated on the ε nitrogen) and anionic Glu211 preserves essential X-ray structural features: i) the complete hydrogen bond network of the chromophore and between the triad residues, ii) the absence of π-stacking between His193 and the chromophore phenolate ring. This protonation state is also the one proposed by Brakeman *et al*[3] on the basis of the chromophore pK properties.

MD simulations of B_{trans} Padron excited state were performed using a specific intra chromophore potential for the S_1 excited state recently developed and implemented[17] in the parallel processing PMEMD module of the AMBER suite.[19] This potential includes a coupling between the τ and φ (phenolate bridge bond) angles an important feature for describing how the chromophore might snake from the *cis* to the *trans* conformation inside the protein. In addition, this implementation allows the removal or the scaling of specific non-bonded interactions (van der Waals or electrostatic) between specified atom pairs of the chromophore and/or the protein along the dynamics, a feature allowing to explore the effect of removing given H bonds.

The AMBER 1999 force field "ff99" was used for all standard amino-acids. The force field of the anionic chromophore in its electronic ground state and the MD protocol are described elsewhere.[17]

MD results

A 10 ns-long MD simulation of B_{trans} Padron in the ground state at low temperature (100 K) confirms strong permanent hydrogen bonds anchoring the chromophore (the phenolate oxygen atom H-bonded to Tyr159 and Wat9 and the imidazolinone carbonyl oxygen atom H-bonded to Arg91 and Arg66). Ground state geometries were sampled as starting coordinates

for 30 excited state MD simulations in order to deepen the understanding of the isomerisation process. In all simulations, a τ twist occurs within a few picoseconds: a τ angle near -70° is reached ($\tau = -71 \pm 4°$ and $\varphi = 0 \pm 7°$) after a time interval of 0.2 to 16 ps (average value of 3 ps). The τ twists occur exclusively in the upper half of the chromophore pocket, i.e. in the opposite side of the triad Glu144 – His193 – Glu211. In the twisted geometries, the chromophore hydrogen bond network is preserved, including unexpectedly the H-bonds of the phenolate oxygen to Tyr159 and Wat9. These hydrogen bonds have a strong hold on the chromophore, keeping it from reaching a completely perpendicular geometry (see Figure S3). In addition, we have found that twisted geometries beyond the perpendicular one can indeed be reached by removing the non-bonded interactions that give rise to these two H-bonds.

The possibility of an actual weakening of these non-bonded interactions has been tested by running MD simulations at 300K. It then appears that the two H-bonds with Tyr159 and Wat9 actually diseappear during 2% of the time.

The loss of these H-bond is probably related to a collective motion of the protein. Indeed, Wat9 is H-bonded to Ser155 and Thr175 located on strands 2 and 3 respectively.[3] If these strands move away from the α-helix, one H-bond of Wat9 (either to Ser155 or Thr175 or the chromophore) is cut. Such collective motions have already been mentioned for GFP.[17] One may wonder if these collective motions occur at 100 K. The answer cannot be easily obtained by MD simulations. But it can be noted that if they still exist, they would rarely reach sufficient amplitude and this is not in contradiction with the low rate of isomerisation observed experimentally at low temperature.

It is also worth mentioning that the fast twisting dynamics observed in all simulations agrees with the short fluorescence lifetime of the *trans* conformer, since the green fluorescence emission is strongly dimed by the twist.[20]

The third step of the isomerisation has been investigated by increasing step by step the τ angle to 180° (*cis* conformation) in a given snapshot (where $|\tau| \sim 75°$) with no relaxation of the cavity. This approach was used instead of a MD simulation because no realistic conformation with $|\tau| > 90°$ was found.

While forcing the return to the *cis* isomer, a strong clash occurs with Met59 when the τ torsion reaches 120°. It involves a close contact between the chromophore and the S atom of Met59; but the Met59 side-chain is flexible and may twist as observed in the non-relaxed I_{cis} X-ray structure. A weakly unfavorable interaction occurs between His193 and the

chromophore near the *cis* conformation ($|\tau|\sim180°$). This is due to a slight displacement of His193 in the twisted and excited conformation from its position in the B_{trans} structure but also to the frozen geometry of the cavity in the present calculations. Small adjustments of His193 and of the chromophore geometry should bypass this situation while promoting a stabilizing π-stacking.

On the whole, the molecular dynamics simulations are consistent with the experimental observations, despite the fact that the whole isomerization cannot be easily observed in the computer due to the low isomerization rate.

References

(1) McGeehan, J.; Ravelli, R. B.; Murray, J. W.; Owen, R. L.; Cipriani, F.; McSweeney, S.; Weik, M.; Garman, E. F. *J. Synchrotron Radiat.* **2009**, *16*, 163-172.
(2) Owen, R. L.; Pearson, A. R.; Meents, A.; Boehler, P.; Thominet, V.; Schulze-Briese, C. *J. Synchrotron Radiat.* **2009**, *16*, 173-182.
(3) Brakemann, T.; Weber, G.; Andresen, M.; Groenhof, G.; Stiel, A. C.; Trowitzsch, S.; Eggeling, C.; Grubmuller, H.; Hell, S. W.; Wahl, M. C.; Jakobs, S. *J. Biol. Chem.* **2010**, *285*, 14603-14609.
(4) Winn, M. D.; Ballard, C. C.; Cowtan, K. D.; Dodson, E. J.; Emsley, P.; Evans, P. R.; Keegan, R. M.; Krissinel, E. B.; Leslie, A. G. W.; McCoy, A.; McNicholas, S. J.; Murshudov, G. N.; Pannu, N. S.; Potterton, E. A.; Powell, H. R.; Read, R. J.; Vagin, A.; Wilson, K. S. *Acta Crystallogr. D* **2011**, *67*, 235-242.
(5) Ursby, T.; Bourgeois, D. *Acta Crystallogr. A* **1997**, *53*, 564-575.
(6) Paithankar, K. S.; Garman, E. F. *Acta Crystallogr. D* **2010**, *66*, 381-388.
(7) Owen, R. L.; Rudino-Pinera, E.; Garman, E. F. *Proc. Natl. Acad. Sci. U. S. A.* **2006**, *103*, 4912-4917.
(8) Kabsch, W. *J. Appl. Cryst.* **1988**, *21*, 67-72.
(9) McCoy, A. J.; Grosse-Kunstleve, R. W.; Adams, P. D.; Winn, M. D.; Storoni, L. C.; Read, R. J. *J. Appl. Cryst.* **2007**, *40*, 658-674.
(10) Afonine, P. V., Grosse-Kunstleve, R.W. , Adams, P.D. *CCP4 Newsl.* **2005**, *contribution 8*.
(11) Brunger, A. T.; Adams, P. D. *Acc. Chem. Res.* **2002**, *35*, 404-412.
(12) DeLano, W. L. *The PyMol Molecular Graphics System* Palo Alto, CA, USA, 2008.
(13) Bourgeois, D.; Vernède, X.; Adam, V.; Fioravanti, E.; Ursby, T. *J. App. Cryst.* **2002**, *35*, 319-326.
(14) Frauenfelder, H.; Sligar, S. G.; Wolynes, P. G. *Science* **1991**, *254*, 1598-1603.
(15) Henry, E. R.; Eaton, W. A.; Hochstrasser, R. M. *Proc. Natl. Acad. Sci. U. S. A.* **1986**, *83*, 8982-8986.
(16) Faro, A. R.; Adam, V.; Carpentier, P.; Darnault, C.; Bourgeois, D.; de Rosny, E. *Photochem. Photobiol. Sci.* **2010**, *9*, 254-262.
(17) Jonasson, G.; Teuler, J.-M.; Vallverdu, G.; Mérola, F.; Ridard, J.; Lévy, B.; Demachy, I. *J. Chem.Theor. and Comput.* **2011**, *7*, 1990-1997.
(18) Martin, M. E.; Negri, F.; Olivucci, M. *J. Am. Chem. Soc.* **2004**, *126*, 5452-5464.
(19) Case, D. A.; Darden, T. A.; Cheatham, T. E.; Simmerling, C. L.; Wang, J.; Duke, R. E.; Luo, R.; Crowley, M.; Walker, R. C.; Zhang, W.; Merz, K. M.; Wang, B.; Hayik, S.; Roitberg, A.; Seabra, G.; Kolossváry, I.; Wong, K. F.; Paesani, F.; Vanicek, J.; Wu, X.; Brozell, S. R.; Steinbrecher, T.; Gohlke, H.; Yang, L.; Tan, C.; Mongan, J.; Hornak, V.; Cui, G.; Mathews, D. H.; Seetin, M. G.; Sagui, C.; Babin, V.; Kollman, P. A. *AMBER 10* University of California, San Francisco. , 2008; Vol. null.
(20) Olsen, S.; Smith, S. C. *J. Am. Chem. Soc.* **2008**, *130*, 8677-8689.

TABLE S1. Crystallographic data collection statistics

	On (**I**$_{cis}$)	On (**AB**$_{cis}$)	Off (**B**$_{trans}$)	On (**I**$_{cis}$)	On (**B**$_{cis,LT}$)	Off **B**$_{trans}$
Space group	$P\,2_12_12$					
Average unit cell	a = 107.78 Å, b = 180.52 Å, c = 72.17 Å					
Beamline	ESRF / ID14-2	ESRF / ID14-2	ESRF / ID23-2	SLS / X10SA	SLS / X10SA	SLS / X10SA
Wavelength, (Å)	0.933	0.933	0.873	0.999	0.999	0.999
Resolution, (Å)	50.00 - 2.30	50.00 - 2.34	50.00 - 2.20	50.00 - 2.60	50.00 - 2.68	50.00 - 2.60
No. uniq. reflections	64825 [10220]	61045 [9666]	73775 [11565]	205376 [29184]	165854 [26404]	236814 [34381]
Redundancy	4.4 [4.3]	5.2 [5.3]	3.5 [3.3]	3.8 [3.8]	3.80 [3.80]	3.9 [3.9]
Completeness, (%)	99.4 [98.4]	98.8 [98.3]	98.4 [96.9]	95.9 [99.3]	93.7 [99.3]	97.0 [99.2]
R_{sym}, (%)‡	11.3 [50.1]	7.0 [32.2]	7.8 [41.7]	16.7 [44.4]	18.0 [61.8]	16.6 [43.0]
Mean I/σ(I)	12.4 [3.1]	19.9 [5.3]	13.42 [3.5]	5.60 [2.52]	5.45 [1.71]	5.58 [2.76]
Wilson B $_{factor}$, (Å^2)	29.20	31.87	35.80	49.84	51.02	46.41

Numbers in brackets refer to the last resolution shell.

‡ $R_{sym} = \sum_j \sum_h \left| I_{h,j} - \langle I_h \rangle \right| / \sum_j \sum_h I_{h,j}$

TABLE S2. Model refinement statistics

	On (**I**$_{cis}$)	On (**AB**$_{cis}$)	Off (**B**$_{trans}$)
R_{work} (%) #	0.21	0.19	0.20
R_{free} (%) Δ	0.25	0.30	0.24
Mean B value, (Å²)	23.90	26.50	32.90
RMSD bond length, (Å)	0.01	0.01	0.02
RMSD bond angles, (°)	1.24	1.26	1.55
Chro. Planarity,(°) $			
chain A	168.9, -1.4	173.8, 3.8	-16.3, 0.6
chain B	167.5, -2.7	174.9, 3.3	-16.7, 1.5
chain C	170.2, -2.6	177.4, 4.1	-20.7, 2.1
chain D	167.4, -3.2	175.2, 3.8	-18.7, 1.7
chain E	162.5,-2.6	174.5, 2.9	-23.4, 1.6
chain F	170.3, -3.6	177.3, 3.4	-23.1, 2.7
Ramachandran statistics (%) §			
allowed	99.2	99.3	99.1
outliers	0.1	0.2	0.0

$R_{work} = \sum_h \left| F_{obs} - F_{cal} \right| / \sum_h F_{obs}$.

Δ R_{free} is calculated with a small fraction (5 %) of reflections chosen to be part of a test group.

$ Chromophore planarity was assessed by measurement of the average dihedral angles τ and φ, linking atoms N_2-C_{A2}-C_{B2}-C_{G2} and C_{A2}-C_{B2}-C_{G2}-C_{D2}, respectively.

§ Determined by PHENIX.[10]

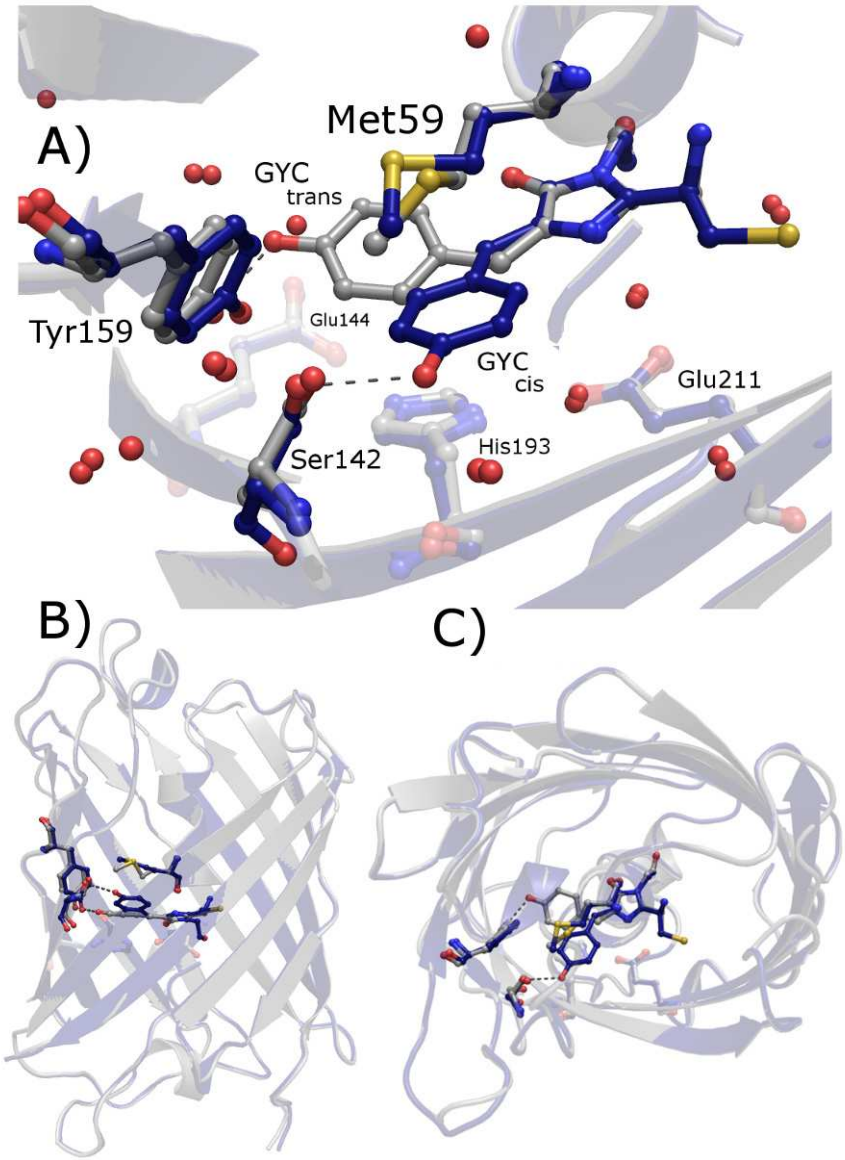

Figure S1: Room-temperature chromophore isomerization in Padron. Crystal structures of Padron in the nonfluorescent off-state B_{trans} (white) and fluorescent on-state AB_{cis} (blue). A: zoom on the chromophore pocket. B and C: overall views from the side and the top of the β-barrel, respectively. Key residues of the chromophore pocket (except Arg66 , omitted for clarity) are represented in ball and stick mode, and the protein matrix in cartoon mode. Water molecules are shown as red balls.

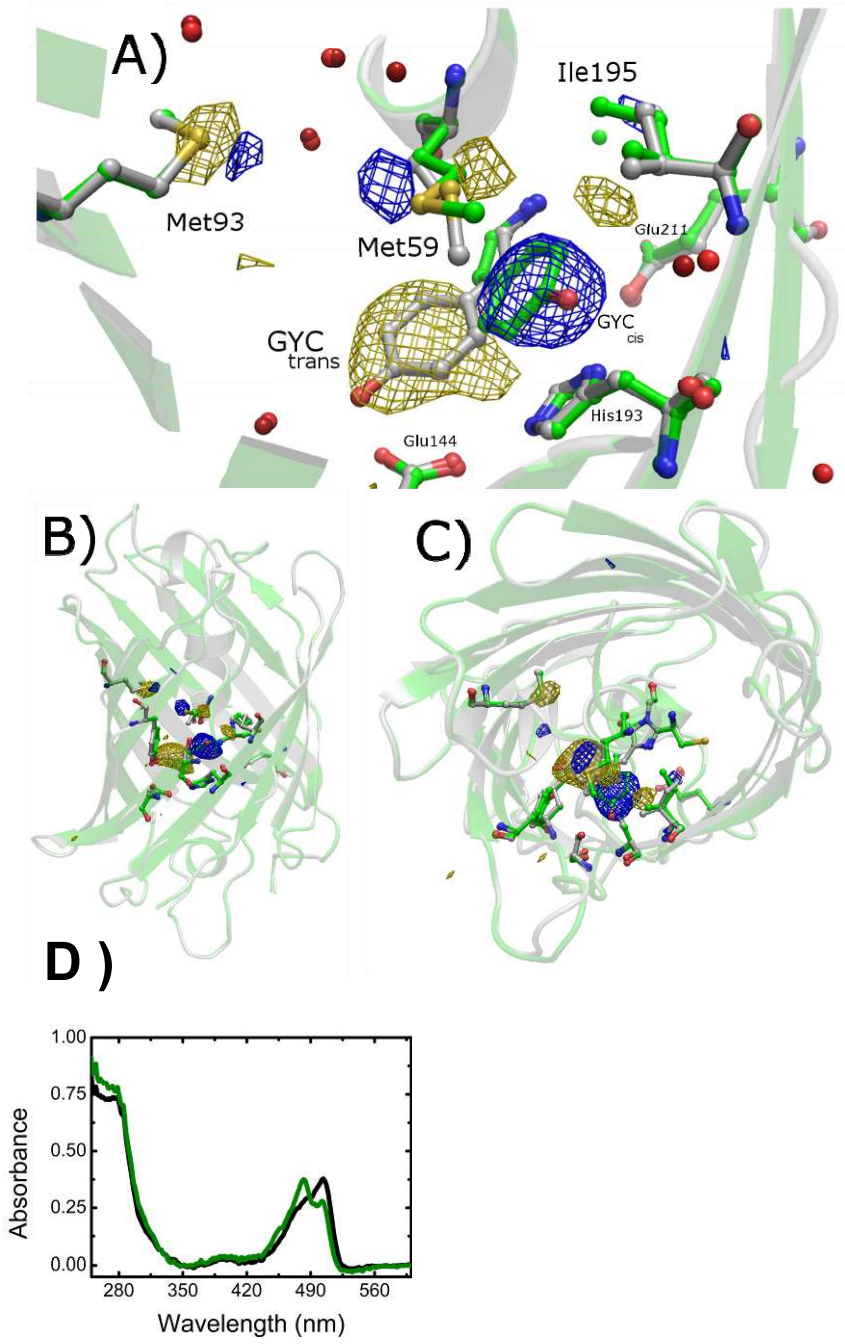

Figure S2: Overall view of the structural differences between B_{trans} and I_{cis}. Crystal structures of Padron in the non-fluorescent *off*-state B_{trans} (white) and intermediate fluorescent state I_{cis} (green) are shown. A, B and C: similar representations as in Figure S1. The experimental difference electron density map (yellow, -4.5σ; blue, +4.5σ) computed as described in the legend of Figure 2 is shown over the whole structure of Padron monomer A. Difference electron densities on Met93, Met59 and Ile195 witness the slight conformational change undergone by the protein under cryo-photoisomerization. No other significant difference electron density appear elsewhere, highlighting the satisfactory quality of the diffraction data. D: Formation of I_{cis} *in crystallo* monitored by online microspectrophotometry on the ESRF ID14-1 beamline, before (black) and after (green) Padron illumination at 521 nm at 100 K. Data sets used for refinement were collected on different crystals treated with similar cryo-illumination protocols.

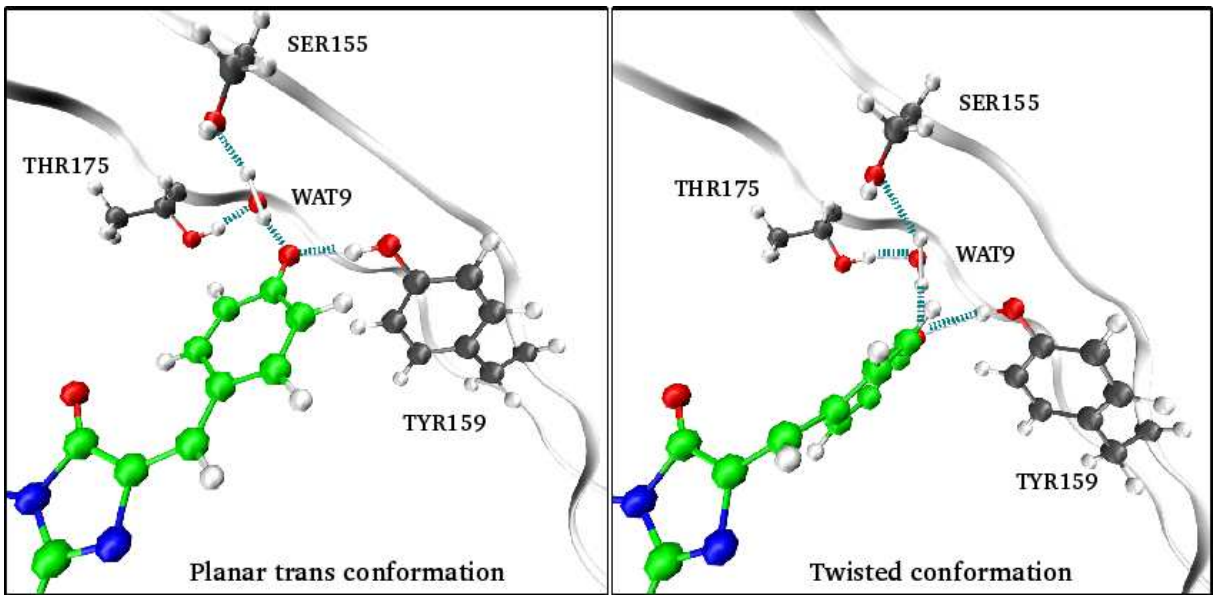

Figure S3: The hydrogen bond network in the vicinity of the phenolate oxygen of the Padron chromophore (green carbon atoms). The B_{trans} geometry (left) and the excited state twisted geometry (right) are shown. H-bonds are represented by blue dashed lines.

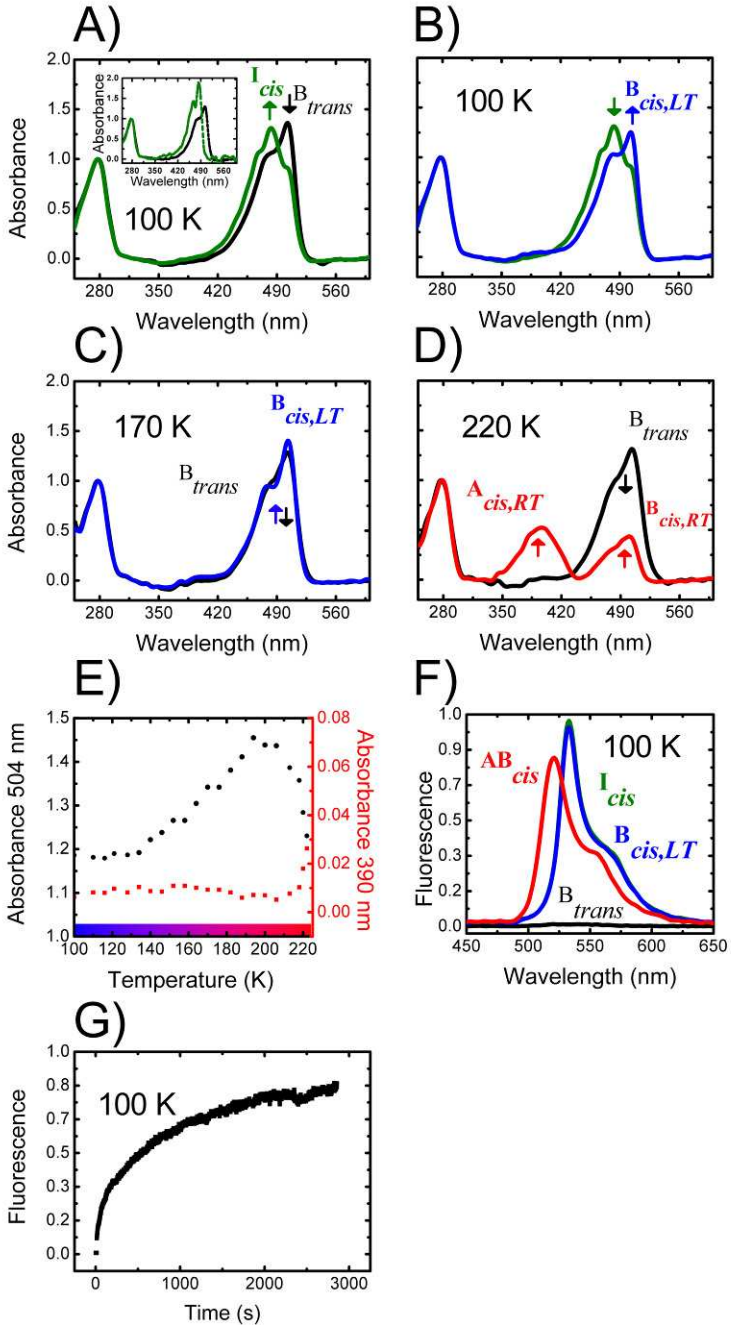

Figure S4: Spectroscopic properties of Padron along its off-on photoswitching pathway recorded in solution. **(A, B, C, D)** Absorbance spectra recorded at different temperatures, normalized at 280 nm. **(A)** Illumination at 532 nm (1.6 kW/cm^2) at 100 K of the Padron off state (B_{trans}, black line) yields a first intermediate (I_{cis}, green line). Inset: absorbance spectrum of the pure I_{cis} (green), crudely obtained by subtracting a fraction of B_{trans} from the green spectrum in the main panel, and compared to that of B_{trans} (black). **(B)** Spontaneous relaxation of I_{cis} in the dark at 100 K yields a second intermediate ($B_{cis,LT}$, blue line). However, the relaxation is incomplete and slow. **(C)** At 170 K, B_{trans} is rapidly transformed into $B_{cis,LT}$ and I_{cis} does not build up to a significant population. **(D)** At 220 K, above the glass transition temperature, B_{trans} is readily transformed into AB_{cis} (mixture of $A_{cis,RT}$ and $B_{cis,RT}$, red line). At this temperature, neither I_{cis} not $B_{cis,LT}$ build up to significant populations. **(E)** Evolution of absorbances at 504 nm (black dots) and 390 nm (red squares) during the spontaneous relaxation of I_{cis} during temperature ramping (**6** K/min) in the dark. I_{cis} was light-induced at 100 K. **(F)** Emission spectra of Padron in B_{trans} (black line), I_{cis} (green line), $B_{cis,\ LT}$ (blue line) and B_{cis} (red line). Excitation at 488 nm (2.5 mW/cm^2). The observed red shifts as compared to the spectra collected in crystallo (see Figure 1D) are attributed to the effect of the crystallization medium in the latter spectra. **(G)** Photoactivation of Padron at 488 nm at 100 K (0.36 kW/cm²).

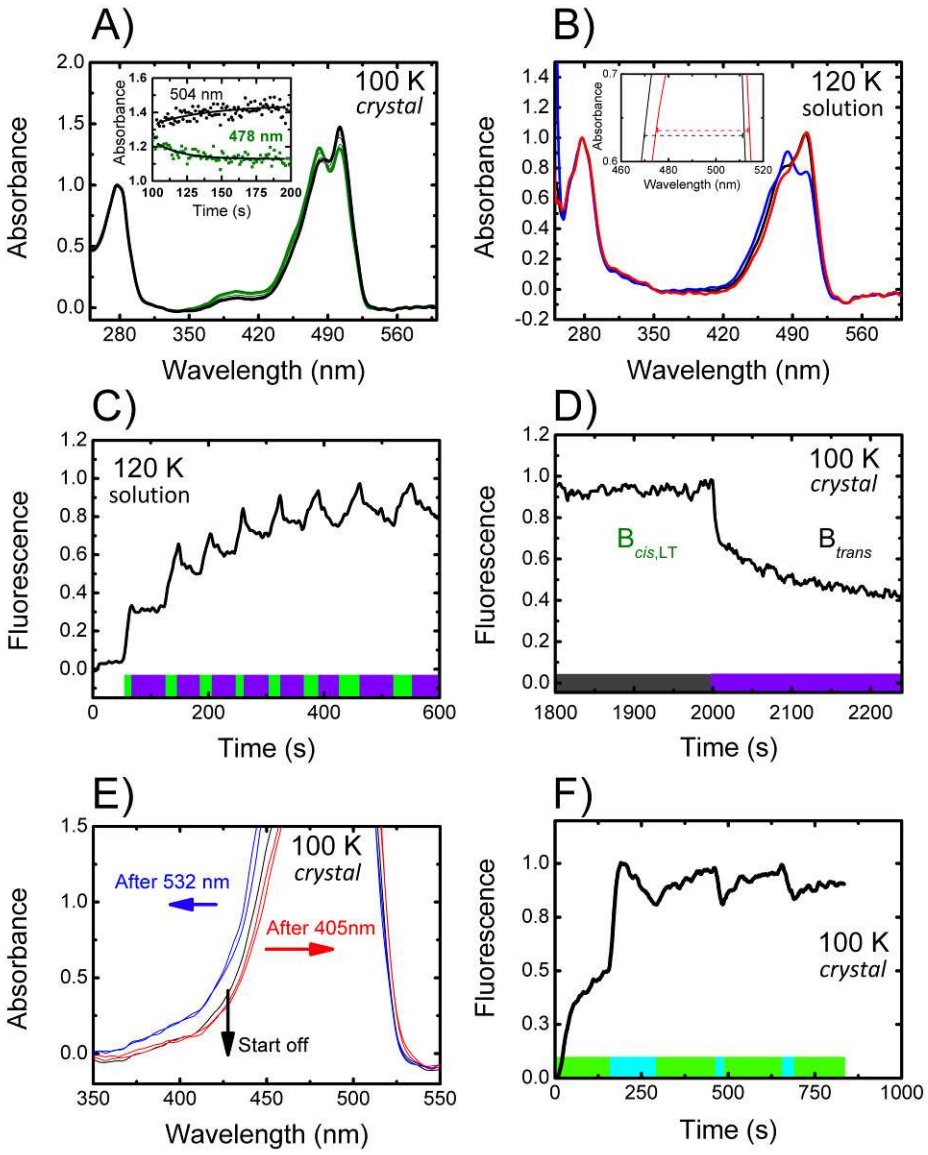

Figure S5: Mechanism of low-temperature Padron reversible photoswitching. **(A)** Absorbance spectral changes upon conversion from I_{cis} (green), mostly into B_{trans} (black), upon illumination at 405 nm at 100 K in the crystalline state. The curve is essentially the reverse of Figure 1A. **(B)** Similar data recorded in solution at 120 K. The absorbance spectra before illumination (black), after illumination at 532 nm (blue) and after subsequent illumination at 405 nm (red) are shown. Inset: detailed comparison between the initial and final absorbance spectra, suggesting a substantial formation of the narrower (and slightly red-shifted) absorption band from $B_{cis,LT}$. **(C)** Padron photoswitching at 120 K in solution, upon alternate actinic irradiation at 532nm (green bars) and 405 nm (violet bars) and with excitation at 488 nm. **(D)** Decay of fluorescence upon illumination of $B_{cis,LT}$ with 405 nm light, recorded on a cystal. $B_{cis,LT}$ was formed by illumination of a frozen crystal at 532 nm followed by transient excursion at 140K. **(E)** Details of absorbance spectra collected on a thick crystal upon alternate excitation at 100 K with green and violet lights. The starting spectrum is shown in black, spectra obtained after 405 nm illumination are shown in red and spectra obtained after 532 nm illumination are shown in blue. No absorption band from a neutral chromophore species seems to be present. **(F)** *In crystallo* Padron photoswitching at 100 K, upon alternate actinic irradiation at 532nm (green bars) and 473 nm (cyan bars) and with excitation at 488 nm. A reduced switching contrast is achieved (compare with inset of Figure 1D). Note the fluorescence increase during the first illumination at 473 nm, suggesting a strong sensitivity of B_{trans} to this wavelength.

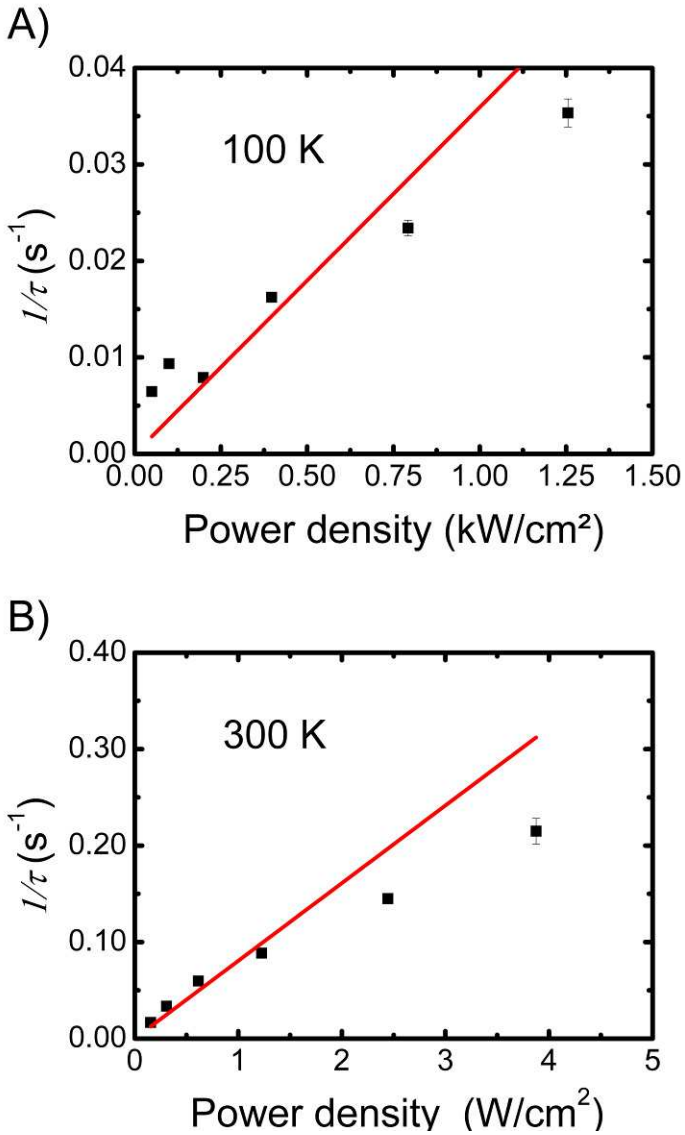

Figure S6: Photoactivation of Padron occurs via a 1-photon absorption process at low to room temperature. **A)** At 100 K, the photoactivation rate reports on the buildup of I_{cis} (actinic laser at 532 nm). **B)** At room temperature, the rate reports on the buildup of AB_{cis} (actinic laser at 488 nm). In both cases the excitation wavelength was 488 nm. Rates ($1/\tau$) were calculated by fitting the rise of fluorescence emission (510-530 nm band) with a mono-exponential kinetic model. Solid red lines show the slopes best fitting the data. Relatively low power densities were used to allow fine sampling of the photoactivation process with the limited time-resolution of our spectrometer.

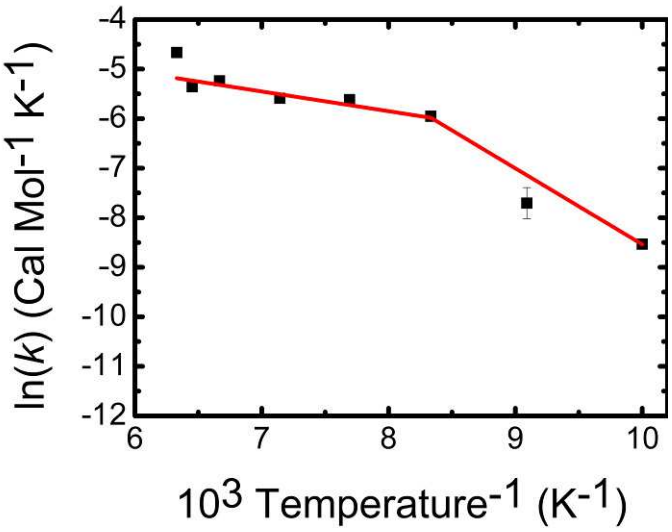

Figure S7: Arrhenius representation of the thermally-induced relaxation of I_{cis} to $B_{cis,LT}$. The logarithm of the relaxation rate $I_{cis} \rightarrow B_{cis,LT}$ is reported as a function of the inverse temperature. The plotted rates *k* were obtained by fitting the decay of I_{cis} (501-507 nm absorbance band) during relaxation in the dark by a stretched exponential model. The solid red lines show the slope best fitting the data for two temperature windows where the reaction appears to show a linear behavior.

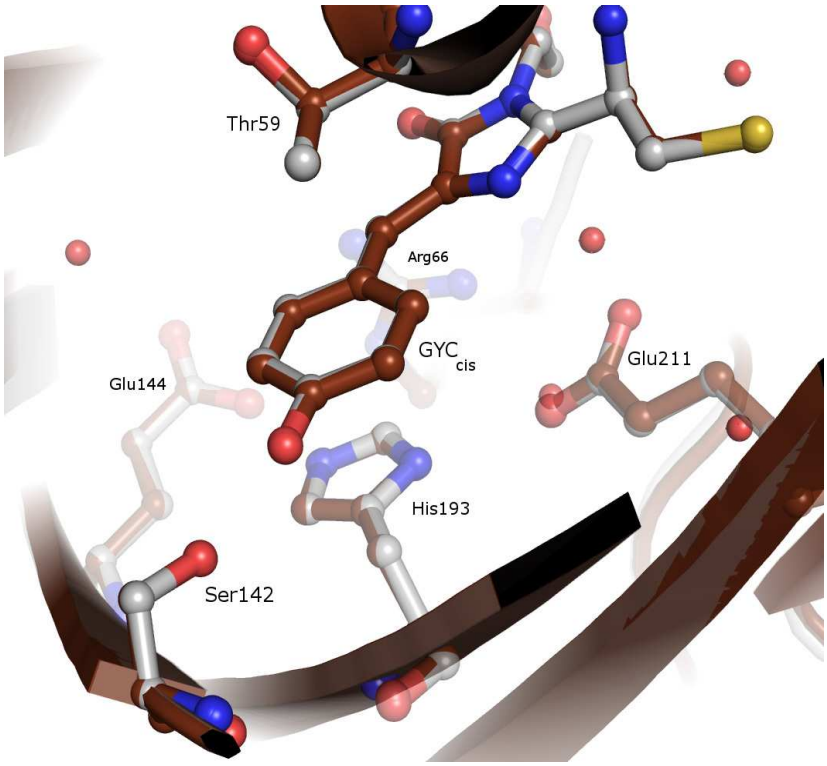

Figure S8: Crystal structure of Dronpa recorded under similar experimental conditions as that yielding I_{cis} in Padron. The structure of Dronpa in its fluorescent on-state is shown in white and the structure obtained upon actinic illumination at 100 K with 521 nm laser light is shown in brown. No significant differences can be seen between the two structures.